Optimization of bistable molecular materials

Hongfeng Wang

N° d'ordre : 4733

THÈSE

PRÉSENTÉE A

L'UNIVERSITÉ BORDEAUX 1

ÉCOLE DOCTORALE DES SCIENCES CHIMIQUES

Par Hongfeng WANG

POUR OBTENIR LE GRADE DE

DOCTEUR

SPÉCIALITÉ : Physico-Chimie de la Matière Condensée

OPTIMISATION DE MATERIAUX MOLECULAIRES BISTABLES

Directeurs de thèse : Jean-François LETARD
Cédric DESPLANCHES

Date de soutenance : 19 décembre 2012

Devant la commission d'examen formée de :

M. Smaïl TRIKI	Professeur	Université de Bretagne Occidentale	Rapporteurs
M. Keitaro NAKATANI	Professeur	ENS Cachan	
M. Mario MAGLIONE	Directeur de Recherche	ICMCB-CNRS	Examinateurs
M. Miguel CLEMENTE-LEON	Maître de conférences	Universidad de Valencia	
M. Cédric DESPLANCHES	Maître de conférences	Université Bordeaux 1	
M. Jean-François LETARD	Directeur de Recherche	ICMCB-CNRS	

A mes parents et Yin LIN

Remerciements

Je tiens à remercier Jean -François LETARD qui m'a encadré pendant la durée de cette thèse et qui m'a fait partager ses brillantes intuitions. J'ai sincèrement apprécié de travailler avec lui et je lui suis reconnaissant pour le temps qu'il m'a consacré et toutes les opportunités qu'il m'a données au cours de cette thèse.

Mes remerciements vont également à Cédric DESPLANCHES pour avoir co-encadré cette thèse. Il a grandement contribué à ma formation en répondant avec patience à mes questions de jeune naïf.

Je suis également très reconnaissant à Smaïl TRIKI et Keitaro NAKATANI d'avoir accepté d'être rapporteurs de cette thèse, ainsi qu'aux autres membres du jury, Miguel CLEMENTE-LEON et Mario MAGLIONE pour toutes leurs questions, suggestions et remarques.

Un remerciement spécial à Philippe GUIONNEAU qui a bien voulu relire ce manuscrit et m'a appris les bases de la cristallographie au long de ces trois années.

Par ailleurs, je voudrais remercier Claude DELMAS et Mario MAGLIONE, qui m'ont accueilli pendant trois ans au sein de l'ICMCB. C'est grâce à eux que j'ai pu travailler avec bonheur pendant cette thèse.

Un grand merci au groupe des Sciences Moléculaires : Nathalie DARO, Olivier NGUYEN, Cindy MAURIAC, Guillaume CHASTANET, Samir MATAR, Patrick ROSA, Daniel CHASSEAU, Corine MATHONIERE, Arnaud GROSJEAN, Nicolas PARADIS, Sergiu CALANCEA, Sabine LAKHLOUFI, Lucie MOULET qui m'ont permis de compléter ma formation. Je souhaite les remercier ici pour toute l'aide, le soutien, les conseils qu'ils m'ont apportés ainsi que pour leur bonne humeur et leur joie de vivre qui ont fait de ces trois années une aventure incroyable.

Un merci particulier à Jean ETOURNEAU pour m'avoir conseillé pendant trois ans.

Mes derniers mots, je les adresse à ma famille. Merci infiniment à vous d'avoir supporté mon éloignement et mon peu de disponibilité au cours de ces trois dernières années.

Table of Contents

Résumé en français.

Durant les dernières décennies, le développement des technologies de l'information a donné naissance à de très nombreuses recherches visant à réduire la taille et augmenter la capacité des composants électroniques. Dans ce contexte, la conception de matériaux moléculaires présentant des propriétés commutables à température ambiante est un défi actuel. L'intérêt de ces matériaux réside dans le fait qu'ils peuvent présenter plusieurs états magnétiques qui commutent sous l'effet d'une perturbation externe, comme la température, la pression ou la lumière. Cette propriété (bistabilité ou multi-stabilité) leur permet d'enregistrer et de stocker des informations. Dans certains cas, le changement de propriété magnétique (changement de spin) est accompagné d'un changement de couleur du composé, fournissant potentiellement des applications dans le domaine de l'affichage. Au sein de tous les matériaux étudiés depuis plusieurs années, les composés à conversion de spin (SCO) à base de fer sont parmi les plus étudiés. Une propriété particulièrement prometteuse de ces composés est le phénomène de piégeage d'un état de spin par irradiation ou par trempe thermique : effet LIESST (Light Induced Excited Spin State Trapping) ou TIESST (Thermally Induced Spin State Trapping). Par irradiation à basse température ou à l'aide d'un refroidissement rapide, il est possible de piéger un état haut spin métastable présentant une longue durée de vie à basse température. Cet état métastable peut présenter des durées de vie à basses températures très longues, allant jusqu'à plusieurs semaines ou mois. Toutefois, au dessus d'une température limite, dénommée T(LIESST) ou T(TIESST), la relaxation de l'état métastable est très rapide, de l'ordre de quelques secondes ou moins, empêchant l'utilisation de ces composés dans des dispositifs au dessus de T(LIESST). A l'heure actuelle, aucun composé présentant un T(LIESST) proche de l'ambiante n'est encore connu.

Pour augmenter cette température limite T(LIESST), il a été tenté d'identifier les facteurs responsables de la stabilisation de l'état métastable. Avec cet objectif en vue, le groupe des sciences moléculaires de l'ICMCB (Bordeaux) a déjà comparé plus de 60 matériaux présentant l'effet LIESST et a établi une base de donnée reliant T(LIESST) à la température de conversion thermique $T_{1/2}$. Une relation linéaire a été mise en évidence, permettant de relier ces deux grandeurs : $T(LIESST) = T_0 - 0{,}3\ T_{1/2}$ (figure a). Il a été démontré que la sphère de coordination du centre métallique joue un rôle majeur dans la stabilisation de l'état métastable HS, les ligands polydentes permettant d'obtenir les valeurs de T(LIESST) les plus élevées. En particulier, un complexe macrocyclique $[Fe(L_{222}N_3O_2)(CN)_2]\cdot H_2O$ présentant une température T(LIESST) particulièrement élevée a été découvert. Dans cette thèse, nous ciblerons notre étude sur les propriétés de ce complexe $[Fe(L_{222}N_3O_2)(CN)_2]\cdot H_2O$ et de ses analogues. Naïvement, le complexe $[Fe(L_{222}N_3O_2)(CN)_2]\cdot H_2O$ peut être vu comme étant constitué de quatre parties : le centre métallique Fe(II), le ligand macrocyclique $L_{222}N_3O_2$, le ligand anionique cyano et la molécule d'eau. Cette thèse sera consacrée à l'étude des effets sur la température T(LIESST) des modifications de ces quatre parties.

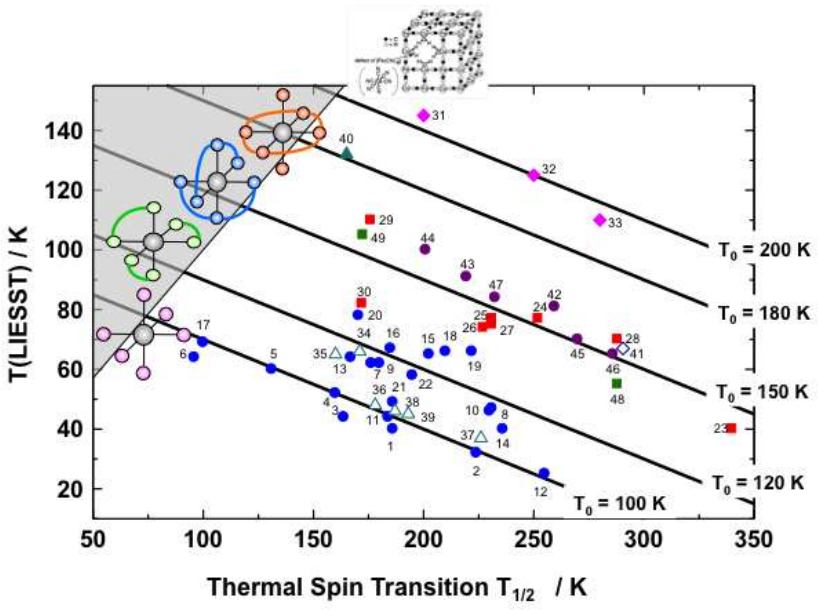

Figure a. Variation de T(LIESST) en fonction de $T_{1/2}$ pour des composés à conversion de spin

La partie I sera consacrée à un bref rappel de l'ensemble des propriétés des complexes de Fe(II) à conversion de spin. Nous présenterons le concept d'excitation photo-induite ou effet LIESST. L'idée d'une relation étroite entre la nature du ligand et la durée de vie de l'état métastable sera présentée au travers de la base de données $T(LIESST)/T_{1/2}$. Nous examinerons enfin brièvement l'évolution de cette base de données, ce qui nous conduira à justifier le choix du complexe $[Fe(L_{222}N_3O_2)(CN)_2]\cdot H_2O$ pour la suite des études décrites dans cette thèse.

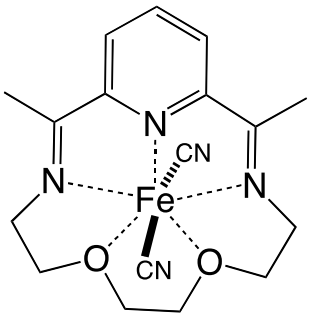

Schéma a. Complexe $[Fe(L_{222}N_3O_2)(CN)_2]$

La partie II de cette thèse sera consacrée à la présentation des propriétés structurales et magnétiques de la série métallique diluée $[Fe_xMn_{(1-x)}(L_{222}N_3O_2)(CN)_2]\cdot H_2O$. Des monocristaux du composés ne contenant que du manganèse $[Mn(L_{222}N_3O_2)(CN)_2]\cdot H_2O$ ainsi que des monocristaux de composés dilués $[Fe_xMn_{(1-x)}(L_{222}N_3O_2)(CN)_2]\cdot H_2O$ ont été synthétisés, le principe de synthèse étant décrit sur le schéma b. L'étude des propriétés de ces composés a permis la réalisation d'un diagramme de phase pour différentes températures et différentes dilutions.

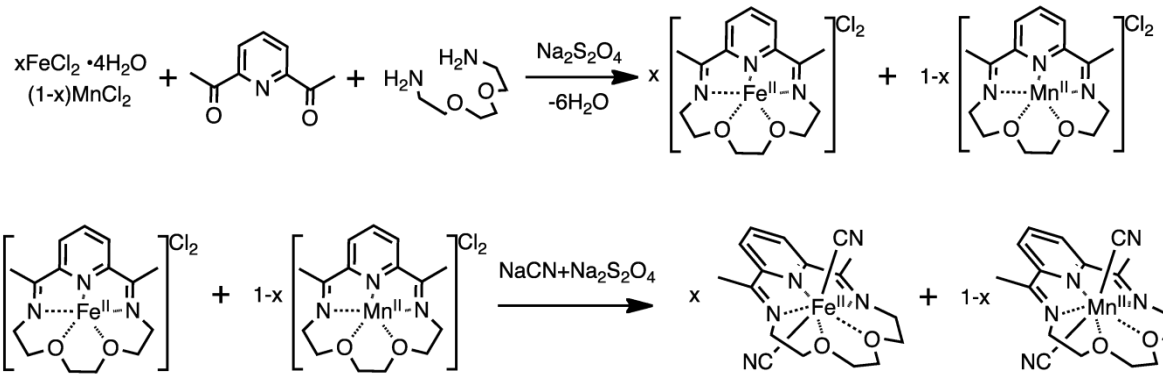

Schéma b. Synthèse de la série métallique diluée $[Fe_xMn_{(1-x)}(L_{222}N_3O_2)(CN)_2]\cdot H_2O$

La partie III sera consacrée à l'étude des modifications chimiques sur les analogues du complexe $[Fe(L_{222}N_3O_2)(CN)_2]\cdot H_2O$. Dans ces analogues, d'une part, les atomes de coordination d'oxygène seront remplacés par des atomes d'azote. D'autre part, le nombre d'atome de carbone entre les atomes d'azote de coordination sera modifié afin d'étudier l'influence de la flexibilité du ligand sur les propriétés photomagnétiques de cette série de composés. Quatre composés seront synthétisés et étudiés (schéma c). Les quatre composés sont $[Fe(L_{222}N_5)(CN)_2]\cdot H_2O$ ($L_{222}N_5$ = 2,13-dimethyl-3,6,9,12,18-pentaazabicyclo[12.3.1]-octadéca-1(18),2,12,14,16-pentaene), $[Fe(L_{232}N_5)(CN)_2]\cdot 2.5H_2O$ ($L_{232}N_5$ = 2,14-dimethyl-3,6,10,12,19-pentaazabicyclo[13.3.1]-nonadeca-1(19),2,13,15,17-pentaene), $[Fe(L_{223}N_5)CN)_2]\cdot 2.5H_2O$ ($L_{223}N_5$=2,14-dimethyl-3,7,10,13,19-pentaazabicyclo[13.3.1]-nonadeca-1(19),2,13,15,17-pentaene) et $[Fe(L_{323}N_5)(CN)_2]\cdot 1.5H_2O$ ($L_{323}N_5$ = 2,15-dimethyl-3,7,10,14,20-pentaaro- bicyclo[14.3.1]- icosan-1(20),2,14,16,18-pentaene).

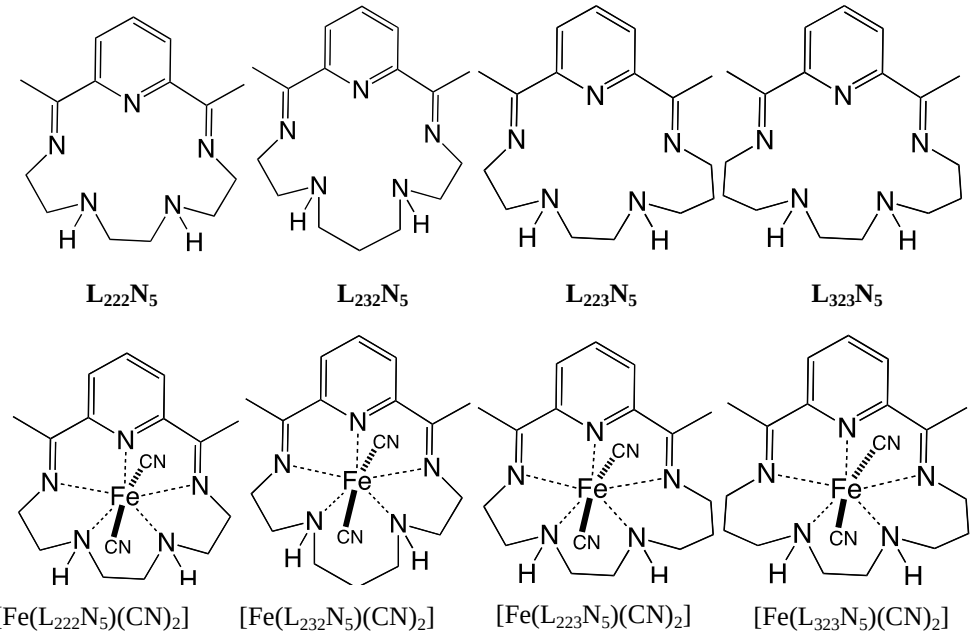

Schéma c. Ligands et complexes $[Fe(L_{xyz}N_5)(CN)_2]\cdot H_2O$ avec L_{xyz} = L_{222}, L_{232}, L_{223} and L_{323}

La partie IV portera sur l'effet du ligand anionique sur les propriétés structurales des complexes macrocycliques de Fe(II). La stratégie retenue consiste à remplacer le ligand cyano

en position axiale par un ligand thiocyanate ou sélénocyanate (schéma d). Les propriétés structurales de huit composés macrocycliques de Fe(II) seront étudiées à hautes et à basses températures et comparées aux propriétés structurales du complexe $Fe(L_{222}N_3O_2)(CN)_2]\cdot H_2O$.

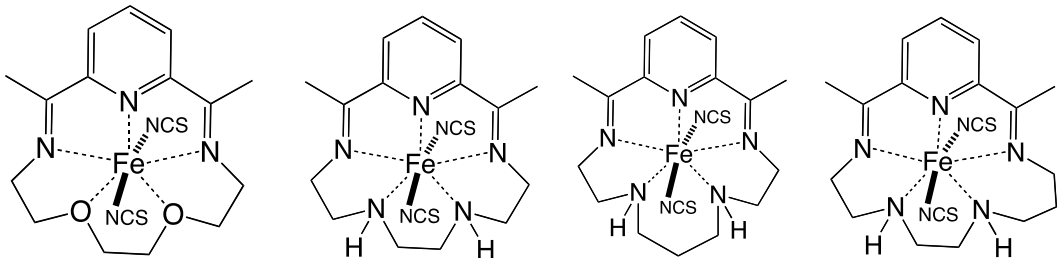

$[Fe(L_{222}N_3O_2)(NCS)_2]$ $[Fe(L_{222}N_5)(NCS)_2]$ $[Fe(L_{232}N_5)(NCS)_2]$ $[Fe(L_{223}N_5)(NCS)_2]$

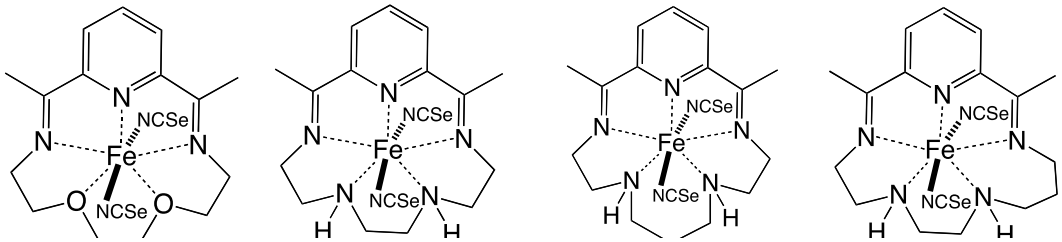

$[Fe(L_{222}N_3O_2)(NCSe)_2]$ $[Fe(L_{222}N_5)(NCSe)_2]$ $[Fe(L_{232}N_5)(NCSe)_2]$ $[Fe(L_{223}N_5)(NCSe)_2]$

Schéma d. Complexes macrocycliques présentant des ligands thiocyanate ou sélénocyanate

Enfin, dans la partie V, nous étudierons la dépendance en fonction du solvant de cristallisation du complexe $Fe(L_{222}N_3O_2)(CN)_2]\cdot H_2O$. Dans un premier temps, une étude d'un composé dans lequel la molécule d'eau a été remplacée par une molécule de chloroforme sera décrite. Dans un second temps, nous nous focaliserons sur les propriétés magnétiques du composé $Fe(L_{222}N_3O_2)(CN)_2]\cdot H_2O$ déshydraté puis réhydraté.

Nous conclurons enfin en rappelant les principaux résultats et leur contribution à la recherche de composés présentant une température T(LIESST) élevée. Quelques perspectives de recherche sur les résultats de ces travaux seront données.

General Introduction

In recent decades, the development of the electronics led to a tremendous growth of information technology to reduce the size and to increase the capacity of components. In this context, the design of molecular materials with switchable properties at room temperature application is a current challenge. The advantage of developing such materials may be linked for instance to the presence of several magnetic states which commute under the effect of an external perturbation such as temperature, pressure or light. This property (bistability or multi-stability), allows them to record and store information. In some cases, the change in spin is accompanied by a color change of the compound which provides some application in the field of the display. Along all the materials investigated since several years, iron spin-crossover (SCO) compounds have been extensively studied. A promising property is the potentiality for some of the SCO systems to display the excited spin state trapping phenomenon (either light-induced, i.e. LIESST effect or thermally induced, i.e. TIESST effect). Upon irradiation or fast cooling, a metastable high-spin (HS, $^5T_2$) state can be populated at low temperature. The main limitation for application is the stability of the metastable HS state. Above a limiting temperature, i.e. T(LIESST) or T(TIESST), the metastable HS state decays within seconds or less.

To overpass this limitation, it has been attempted to identify the factors responsible for stabilizing the metastable state. With this objective, the Molecular Science Group at the ICMCB (Bordeaux) has previously compared more than 60 SCO materials, and established a database with a $T(LIESST)=T_0 - 0.3\ T_{1/2}$ relationship. It has been evidenced that the degree of coordination of the metal center plays a major role in the stabilization of metastable HS state. Following this strategy, Fe(II) macrocyclic complex $[FeL_{222}N_3O_2(CN)_2]\cdot H_2O$ has been reported with an exceptional high T(LIESST) value. In this thesis, we will focus our attention on the influence of chemical modifications on the SCO properties of the $[Fe(L_{222}N_3O_2)(CN)_2]\cdot H_2O$ complex and its analogues. Naively, the $[Fe(L_{222}N_3O_2)(CN)_2]\cdot H_2O$ complex can be separated in four interconnected parts: the Fe(II) coordination center, the macrocyclic ligand, the anionic ligand (cyano group) and the water molecule. We will devote this thesis to a comprehensive investigation on these four different parts.

The Part I will be dedicated to the brief recall and overview of the spin crossover properties on Fe(II) compounds. We will present the light induced phenomenon associated to the LIESST effect, including the concept of T(LIESST). The idea of a close relationship between the nature of the ligand and the lifetime of the metastable state will be presented, i.e. the T(LIESST) database. We will then briefly review the development of this database, which lead us to the study of chemical modifications on the $[Fe(L_{222}N_3O_2)(CN)_2]\cdot H_2O$ complex and its analogues.

The Part II will be dedicated to the presentation of the magnetic and structural properties of the metal diluted series $[Fe_xMn_{(1-x)}(L_{222}N_3O_2)(CN)_2]\cdot H_2O$. The metal dilution method is considered as a modification of Fe(II) coordination center. A discussion of the properties recorded as a function of temperature will be given based on the phase diagram of this series.

The Part III will be dedicated to the study of chemical modifications on the analogues of $[Fe(L_{222}N_3O_2)(CN)_2]\cdot H_2O$ complex. In these analogues, the oxygen coordination atoms are

replaced by nitrogen atoms. The selected modification method is to change the number of carbon atoms between the nitrogen coordination atoms. We will thus be in a position to investigate the influence of macrocylic ligands on the SCO properties.

The Part IV will concern the effect of anionic ligand on the structural properties of Fe macrocyclic complexes. The selected strategy is to change the cyano group at the axial position with thiocyanate / selenocyanate group. By a systematic structural investigation of eight Fe(II) macrocyclic complexes at both high and low temperatures, we will compare the structural properties with the $Fe(L_{222}N_3O_2)(CN)_2]\cdot H_2O$ complex.

Finally, in Part V we will report the investigation of the solvent dependence on $Fe(L_{222}N_3O_2)(CN)_2]\cdot H_2O$ complex. We will first report a structural study on $Fe(L_{222}N_3O_2)(CN)_2]\cdot CHCl_3$ complex, and then focus on the magnetic properties of the dehydrated and rehydrated $Fe(L_{222}N_3O_2)(CN)_2]\cdot H_2O$.

We will conclude by recalling the main results and their significant contribution to the broad topic of research. Some research perspectives on the result of this work will be given.

Part I. Introduction

Chapter I.1. Spin crossover phenomena of Fe(II) complexes

I.1.1. General introduction of spin crossover

The design of switchable molecular materials towards room temperature application is a current challenge in information technology [1-3]. Many iron spin crossover compounds have been studied with this aim [4]. The first experiment on the spin crossover was reported by Cambi and Szegö in 1931 in a series of complexes of Fe(III) tris (dithiocarbamate) [5]. Since that first observation, the spin crossover phenomenon has been described in transition metals with the electronic configuration of $3d^4$ to $3d^7$, i.e. Fe(II), Fe(III), Co(II), Co(III), Mn(II) and Mn(III) [6-15]. Today, most of the compounds displaying spin crossover properties involve Fe(II) metal ions in octahedral geometry [4,6]. For this reason, we will take the case of the Fe(II) as an example to illustrate the phenomenon of spin crossover in details.

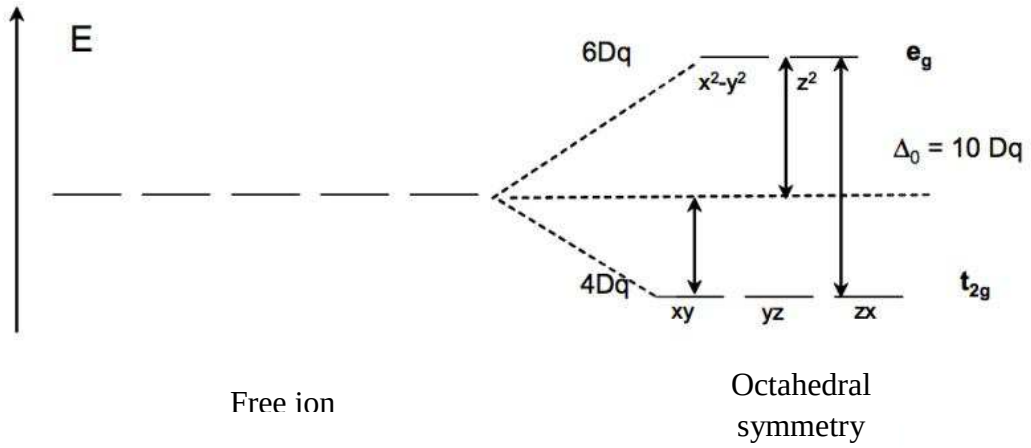

Scheme I. 1: Energy diagram of the d orbitals of the Fe (II).

The electronic configuration of the Fe(II) ion in its free state is [Ar] $3d^6$. It has five d orbitals with the same energy level as presented in Scheme I. 1. In an octahedral complex, the d orbitals have different energy levels. They fall into two sublevels called t_{2g} and e_g. The level corresponding to three t_{2g} orbitals d_{xy}, d_{xz} and d_{yz}, and the e_g level corresponding to the two orbitals of higher energy $d_{x^2-y^2}$ and d_{z^2}. e_g type orbitals have energy higher than the t_{2g} orbitals. The energy difference between t_{2g} and e_g is Δ_0 = 10 Dq (Dq, crystal field splitting parameter).

There are two options for filling the six 3d elections of Fe(II) complex: the low spin state (LS, $^1A_{1g}$: t_{2g}^6 e_g^0, S =0), diamagnetic and the high spin state (HS, $^5T_{2g}$ t_{2g}^4 e_g^2, S =2), paramagnetic as presented in Scheme I. 2. The system will adopt one or the other type of filling depending of the ligand field Δ_0 and the pairing energy Π.

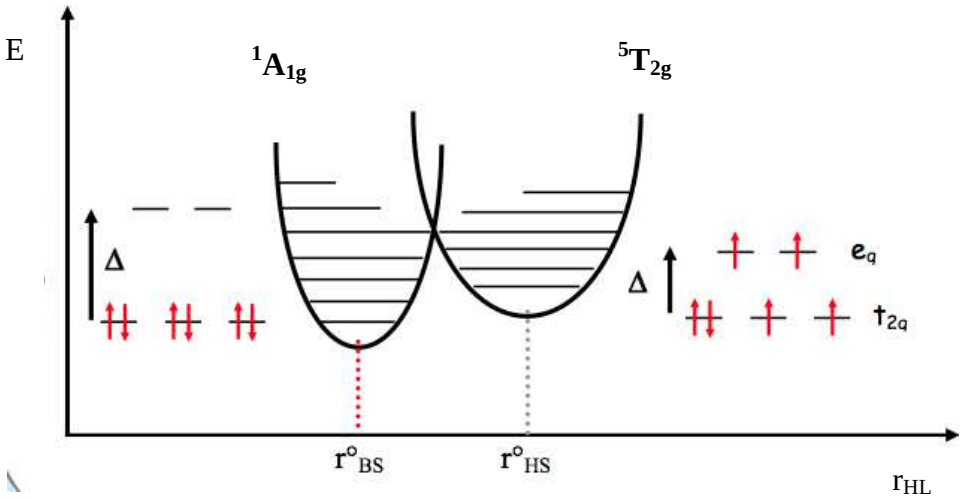

Scheme I. 2: Diagram of energy levels and spin states of Fe (II).

In the case $\Delta_0 << \Pi$, the electrons occupy the maximum possible orbitals following Hund's rule. There are then four unpaired electrons and the resulting electron spin S is equal to 2: this is the high spin state (HS). In the case $\Delta_0 >> \Pi$, for a d^6 configuration, all electrons are paired in the lowest energy orbitals t_{2g}, (i.e. violating Hund's rule). The resulting electron spin S is equal to 0: this is the low spin state (LS). The phenomenon of spin crossover takes place when Δ and Π are the same order of magnitude, with Δ of about 12000 cm^{-1}. Under the effect of an external perturbation, for example changes in temperature, in excitation by an electromagnetic wave, a magnetic field variation and, in pressure, the complex can change from low-spin state to high spin state or on the contrary. If we consider for instance the case of spin state induced by a change of temperature five classes of behavior have been reported [4,16] (Scheme I. 3) : a) gradual; b) abrupt c) abrupt with hysteresis, d) in steps e) incomplete.

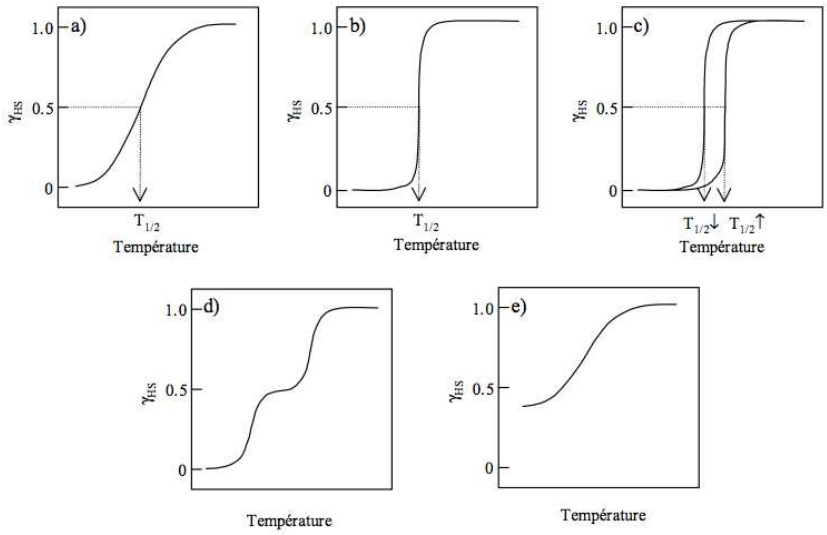

Scheme I. 3: Schematic representation of the different spin crossover (SCO) in function of temperature (high spin fraction, γ_{HS}): a) gradual b) abrupt c) abrupt with hysteresis d) in steps e) incomplete [4,16].

a) Gradual properties (Scheme I. 3a) correspond to complexes with weak interaction, for example, in highly diluted systems or in the case that the sites of Fe(II) are far away from each other due to bulky ligand.

b) Abrupt behavior (Scheme I. 3b) is associated to the complexes in which Fe(II) centers have stronger interaction [17]. In this case, the spread of spin state change in the material is accelerated by the network in particular interaction between the molecules. It is the case for example, the compounds $[Fe(phen)_2(NCS)_2]$ [17,18], $[Fe(PM\text{-}BIA)_2(NCS)_2]$ (with PM-BIA = N-(2'-pyridylmethylene) aminobiphenyl) [19] and $[Fe(bpp)_2](NCSe)_2$ [20,21].

c) The third type of behavior is the presence of a thermal hysteresis (Scheme I. 3c) [22]. In general, the presence of hysteresis can be associated with either a change in crystallographic phase, or in the presence of strong long-range interactions in the material. Two approaches are used to enhance the interaction between Fe(II) to increase the width of the hysteresis. The first strategy is to ensure the cohesion of the crystal lattice via weak interactions (π-π interaction, hydrogen bonds) [4,16,23]. The second strategy is to link the metal atoms together by chemical bridges to generate a network of strong interactions (covalent bonds). This is typically the case of polymeric systems based triazole ligand [24-31].

d) The forth class is the occurrence of spin crossover in steps (Scheme I. 3d). The first spin crossover in two steps was observed on a complex of Fe(III) in 1981 by Zelentsov [32]. This can be caused by the existence of different coordination sites [33] and/or the presence in a SCO complex of several Fe(II) metal center, like in the case of binuclear complexes [34-36]. In the latter case, change may occur between the two entities in the high spin state, state [HS-HS], to an intermediate state where one of the two entities is in high-spin state, state [HS-LS], and then to the ground state with all entities in the low spin state, state [LS-LS]. Finally, a two-step transition was also observed for systems with only one coordination site as the family of complexes $[Fe(2\text{-}pic)_3]Cl_2 \cdot EtOH$ (with 2-pic = 2-picolylamine) [37]. This behavior was attributed to the existence of short range interactions and the formation of HS / LS pairs throughout the spin crossover [38,39].

e) The last class is incomplete spin crossover (Scheme I. 3d). In some cases, this behavior can be justified by an effect of iso-energy states between HS and LS states [40]. The relaxation kinetics at low temperature is slow enough that the phenomenon of "spin freezing" is observed. It is also possible to switch from an incomplete spin crossover to a complete transition by applying external pressure to the system. These studies were conducted in 1998 by Kahn and Gütlich on the complex $[Fe(PM\text{-}A)_2(NCS)_2]$ (with PM-A = N-(2'-pyridylmethylene) aniline) [41,42]. In other cases, the incomplete transition is due to a partial transition of some of the metal sites.

I.1.2. Thermodynamics of spin crossover

The phenomenon of spin crossover can be thermodynamically described as a physical balance between LS and HS state. This equilibrium is governed by the variation of free enthalpy or Gibbs free energy ΔG (Eq 1). ΔH (= H_{HS} - H_{LS}) and ΔS (= S_{HS} - S_{LS}) are, the changes of enthalpy and entropy of the system, respectively.

$$\Delta G = G_{HS} - G_{LS} = \Delta H - T\Delta S \qquad \text{(Eq. 1)}$$

The enthalpy changes, ΔH, and entropy, ΔS, are divided into two contributions: electronic contribution (ΔH_e and ΔS_e) and vibrational contribution (ΔH_{vib} and ΔS_{vib}).

The enthalpy change, ΔH is variable between the compounds, and may be directly connected to the electronic contribution ΔH_e, which is estimated at 1000 cm^{-1} [9,43].

The entropy change, ΔS is the sum of two contributions, the electronic contribution (ΔS_e) and vibrational contribution (ΔS_{vib}) [44-46]. The entropy change of the electronic contribution (ΔS_e) is the sum of contributions, changes in spin (ΔS_e^{spin}) and orbital moment (ΔS_e^{orb}), respectively. This orbital contribution is usually neglected due to the lowering of the symmetry around the Fe(II) [9,43]. Overall, $\Delta S_e = \Delta S_e^{spin} = R\,[\ln\{(2S+1)_{HS} / (2S+1)_{LS}\}] = R \ln 5 = 13.38$ J K mol^{-1}. The electronic contribution is constant. The vibrational contribution (ΔS_{vib}) and the electronic contribution affect the total change in entropy.

ΔG is positive when the LS state is stabilized, and it is negative when HS state is stabilized. Therefore at the equilibrium temperature denoted $T_{1/2}$, ΔG vanishes and the free energies of the HS and LS forms are equal. Transition temperature $T_{1/2}$ is defined by:

$$T_{1/2} = \frac{\Delta H}{\Delta S} \qquad \text{(Eq. 2)}$$

Below $T_{1/2}$ ($\Delta G > 0$), ΔH is greater than TΔS, the enthalpy factor dominates and LS state is stable. On the contrary, above $T_{1/2}$ ($\Delta G < 0$), ΔH is less than TΔS, the entropic factor dominates and the HS state is stable (Scheme I. 4). Based on all that, it may be considered that the spin crossover is a thermo-induced molecular process driven by entropy, like all thermal transitions.

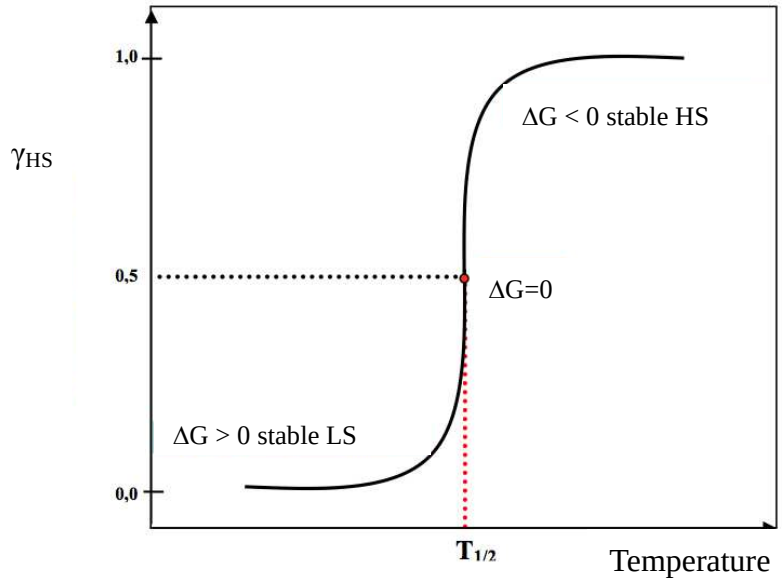

Scheme I. 4: Variation of the HS fraction depending on the temperature [47].

The spin crossover is under the influence of intermolecular interactions and pressure.

a) Influence of intermolecular interactions

If we consider a set of randomly distributed molecules in the solid with molar fractions γ and (1 -γ), respectively associated with the HS and LS states, then the free energy of the system consisting of Fe(II) interacting, is expressed in the form:

$$G = (1 - \gamma)G_{LS} + \gamma G_{HS} - TS_{mix} + \Gamma\gamma(1 - \gamma) \qquad \text{(Eq. 3)}$$

Where Γ stands for the intermolecular interaction term between Fe(II) metal centers. The entropy of mixing S_{mix} is expressed as: / $S_{mix} = -R[(1-\gamma)\ln(1-\gamma) +\gamma\ln(\gamma)]$ /, where R is the ideal gas constant. Taking G_{LS} as original energy ($G_{LS} = 0$) and $\Delta G = G_{HS} = \Delta H - T\Delta S$, the Eq. 2 becomes:

$$G =\gamma\Delta H + \Gamma\gamma(1 - \gamma) - RT[(1 - \gamma)\ln(1 - \gamma) + \gamma\ln(\gamma) + \gamma\Delta S/R] \qquad \text{(Eq. 4)}$$

At thermodynamic equilibrium of the system, the condition $(\partial G / \partial\gamma)_{T,\ P} = 0$, the temperature as a function of the HS fraction (Eq. 5) can be expressed.

$$T = \frac{\Delta H+\Gamma(1\ -2\gamma)}{R\ln\left(\frac{1-\gamma}{\gamma}\right)+\Delta S} \qquad \text{(Eq. 5)}$$

For γ= 0.5, that is to say, when the LS entities and HS entities are equal, the expression of the transition temperature is found to be $T_{1/2} = \Delta H / \Delta S$.

Eq. 5 allows us to follow the evolution of the HS fraction, γ, depending on the temperature T. Several types of transition can be considered depending on the nature of the interactions Γ within the system:

- Gradual, for $\Gamma < 2RT_{1/2}$, which is characteristic of weak intermolecular interactions.
- Abrupt, for $\Gamma = 2RT_{1/2}$ which is characteristic of strong intermolecular interactions.
- Abrupt with hysteresis values $\Gamma > 2RT_{1/2}$, which is characteristic of very strong intermolecular interactions.

b) Spin crossover induced by pressure

The first study of the effect of pressure on a SCO material was reported almost 40 years ago. One of the pioneers in this field, Ewald in 1969 [48] assumes that the application of pressure stabilizes the LS state characterized by a smaller volume than the HS state. The consequence is a shift of the transition temperature towards higher temperatures. The effect of the pressure on the SCO phenomenon has been interpreted along the mean field approximation [49-51], where the dependence of $T_{1/2}$ with the pressure obeys to the Clausius-Clapeyron law:

$$\frac{\partial T_{\frac{1}{2}}}{\partial P} = \frac{\Delta V}{\Delta S_{HL}} \qquad \text{(Eq. 6)}$$

In this approach, the effect of the pressure on the spin crossover is determined by the magnitude of the volume change of the cell unit per molecule having a spin crossover ΔV and intermolecular interactions of the free energies $F_{int}(\gamma, T)$. Thus, the change in free enthalpy or Gibbs free energy to external pressure P, is defined as:

$$\Delta G = \gamma \Delta F_{HL} + F_{int}(\gamma, T) - TS_{mix}(\gamma) + \gamma P \Delta V \qquad \text{(Eq. 7)}$$

With γ = HS mole fraction; ΔF_{HL} = free energy change due to the spin crossover $S_{mix}(\gamma) = -k_B [(1-\gamma) \ln(1-\gamma) + \gamma \ln(\gamma)]$ and $F_{int}(\gamma, T) = \Delta_s \gamma - \Gamma \gamma^2$ wherein Δ_s and Γ denote the displacement of the energy and cooperativity coefficient, respectively [50]. The variation of free energy is expressed as:

$$\Delta F_{HL} = \Delta H(T_{1/2}) - T\Delta S_{HL} \qquad \text{(Eq. 8)}$$

Here $\Delta H(T_{1/2})$ and ΔS_{HL} represent, the variations of enthalpy and entropy of the system at atmospheric pressure, respectively.

At the thermodynamic equilibrium of the system, the condition $(\partial G / \partial \gamma)_{T, P} = 0$ is used to describe the influence of pressure on the spin crossover (Eq. 9)

$$T = \frac{(\Delta H\left(T_{\frac{1}{2}}\right) + \Delta_s + P\Delta V - 2\gamma\Gamma)}{k_B \ln\left(\frac{1-\gamma}{\gamma}\right) + \Delta S_{HL}} \qquad \text{(Eq. 9)}$$

Based on Eq. 9 the variation in $T_{1/2}$ under the pressure can be explained in many cases. Today, various techniques have been used, magnetic susceptibility measurements [4,7,41,42,53,54,55], absorption and optical reflectivity [56,57] and Mössbauer [58], to study the pressure on a SCO materials.

Main of these studies confirm the increase in the transition temperature with the increase of pressure, such as for $[Fe(Phen)_2(NCS)_2]$ and for $[Fe(PM\text{-}Aza)_2(NCS)_2]$ with N = PM-Aza-(2'-pyridyl-methylene)-4-(phenylazo) aniline [42]. Nevertheless in very few examples, it was reported the opposite effect: a decrease of $T_{1/2}$ with the pressure [41,57,59-63]. In those cases, the crystal unit cell in HS state is smaller than in LS state. The thermodynamic approach of the spin crossover under external pressure can be also extended to dilute systems, subject to a change of internal pressure in reason of the insertion of guest metal dilution [52].

Chapter I.2. Photo-induced spin crossover

I.2.1. The phenomena of photomagnetism

The photomagnetism is a fascinating and very promising property from the point of view of applications. This covers all changes of magnetic properties induced by the application of light. There are different families of photoswitching molecular compounds, inorganic or organic. The best known and most studied are [64]:

a) Spin crossover compounds containing Fe(II) center.
b) Metal-ligand charge transfer compounds: the family nitroprussiates [64-67].
c) Metal-metal charge transfer compounds: Prussian blue analogues [68-73].
d) Complexes with photoisomerizable ligands [74-76].
e) Complexes of Co(II) catecholates [77-85].
f) "Magnetic switch" from the diarylethenes family [86-92]

One of the challenges is obviously to get a photo-induced effect with a very long lifetime at room temperature, active in solid state, photoreversible and with a very low fatigability (i.e. high cyclability). In the field of spin crossover materials, three strategies are now developed to achieve these objectives: i) The first is based on the LD-LISC effect (Ligand Driven - Light Induced Spin Change), where the organic ligand is sensitive [75,76], ii) the second is based on the irradiation at the center of the thermal hysteresis [85,93-95], and iii) The third concerns the increase of the lifetime of the photo-induced state based on the LIESST phenomenon (Light-Induced Excited Spin State Trapping) [19,96-99].

The last strategy is the subject of this thesis, and therefore we will describe this strategy in detail in the following paragraphs.

I.2.2. LIESST effect

The LIESST phenomena can be found in both Fe(II) and Fe(III) [100-106] complexes, and nowadays the overwhelming majority is Fe(II) complexes. The first evidence of the Light Induced Excited Spin State Trapping (LIESST) effect in Fe(II) complex was first observed in liquid phase in 1982 [107], and two years later in solid phase [96]. The proposed mechanism for Fe(II) (Scheme I. 5) is related to the existence of two successive intersystems crossing. Under excitation with typically green light at 514 nm, the system is transferred from the LS $^1A_1$ state to the excited $^1T_1$ or $^1T_2$ state, then relaxes non-radiatively to the intermediate triplet state, $^3T_2$ or $^3T_1$, and finally reaches the metastable HS state, $^5T_2$. The lifetime of the metastable HS depends on the temperature. For instance, at 20 K in the solid phase the lifetime of the metastable HS state was higher than 10^6 s [96]. An alternative way to return to the stable LS $^1A_1$ state is the reverse-LIESST phenomenon [98]. Under excitation with a red light at 820 nm, i.e. irradiation in the absorption band of the HS state the excited state ^5E is

populated, followed by relaxation in $^3T_2$ or $^3T_1$, and finally to the stable LS $^1A_1$ state.

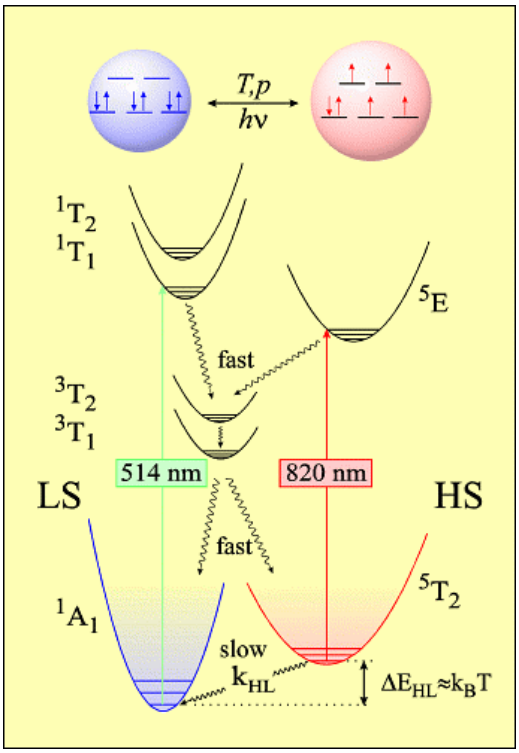

Scheme I. 5: Schematic illustration of the LIESST effect and reverse-LIESST effect

Today, many studies have been conducted to investigate the effects LIESST and reverse-LIESST, including the lifetime of the metastable HS. The first comparison of the stability of the photoinduced HS state was made by Herber and Casson in 1986 using infrared spectroscopy [108]. These authors followed the temperature dependence of the vibration of ν_{CN} in six spin crossover materials, and determined a temperature limit above which the light-induced phenomenon is no longer observable.

In 1991, Hauser presented the first guideline concerning the lifetime of the photoinduced HS state [109]. This author has studied the dynamics of the LIESST effect in different diluted spin crossover materials, and noticed a strong correlation between the lifetime of the photoinduced HS state and the spin crossover temperature $T_{1/2}$. More precisely, Hauser observed that the longest lifetimes of the metastable HS were obtained for compounds with the lowest spin crossover temperatures $T_{1/2}$. This relationship is known today as the "inverse energy" law. However one difficulty to use such an approach, is to properly determine the lifetime of in the tunneling region, especially when stabilization of the photoinduced HS state in the tunneling region is very effective, that is to say that it takes long time to be determined.

For this reason, in 1998, in collaboration with Motorola Industrial Research Centre, the Molecular Sciences group has proposed to introduce a procedure for comparing materials, based on the determination of a temperature limit of photo-inscription, denoted as T(LIESST) [110]. The author proposes to use this value for evaluating the ability of a spin crossover compound to store information. Indeed, above the T(LIESST) limit, the photo-induced magnetic information is deleted in the cavity of a SQUID magnetometer.

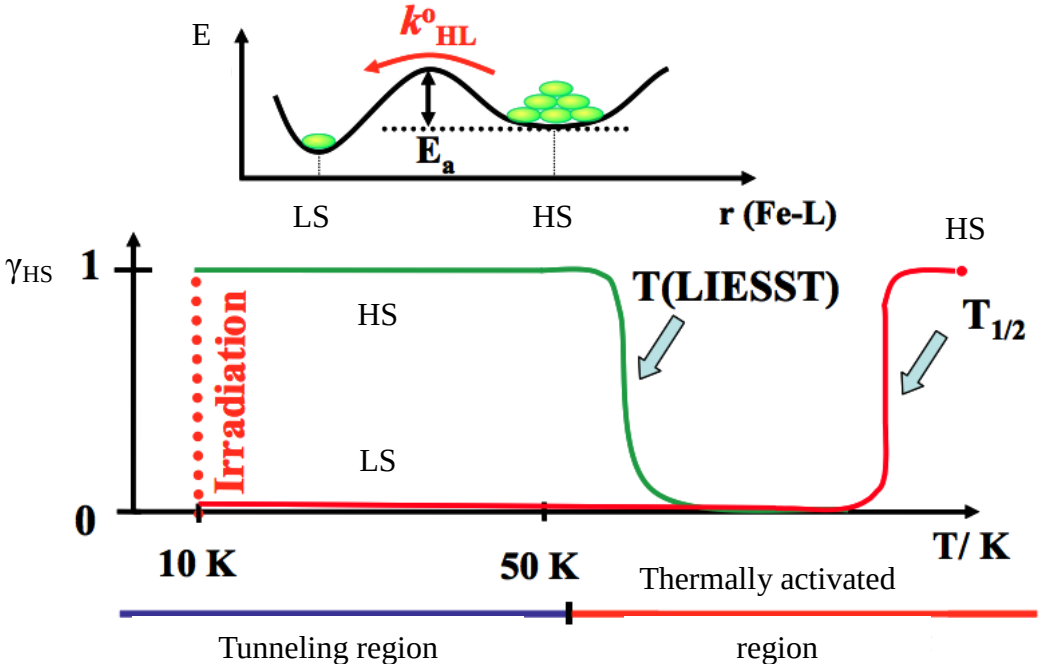

Scheme I. 6: Schematic illustration of the experimental T(LIESST) measurement. [47]

A typical experiment carried out is presented in Scheme I. 6. The compound, generally in its HS state, is placed in the SQUID cavity at room temperature. The temperature is then lowered slowly (10 K min^{-1}) down to 10 K to avoid any trapping of HS fraction. During this thermal treatment, the compound passes from HS state to LS state at 10 K. The system in the LS state is then irradiated with a green light, as soon as an increase of the magnetic signal is observed. After typically some hours the photostationary state is reached and the light irradiation is stopped. The temperature is then increased at a constant speed calculated to be 0.3 $Kmin^{-1}$. The minimum of the $d\chi_M T/dT$ versus T curve determines the T(LIESST) temperature [110].

In parallel to the possibility to reach an excited spin state by photoexcitation, rapid quench cooling also gives access to a metastable HS state. This phenomenon is known today as the Thermal Induced Excited Spin State Trapping (TIESST) [100-102]. To further investigate this effect, the Molecular Sciences group has used an identical procedure that for measuring the T(LIESST). The unique difference concerns the preparation of the metastable HS state. In the case of TIESST experiment, the sample from room temperature is quickly frozen in the SQUID cavity placed at 10 K. Temperature is then increased at a constant speed calculated to be 0.3 $Kmin^{-1}$ and the minimum of the $d\chi_M T/dT$ versus T curve determines the T(TIESST) temperature.

I.2.3. T(LIESST) database

Since many years, the molecular group in collaboration with many teams attempts to identify the factors responsible for stabilizing the metastable state [111-114]. Today, it seems that a relation exists, $T(LIESST)=T_0 - 0.3\ T_{1/2}$ relation [115-118] (Figure I. 1), and the role of

inner coordination sphere seems to play a key role on the stabilization of metastable HS state.

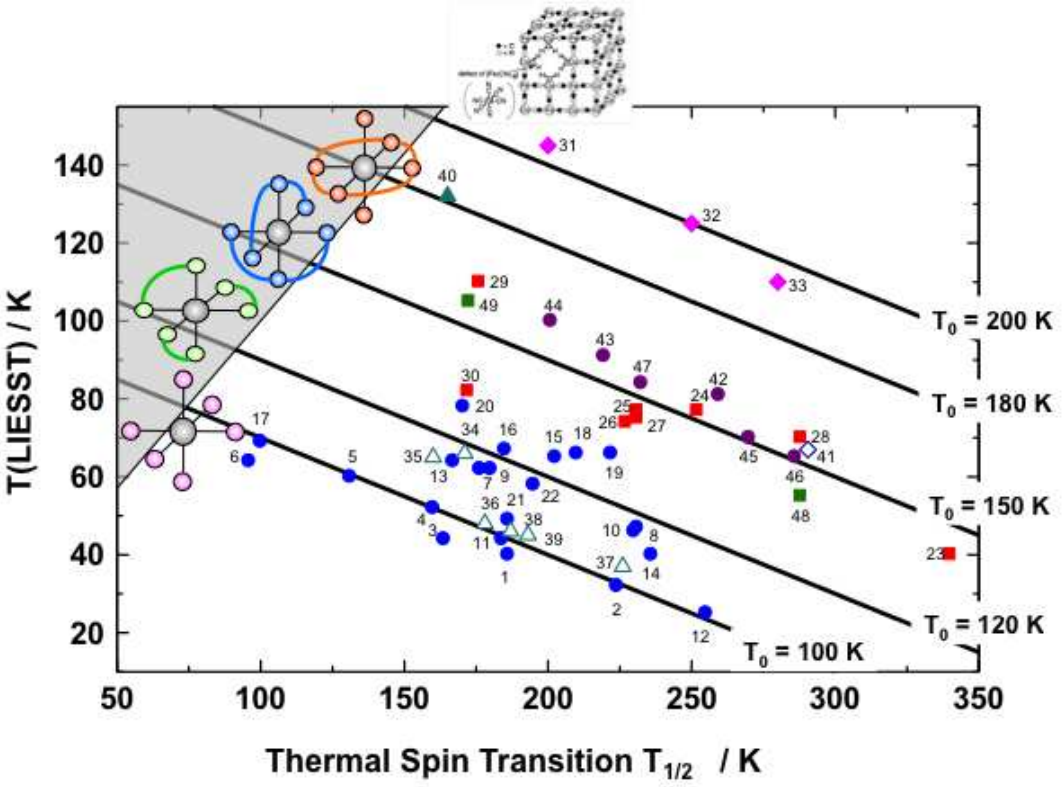

Figure I. 1: Variation of T(LIESST) versus T1/2 for spin crossover compounds [117].

The first work based on a comparison of T(LIESST) temperatures was performed in 1999 [115]. In this study, the magnetic and the photomagnetic properties of twenty-two SCO compounds were determined (Figure I. 1, samples 1–22); i.e. the thermal spin crossover $T_{1/2}$ as well as the T(LIESST) temperatures. When all these data were plotted in a graph defined by T(LIESST) temperature versus $T_{1/2}$, it was firstly observed a large distribution of points. But by considering the chemical formula of the different complexes, it was realized that the physical properties of the complexes followed some general tendencies. Most of the investigated SCO complexes in these cases are members of the $[FeL_2(NCX)_2]$ family (samples 1–22), with L an aromatic unit ligand and X a thiocyanato (= S) or a selenocyanato (= Se) unit. The original idea was to compare a couple when two complexes possessed the same aromatic L unit ligand but involved either a S or a Se unit. By doing this, several couples (S and Se) were found to follow the same tendency (samples 1–2, 7–8, 9–10, 11–12, 13–14) and two virtual lines were proposed with a general equation, $T(LIESST)=T_0 - 0.3\ T_{1/2}$. The extrapolated T_0 values, at $T \rightarrow 0$, were 100 K and 120 K [115].

Later on, this analysis was confirmed by an additional study where the magnetic and the photomagnetic studies of eight new SCO materials were investigated (Figure I. 1, samples 23–30) [116]. The idea was to compare a series of Fe(II) metal complexes possessing various $T_{1/2}$ and T(LIESST) values without changing the FeN_6 coordination sphere. The studies family was the $[Fe(bpp)_2]X_2 \cdot nH_2O$ series. This family was well known for exhibiting various thermal spin-crossover behaviours depending on the nature of the anion and the degree of hydration. The iron(II) metal center of this family was surrounded by six donor nitrogen atoms with two

ligand molecules coordinated in an octahedral plane [119-122]. These authors systematically determined the thermal spin crossover and the limit temperature of the LIESST phenomenon of all the series of hydrated and dehydrated $[Fe(bpp)_2]X_2 \cdot nH_2O$ complexes, with $X = PF_6^-$, NCS^-, $NCSe^-$, BF_4^-, Br^- and I^-. Interestingly, the $[Fe(bpp)_2]X_2 \cdot nH_2O$ data on the T(LIESST) vs. $T_{1/2}$ plot were distributed in a such way that the $T(LIESST)=T_0 - 0.3\ T_{1/2}$ relation established earlier remained valid. A third line with a T_0 value of 150 K was proposed (Figure I. 1, samples 23–30) for this family. What is remarkable is that for the first time the 150 T_0 line defines some SCO complexes with a $T_{1/2}$ value around room temperature and a measurable T(LIESST) value (sample 28). Such a result is very exciting, as it represents the first step towards the design of switchable SCO materials useable in a genuine device [117].

In parallel, Hashimoto et al. [71] provided a new evidence for the validity of the $T(LIESST)=T_0 - 0.3\ T_{1/2}$ relation. The selected family was the Co–Fe Prussian Blue analogues, $[Na_xCo_yFe(CN)_6]\cdot zH_2O$ with atomic Co/Fe composition ratios of 1.37, 1.32 and 1.26. In those complexes, a change of electronic and spin states may be induced by two methods: (i) by a temperature gradient, i.e. from room temperature Fe(III) ($t_{2g}^5e_g^0$, LS, S = 1/2)–CN–Co(II) ($t_{2g}^5e_g^2$, HS, S = 3/2) to low temperature Fe(II) ($t_{2g}^6e_g^0$, LS, S = 0) –CN–Co(III) ($t_{2g}^6e_g^0$, LS, S = 0); (ii) by light irradiation at 5 K with the population of the metastable Fe(III) ($t_{2g}^5e_g^0$, LS, S = 1/2)–CN–Co(II) ($t_{2g}^5e_g^2$, HS, S = 3/2) state. The authors consequently determined for each Co/Fe composition the $T_{1/2}$ and T(LIESST) temperatures and observed the presence of a new T_0 line (Figure I. 1, samples 31–33) parallel to the three previous ones [71]. The T_0 value was estimated at 200 K. Of course, on one hand it is clear that the physical process involved in these Prussian Blue complexes is not strictly speaking a pure spin crossover phenomenon but a Charge-Transfer-Induced Spin Transition (CTIST) effect [69], and any overall comparison has to be made cautiously. On the other hand, this indicates that the T(LIESST) relation ($T(LIESST)=T_0 - 0.3\ T_{1/2}$) is probably more general.

Based on this evidence that some relations exist between compound (existence of T_0 line) many efforts have been dedicated to study the factors able to affect the T_0 value such as a) cooperativity, b) influence of the electronic factor c) tuning the Fe(II) bond length and d) distortion of the FeN_6 octahedron.

a) Cooperativity

It is sometime proposed that the cooperativity factor stabilise the photo-induced HS state [31]. In this context, in the $[Fe(PM\text{-}L)_2(NCX)_2]$ family, it has been demonstrated that for an almost constant $T_{1/2}$ temperature of about 170 K, the T(LIESST) value increased from 31 K, for the gradual SCO $[Fe(PM\text{-}AzA)_2(NCS)_2]$ (sample 11), to 78 K for the abrupt SCO $[Fe(PM\text{-}BiA)_2(NCS)_2]$ (sample 20). Based on that a general relation between the T(LIESST) temperature and the cooperativity factor was proposed [123,124]. However it should be admitted that it is not so easy to properly disconnect the cooperativity factor from the effects of both local deformation (such as a twist of the FeN_6 core or an elongation of the Fe–N bond length) and change of the electronic distribution (modification of the aromatic unit) [125]. The X-ray structures of the thermodynamically stable states (LS and HS) and the metastable state (photoinduced HS) have really to be systematically solved. Unfortunately, up to now

only a few articles report a careful comparison of all these structures and it is not yet possible to obtain an overview of the effect of the cooperativity. Considering the influence of the cooperativity on the HS to LS relaxations, it is well known from the work of Hauser [99] that the activation energy barrier is a function of the HS (or LS) fraction because of an internal pressure created by the large modification of the metal–ligand bond lengths occurring between the HS and the LS states. As a consequence, the activation energy barrier for a given HS fraction is reduced when the cooperativity is increased, and thus, as recently demonstrated by doing some theoretical simulations, the T(LIESST) temperature is slightly reduced [126,127]. In fact, the influence of the cooperativity on the T(LIESST) temperature appears to be very weak. This conclusion is also supported by the experimental work performed on the $[Fe(bpp)_2]X_2 \cdot nH_2O$ family (samples 23–30) [116]. The photomagnetic property of these series was found to follow the same T_0 = 150 K line, whatever the cooperativity; i.e. from an incomplete spin conversion to a gradual or an abrupt spin transition without or with thermal hysteresis. All this indicated that the cooperativity factor is not the key factor for stabilizing the photo-induced HS state.

b) Influence of the electronic factor

Basically in a coordination sphere, the first important factor which has to be taken into account is the electronic contribution of the ligand. In this peculiar context, the work performed on the $[Fe(bpp)_2]X_2 \cdot nH_2O$ family (23–30) gives some interesting information. Goodwin et al. [119-122] showed that the thermal SCO properties of the $[Fe(bpp)_2]X_2 \cdot nH_2O$ series are strongly affected by the hydration degree, because the hydrated salts participated in an extended hydrogen-bonded network involving the uncoordinated NH groups of the pyrazole moieties, the anion and the water molecules. Consequently, any change of the hydration degree affects the electronics of the ligand and modifies the thermal spin crossover behaviour. Interestingly the photomagnetic properties of the hydrate and of the dehydrated compounds follow the same T_0 line, suggesting that the influence of the electronic factor on the T_0 factor is negligible [116]. This idea is also supported by the results found for the $[Fe(PM\text{-}L)_2(NCX)_2]$ family (samples 1–22), where for a given aromatic ligand (L) the T(LIESST) – $T_{1/2}$ values of thiocyanato (X = S) and selenocyanato (Se) compounds have been found to follow the same T_0 line, independently of the electronic modification accompanying the S/Se substitution [115].

c) Tuning the Fe(II)-ligand bond length

To investigate the influence of the Fe-ligand bond length, it was decided to study thermal and light-induced properties of SCO materials based on phosphorous ligand. For instance, in the peculiar case of $[Fe(dppen)_2Cl_2] \cdot 2(CH_3)_2CO$ compound, the single crystal structures have been determined in both HS and LS states. As expected the a Δr_{HL}(Fe–P) variation of 0.3 Å [128] has been formed, larger than the average Δr_{HL}(Fe–N) variation of 0.2 Å for FeN_6 coordination complexes [129-131]. Interestingly, the relaxation kinetics of the HS → LS conversion occurring after the LIESST effect was found to be slower than those for classical FeN_6 complexes. Thus the Fe(II) phosphorous complexes were expected to obey to a higher T_0 line. However, by examining the T(LIESST) and $T_{1/2}$ values of several iron(II)

phosphorous complexes (samples 34–39), it was realized that the T(LIESST) vs. $T_{1/2}$ data (Figure I. 1, samples 34–39) remained close to the T_0 = 100 K and 120 K lines and that the latitude to further increase the T_0 value by tuning the iron(II) ligand bond length appears not so large [117].

d) Distortion of the FeN_6 octahedron.

The attention has been then focused on the distortion of the FeN_6 octahedron [114]. Here also the determination of the structure is essential. However, by using the few X-ray data available on mononuclear iron(II) complexes of general formula $[FeL_2(NCS)_2]$, an exciting result has been obtained: i.e. the T(LIESST) value shows a linear correlation with the distortion of the metal environment sphere [114]. The stronger the distortion of the FeN_6 octahedron the higher T(LIESST). Such a result confirms the assumption that the T(LIESST) value is mainly dependent on the coordination sphere, not the cooperativity.

e) Role of the inner coordination sphere

Based on the comparison of the different T(LIESST) – $T_{1/2}$ values, Létard et al. [117] investigated chemical nature of the ligand involved in the inner coordination sphere. For this iron(II) complexes were arbitrarily separated between those involving six independent monodentate ligands (FeL_6 coordination sphere), those possessing three bidentate ligands (FeL_3), and those involving only two tridentate ligands (FeL_2). Interestingly, in each of the three cases (FeL_6, FeL_3 and FeL_2) the highest T(LIESST) values are found on a different T_0 line. More precisely, the highest T(LIESST) temperature of the FeL_6 complexes corresponds to the well-known $[Fe(ptz)_6](BF_4)_2$, situated close to the T_0 = 100 K line (sample 5), while for the FeL_3 systems it is the $[Fe(PM\text{- }BiA)_2(NCS)_2]$ complex (78 K, sample 20), situated on the T_0 = 120 K line, and for the FeL_2 compounds it is the $[Fe(bpp)_2](BF_4)_2$ complex at the T_0 = 150 K line (sample 29). Such a finding really supports the idea that the influence of the inner coordination sphere on the T_0 value is significant.

As a continuation of this approach, attempt was focused on Fe(II) macrocyclic spin crossover complexes. Two complexes have been reported for this attempt (Scheme I. 7). The first one is $[Fe(L_{222}N_3O_2)(CN)_2]\cdot H_2O$ (in which $L_{222}N_3O_2$ is a Schiff-base macrocyclic ligand derived from the condensation of 2,6-diacetylpyridine with 3,6-dioxaoctane-1,8-diamine) [132-138]. This complex has presented a atypical long-lived lifetime giving a T(LIESST) temperature of 132 K. The position of the T(LIESST) vs. $T_{1/2}$ point is in the vicinity of a virtual T_0 = 180 K line (Figure I. 1, sample 40), which is in perfect agreement with the proposed evolution of the nature of the coordination sphere. [117]. The second example concerns $[Fe(L_{222}N_5)(CN)_2]\cdot H_2O$ complex, which is an analogue to the $[Fe(L_{222}N_3O_2)(CN)_2]\cdot H_2O$ by the replacement of oxygen by nitrogen atoms. This example $[Fe(L_{222}N_5)(CN)_2]\cdot H_2O$ is found to be in LS state from 10 K until decomposition and the T(LIESST) value was estimated at 105 K [139], which evidenced an exceptional stability for the photoinduced HS state.

All these studies emphasize that the role of the inner coordination sphere. Moreover by

investigating Fe(II) macrocyclic SCO materials, the T(LIESST) values seem to obey to the T_0 = 180 K. It becomes consequently crucial to systematically investigate on the macrocyclic $[Fe(L_{222}N_3O_2)(CN)_2]\cdot H_2O$ and $[Fe(L_{222}N_5)(CN)_2]\cdot H_2O$ complexes, the influence of chemical modification on the stabilizing the metastable state.

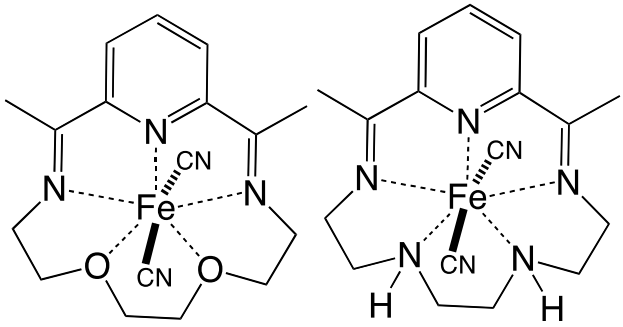

$[Fe(L_{222}N_3O_2)(CN)_2]$ $[Fe(L_{222}N_5)(CN)_2]$

Scheme I. 7: Complexes $[Fe(L_{222}N_3O_2)(CN)_2]$ and $[Fe(L_{222}N_5)(CN)_2]$

I.2.4. Chemical modification strategies of complex macrocyclic complexes

The selected parameters to study in this thesis are a) metal dilution, b) ligand flexibility, c) anionic group and d) solvent dependence.

a) Mn(II) metal dilution

In Part II, we will first report the structure of the pure $[Mn(L_{222}N_3O_2)(CN)_2]\cdot H_2O$ as well as the structures of diluted crystals. Then we will systematically investigate the transition behaviors of $[Fe_xMn_{1-x}(L_{222}N_3O_2)(CN)_2]\cdot H_2O$ in the form of polycrystalline powder. The purpose of this part is to study the influence of Mn(II) dilution on the properties of $[Fe(L_{222}N_3O_2)(CN)_2]\cdot H_2O$ complex.

b) Modification of macrocyclic ligand

In Part III, we will describe the synthesis, characterization and properties of several macrocyclic complexes where the amine unit has been modified in order to change the flexibility of the ligand. A family of compounds $[Fe(L_{xyz}N_5)(CN)_2]\cdot nH_2O$ with x,y,z = 2, 3, 2; 3, 2, 3 or 2, 2, 3 will be reported. Their magnetic and photomagnetic properties will be investigated and a comparison with the previously described $[Fe(L_{222}N_5)(CN)_2]\cdot H_2O$ will be done.

c) Modification of anionic ligands

In Part IV, thiocyanate and selenocyanate coordinated macrocyclic complexes will be studied, in order to investigate the similarity, or not, with cyano group coordinated

$[Fe(L_{222}N_3O_2)(CN)_2]\cdot H_2O$ complex, where change of coordination and spin crossover have been evidenced. Structural investigation will be reported at different temperature and new examples of change of coordination in Fe(II) macrocyclic SCO complex will be discussed.

d) Solvent dependence

In Part V, we will study the influence of solvent modification on metastable HS state of $[FeL_{222}N_3O_2(CN)_2]\cdot nX$ (X= $CHCl_3$ and H_2O). Firstly, the structure of $[FeL_{222}N_3O_2(CN)_2]\cdot 2CHCl_3$ will be introduced. Then powder XRD studies as well as magnetic and photomagnetic properties of dehydration and rehydration of $[FeL_{222}N_3O_2(CN)_2]\cdot H_2O$ will be presented.

References

1 O. Kahn, C. J. Martinez, *Science* **1998**, *279*, 44.

2 C. Joachim, J. K. Gimzewski, A. Aviram, *Nature* **2000**, *408*, 541.

3 J. K. Gimzewski, C. Joachim, *Science* **1999**, *283*, 1683.

4 Spin Crossover in Transition Metal Compounds, in Topics in Current Chemistry, ed. P. Gütlich and H. A. Goodwin, Springer-Verlag, Berlin– Heidelberg–New York, **2004**, vol. I, II and III.

5 L. Cambi, L. Szegö, *Ber. Deutsch. Chem. Gesell.* **1931**, *10*, 2591.

6 H. A Goodwin, *Top. Curr. Chem.* **2004**, *234*, 23.

7 Y. Garcia, P. Gütlich, *Top. Curr. Chem.* **2004**, 234, 49.

8 H. Toftlund, *Coord. Chem. Rev.* **1989**, *94*, 67.

9 P. Gütlich, *Structure and Bonding, Vol. 44*, Springer-Verlag, Berlin, **1981**, pp. 83-196.

10 L. Cambi, L. Szegö, *Bericht. d. D. Chem. Gesell.* **1933**, *66*, 656.

11 A. H. Ewald, R. L. Martin, I. G. Ross, A. H. White, *proc. Roy. Soc. A.* **1964**, *280*, 235.

12 R. C. Stouter, D. W. Smith, E. A. Cleavenger, T. E. Norris, *Inorg. Chem.* **1966**, *5*, 1167.

13 W. Kläui, *J. Chem. Soc. Chem. Comm.* **1979**, 700.

14 J. H. Ammeter, R. Bucher, N. Oswald, *J. Am. Chem. Soc.* **1974**, *96*, 7883.

15 P. G. Sim, E. Sinn, *J. Am. Chem. Soc.* **1981**, *103*, 241.

16 P. Gütlich, A. Hauser, H. Spiering, *Angew. Chem. Int. Ed. Engl.* **1994**, *33*, 2024.

17 W. A. Baker, H. M. Bobonich, *Inorg. Chem.* **1964**, *3*, 1184.

18 E. König, K. Madeja, *Inorg. Chem.* **1967**, *6*, 48.

19 J.-F. Létard, P. Guionneau, L. Rabardel, J. A. K. Howard, A. Goeta, D. Chasseau, O. Kahn, *Inorg. Chem.* **1998**, *37*, 4432.

20 K. H. Sugiyarto, D. C. Craig, A. D. Rae, H. A. Goodwin, *Aust. J. Chem.* **1994**, *47*, 869.

21 K. H. Sugiyarto, M. L. Scudder, D. C. Craig, H. A. Goodwin, *Aust.J. Chem.* **2000**, *53*, 755.

22 E. König, G. Ritter, *Sol. State. Comm.* **1976**, *18*, 279.

23 J.-F. Létard, P. Guionneau, E. Codjovi, O. Lavastre, G. Bravic, D. Chasseau, O. Kahn, *J. Am. Chem. Soc.* **1997**, *119*, 10861.

24 J. G. Haasnoot, G. Vos, W. L. Groeneveld, *Z. Naturforsch.* **1977**, *32b*, 1421.

25 L. G. Lavrenova, V. N. Ikorskii, V. A. Varnek, I. M. Oglezneva, S. V. Larionov, *Koord. Khim.* **1986**, *12*, 207.

26 L. G. Lavrenova, V. N. Ikorskii, V. A. Varnek, I. M. Oglezneva, S. V. Larionov, *Koord. Khim.* **1990**, *16***,** 654.

27 E. Codjovi, L. Sommier, O. Kahn, C. Jay, *New. J. Chem.* **1996**, *20***,** 503.

28 W. Vreugdenhil, J. H. van Diemen, R.A-G de Graaff, J. G. Haasnoot, J. Reedijk, A. M. van der Kraan, O. Kahn, J. Zarembowitch, *Polyhedron.* **1990**, *9*, 2971.

29 J. Zarembowitch, O. Kahn, *New J. Chem.* **1991**, *15***,** 181.

30 O. Kahn, J. Kröber, C. Jay, *Adv. Mater.* **1992**, *4*, 178.

31 O. Kahn, E. Codjovi, *Phil. Trans. R. Soc. London A.* **1996**, *354*, 359.

32 V. V. Zelentsov, *Sov. Sci. Rev B. Chem.* **1981**, *81***,** 543.

33 G. S. Matouzenko, J.-F. Létard, S. Lecocq, A. Bousseksou, L. Capes, L. Salmon, M. Perrin, O. Kahn, E. Collet, *Eur. J. Inorg. Chem.* **2001**, 2935.

34 J. A. Real, H. Bolvin, A. Bousseksou, A. Dworkin, O. Kahn, F. Varret, J. Zarembowitch, *J. Am. Chem. Soc.* **1992**, *114***,** 4650.

35 J. A. Real, B. Gallois, T. Granier, F. Suezpanama, J. Zarembowitch, *Inorg. Chem.* **1992**, *31*, 4972.

36 V. Ksenofontov, A. B. Gaspar, V. Niel, S. Reiman, J. A. Real, P. Gütlich, *Chem.Eur. J.* **2004**, *10*, 1291.

37 H. Köppen, E.W. Müler, C. P. Köhler, H. Spiering, E. Meissner, P. Gütlich, *Chem. Phys. Lett.* **1982**, *91*, 348.

38 R. Jakobi, H. Spiering, P. Gütlich, *J. Phys. Chem. Solids.* **1992**, *53*, 267.

39 H. Romstedt, A. Hauser, H. Spiering, *J. Phys. Chem. Solids.* **1998**, *59*, 265.

40 A. Bousseksou, H. C. Machado, F. Varret, *J. Phys. I France.* **1995,** *5*,747.

41 V. Ksenofontov, G. Levchenko, H. Spiering, P. Gütlich, J.-F. Létard, Y. Bouhedja, O. Kahn, *Chem. Phys. Lett.* **1998**,*294*, 545.

42 V. Ksenofontov, A. B. Gaspar, P. Gütlich, *Top. Curr. Chem.* **2004**, *235*, 23.

43 L. F. Lindoy, S. E. Livingstone, *Coord. Chem. Rev.* **1967**, *2*,173.

44 M. Sorai, S. Seki, *J. Phys. Chem. Solids.* **1974**, *35*, 555.

45 K. Boukheddaden, I. Shteto, B. Hôo, F. Varret, *Phys. Rev B.* **2000**, *62*, 14796.

46 J. P. Tuchagues, A. Bousseksou, G. Molnar, J. J. McGarvey, F. Varret, *Top. Curr. Chem.* **2004**, *235*, 85.

47 C. Baldé, PhD Thesis, Université Bordeaux I, 2008.

48 A. H. Ewald, R. L. Martin, E. Sinn, A. H. White, *Inorg. Chem.* **1969**, *8*, 1837.

49 H. Spiering, E. Meissner, H. Köppen, E.W. Müller, P. Gütlich, *J. Chem. Phys.* **1982**, *68,* 65.

50 E. Meissner, H. Köppen, H. Spiering, P. Gütlich, *Chem. Phys. Lett.* **1983**, *95*, 163.

51 P. Adler, L. Wiehl, E. Meissner, C. P. Köhler, H. Spiering, P. Gütlich, *J. Phys. Chem. Solids.* **1987**, *48*, 517.

52 C. P. Köhler, R. Jakobi, E. Meisner, L. Wiehl, H. Spiering, P. Gütlich, *J. Phys. Chem. Solids.* **1990**, *51*, 239.

53 J. Gaultier, T. Granier, B. Gallois, J. A. Real, J. Zarembowitch, *Hight. Press. Res.* **1991**, *7*, 336.

54 T. Granier, B. Gallois, J. Gaultier, J. A. Real, J. Zarembowitch, *Inorg.Chem.* **1993**, *32*, 5305.

55 P. Guionneau, C. Brigouleix, Y. Barrans, A. Goeta, J.-F. Létard, J. A. K. Howard, J. Gaultier, D. Chasseau, *C. R. Acad. Sci. Series II. C.* **2001**, *4*, 161.

56 A. Hauser, J. Jeftic, H. Romstedt, R. Hinek, *Mol. Cryst. Liq.Cryst.* **1996**, *286*, 217.

57 E. Codjovi, N. Menendez, J. Jeftic, F. Varret, *C. R. Acad. Sci. Chim.* **2001**, *4*, 181.

58 P. Adler, H. Spiering, P. Gütlich, *J. Phys. Chem. Solids.* **1989**, *50*, 587.

59 Y. Garcia, V. Ksenofontov, G. Levchenko, G. Schimtt, P. Gütlich, *J. Phys. Chem.* **2000**, *B104*, 5045.

60 Y. Garcia, V. Ksenofontov, P. Gütlich, *C. R. Acad. Sci. Series. C* **2001**, *4,* 227.

61 G. G. Levchenko, V. Ksenofontof, A. V. Stupakov, H. Spiering, Y. Garcia, P. Gütlich, *Chem. Phys.* **2002**, *277*, 125.

62 H. Spiering, K. Boukheddaden, J. Linares, F. Varret, *Phys. Rev. B.* **2004**, *70*, 184106.

63 F. Legac, PhD Thesis, Université Bordeaux 1, **2008**.

64 P. Gütlich, Y. Garcia, T. Woike, *Coord. Chem. Rev.* **2001**, *219*, 839.

65 Z. Z. Gu, O. Sato, T. Iyoda, K. Hashimoto, A. Fujishima, *J. Phys. Chem.* **1996**, *100*, 18289.

66 Z. Z. Gu, O. Sato, T. Iyoda, K. Hashimoto, A. Fujishima, *J. Chem.Mater.* **1997**, *9*, 1092.

67 J. Tritt-Goc, N. Pislewski, S. K. Hoffmann, *Chem. Phys. Lett.* **1997**, *268*, 471.

68 M. Verdaguer, *Science.* **1996**, *272*, 698.

69 O. Sato, T. Iyoda, A. Fujishima, K. Hashimoto, *Science.* **1996**, *272*, 704.

70 N. Shimamoto, S. S. Ohkoshi, O. Sato, K. Hashimoto, *Chem Lett.* **2002**, *31*, 486.

71 N. Shimamoto, S. S. Ohkoshi, O. Sato, K. Hashimoto, *Inorg. Chem.* **2002**, *41*, 678.

72 A. Bleuzen, V. Escax, A. Ferrier, F. Villain, M. Verdaguer, P. Münsch, J. P. Itié, *Angew. Chem. Int. Ed.* **2004**, *43*, 3728.

73 A. Bleuzen, V. Escax, J. P. Itié, P. Münsch, Verdaguer M, *C. R. Chimie.* **2003**, *6*, 343.

74 J. S. Kolb, M. D. Thomson, M. Novosel, K. Sénéchal-David, E. Riviére, M. L. Boillot, H. G. Roskos, *C. R. Chimie.* **2007**, *10*, 125.

75 M. L. Boillot, C. Roux, J. Zarembowitch, A. Sour, *Top. Curr. Chem.* **2004**, *234*, 261.

76 J. Zarembowitch, C. Roux, *Brevet Français 9205928*, **1992**.

77 D. M. Adams, A. Dei, A. L. Rheingold, D. N. Hendrickson, *J. Am. Chem. Soc.* **1993**, *115*, 8221.

78 D. M. Adams, B. Li, J. D. Simon, D. N. Hendrickson, *Angew. Chem.Int. Ed. Engl.* **1995**, *34*, 1481.

79 D. M. Adams, D. N. Hendrickson, *J. Am. Chem. Soc.* **1996**, *118*, 11515.

80 D. M. Adams, L. Noodleman, D. N. Hendrickson, *Inorg. Chem.* **1997**, *36*, 3966.

81 R. M. Buchanan, C. G. Pierpont, *J. Am. Chem. Soc.* **1980**, *102*, 4951.

82 F. Varret, M. Nogues, A. Goujon, in: J.S. Miller, M. Drillon (Eds.), Magnetism: Molecules to Materials, Wiley-VCH. **2001**, 257.

83 O. Sato, S. Hayami, Z.-Z. Gu, K. Seki, R. Nakajima, A. Fujishima, *Chem. Lett.* **2001**, 874.

84 O. Sato, S. Hayami, Z.-Z. Gu, K. Takahashi, R. Nakajima, A. Fujishima, *Phase Transitions.* **2003**, *75*, 779.

85 O. Sato, *J. Photochem. Photobiol. C. Photo. Chem. Rev.* **2004**, *5*, 203.

86 K. Matsuda, M. Irie, *J. Am. Chem. Soc.* **2000**, *122*, 7195.

87 K. Matsuda, M. Irie, *Chem. Eur. J.* **2001**, *7*, 3466.

88 K. Matsuda, M. Irie, *J. Am. Chem. Soc.* **2001**, *123*, 9896.

89 K. Matsuda, M. Matsuo, S. Mizoguti, K. Higashiguchi, M. Irie, *J.Phys. Chem. B.* **2002**, *106*, 11218.

90 K. Matsuda, K. Takayama, M. Irie, *Inorg. Chem.* **2004**, *43*, 482.

91 B. L. Feringa, R. A. van Delden, N. Koumura, E. M. Geerstsema, *Chem. Rev.* **2000**, *100*, 1789.

92 M. Irie, T. Fukaminato, T. Sasaki, T. Tamai, T. Kawai, *Nature.* **2002**, *420*, 759.

93 F. Renz, H. Spiering, H. A. Goodwin, P. Gütlich, *Hyperfine Interact.* **2000**, *126*, 155.

94 S. Bonhommeau, G. Molnár, A. Galet, A. Zwick, J. A. Real, J. J. McGarvey, A. Bousseksou, *Angew. Chem., Int. Ed.* **2005**, *44*, 4069.

95 S. Bonhommeau, N. Bréfuel, V. K. Pálfi, G. Molnár, A. Zwick, L. Salmon, J. P. Tuchagues, J. S. Costa, J.-F. Létard, H. Paulsen, A. Bousseksou, *Phys. Chem. Chem. Phys.* **2005**, *7*, 2909.

96 S. Decurtins, P. Gütlich, C. P. Köhler, H. Spiering, A. Hauser, *Chem. Phys. Lett.* **1984**, *105*,1.

97 S. Decurtins, P. Gütlich, K. M. Hasselbach, A. Hauser, H. Spiering, *Inorg. Chem.* **1985**, *24*, 2174.

98 A. Hauser, P. Gütlich, H. Spiering, *Inorg. Chem.* **1986**, *25*, 4245.

99 A. Hauser, *Top. Curr. Chem*. **2004**, *234*, 155.

100 G. Ritter. E. König. W. Irler, H. A. Goodwin. *Inorg. Chem*. **1978**,*17*.224

101 H. A. Goodwin, K. H. Sugiyarto, Chent. *Phys. Lett.* **1987**.*139*,470.

102 T. Buchen, P. Gütlich, H. A. Goodwin, *Inorg. Chem.* **1994**.*33*, 4573.

103 S. Hayami, Z.-Z. Gu, M. Shiro, Y. Einaga, A. Fujishima and O. Sato, *J. Am. Chem. Soc*., **2000**, *122*, 7126.

104 G. Juhász, S. Hayami, O. Sato and Y. Maeda, *Chem. Phys. Lett*., **2002**, *364*, 164.

105 S. Hayami, K. Hiki, T. Kawahara, Y. Maeda, D. Urakami, K. Inoue, M. Ohama, S. Kawata and O. Sato, *Chem.–Eur. J.*, **2009**, *15*, 3497.

106 M. Clemente-León, E. Coronado, M. López-Jordà, C. Desplanches, S. Asthana, H. Wang, J.-F. Létard, *Chem. Sci.*, **2011**, *2*, 1121.

107 J. J. McGarvey, I. Lawthers, *J. Chem. Soc., Chem. Comm.* **1982**, 906.

108 R. H. Herber, L. M. Casson, *Inorg. Chem.* **1986**, 25, 847.

109 A. Hauser, A. Vef, P. Adler, *J. Chem. Phys.* **1991**, 95, 8710.

110 J.-F. Létard, P. Guionneau, L. Rabardel, J.A.K. Howard, A.E. Goeta, D. Chasseau, O. Kahn, *Inorg. Chem.* **1998**, *37*, 4432.

111 A. Hauser, *Coord. Chem. Rev.* **1991**, *111*, 275.

112 A. Hauser, *Comments Inorg. Chem.* **1995**, *17*, 17.

113 A. Hauser, C. Enaschescu, M.L. Daku, A. Vargas, N. Amstutz, *Coord. Chem. Rev.* **2006**, *250*, 1642.

114 M. Marchivie, P.Guionneau, J.-F. Létard, D. Chasseau, *Acta Crystallogr., Sect. B: Struct. Sci.* **2005**, *61*, 25.

115 J.-F. Létard, L. Capes, G. Chastanet, N. Moliner, S. Létard, J. A. Real, O. Kahn, *Chem. Phys. Lett.* **1999**, *313*, 115.

116 S. Marcén, L. Lecren, L. Capes, H. A. Goodwin, J.-F. Létard, *Chem. Phys. Lett.* **2002**, *358*, 87.

117 J.-F. Létard, P. Guionneau, O. Nguyen, J. S. Costa, S. Marcén, G. Chastanet, M. Marchivie, L. Goux-Capes, *Chem. Eur. J.* **2005**, *11*, 4582.

118 J.-F. Létard, *J. Mater. Chem.* **2006**, *16*, 2550.

119 K. H. Sugiyarto, H. A. Goodwin, *Aust. J. Chem.* **1988**, *41*, 1645.

120 K. H. Sugiyarto, D. C. Craig, A. D. Rae, H. A. Goodwin, *Aust. J. Chem.* **1994**, *47*, 869.

121 K. H. Sugiyarto, K. Weitzner, D. C. Craig, H. A. Goodwin, *Aust. J. Chem.* **1997**, *50*, 869.

122 K. H. Sugiyarto, M. L. Scuddler, D. C. Criag, H. A. Goodwin, *Aust. J. Chem.* **2000**, *53*, 755.

123 L. Capes, J.-F. Létard, O. Kahn, *Chem.Eur.J.* **2000**, *6*, 2246.

124 S. Hayami, Z.-Z. Gu, M. Shiro, Y. Einaga, A. Fujishima, O. Sato, *J. Am. Chem. Soc.*, **2000**, *122*, 7126.

125 P. Guionneau, M. Marchivie, G. Bravic, J.-F. Létard and D. Chasseau, Structural aspects of spin crossover, in Spin Crossover in Transition Metal Compounds, ed. P. Gütlich, H. A. Goodwin, Topics in Current Chemistry, Springer, Wien and New York **2004**, vol. 234, p. 97.

126 J.-F. Létard, G. Chastanet, O. Nguyen, S. Marcen, M. Marchivie, P. Guionneau, D. Chasseau, P. Gütlich, *Monatsh. Chem.*, **2003**, 134, 165

127 J.-F. Létard G. Chastanet, O. Nguyen, S. Marcén, M. Marchivie, P. Guionneau, D. Chasseau, P. Gütlich Molecular *Magnets Recents Highlights*, ed. W. Linert, M. Verdaguer, Springer, Wien and New York, **2003**, p. 49.

128 F. Cecconi, M. Di Vaira, S. Midollini, A. Orlandini, L. Sacconi, *Inorg. Chem*. **1981**, *20*, 3423.

129 A.G. Orpen, L. Brammer, H.A. Frank, O. Kennard, D.G. Watson, R. Taylor, *J. Chem. Soc. Dalton Trans., Suppl.* **1989**, *171*, S1.

130 H. Montgomery, R.V. Chastain, J.J. Natt, A.M. Witowsak, E. Lingfelter, *Acta Cryst.* **1967,** *22*, 775.

131 S. Dick, *Zeitschrift für Kristallographie – New Crystal Structures***1998**, *213*, 356.

132 S. M. Nelson, P. D. A. Mcllroy, C. S. Stevenson, E. König, G. Ritter, J. Waigel, *J. Chem. Soc. Dalton Trans.* **1986**, 991

133 E. König, G. Ritter, J. Dengler, S. M. Nelson *Inorg. Chem.* **1987**, *26*, 3582.

134 S. Hayami, Z. Gu, Y. Einaga, Y. Kobayasi, Y. Ishikawa, Y. Yamada, A. Fujishima, O. Sato, *Inorg. Chem.* **2001**, *40*, 3240.

135 H. Liu, A. Fujishima, O. Sato, *Appl. Phys. Lett.* **2004**, *85*, 2295.

136 P. Guionneau, J. S. Costa, J.-F. Létard, *Acta Cryst.* **2004**, *C60*, m587

137 P. Guionneau, F. Le Gac, A. Kaiba, J. S. Costa, D. Chasseau, J.-F. Létard, *Chem. Commun*. **2007**, *36*, 3723

138 J. S. Costa, P. Guionneau, J.-F. Létard, *J. Phys.: Conf. Ser.* **2005**, *21*, 67.

139 J. S. Costa, C. Baldé, C. Carbonera, D. Denux, A. Wattiaux, C. Desplanches, J.-P. Ader, P. Gütlich, J.-F. Létard, *Inorg. Chem.* **2007**, *46*, 4114

Part II. Metal dilution of $[Fe_xMn_{1-x}(L_{222}N_3O_2)(CN)_2]\cdot H_2O$ series

Chapter II.1. Introduction of metal dilution method

II.1.1. Influence of metal dilution on thermal spin crossover

The influence of dilution on the thermal SCO properties of molecular materials has been extensively studied [1-23]. Most of those studies have been carried out on Fe(III) and Fe(II) complexes. In 1980, Haddad and Hendrickson have focused on complexes of Fe(III) especially in the isomorphous metal diluted series $[Fe_xM_{1-x}(3\text{-}OCH_3\text{-}SalEen)_2]PF_6$ and $[Fe_xM_{1-x}(SalEen)_2]PF_6$, with SalEen = schiff base and M = Cr(III), Co(III) [1-3]. Regarding the metal dilution of Fe(II) SCO complexes, Gütlich investigated in particular three families: the family $[Fe_xM_{1-x}(phen)_2(NCS)_2]$ (phen = 1,10-phenanthroline and M = Co(II), Mn(II), Ni(II), Zn(II)) [4-7], the family $[Fe_xM_{1-x}(2\text{-}pic)_3]Cl_2\cdot Sol$ (2-pic = 2-picolylamine, Sol = EtOH, MeOH and M = Co(II), Mn(II), Zn(II)) [3,4,8-17] and the $[Fe_xM_{1-x}(btr)_2(NCS)_2]\cdot H_2O$ (btr = 4,4'-bis(1,2,4-triazole) and M = Co, Ni) [18-23].

To illustrate the effects of the metal dilution on the thermal SCO properties, let us consider the well known $[Fe(phen)_2(NCS)_2]$ complex which exhibits an abrupt transition at around 176 K with a hysteresis loop of a few kelvins. Gütlich et al. [6] have evidenced that metal dilution induced a shift of the transition depending on the size of the guest metal.

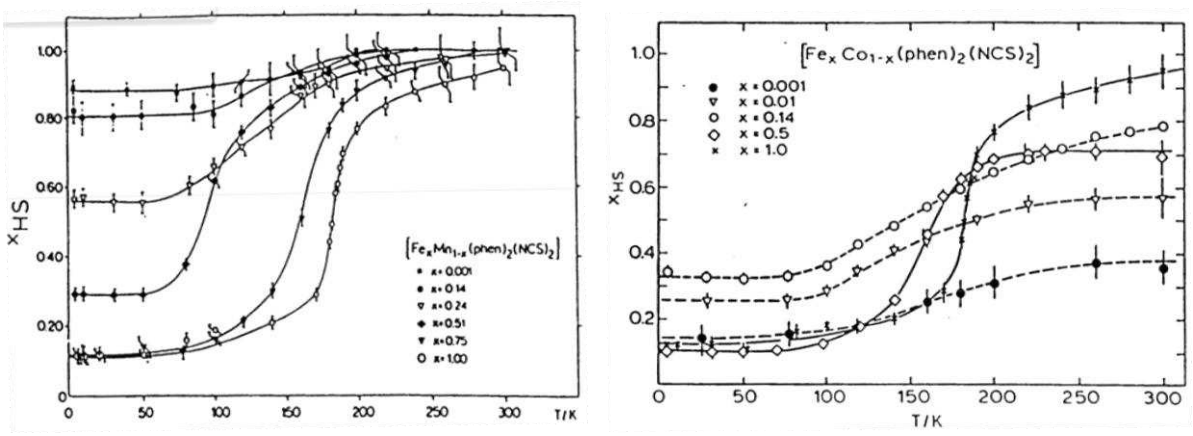

Figure II. 1: HS fraction as a function of temperature for the mixed compounds. Left: $[Fe_xMn_{1-x}(phen)_2(NCS)_2]$, Right: $[Fe_xCo_{1-x}(phen)_2(NCS)_2]$.[6]

a) When the size of the dilution metal is larger than Fe(II) ion (for example Mn (II) ion) the transition temperature $T_{1/2}$ is shifted towards low temperature and transition becomes more gradual with an increase of the HS residual fraction at low temperature (Figure II. 1left) [6].

b) When the size of the host ion is close to, or smaller than Fe(II) ion (for example Co(II) ion), the transition temperature $T_{1/2}$ remains almost constant, or even shifts towards higher temperature. It can be also noticed that the SCO behavior becomes more gradual with the increase of the metal dilution and a slight LS residual at high temperature can be observed.

(Figure II. 1ight) [6]. The decrease of the cooperativity with the metal dilution was attributed to the decrease of the interactions between Fe(II) centers [6].

II.1.2. Influence of metal dilution on the stability of the photo-induced HS state

The influence of the metal dilution on the stability of the photo-induced state was particularly studied by Hauser et al. [24-26]. Figure II. 2 shows the variation of the relaxation constant k_{HL} as a function of the reciprocal temperature for the series $[Fe_xM_{1-x}(bpy)_3](PF_6)_2]$ (bpy = 2,2 '-bipyridine and M = Co(II), Zn(II), Mn(II), Cd(II)) [24-26].

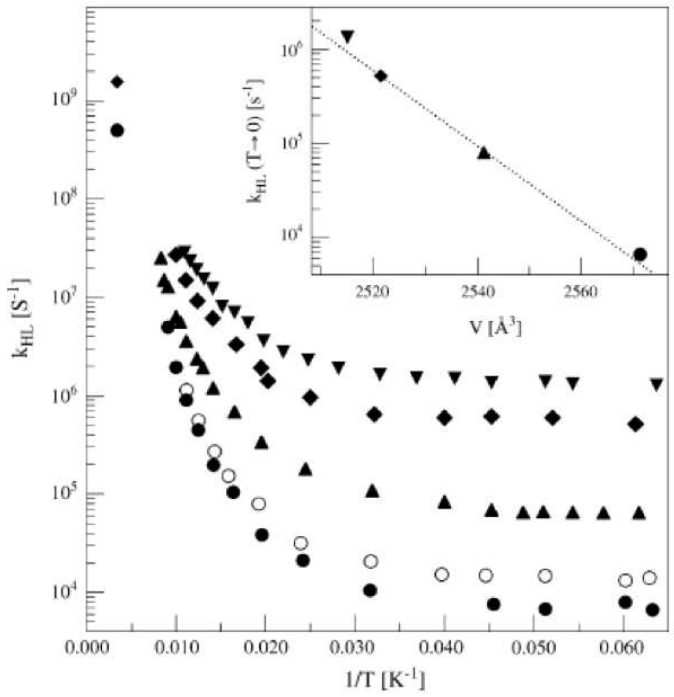

Figure II. 2: Evolution of the relaxation constant, k_{HL}, as a function of 1/T for the mixed series $[Fe_xM_{1-x}(bpy)_3](PF_6)_2]$, M = Co (▼), Zn (♦), Mn (▲) and Cd (●) at atmospheric pressure and Cd (○) at 1 kbar pressure. Insert: evolution of the relaxation constant of the tunneling effect, k_{HL} (T→0), as a function of the of the unit cell volume [24].

Hauser et al. [24-26] estimated the relaxation constant in the tunneling region, $k_{HL}(T\rightarrow 0)$, in a large number of complexes. This author demonstrated that at room temperature the value of the relaxation constant of metal diluted compounds is close to that observed in solution (10^6 to 10^8 s^{-1}) and does not depend too much of the metal ion used for dilution. On the contrary, at low temperature the relaxation constant depends strongly on the nature of metal ion. Indeed, k_{HL} varies from 6×10^3 s^{-1} (τ = 160 μs) for metal diluted with M = Cd(II) (the largest metal ion) to 1.6×10^6 s^{-1} (τ = 650 ns) for M = Co(II) (the smallest metal ion) [24]. The relaxation constant was found to be multiplied by a factor ca. 300, when the volume of the unit cell decreases. The author attributes this effect to the pressure (positive or negative) associated by the insertion of metal ions (of larger or smaller volume, Figure II. 3). Metal dilution with volume smaller than the Fe (II) destabilizes the HS state by creating a "negative pressure" [25] while the incorporation of ions with larger volume than Fe(II) creates positive pressure on the system and stabilize the HS state. This pressure is estimated at about 8 kbar for Cd(II) [26].

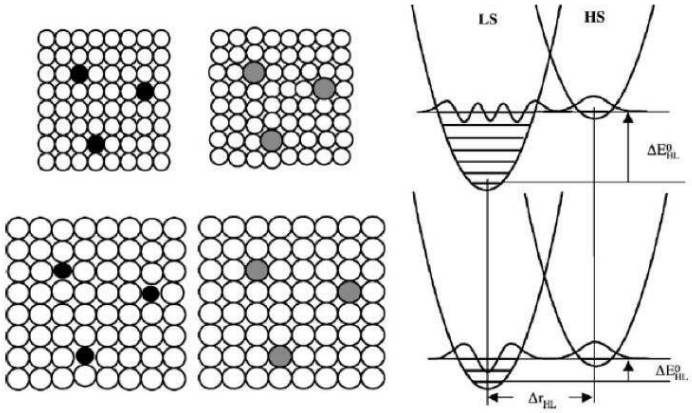

Figure II. 3: Evolution of the potential well of metal diluted complexes of Fe (II): influence of internal pressure [25].

In fact, the dilution leads to a vertical displacement of the potential well (Figure II. 3). It means a change of ΔE^0_{HL}, and thus $T_{1/2}$ according to Eq.1.

$$\Delta E^0_{HL} \approx \Delta H^0_{HL} = T_{1/2}\Delta S^0_{HL} \qquad \text{(Eq.1)}$$

II.1.3. Influence of metal dilution on T(LIESST) / $T_{1/2}$ relation

Later on, the influence of the metal dilution on T(LIESST) values were investigated on several dilution series, such as $[Fe_xZn_{1-x}(phen)_2(NCS)_2]$ [27,28], $[Fe_xMn_{1-x}(bpp)_2](NCSe)_2$ [29], $[Fe_xZn_{1-x}(btzp)_3](BF_4)_2$ and $[Fe_xZn_{1-x}(endi)_3](BF_4)_2$ (bpp = 2,6-bis(pyrazol-3-yl)pyridine, btzp = 1,2-Bis(tetrazol-1-yl)propane and endi = 1,2-Bis(tetrazol-1- yl)ethane) [30].

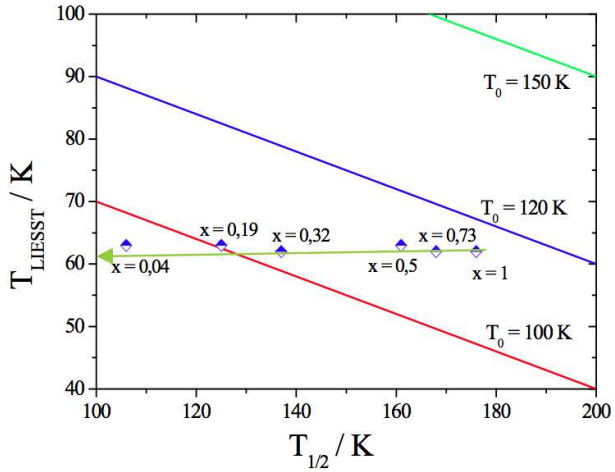

Figure II. 4: Evolution of T(LIESST) as a function of $T_{1/2}$ for the metal diluted $[Fe_xZn_{1-x}(phen)_2(NCS)_2]$ [31]

For the metal diluted $[Fe_xZn_{1-x}(phen)_2(NCS)_2]$ series, the various results evidenced that the values of T(LIESST) remain constant for the whole series of complexes (form x = 0.73 to 0.04), while the values of $T_{1/2}$ decrease continuously with the dilution [27,28] (Figure II. 4). Similar phenomenon was also observed for the $[Fe_xMn_{1-x}(bpp)_2](NCSe)_2$ series (Figure II. 5), where the T(LIESST) remains constant (around 85 K), while $T_{1/2}$ decreases with Mn(II) metal dilution. Based on these studies, Létard et al. [27,28] proposed that photo-induced HS properties are strongly correlated to the molecular properties while the thermal SCO regime depends on thermodynamical region.

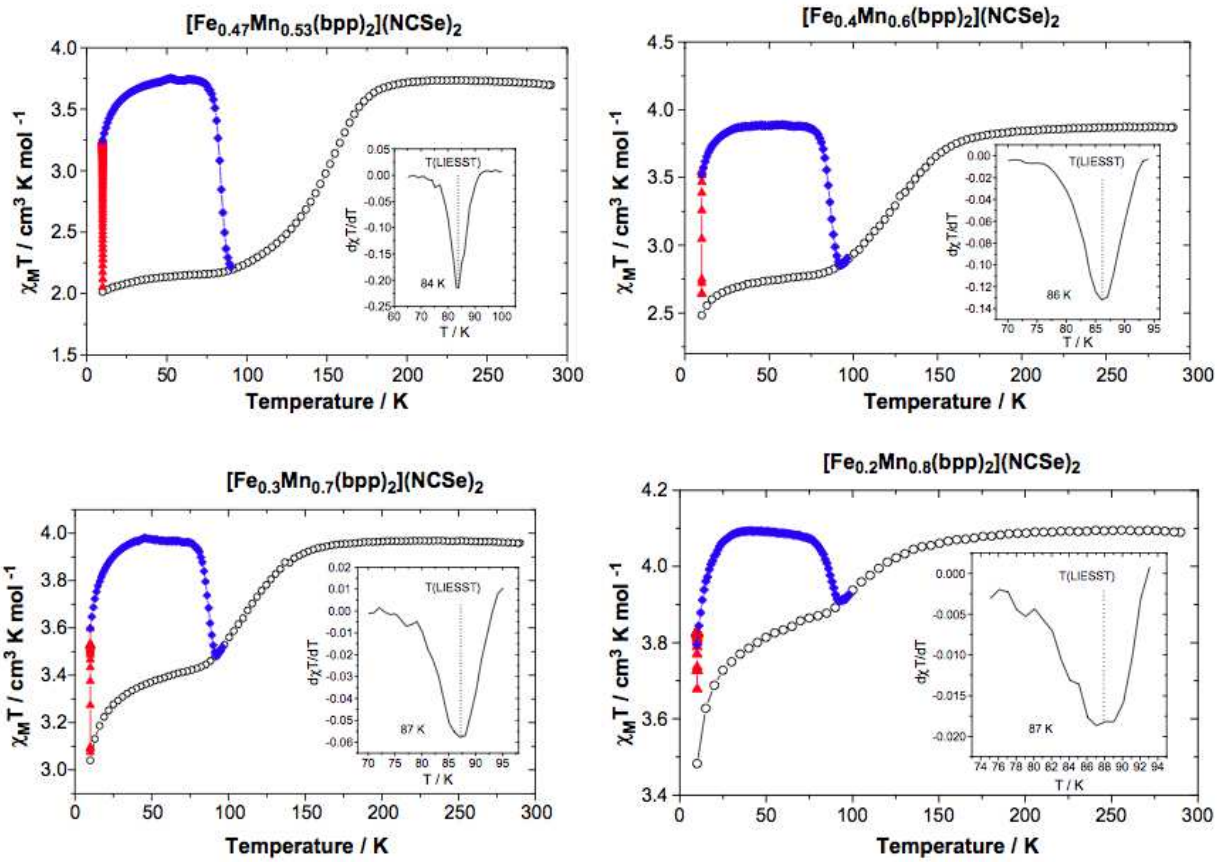

Figure II. 5: emperature dependence of $\chi_M T$ for $[Fe_xMn_{1-x}(bpp)_2](NCSe)_2$ [29] during LIESST experiment.

II.1.4. When T(LIESST) reaches $T_{1/2}$

Following the idea that by using metal dilution, the $T_{1/2}$ can be lowered without affecting the T(LIESST) value, a series of metal diluted SCO materials $[Fe_xMn_{1-x}(bpp)_2](BF_4)_2$ [32] was rationally designed. The ultimate goal was to reach the peculiar situation where the high temperature stable HS phase overlaps with and the low temperature metastable HS state. A phase diagram was established based on the systematic investigation of the thermal SCO properties and the metastability occurring at low temperature generated either by light (LIESST) effect or either by a rapid frozen effect (TIESST effect) (Figure II. 6). It was demonstrated that the overlap between two regimes occurs at $x \leq 0.96$.

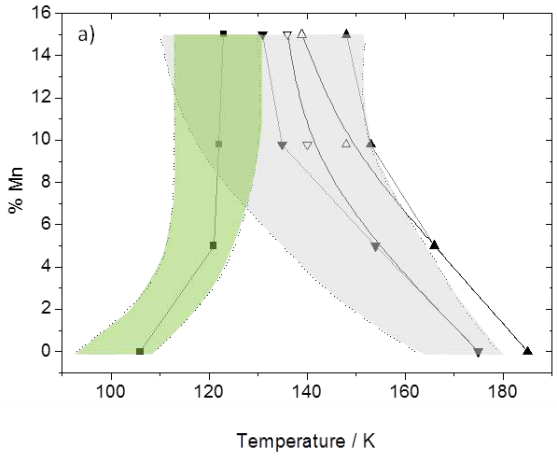

Figure II. 6: Phase diagram of the $[Fe_xMn_{1-x}(bpp)_2](BF_4)_2$ series reporting the region (in gray) delimiting 5-95 % of the thermal SCO phenomenon on the cooling branch. The green zone stands for the region delimiting 95-5% of the relaxation associated to the T(TIESST) curve. The symbols ▲ and ▼ correspond respectively to the $T_{1/2}$ in the warming and cooling mode measured at a rate of 0.4 K/mn while Δ and ∇ stand for the stationary limit. (■) represents the T(TIESST) values.

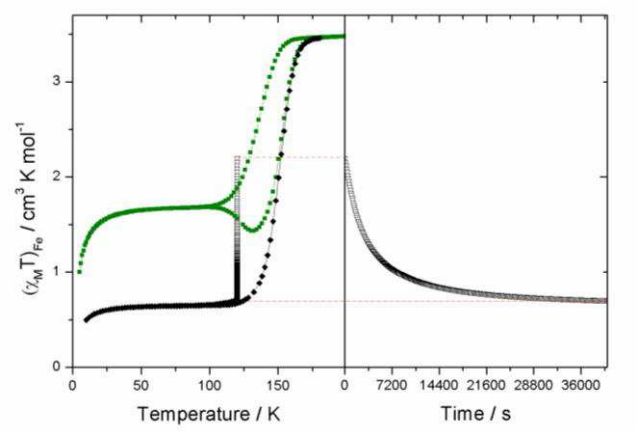

Figure II. 7: Relaxation of the Thermally-Induced Excited Spin-State in **3** (∇) and the following thermal spin-crossover (●).

As a typical example, Figure II. 7 presents the peculiar case of $[Fe_xMn_{1-x}(bpp)_2](BF_4)_2$ with x = 0.9. In this complex, only 50 % of the Fe(II) ions are involved in the thermal spin transition (Figure II. 7). It was demonstrated that by investigating the kinetic during 10 hours at 120 K, the magnetic response reaches a stationary $(\chi_M T)_{Fe}$ value of 0.62 cm^3 K mol^{-1} which does not change upon further relaxation time, which indicate that 83 % of the Fe(II) centers exhibit the SCO process. This type of experiment was performed at several temperatures and the authors conclude that when the T(LIESST) regime starts to reach $T_{1/2}$, the SCO process is strongly affected by the kinetic.

II.1.5. Objective of Part II.

The main purpose of this part is to investigate the influence of Mn(II) metal dilution on the coordination properties of $[Fe(L_{222}N_3O_2)(CN)_2]\cdot H_2O$ complex. Inspired by those recent results, we have decided to elaborate a series of metal diluted $[Fe_xMn_{1-x}]$ complexes, in which

the lattice contains increasing proportion of $\{(1-x)[Mn(L_{222}N_3O_2)(CN)_2]\cdot H_2O\}/\{x[Fe(L_{222}N_3O_2)(CN)_2]\cdot H_2O\}$. We expect that by varying the Mn(II)/Fe(II) ratio, SCO properties will be affected.

We will first briefly report the various works already published on $[Fe(L_{222}N_3O_2)(CN)_2]\cdot H_2O$. Then, we will present our contributions beginning with the report of the structure for the pure $[Mn(L_{222}N_3O_2)(CN)_2]\cdot H_2O$ as well as the structures of several metal diluted crystals. Then, we will systematically investigate the thermal SCO and the photo-induced properties of $[Fe_xMn_{1-x}(L_{222}N_3O_2)(CN)_2]\cdot H_2O$ for polycrystalline powder. Finally, we will compare our results with the literature.

Chapter II.2. Complex $[Fe(L_{222}N_3O_2)(CN)_2]\cdot H_2O$

II.2.1. Fe(II) macrocyclic complex $[Fe(L_{222}N_3O_2)(CN)_2]\cdot H_2O$

In this chapter, we will first recall the literature works already published on the complex $[Fe(L_{222}N_3O_2)(CN)_2]\cdot H_2O$ (Scheme II. 1), which is up to now Fe(II) SCO materials with the highest T(LIESST) value.

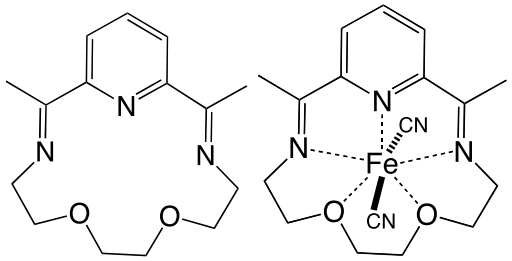

Ligand $L_{222}N_3O_2$ $[Fe(L_{222}N_3O_2)(CN)_2]$

Scheme II. 1: Macrocyclic ligand and the macrocyclic complex of $[Fe(L_{222}N_3O_2)(CN)_2]$

II.2.2. Publication of Nelson et al. (1986) [33]

The synthesis of the macrocyclic complex $[Fe(L_{222}N_3O_2)(CN)_2]\cdot H_2O$ was initially reported by Nelson et al. in 1986 [33]. These authors also reported some primary magnetic studies (Figure II. 8). At room temperature, the complex was HS state and by lowering the temperature some thermal spin crossover and quenching properties were indicated.

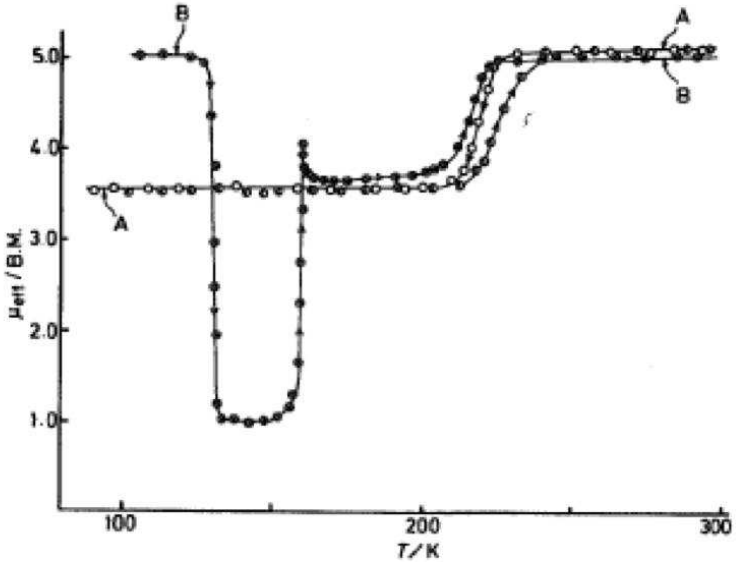

Figure II. 8: Variation of magnetic moment in the unit of μ_{eff}/B.M. of complex $[Fe(L_{222}N_3O_2)(CN)_2]\cdot H_2O$ with temperature. Curve A, specimen A on descending and ascending temperature. Curve B, specimen B on slow warming following rapid quenching to 80 K [33].

Nelson et al. [33] mentioned the existence of two magnetic behaviors (sample A and B) depending of the synthetic conditions. On the sample A, Nelson investigated the thermal spin

crossover properties (Figure II. 8, curve A). At room temperature, the complex is HS with an S = 2 configuration. When the temperature is slowly cooled (at a rate of ca. 2 K min^{-1}), the magnetic moment remains constant down to ca. 225 K and then suddenly decreases to reach a value close to 1 B.M. Further cooling down to 90 K induces no significant change. Initially the magnetic change at about 200 K was firstly attributed to the population of the spin triplet (S = 1) ground state [33] but Mössbauer spectra studies lead the authors to attribute the apparent S = 1 ground state of the specimen A to a mixed HS (S = 2) / LS (S = 0) state [33].

On the sample B, Nelson et al. [33] reported some quench cooling experiments (Figure II. 8 Curve B). The complex was rapidly quenched in liquid nitrogen and then warmed from 100 K to room temperature. Below 130 K, the possibility of quenching the metastable HS state was confirmed by the magnetic moment of 5.0 B.M. At about 130 K, the authors noticed a strong decrease of the magnetic signal and then a re-increase. The authors also indicated an unusual 'peak' at around 165 K, and mentioned that the magnetic behavior is dependent on thermal pre-history treatment and/or the sample preparation.

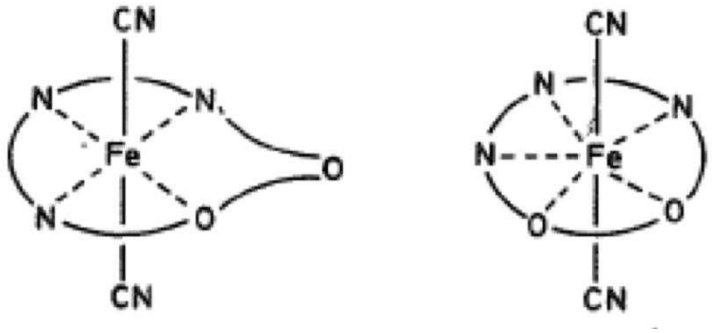

Scheme II. 2: Possible coordination for $[Fe(L_{222}N_3O_2)(CN)_2]\cdot H_2O$, proposed by Nelson et al.[33]

Based on all these atypical results, Nelson et al. [33] proposed that the coordination structure of the Fe(II) metal center may be different at high and low temperatures. By comparing the Mossbauer studies of several similar CN coordinated macrocyclic complexes which are LS at low temperature, the authors proposed that at low temperature (in LS state) the $[Fe(L_{222}N_3O_2)(CN)_2]\cdot H_2O$ complex is six coordinated. For high temperature in the HS state, the authors indicated that the complex is either six coordinated as at low temperature or either seven coordinate with a pentagonal bipyramidal structure (Scheme II. 2), as in complexes with other anionic ligands such as $[Fe(L_{222}N_3O_2)(NCS)_2]$ [34].

II.2.3. Publication of E. König et al. (1987) [35]

Later in 1987, complementary studies were performed by König et al. [35] on the quenching properties by Mossbauser and powder X-ray diffraction. These authors mentioned that by quenching the sample at 77 K, the relaxation of HS state is 'frozen in' and the HS to LS transition was quenched within several days. When the temperature was slowly warmed up, the relaxation becomes faster. These authors [35] reported the quenching study of HS state from room temperature to the 130 K -180 K region (Figure II. 9).

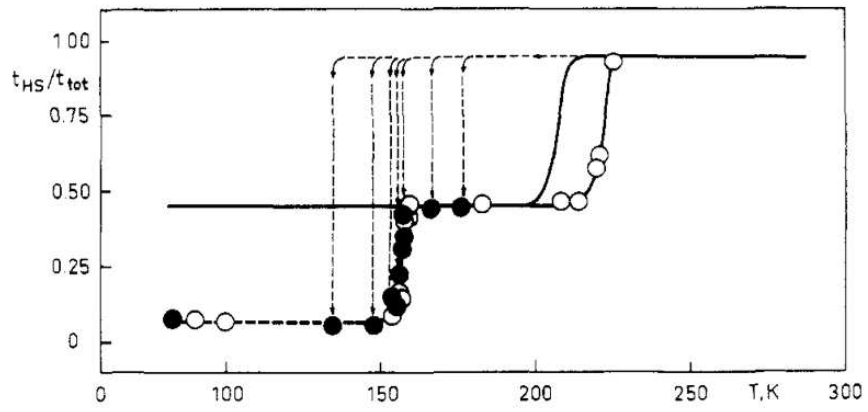

Figure II. 9: Schematic diagram of the temperature dependence of t_{HS}/t_{tot} for reasonably fast decrease of temperature (10-20 K min^{-1}) from 250.0 K into the region between 176.5 and 134.8 K (●) and subsequent increase of temperature(○). The transition temperature is T_c = 157 K [35].

They also preformed some investigation by frozing the sample from room temperature down to liquid nitrogen (Figure II. 10). In that condition, when temperature was warmed up to 130 K, the metastable quenched state relaxed to the LS state, then changed to the mixed HS/LS between 160 K and 180 K, and finally come back to the HS state at high temperature.

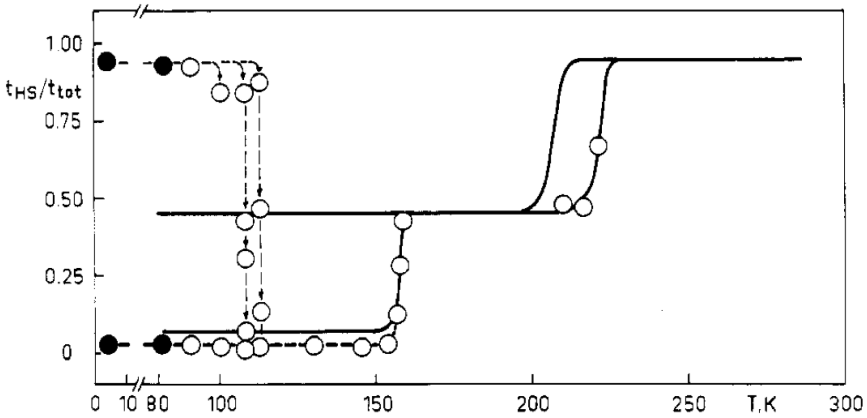

Figure II. 10: Schematic diagram of the temperature dependence of t_{HS}/t_{tot} for a sample of $[Fe(L_{222}N_3O_2)(CN)_2]\cdot H_2O$ quenched in liquid nitrogen [35]

II.2.4. Publication of Hayami et al. (Group of O. Sato) (2001) [36]

In 2001, Sato et al. re-investigated the $[Fe(L_{222}N_3O_2)(CN)_2]\cdot H_2O$ complex [36]. Figure II. 11a shows the X-ray crystallography structure determined at 270 K which indicates, for the $[Fe(L_{222}N_3O_2)(CN)_2]\cdot H_2O$ complex, a seven coordination. The proposed space group in their study was C c with one of the Fe-O bond being 2.41 Å. The water molecule was connected with CN ligand by hydrogen bond, forming a chain structure.

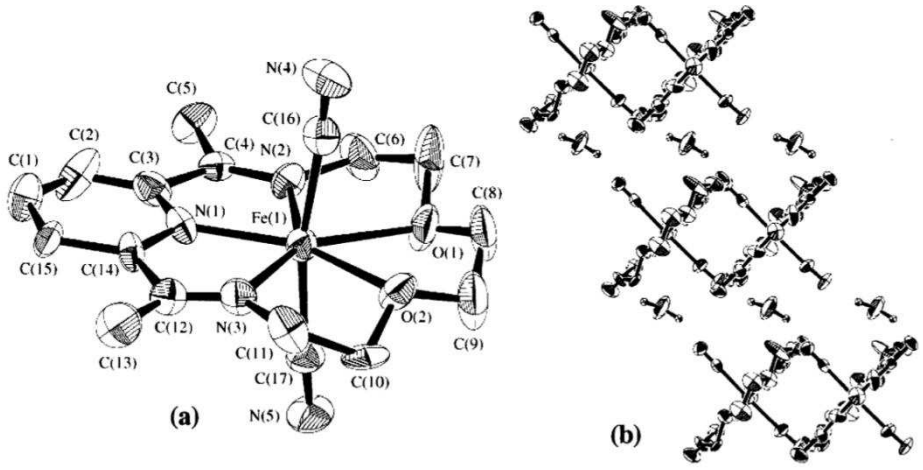

Figure II. 11: Molecular structures in the high-spin (270 K) states. (a) ORTEP view for $[Fe(L_{222}N_3O_2)(CN)_2]\cdot H_2O$ (with the exception of the hydrogen atoms and a water molecule). (b) Projection of the crystal structure of complex $[Fe(L_{222}N_3O_2)(CN)_2]\cdot H_2O$ along the *ac* plane.[36]

In this study, Sato et al. [36] also completed the thermal crossover properties of the complex $[Fe(L_{222}N_3O_2)(CN)_2]\cdot H_2O$ on single crystal and confirmed that the magnetic behavior is dependent on the pre-history (Figure II. 12). On the first cooling an abrupt transition was described at $T_{1/2}$ = 159 K and the sample at 130 K was in LS state. In the first warming mode (Figure II. 12, position 2), the $\chi_M T$ product was observed to strongly increase at $T_{1/2}$ = 172 K, then to decrease to the mixed HS:LS (1:1) state (already described by the previous authors [33,35]) and reaches the HS state at around 225 K. The magnetic behaviors in subsequent thermal cycles were totally different from first cycle. A classical spin crossover between HS state and mixed HS:LS (1:1) state was described at $T_{1/2}\uparrow$ = 225 K and $T_{1/2}\downarrow$ = 198 K with a thermal hysteresis.

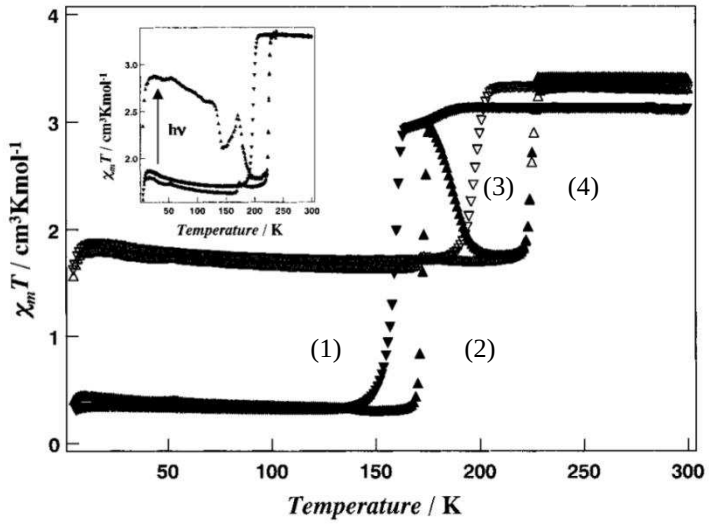

Figure II. 12: $\chi_M T$ versus *T* plots for complex $[Fe(L_{222}N_3O_2)(CN)_2]\cdot H_2O$. (1): Cooling mode of first cycle. (2): Warming mode of first cycle. (3): Cooling mode of second cycle. (4): Warming mode of second cycle. The temperature was varied at the rate of 1 K min^{-1} without temperature overshoot. The $\chi_M T$ versus *T* plot in the insert was recorded in the warming mode after the sample was exposed to light illumination for 1 h.[36]

Sato et al. also reports the photomagnetic properties. The sample was irradiated at 5 K

using Hg-Xe lamp with $\lambda \approx 550$ nm. The authors observed a clear increase of the magnetic signal in agreement with the LIESST process and described a two steps transition after irradiation (Figure II. 12 insert). A T(LIESST) value of 130 K was calculated from the first step, being the highest value at that moment.

II.2.5. Publication of H. Liu et al. (Group of O. Sato) (2004) [37]

In 2004, Sato et al. [37] completed the investigation of the photomagnetic properties by carefully studying what happens from the mixed HS:LS(1:1) state. These authors demonstrated that under irradiation (with 520, 980 or 1340 nm) the metastable HS state can be obtained with a T(LIESST) value of around 70 K which is much lower than the previous study (Figure II. 13 Curve L → H). These authors also indicated that by using a 980 nm excitation at 50 K, the mixed HS-LS state can be fully photoconverted into LS state (Figure II. 13 Curve H → L).

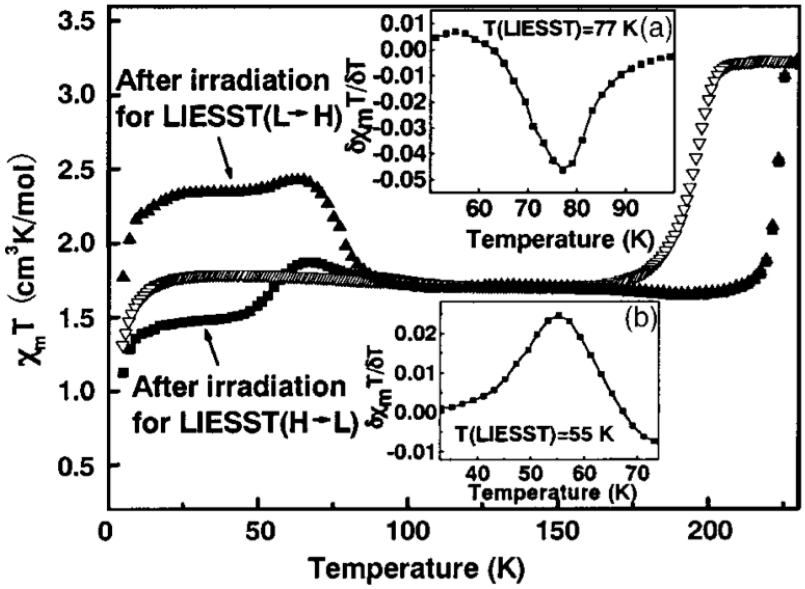

Figure II. 13: Temperature dependence of $\chi_M T$ for $[Fe(L_{222}N_3O_2)(CN)_2]\cdot H_2O$: (▽) data re-corded in cooling mode at 1 K min^{-1} without irradiation; (▲) data recorded in heating mode at 2 K min^{-1} after sequential irradiation with 520, 980, and 1340 nm light for LIESST (*L*→*H*) at 5 K; (■) data recorded in heating mode at 2 K min^{-1} after irradiation with 980 nm light for LIESST (*H* → *L*) at 5 K. Inserts (a) and (b) show the derivative $d\chi_M T / dT$ as a function of temperature for LIESST (*L* → *H*) and LIESST (*H* → *L*), respectively.[37]

II.2.6. Publications of P. Guionneau et al. (2004 and 2007) [38,39]

In 2004, Guionneau et al. revised the HS structure (Figure II. 14 left) [38], and in 2007 the LS structure was determined (Figure II. 14 right) [39].

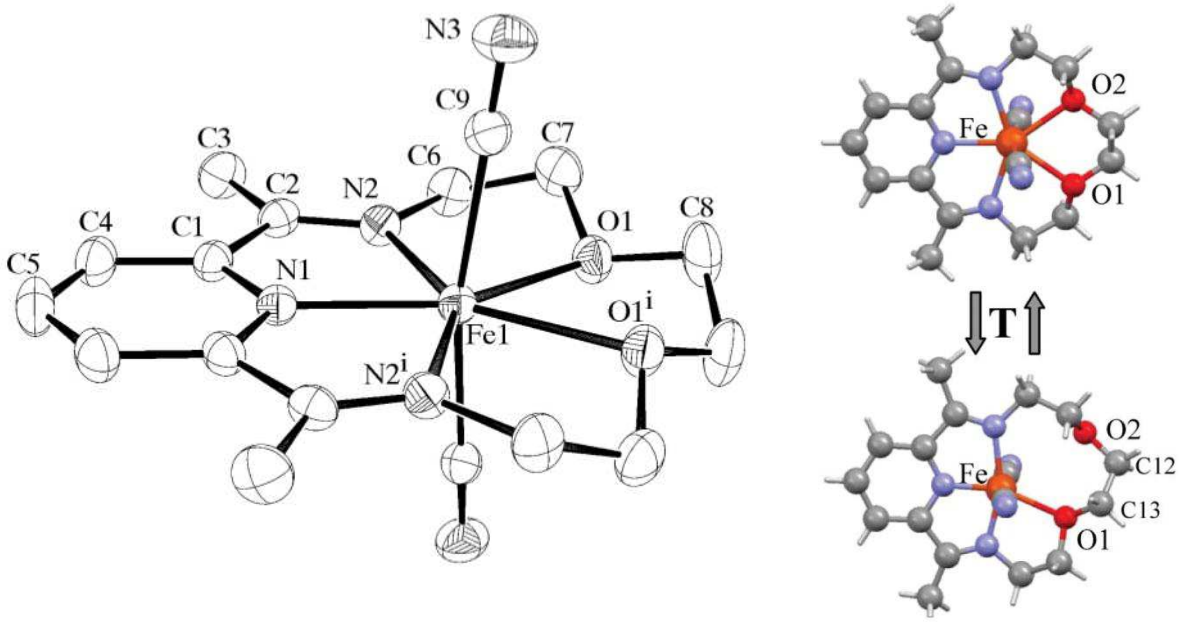

Figure II. 14: Left: An ORTEP-3 (Farrugia, 1997) view of the complex $[Fe(L_{222}N_3O_2)(CN)_2]\cdot H_2O$ at room temperature. The water molecules have been omitted for clarity. [38] Right: View of the two X-ray diffraction molecular structures of $[Fe(L_{222}N_3O_2)(CN)_2]\cdot H_2O$ in HS A (top) and LS B (bottom) showing the reversible transition from a hepta-coordinate high spin state (HS-7, $FeN_3C_2O_2$) to a hexa-coordinate low spin state (LS-6, FeN_3C_2O) for $[Fe(L_{222}N_3O_2)(CN)_2]\cdot H_2O$ in the solid state [39].

The HS state determined at 293 K, was hepta-coordinate high spin state (HS-7, $FeN_3C_2O_2$) and the space group was monoclinic C 2/c [38]. The iron(II) ion was in a pentagonal bipyramidal environment and lied on a twofold axis. The Fe–O bonds are consequently geometrically strictly identical by symmetry [38]. The authors also indicated that if the crystal structure was solved by C c space group, previously reported by Sato et al. [36], the same anomaly was observed.

The LS structure was latter determined at 120 K, showing a hexa-coordinate low spin state (LS-6, FeN_3C_2O) [39]. The space group was monoclinic P 2_1/c with a loss of the twofold axis. Consequently, the symmetry breaking induced a splitting of the Fe-O distances from 2.334(1) Å in HS to 2.243(1) Å for Fe–O1 and 3.202(1) Å for Fe–O2 in LS [39].

II.2.7. Publication of J. S. Costa (2005) [40]

In 2005, J. S. Costa (PhD) [40] reinvestigated the magnetic and photomagnetic properties and recorded the values with the standard procedure of 0.3 K min^{-1} (Figure II. 15). The irradiation of the $[Fe(L_{222}N_3O_2)(CN)_2]\cdot H_2O$ sample initially prepared into the LS state (Figure II. 15a) gave a T(LIESST) of 132 K, and when the sample was placed in the mixed HS:LS(1:1) state the T(LIESST) value was 73 K. These authors also reported the existence of a Light-Induced Thermal Hysteresis (LITH) (Figure II. 16).

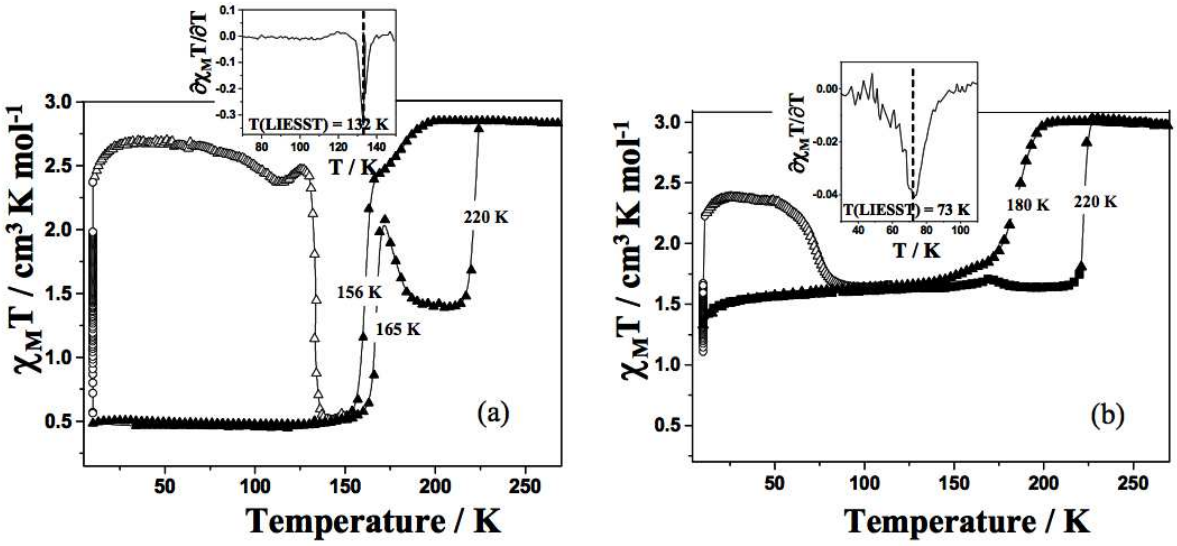

Figure II. 15: Temperature dependence of $\chi_M T$ for $[Fe(L_{222}N_3O_2)(CN)_2]\cdot H_2O$ a) in a first thermal cycle and b) in a second and/or a subsequent thermal cycles. (▲) data recorded in the cooling and warming mode without irradiation; (○) data recorded with irradiation at 10 K; (Δ) T(LIESST) measurement, data recorded in the warming mode after an optical irradiation of 24 hours. The insert graph reports the derivate of the magnetic product as function of the temperature. The minimum of the curve gave the T(LIESST) temperature [40] .

These authors also mentioned that by maintaining the irradiation during the cooling and the warming on the sample initially prepared to reach the fully LS state, a LITH loop appears due to the competition between the photoexcitation and the self accelerated thermal relaxation. At the opposite, excitation from the LS:HS form produced no LITH loop. This difference led the authors to conclude that the cooperativity along the relaxation process was different from the HS to LS form and the HS to LS:HS form

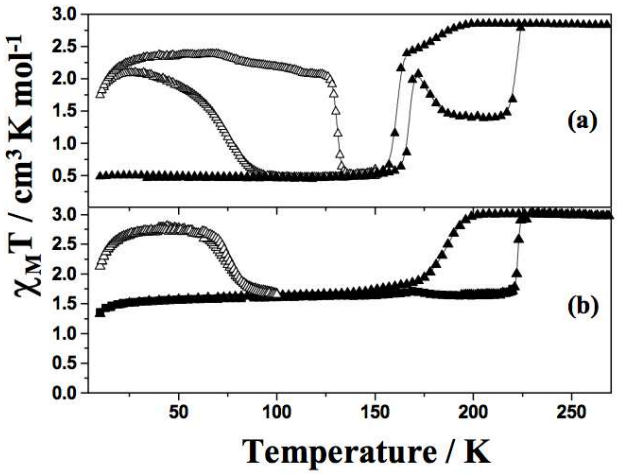

Figure II. 16: LITH experiments for a $[Fe(L_{222}N_3O_2)(CN)_2]\cdot H_2O$ sample initially prepared a) in the first thermal cycle and b) subsequent thermal cycles. [40].

II.2.8. Summary

This rapid overview of the different works already done demonstrates that the $[Fe(L_{222}N_3O_2)(CN)_2]\cdot H_2O$ complex displays atypical properties. Figure II. 17 presents a summary of the various correlations between structure and properties [41]. Briefly the phase B (LS-6 coordination) occurs from the slow cooling (of typically 2 hours) of the high spin state (HS-7 coordination), namely phase A. The phase C attributed to the mixed HS/LS state may be reached if the cooling is much slower than 2 h. This phase is still under investigation. From phase B by irradiation a metastable HS state, Phase B* can be obtained with a T(LIESST) of 132K. In addition, irradiation of Phase C leads to the C* phase with a T(LIESST) of 73 K.

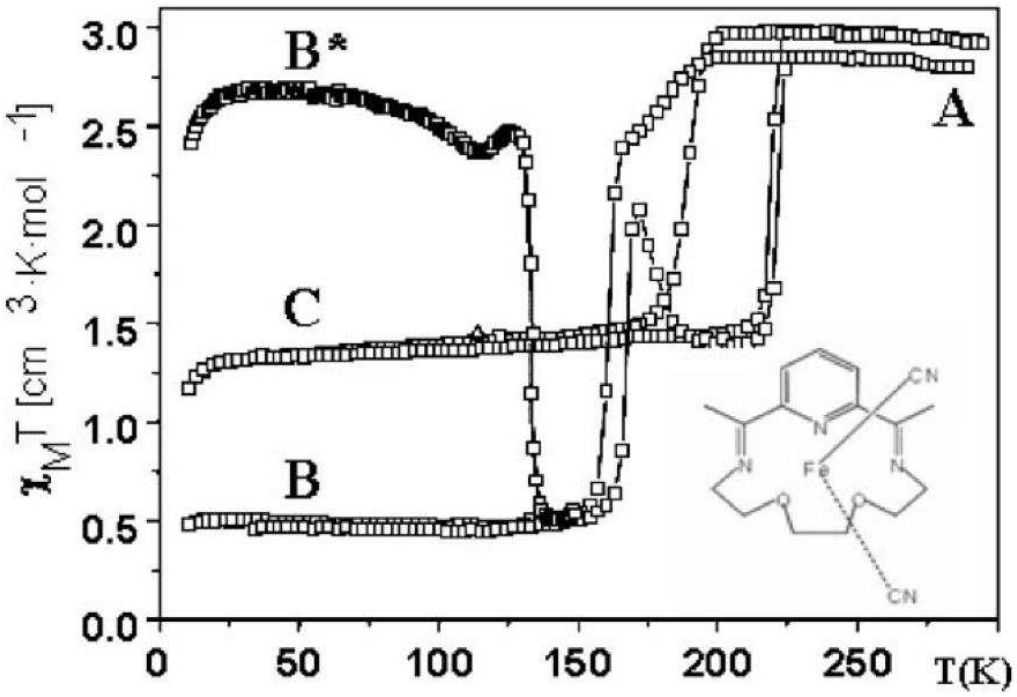

Figure II. 17: Magnetic property diagram for $[Fe(L_{222}N_3O_2)(CN)_2]\cdot H_2O$ from previously reported SQUID measurements. Depending on the method of cooling the conversion levels appear different. The present paper deals with the A to B solid state transition, where B* corresponds to the photo-induced HS phase obtained after light irradiation of the sample in B [39].

Chapter II.3. Complex $[Mn(L_{222}N_3O_2)(CN)_2]\cdot H_2O$

II.3.1. Synthesis and crystallization of $[Mn(L_{222}N_3O_2)(CN)_2]\cdot H_2O$

The synthesis of the $[Mn(L_{222}N_3O_2)(CN)_2]\cdot H_2O$ complex was performed by using the same protocol described by Nelson [42] for the $[Fe(L_{222}N_3O_2)(CN)_2]\cdot H_2O$. The macrocyclic ligand $L_{222}N_3O_2$ is a Schiff base formed by condensation of a diketone and a diamine. Upon formation of the macrocyclic complex, Mn(II) ion is coordinated to the interior of $L_{222}N_3O_2$ ligand and two cyanide groups are then completing the coordination sphere of the ion Mn(II) in axial position. In detail, the synthesis of complex $[Mn(L_{222}N_3O_2)(CN)_2]\cdot H_2O$ was performed under anaerobic conditions (Schlenk line) and all solvents used are degassed. The reaction route is represented in Scheme II. 3. The synthesis is carried out in 10 mL of methanol and 5 mL of water in which are dissolved 0.188 g (1.5 mmol) of manganese chloride, 0.25 g (1.5 mmol) of 2,6-diacetylpyridine, and 0.05 g of sodium dithionite. The 3,6-diamine dioxaoctane-1,8-diamine (0.23 mL, 1.5 mmol) was added dropwise. The mixture was kept at reflux under nitrogen gas for 16 h. A transparent orange solution is obtained. After filtration to remove impurities, 5 mL of aqueous solution containing an excess of sodium cyanide NaCN (1 g, 0.02 mol) was added, the solution turns dark orange. This solution was left in the fridge for two days, and then the brown crystals appeared in a cubic shape.

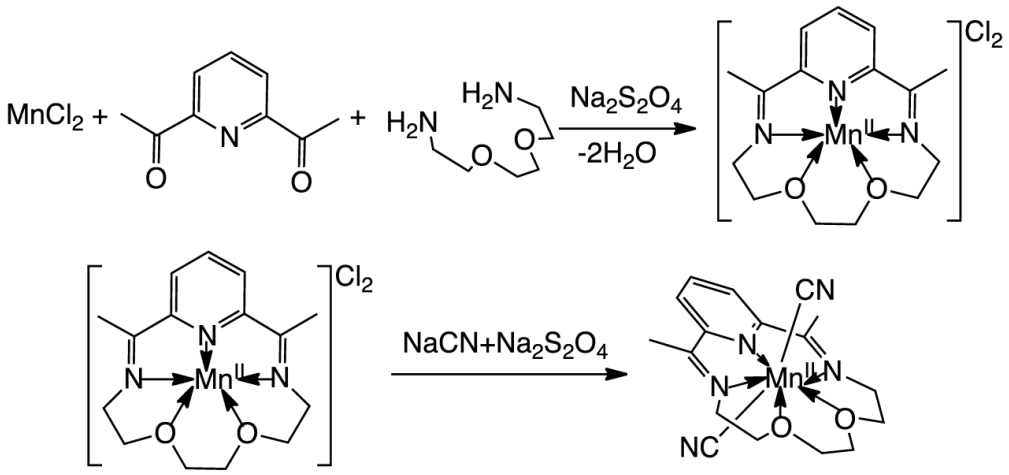

Scheme II. 3: The synthesis of $[Mn(L_{222}N_3O_2)(CN)_2]\cdot H_2O$

II.3.2. Structure of $[Mn(L_{222}N_3O_2)(CN)_2]\cdot H_2O$

a) Structure at 270 K

Structural determination was firstly performed at 270 K (Figure II. 18). At this temperature, the molecule is centered aroud a special position. The complex $[Mn(L_{222}N_3O_2)(CN)_2]\cdot H_2O$ presents a hepta-coordinate state ($MnN_3C_2O_2$), in a monoclinic C 2/c space group. The Mn(II) atom is in a pentagonal bipyramidal environment and is located on a twofold axis. The Mn–O bonds are geometrically identical by symmetry. The selected geometric parameters are presented in Table II. 1. The metal–ligand bond distances in the

macrocyclic ring are 2.214(1) Å for Mn–N1, 2.2676(9) Å for Mn–N2 and 2.308(1) Å for Mn–O1. The metal–ligand bond distance for the cyano group is 2.284(2) Å for Mn–C1. The volume of coordination sphere is 18.6 $Å^3$, calculated from the atomic positions using IVTON. There is one water molecule per Mn(II) center. It links the $[Mn(L_{222}N_3O_2)(CN)_2]$ molecules by hydrogen bonds, through the two cyanide nitrogen atoms in the axial positions. The bond lengths (N···O distance) are 2.916(5) Å and 2.806(5) Å. This interaction forms infinite one dimensional chain (Figure II. 19a).

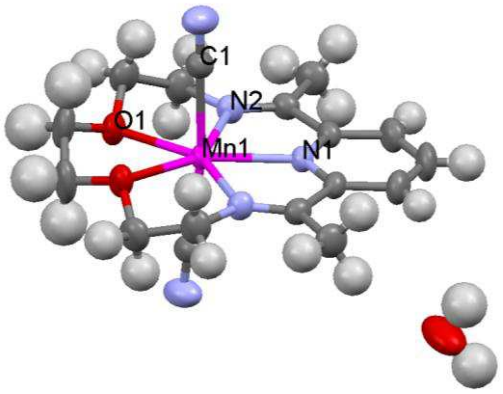

Figure II. 18: Molecular structure of the pure Mn(II) complex $[Mn(L_{222}N_3O_2)(CN)_2]\cdot H_2O$ at 270 K.

Mn1 — N1	2.214(1)	Mn1 — N2	2.2676(9)
Mn1 — O1	2.308(1)	Mn1 — C1	2.284(2)
N1 — Mn1 — N2	70.94(5)	C1 — Mn1 — N1	94.14(5)
N1 — Mn1 — O1	143.32(4)	C1 — Mn1 — N2	92.81(5)
N2 — Mn1 — O1	72.53(4)	C1 — Mn1 — O1	84.51(4)
N2 — Mn1 — $N2^i$	141.88(4)	C1 — Mn1 — $O1^i$	88.86(4)
N2 — Mn1 — $O1^i$	145.50(4)	C1 — Mn1 — $N2^i$	89.89(5)
O1 — Mn1 — $O1^i$	73.35(4)	C1 — Mn1 — $C1^i$	171.73(5)

Table II. 1: Selected geometric parameters (Å, °) for the pure $[Mn(L_{222}N_3O_2)(CN)_2]\cdot H_2O$ at 270 K Symmetry code: (i) 2-x, y, 3/2-z.

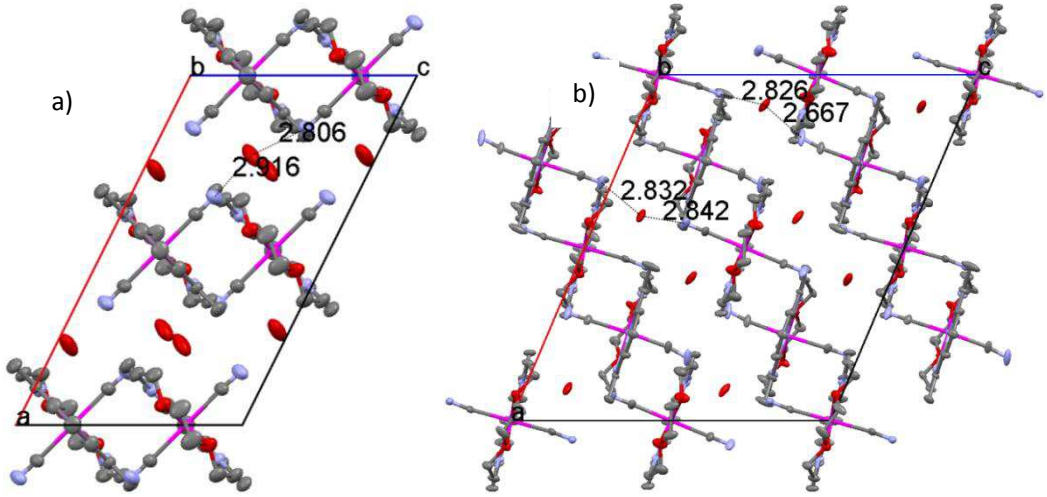

Figure II. 19: Projection of the crystal packing of $[Mn(L_{222}N_3O_2)(CN)_2]\cdot H_2O$: a) 270 K; b) 120 K. Hydrogen atoms have been omitted for clarity.

b) Structure at 120 K

The molecular structure of the $[Mn(L_{222}N_3O_2)(CN)_2]\cdot H_2O$ crystal was also determined at 120 K. Temperature was cooled with a rate of ca. 1 $Kmin^{-1}$. At 120 K, after slow cooling from 270 K, the complex $[Mn(L_{222}N_3O_2)(CN)_2]\cdot H_2O$ adopts the monoclinic C 2 space group (Figure II. 19b), with an increase in unit cell volume of around 95 %. From Table II. 2, it is evident that this increase comes from the doubling of c axes.

Compound	$[Mn(L_{222}N_3O_2)(CN)_2]\cdot H_2O$	
Formula	$C_{17}H_{23}MnN_5O_3$	$C_{17}H_{23}MnN_5O_3$
λ (Å)	0.71073	0.71073
M_r ($g.mol^{-1}$)	400.34	400.34
Colour	brown	brown
Crystal size (mm^3)	0.45 × 0.25 × 0.25	0.45 × 0.25 × 0.25
Crystal morphology	cubic	cubic
Temperature (K)	270(2)	120(2)
Crystal system	Monoclinic	Monoclinic
Space group	C 2/c	C 2
a (Å)	17.5613(3)	17.0933(5)
b (Å)	12.0994(2)	11.9898(3)
c (Å)	10.17850(10)	20.0712(4)
β (°)	116.5790(10)	113.011(2)
V ($Å^3$)	1934.18(5)	3786.18(16)
Z	4	8
Density ($g.cm^{-3}$)	1.375	1.405
μ (mm^{-1})	0.708	0.724
No. of total reflections	2815	10706
R_{obs}	0.0309	0.055
$wR2_{obs}$	0.0839	0.1303
S	1.042	1.126

Table II. 2: Crystal data of $[Mn(L_{222}N_3O_2)(CN)_2]\cdot H_2O$ at 270 K and at 120 K.

Indeed, at 120 K the asymmetric unit of this complex contains one macrocyclic molecule and two independent half-molecules (Figure II. 20a). One of the three Mn(II) atom locates in a general position (Mn3), while the other two Mn(II) atoms locate in two fold axis (Mn1 and Mn2). Despite this difference, the three Mn(II) centers are in hepta-coordinate state, and locate in a pentagonal bipyramidal environment. The bond distances are listed in Table II. 3. The difference between the corresponding metal-ligand bonds are less than 0.05 Å for each Mn-C, Mn-N and Mn-O bonds of the three molecules.

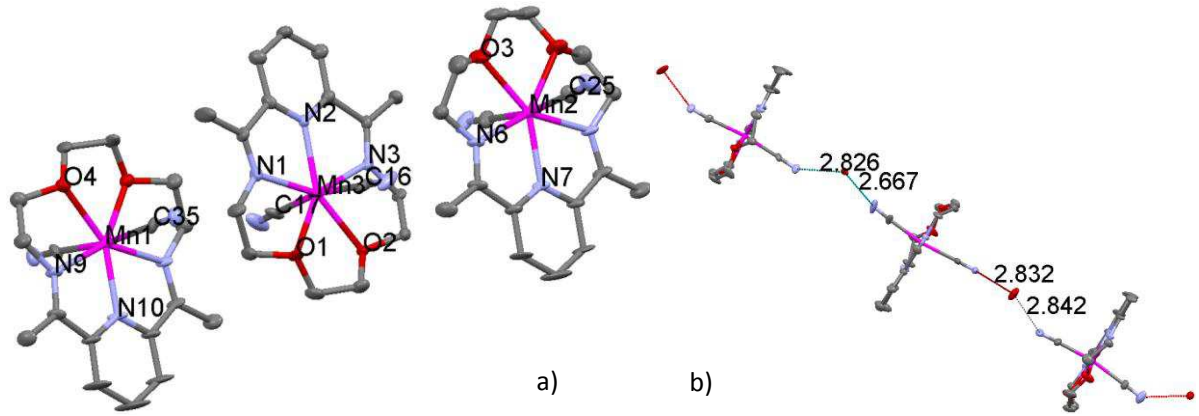

Figure II. 20: Molecular structure of $[Mn(L_{222}N_3O_2)(CN)_2]\cdot H_2O$ at 120 K: a) Coordination environment of Mn(II) centers. b) Intermolecular interactions from hydrogen bond. Hydrogen atoms have been omitted for clarity.

Mn3 — N1	2.285(6)	Mn1 — N9	2.276(4)
Mn3 — N2	2.215(7)	Mn1 — N10	2.214(7)
Mn3 — N3	2.270(6)	Mn1 — O4	2.320(5)
Mn3 — O1	2.315(5)	Mn1 — C35	2.269(5)
Mn3 — O2	2.309(4)		
Mn3 — C16	2.287(5)	Mn2 — N6	2.246(4)
Mn3 — C17	2.265(5)	Mn2 — N7	2.217(7)
		Mn2 — O3	2.310(6)
		Mn2 — C25	2.269(5)

Table II. 3: Selected geometric parameters (Å) for pure $[Mn(L_{222}N_3O_2)(CN)_2]\cdot H_2O$ at 120 K

Concerning the hydrogen interactions, at 120 K the water molecules remain linked to the $[Mn(L_{222}N_3O_2)(CN)_2]$ molecules by strong hydrogen bond through the two cyanide nitrogen atoms in the axial positions. The bond lengths (N···O distance) are 2.826(9) Å, 2.667(8)Å for N11—O7, N5—O7 and 2.832(5) Å, 2.842(7) Å for N4—O5, N8—O5. This type of hydrogen interaction forms an infinite one dimensional chain.

II.3.3. Concluding remarks

The investigation of the crystal structure of the $[Mn(L_{222}N_3O_2)(CN)_2]\cdot H_2O$ complex in comparison with the published $[Fe(L_{222}N_3O_2)(CN)_2]\cdot H_2O$ analogue [38] reveals that at room temperature the two complexes are isomorphous with the same crystal packing. At low temperature, the situation is much more complicated. On the $[Fe(L_{222}N_3O_2)(CN)_2]\cdot H_2O$ complex, the study indicates a strong dependence of the thermal condition with the population of either LS or HS/LS state, while on the $[Mn(L_{222}N_3O_2)(CN)_2]\cdot H_2O$ complex, a phase transition occurs with a change of space group (monoclinic C 2/c at 270 K and C 2 at 120 K) and a doubling of the unit cell volume. Nevertheless, it is reasonable to expect from the room temperature structure that $[Fe_xMn_{1-x}(L_{222}N_3O_2)(CN)_2]\cdot H_2O$ complexes can be synthesized with homogenous metal dilution.

Chapter II.4. Metal diluted series

$[Fe_xMn_{1-x}(L_{222}N_3O_2)(CN)_2]\cdot H_2O$

II.4.1. Synthesis of $[Fe_xMn_{1-x}(L_{222}N_3O_2)(CN)_2]\cdot H_2O$ series

Complexes $[Fe_xMn_{1-x}(L_{222}N_3O_2)(CN)_2]\cdot H_2O$ in polycrystalline powder form were obtained following the procedure initially described by Nelson et al. [42]. In detail, the synthesis was performed under anaerobic conditions (Schlenk line) and all solvents used were degassed. Mixtures of iron chloride tetrahydrate and manganese chloride with appropriated molar ratios (1.5 mmol in total) were initially prepared. This mixture was then dissolved in a solution containing 10 mL of methanol and 5 mL of water, 0.25 g (1.5 mmol) of 2,6-diacetylpyridine, and 0.03 g of sodium dithionite (used as reducing agent to remove traces of trivalent Fe ion). The 3,6-diamine dioxaoctane-1,8-diamine (0.23 mL, 1.5 mmol) was added dropwise. The mixture was kept at reflux under nitrogen gas for 16 h. After filtration, 5 mL of aqueous solution containing an excess of sodium cyanide NaCN (1 g, 0.02 mol) was added. The entire solutions were kept stirring during 2 hours at 293 K. Polycrystalline powders of $[Fe_xMn_{1-x}(L_{222}N_3O_2)(CN)_2]\cdot H_2O$ in dark blue color were obtained after filtration.

The dilution factor x was carefully determined from the results of ICP (Inductively Coupled Plasma) analysis (Figure II. 21). The amount of experimental Fe(II) is found slightly higher than the theoretical value estimated from the synthesis protocol. This can be associated to the higher solubility of Mn(II) complex in regard to the Fe(II) analogue. Despite of this slight difference, the elemental microanalyses of the various complexes, given in Table II. 4 are in good agreement with calculated formula.

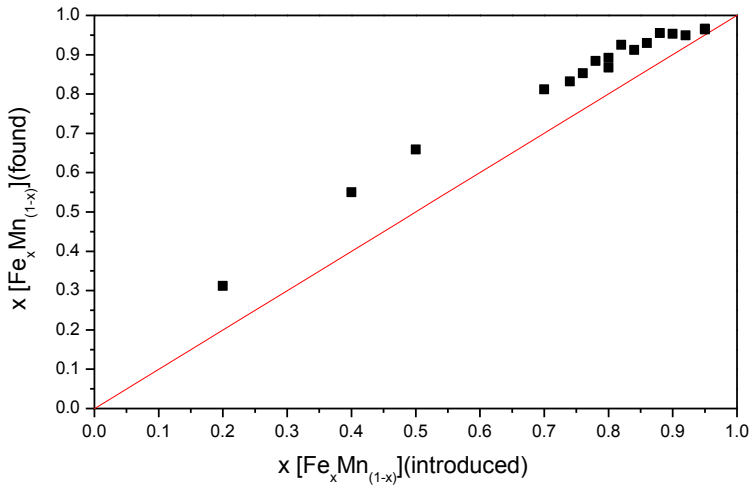

Figure II. 21: Dilution factor obtained as a function of the dilution factor expected for $[Fe_xMn_{1-x}(L_{222}N_3O_2)(CN)_2]\cdot H_2O$.

x	C	H	N	Fe	Mn
1	50.78(50.89)	5.88(5.78)	17.61(17.45)	14.22(13.92)	-
0.966	50.59(50.89)	5.94(5.78)	17.51(17.46)	13.82 (13.45)	0.49 (0.47)
0.964	49.58(50.89)	5.75(5.78)	16.96(17.46)	14.64(13.42)	0.55(0.49)
0.953	50.29(50.89)	5.76(5.78)	17.21(17.46)	13.98(13.27)	0.69(0.64)
0.949	50.04(50.89)	5.79(5.78)	17.19(17.46)	14.18 (13.21)	0.76 (0.70)
0.930	50.76(50.90)	5.95(5.78)	17.48(17.46)	12.39 (12.95)	0.94 (0.96)
0.912	50.68(50.90)	5.79(5.78)	17.45(17.46)	12.70 (12.70)	1.22 (1.21)
0.892	50.90(50.90)	5.66(5.78)	17.56(17.46)	12.86 (12.42)	1.56 (1.48)
0.867	50.46(50.9)	5.83(5.78)	17.31(17.46)	12.77(12.17)	1.83(1.73)
0.853	51.04(50.90)	5.83(5.78)	17.38(17.46)	12.03 (12.02)	1.91(1.88)
0.832	50.90(50.90)	5.84(5.78)	17.52(17.46)	11.71(11.58)	2.32(2.30)
0.812	50.84(50.90)	5.78(5.78)	17.54(17.46)	11.22(11.31)	2.55(2.58)
0.659	49.31(50.93)	5.64(5.78)	16.84(17.47)	9.24(9.18)	4.77(4.67)
0.550	49.68(50.94)	5.77(5.78)	16.89(17.47)	7.99(7.66)	6.53(6.17)
0.312	50.04(50.97)	5.34(5.78)	16.02(17.48)	4.41(4.35)	9.73(9.43)

Table II. 4: Elemental microanalyses of the solid solution materials $[Fe_xMn_{1-x}(L_{222}N_3O_2)(CN)_2]\cdot H_2O$ [found, % (calcd, %)].

Figure II. 22 shows a selection of powder diffraction data for the metal diluted complexes $[Fe_xMn_{1-x}(L_{222}N_3O_2)(CN)_2]\cdot H_2O$, compared to the simulated powder diffraction patterns from the single crystal of pure Fe(II) and Mn(II) complexes (red lines). This series of result provides an indication that all the metal diluted $[Fe_xMn_{1-x}(L_{222}N_3O_2)(CN)_2]\cdot H_2O$ analogues are isomorphous. The only difference is that when x is less than 0.659, X-ray diffraction pattern indicates a significant loss of crystallinity.

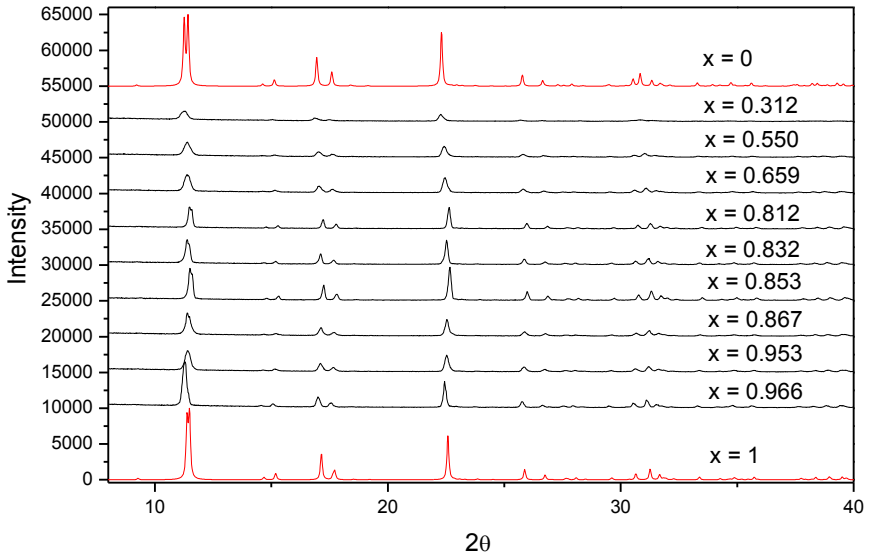

Figure II. 22: Powder diffraction data for the series of $[Fe_xMn_{1-x}(L_{222}N_3O_2)(CN)_2]\cdot H_2O$. Red lines are simulated powder diffraction from single crystals of pure Fe(II) x = 1, and Mn(II) complexes x = 0.

II.4.2. Crystallization and structure of $[Fe_xMn_{1-x}(L_{222}N_3O_2)(CN)_2]\cdot H_2O$ series

In addition to the powder form, single crystals of $[Fe_xMn_{1-x}(L_{222}N_3O_2)(CN)_2]\cdot H_2O$ complexes were also obtained by vapor diffusion method. In detail, an excess of approximately 3 mg of $[Fe_xMn_{1-x}(L_{222}N_3O_2)(CN)_2]\cdot H_2O$ in polycrystalline powder form was dissolved in 3 mL of dichloromethane (SIGMA-ALDRICH ACS reagent, ≥ 99.9% (GC) without degassing). After 30 minutes of stirring, the formed suspension was filtered. 1 mL of the solution was then placed into a small tube (of ca. 1 cm in diameter and 3 cm in depth), which is later on introduced into a bigger bottle (of ca. 2.5 cm in diameter and 5 cm depth) containing 10 mL of ether for vapor diffusion. The bottle is closed tightly and left in the fridge for a week, and dark blue rectangular crystals were obtained later.

Based on this protocol, several crystals were obtained using polycrystalline powder with different x values. Structure determination was performed on two of those crystals. The first one is obtained using the metal diluted $[Fe_xMn_{1-x}(L_{222}N_3O_2)(CN)_2]\cdot H_2O$ complex with x = 0.892. The second structure determination was performed with x = 0.312.

The Fe/Mn percentage was firstly evaluated by EPMA (electron probe microanalyzer) on surface. Indeed, the Fe/Mn percentages of the crystals used for structure determination are evaluated by an average of about 10 crystals in the same batch and the standard deviations are also calculated. For the first set of crystals obtained with an initial solution possessing a Fe_xMn_{1-x} ratio of x = 0.892, the experimental value calculated from eight different crystals (Figure II. 23) is an average of x= 0.963±0.005. For the second set of crystals starting with x = 0.312, an average of x= 0.638±0.009 is calculated from nine crystals (Figure II. 24). These data indicate that for single crystal, a strong deviation happens between the experimental and theoretical metal dilution.

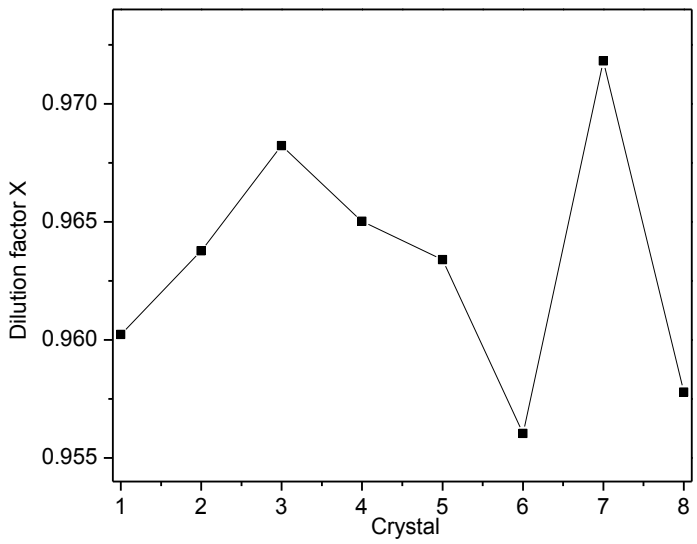

Figure II. 23: Percentage of Fe(II) ion on the surfaces of eight crystals obtained by EPMA. The dilution factor x is 0.963 ± 0.005. The eight crystals were obtained from $[Fe_xMn_{1-x}(L_{222}N_3O_2)(CN)_2]\cdot H_2O$ complex with x = 0.892

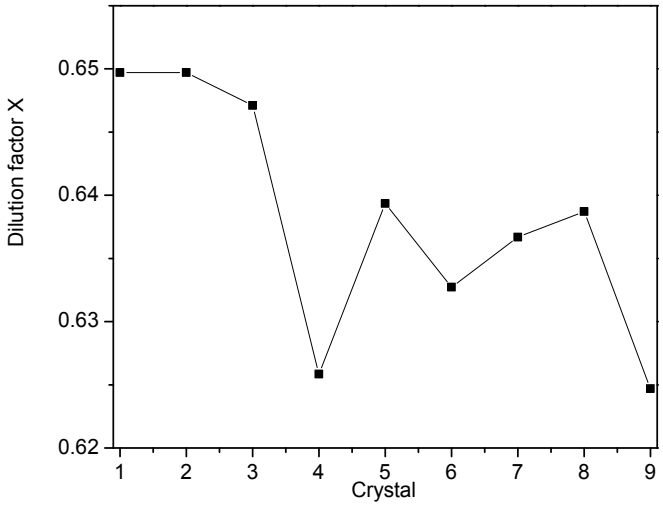

Figure II. 24: Percentage of Mn(II) ion on the surfaces of nine crystals obtained by EPMA. The dilution factor x is 0.638±0.009. The nine crystals were obtained from $[Fe_xMn_{1-x}(L_{222}N_3O_2)(CN)_2]\cdot H_2O$ complex with x = 0.312

a) Crystal of $[Fe_xMn_{1-x}(L_{222}N_3O_2)(CN)_2]\cdot H_2O$ complex with x = 0.963±0.005

Crystal determination of $[Fe_xMn_{1-x}(L_{222}N_3O_2)(CN)_2]\cdot H_2O$ with x = 0.963±0.005 was performed at room temperature. The x value was calculated from Figure II. 23. The crystal adopts the monoclinic C 2/c space group. The metal still lies on a twofold axis, within a pentagonal bipyramidal environment (Figure II. 25a). The selected geometric parameters are presented in Table II. 5. The metal ligand bond distances are 2.122(5) Å for Fe — N1, 2.211(3) Å for Fe — N2, 2.337(3) Å for Fe — O1 and 2.174(6) Å for Fe — C9. The volume of coordination sphere is 17.3Å^3. There is one water molecule per metal center, which links the macrocyclic molecule through the two cyanide nitrogen atoms in the axial positions by hydrogen bond. The hydrogen bond lengths (N···O distance) are 2.93(1) Å and 2.85(2) Å and forms infinite one dimensional chain (Figure II. 25b).

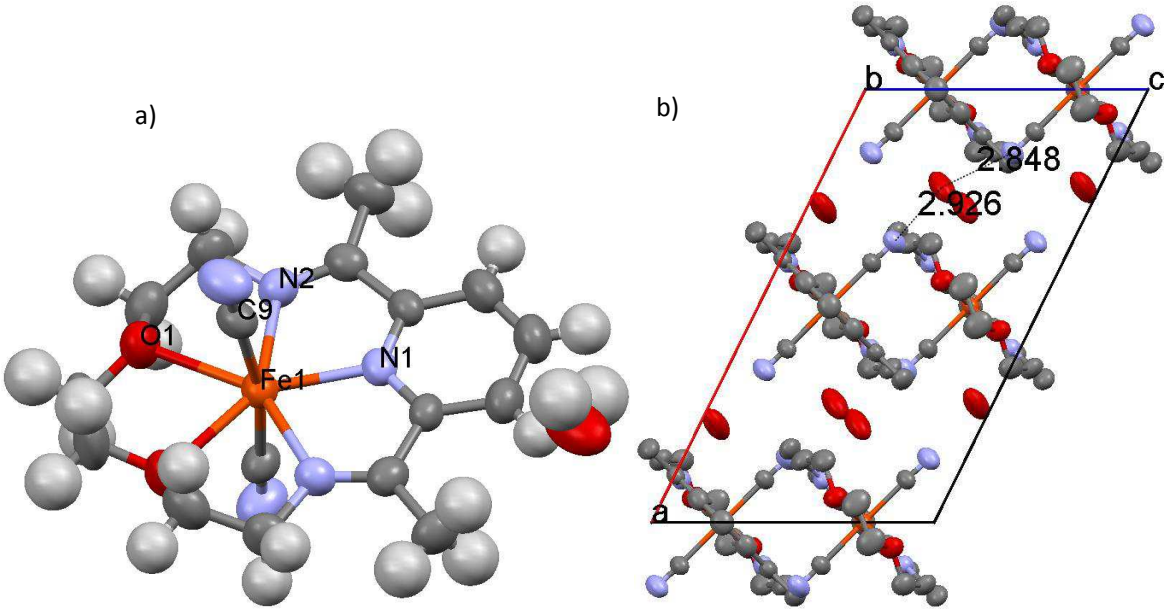

Figure II. 25: Molecular structure (a) and packing (b) of $[Fe_xMn_{1-x}(L_{222}N_3O_2)(CN)_2]\cdot H_2O$ with x = 0.963±0.005 at 293 K. The hydrogen atoms have been omitted for clarity. The x value was calculated from Figure II. 23.

Fe1 — N1	2.122(5)	Fe1 — N2	2.211(3)
Fe1 — O1	2.337(3)	Fe1 — C9	2.174(6)
N1 — Fe1 — N2	72.7(2)	C9 — Fe1 — N1	95.0(2)
N1 — Fe1 — O1	144.5(2)	C9 — Fe1 — N2	92.9(2)
N2 — Fe1 — O1	71.9(1)	C9 — Fe1 — O1	84.2(2)
N2 — Fe1 — $N2^i$	145.3(1)	C9 — Fe1 — $O1^i$	87.7(2)
N2 — Fe1 — $O1^i$	142.7(1)	C9 — Fe1 — $N2^i$	90.0(2)
O1 — Fe1 — $O1^i$	71.1(1)	C9 — Fe1 — $C9^i$	170.0(2)

Table II. 5: Selected geometric parameters (Å, °) for the $[Fe_xMn_{1-x}(L_{222}N_3O_2)(CN)_2]\cdot H_2O$ with x = 0.963±0.005 at room T. Symmetry code: (i) 1-x, y, 1/2-z. The x value was calculated from Figure II. 23

Interestingly, the metal-ligand bond distances of this $[Fe_xMn_{1-x}(L_{222}N_3O_2)(CN)_2]\cdot H_2O$ with x = 0.963 ± 0.005 crystal (Table II. 5) are very close to the complex of $[Fe(L_{222}N_3O_2)(CN)_2]\cdot H_2O$ previously studied at room temperature [38]. The difference is indeed within 0.03 Å range. The unit cell parameter of the metal diluted (Table II. 6) and the pure $[Fe(L_{222}N_3O_2)(CN)_2]\cdot H_2O$ are also close to each other as well ([38]). In conclusion, this sudy suggest that the metal diluted crystals are isomorphous to the pure $[Fe(L_{222}N_3O_2)(CN)_2]\cdot H_2O$ analogue at room temperature. Nevertheless, despite our efforts it was impossible to determine the position of the Mn atom. More precisely it was impossible to solve the structure with the co-existence of Fe and Mn atom.

Compound	$[Fe_xMn_{1-x}(L_{222}N_3O_2)(CN)_2]\cdot H_2O$, x = 0.963±0.005
Formula	$C_{17}H_{23}Mn_{0.04}Fe_{0.96}N_5O_3$
λ (Å)	0.71073
M_r (g.mol^{-1})	401.22
Colour	dark blue
Crystal size (mm^3)	0.08 × 0.08 × 0.08
Crystal morphology	cubic
Temperature (K)	293(2)
Crystal system	Monoclinic
Space group	C 2/c
a (Å)	17.3438(8)
b (Å)	12.0771(7)
c (Å)	10.1378(7)
β (°)	116.269(3)
V (Å^3)	1904.19(19)
Z	4
Density (g.cm^{-3})	1.400
μ (mm^{-1})	0.818
No. of total reflections	2586
R_{obs}	0.0773
$wR2_{obs}$	0.1536
S	0.989

Table II. 6: Crystal data of $[Fe_xMn_{1-x}(L_{222}N_3O_2)(CN)_2]\cdot H_2O$ with x = 0.963±0.005 at room T. The x value was calculated from Figure II. 23.

b) Crystal of $[Fe_xMn_{1-x}(L_{222}N_3O_2)(CN)_2]\cdot H_2O$ complex with x = 0.638±0.009

Concerning the metal dilution with 0.638±0.009, the structure was firstly determined at 250 K. The x value was calculated from Figure II. 24. At this temperature, the complex adopts monoclinic C 2/c space group at this temperature. The metal ion lies on a twofold axis, within a pentagonal bipyramidal environment (Figure II. 26a). The selected geometric parameters are presented in Table II. 7. The volume of coordination sphere is 17.7Å^3. Those parameters are very close to the one of x = 0.963±0.005 at room temperature. There is one molecule of water per metal center. The hydrogen bond lengths (N···O distance) are 2.931(9) Å and 2.836(9) Å Those distances are also similar with the case of x = 0.963±0.005 at room temperature. This interaction forms infinite one dimensional chain Figure II. 26b). Unfortunately, the attempts to distinguish the Mn(II) atom from Fe(II) atom was also unsuccessful.

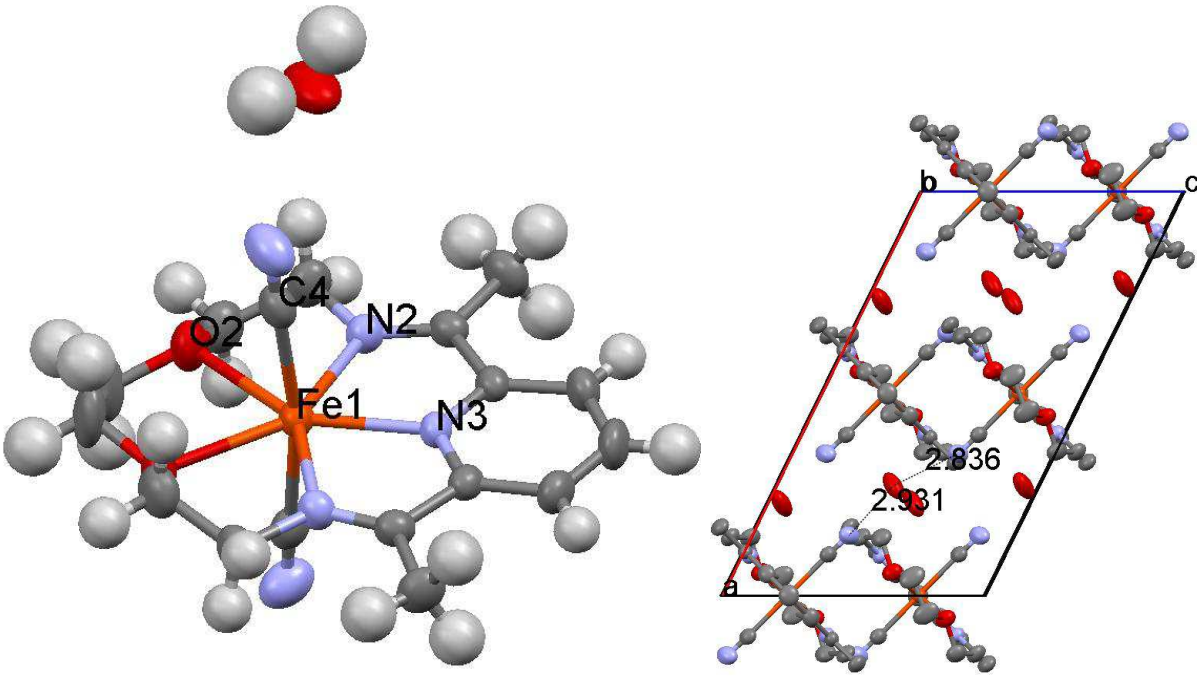

Figure II. 26: Molecular structure (a) and packing (b) of $[Fe_xMn_{1-x}(L_{222}N_3O_2)(CN)_2]\cdot H_2O$ with x = 0.638±0.009 at 250 K. The hydrogen atoms have been omitted for clarity. The x value was calculated from Figure II. 24

Fe1 — N3	2.143(2)	Fe1 — N2	2.225(2)
Fe1 — O2	2.323(2)	Fe1 — C4	2.224(4)
N3 — Fe1 — N2	72.17(9)	C4 — Fe1 — N3	95.0(1)
N3 — Fe1 — O2	144.05(8)	C4 — Fe1 — N2	92.86(9)
N2 — Fe1 — O2	71.99(7)	C4 — Fe1 — O2	84.07(9)
N2 — Fe1 — N2^i	144.35(8)	C4 — Fe1 — O2^i	87.82(9)
N2 — Fe1 — O2^i	143.60(8)	C4 — Fe1 — N2^i	90.21(9)
O2 — Fe1 — O2^i	71.89(7)	C4 — Fe1 — C4^i	170.0(1)

Table II. 7: Selected geometric parameters (Å, °) for the $[Fe_xMn_{1-x}(L_{222}N_3O_2)(CN)_2]\cdot H_2O$ with x = 0.638±0.009 at 250 K. Symmetry code: (i) -x, y, 1/2-z. The x value was calculated from Figure II. 24

The structure of this metal diluted complexes with x = 0.638±0.009 was also determined at 100 K. After slowly cooling down to 100 K in more than 2 hours, structure determination

was performed. At 100 K, the complex adopts the same monoclinic C 2/c space group as at room temperature (Figure II. 27a). It was impossible to evidence any change of the structure and/or change of coordination at the metal center. The selected geometric parameters are presented in Table II. 8. The volume of coordination sphere decrease to 17.5Å^3. The hydrogen bond lengths (N···O distance) at 120 K are 2.910(7) Å and 2.785(8) Å (Figure II. 27b). The identification of Mn atom in the crystal structure was not successful. The crystal data is listed in Table II. 9.

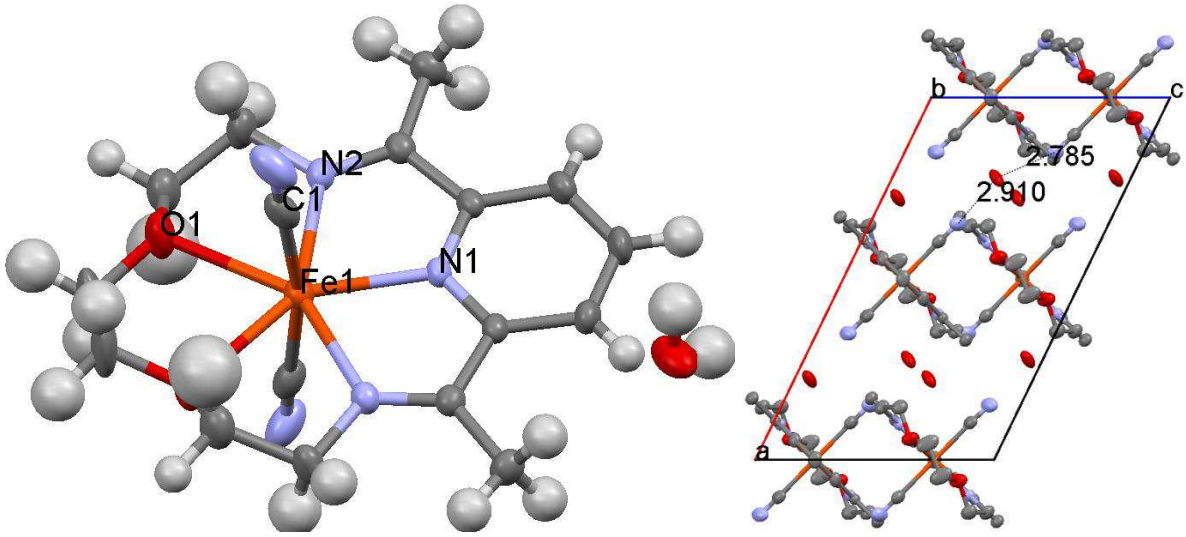

Figure II. 27: Molecular structure (a) and packing (b) of $[Fe_xMn_{1-x}(L_{222}N_3O_2)(CN)_2]\cdot H_2O$ with x = 0.638±0.009 at 100K. The hydrogen atoms have been omitted for clarity. The x value was calculated from Figure II. 24

Fe1 — N1	2.118(4)	Fe1 — N2	2.214(2)
Fe1 — O1	2.329(2)	Fe1 — C1	2.208(4)
N1 — Fe1 — N2	72.6(1)	C1 — Fe1 — N1	95.4(1)
N1 — Fe1 — O1	144.3(1)	C1 — Fe1 — N2	92.9(1)
N2 — Fe1 — O1	71.88(9)	C1 — Fe1 — O1	83.8(1)
N2 — Fe1 — N2^i	145.13(9)	C1 — Fe1 — O1^i	87.5(1)
N2 — Fe1 — O1^i	142.93(9)	C1 — Fe1 — N2^i	90.3(1)
O1 — Fe1 — O1^i	71.33(9)	C1 — Fe1 — C1^i	169.3(1)

Table II. 8: Selected geometric parameters (Å, °) for the $[Fe_xMn_{1-x}(L_{222}N_3O_2)(CN)_2]\cdot H_2O$ with x=0.638±0.009 at 100 K. Symmetry code: (i) 1-x, y, 1/2-z. The x value was calculated from Figure II. 24

Compound	$[Fe_xMn_{1-x}(L_{222}N_3O_2)(CN)_2]\cdot H_2O$, x = 0.638±0.009	
Formula	$C_{17}H_{23}Mn_{0.36}Fe_{0.64}FeN_5O_3$	$C_{17}H_{23}Mn_{0.36}Fe_{0.64}N_5O_3$
λ (Å)	0.71073	0.71073
M_r (g.mol^{-1})	400.93	400.93
Colour	dark blue	dark blue
Crystal size (mm^3)	0.17 × 0.13 × 0.13	0.17 × 0.13 × 0.13
Crystal morphology	prism	prism
Temperature (K)	250(2)	100(2)
Crystal system	Monoclinic	Monoclinic
Space group	C 2/c	C 2/c
a (Å)	17.3332(4)	17.0528(5)
b (Å)	12.0778(4)	12.0023(4)
c (Å)	10.1168(2)	10.0974(3)
β (°)	116.210(2)	115.880(2)
V (Å^3)	1900.16(9)	1859.40(10)
Z	4	4
Density (g.cm^{-3})	1.403	1.433
μ (mm^{-1})	0.820	0.838
No. of total reflections	2164	2116
R_{obs}	0.0589	0.0631
$wR2_{obs}$	0.1105	0.1208
S	1.061	1.08

Table II. 9: Crystal data of $[Fe_xMn_{1-x}(L_{222}N_3O_2)(CN)_2]\cdot H_2O$ with x = 0.638±0.009 at 250 K and 100 K. The x value was calculated from Figure II. 23.

c) Summary

To sum up, structure determination was performed for two metal diluted complexes, i.e. $[Fe_xMn_{1-x}(L_{222}N_3O_2)(CN)_2]\cdot H_2O$ with x = 0.963±0.005 and x = 0.638±0.009. These crystals are isomorphous at room temperature with pure $[Mn(L_{222}N_3O_2)(CN)_2]\cdot H_2O$ and $[Fe(L_{222}N_3O_2)(CN)_2]\cdot H_2O$. At low temperature, the metal diluted $[Fe_xMn_{1-x}(L_{222}N_3O_2)(CN)_2]\cdot H_2O$ x = 0.638±0.009 keeps the same space group and similar cell parameters as in high temperature. The crystal structure of $[Fe_xMn_{1-x}(L_{222}N_3O_2)(CN)_2]\cdot H_2O$ with x = 0.963±0.005 at low temperature is still under investigation.

Based on these data, it is surprising that neither structure transition nor change of coordination is observed for the crystal of $[Fe_xMn_{1-x}(L_{222}N_3O_2)(CN)_2]\cdot H_2O$ with x = 0.638±0.009. It seems that the insertion of Mn(II) complex in the lattice of $[Fe(L_{222}N_3O_2)(CN)_2]\cdot H_2O$ prevent the Fe(II) metal ions to both exhibit the SCO phenomena and/or to change the coordination like it was reported for the pure $[Fe(L_{222}N_3O_2)(CN)_2]\cdot H_2O$. Moreover, at x = 0.638 lowering the temperature does not induce a structural transition as it was described for the pure $[Mn(L_{222}N_3O_2)(CN)_2]\cdot H_2O$ complex.

II.4.3. Magnetic behavior of the metal diluted $[Fe_xMn_{1-x}(L_{222}N_3O_2)(CN)_2]\cdot H_2O$

Let us first briefly recall that for presenting the magnetic value of metal diluted analogues, the paramagnetic contribution of the Mn(II) ion (d^5,S = 5/2) is removed from the measurement according to Eq.2. The $(\chi_M T)_{Mn}$ product was measured on single crystals of value of pure $[Mn(L_{222}N_3O_2)(CN)_2]\cdot H_2O$ complex and the value was constant at 4.38 $cm^3mol^{-1}K$ between 10 K and 290 K, in agreement with the expected spin only value. The value of $(\chi_M T)_{Fe}$, representing 1 mol of iron entities can be extracted (Eq.3) in agreement with the previous work on the metal dilution systems [29,32]. The HS fraction γ_{HS} is determined according to Eq. 4, and the value of $(\chi_M T)_{HS}$ used for Part II is 3.74 $cm^3mol^{-1}K$ obtained from freshly prepared pure Fe(II) analogue.

$$\chi_M T = x \cdot (\chi_M T)_{Fe} + (1 - x) \cdot (\chi_M T)_{Mn} \qquad \text{(Eq.2)}$$

$$(\chi_M T)_{Fe} = \frac{\chi_M T - (1-x)\cdot(\chi_M T)_{Mn}}{x} \qquad \text{(Eq.3)}$$

$$\gamma_{HS} = \frac{(\chi_M T)_{HS}}{(\chi_M T)_{Fe}} \qquad \text{(Eq.4)}$$

The experimental $\chi_M T$ value for the pure $[Mn(L_{222}N_3O_2)(CN)_2]\cdot H_2O$ was measured on single crystals. The magnetic value is almost constant (4.38 $cm^3mol^{-1}K$) between 10 K and 290 K. Figure II. 28 shows the magnetic behavior recorded for two metal diluted $[Fe_xMn_{1-x}(L_{222}N_3O_2)(CN)_2]\cdot H_2O$ complex with respectively x = 0.966 and x = 0.949.

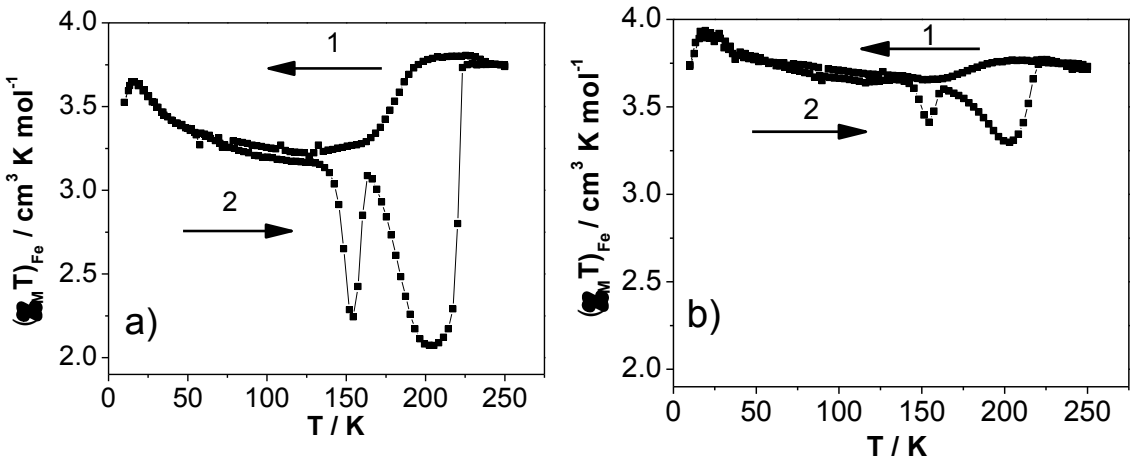

Figure II. 28: Temperature dependence of $(\chi_M T)_{Fe}$ with a rate of 3 $Kmin^{-1}$ for $[Fe_xMn_{1-x}(L_{222}N_3O_2)(CN)_2]\cdot H_2O$ with a) x = 0.966 and b) x = 0.949. Solid lines are added in order to follow the SCO properties. The measurements were performed first on cooling (1), then on warming (2). The control of the temperature variation rate in SQUID was accurately performed by using 'sweep mode'. The thermal spin crossover behavior was firstly investigated with a rate of 3 $Kmin^{-1}$ for the two metal diluted systems.

As compared to the SCO behavior of $[Fe(L_{222}N_3O_2)(CN)_2]\cdot H_2O$ (Figure II. 17), none of the two complexes present a clear HS to LS transition. Indeed, with a rate of 3 $Kmin^{-1}$ for x =

0.966 (Figure II. 28a), on the cooling mode, gradual transitions occur in the vicinity of 200 K - 160 K with a $T_{1/2}\downarrow$ around 180 K. The residual level at low temperature is very high. The $(\chi_M T)_{Fe}$ value of 3.2 $cm^3mol^{-1}K$ indicates that only 15% of the Fe(II) metal centers seems to be in LS state. On the warming mode, the magnetic signal first decreases in the vicinity of 130 K - 150 K reaching a $(\chi_M T)_{Fe}$ value 2.24 $cm^3mol^{-1}K$ (γ_{HS} = 0.60). Then it increases in the 150 K to 165 K up to $(\chi_M T)_{Fe}$ value of 2.07 $cm^3mol^{-1}K$ (γ_{HS} = 0.55). After reaching this maximum, the magnetic signal decreases and reaches a minimum at 200 K. Finally, the signal increases to the initial HS $(\chi_M T)_{Fe}$ value with $T_{1/2}\uparrow$ = 220 K.

For x = 0.949 with a rate of 3 $Kmin^{-1}$ on the cooling, the $(\chi_M T)_{Fe}$ value decreases about 0.1 $cm^3mol^{-1}K$ respectively in the vicinity of 250 K to 110 K. A very high HS residual is also observed at low temperature. On the warming mode, the magnetic product first decreasees in the vicinity of 110 K to 150 K, reaching a $(\chi_M T)_{Fe}$ value of 3.41 $cm^3mol^{-1}K$ (γ_{HS} = 0.91). Then the signal increases slightly in the vicinity of 150 K to 165 K, reaching a $(\chi_M T)_{Fe}$ value of 3.29 $cm^3mol^{-1}K$ (γ_{HS} = 0.88). After that the signal undergoes a second decrease in the vicinity of 165 K to 205 K and finally the signal increases to the initial HS value.

The magnetic properties of these two metal diluted complexes are very unusual. It seems that the insertion of Mn(II) ions strongly influenced the SCO properties of the $[Fe(L_{222}N_3O_2)(CN)_2]\cdot H_2O$. Metal diluted complexes exhibit incomplete SCO from HS state to LS state on cooling. Moreover, on warming those complexes display a decrease of $(\chi_M T)_{Fe}$ value in the vicinity of 150 K to 200 K, and the magnitude becomes more negligible with lower x value.

II.4.4. The influence of the cooling and warming rate on SCO properties

The influence of the rate of changing the temperature was investigated for two complexes with x = 0.966 and x = 0.949. The temperature dependence of $(\chi_M T)_{Fe}$ is presented in Figure II. 29 (x = 0.966) and Figure II. 30 (x = 0.949) with rate from 1 $Kmin^{-1}$ to 5 $Kmin^{-1}$.

a) Case of x = 0.966

For x = 0.966, with a rate of 1 $Kmin^{-1}$ (Figure II. 29a), the spin crossover is incomplete ($T_{1/2}\downarrow$ = 185 K, $T_{1/2}\uparrow$ = 220 K), with a hysteresis loop of 35 K. The $(\chi_M T)_{Fe}$ product at 150 K is equal to 1.98 $cm^3mol^{-1}K$ (γ_{HS} = 0.53). In regard to the pure $[Fe(L_{222}N_3O_2)(CN)_2]\cdot H_2O$ complex, this behavior can be attributed to the transition between HS state and the mixed HS/LS state. Only the width of the hysteresis is slightly reduced in regard to the pure complex (40 K) [40].

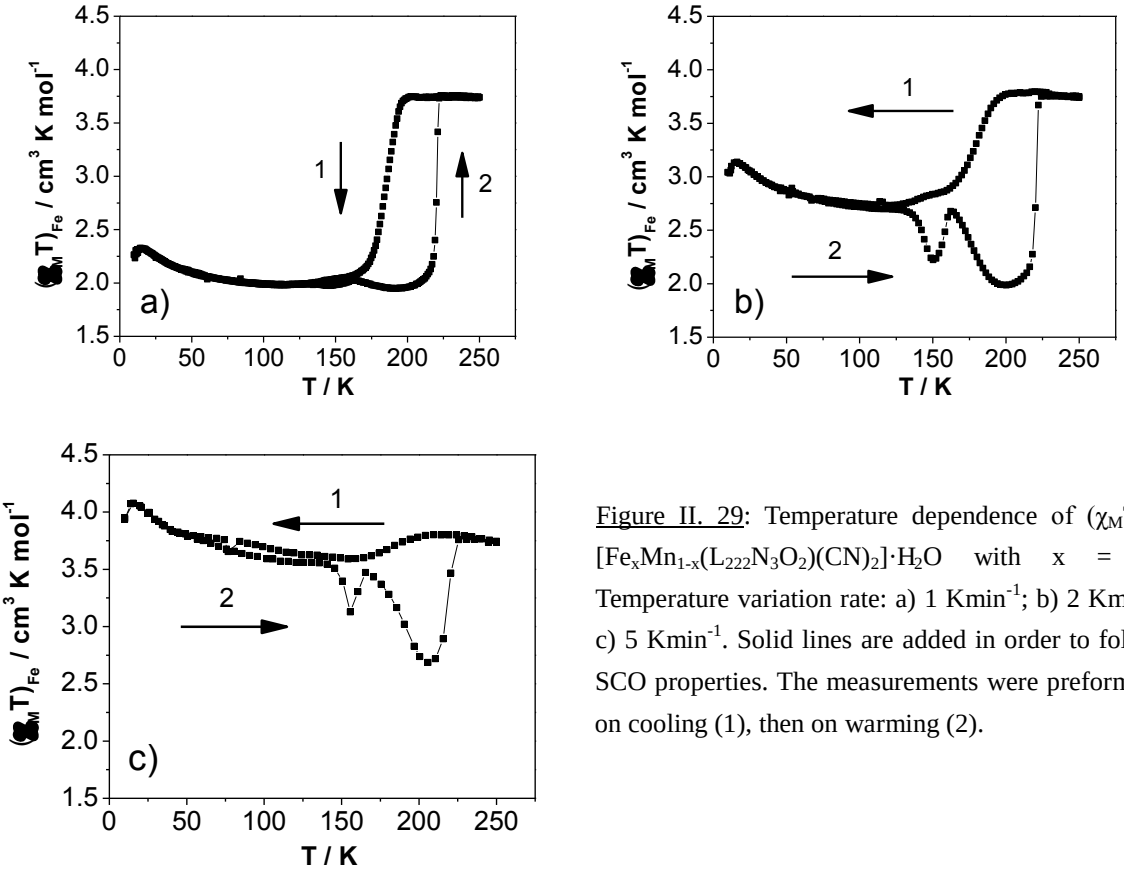

Figure II. 29: Temperature dependence of $(\chi_M T)_{Fe}$ for $[Fe_xMn_{1-x}(L_{222}N_3O_2)(CN)_2]\cdot H_2O$ with x = 0.966. Temperature variation rate: a) 1 Kmin^{-1}; b) 2 Kmin^{-1} and c) 5 Kmin^{-1}. Solid lines are added in order to follow the SCO properties. The measurements were preformed first on cooling (1), then on warming (2).

At a rate of 2 Kmin^{-1} (Figure II. 29b), the SCO behavior is similar with the one previously recorded at 3 Kmin^{-1} (Figure II. 28a). A gradual transition occurs in the vicinity of 200 K- 160 K with $T_{1/2}\downarrow$ = 179 K with a very high residue at 110 K (γ_{HS} = 0.72). On the warming mode, the magnetic signal display the bump and recover the initial HS $(\chi_M T)_{Fe}$ value at $T_{1/2}\uparrow$ = 220 K.

In the case of 5 Kmin^{-1} (Figure II. 29c), the magnetic signal slightly decreases on the cooling mode but remains almost in HS state even until 110 K (γ_{HS} = 0.98). On the warming mode, the magnetic behavior is similar to the rate of 2 Kmin^{-1} and 3 Kmin^{-1}, with the occurrence of a bump.

To summarize, the $[Fe_xMn_{1-x}(L_{222}N_3O_2)(CN)_2]\cdot H_2O$ complex with x = 0.966 presents a strong influence of the rate used for changing the temperature. With a rate of 1 Kmin^{-1}, the behavior is similar to the properties of the pure $[Fe(L_{222}N_3O_2)(CN)_2]\cdot H_2O$ in its second thermal cycle; i.e. a transition from HS state to HS/LS mixed state. With higher cooling rate, the HS state appears quenched. The SCO only occurs on the warming process at around 150 K and 200 K. With a rate of 3 Kmin^{-1}, the transition behavior of the diluted series is totally different from the pure $[Fe(L_{222}N_3O_2)(CN)_2]\cdot H_2O$ complex, which exhibits a complete HS to LS transition for the first thermal cycle.

b) Case of x = 0.949

For x = 0.949, with the cooling mode of 1 $Kmin^{-1}$ (Figure II. 30a), the magnetic signal first decreases down to 3.40 $cm^3mol^{-1}K$ (110 K, γ_{HS} = 0.91) and then remains stable. On the warming mode, the magnetic signal first decreases in the vicinity of 110 K to 150 K, reaching 1.85 $cm^3mol^{-1}K$ at 151 K (γ_{HS} = 0.49), then increases. A second decrease can be observed at 160 K, reaching a minimum of 2.93 $cm^3mol^{-1}K$ at 202 K (γ_{HS} = 0.78). Finally $(\chi_MT)_{Fe}$ value recovers the initial value of HS state. For 2 $Kmin^{-1}$ (Figure II. 30b), the magnetic behavior is very similar to results obtained with a cooling rate of 1 $Kmin^{-1}$. We observe the same bump on the warming mode with two minimum at 152 K with a value of 3.05 $cm^3mol^{-1}K$ (γ_{HS} = 8.16) and at 202 K with a value of 2.73 $cm^3mol^{-1}K$ (γ_{HS} = 0.73). For 5 $Kmin^{-1}$ (Figure II. 30c), the behavior is totally different. The magnetic signal remains stable during the cooling mode and the warming mode. The system remains in HS state.

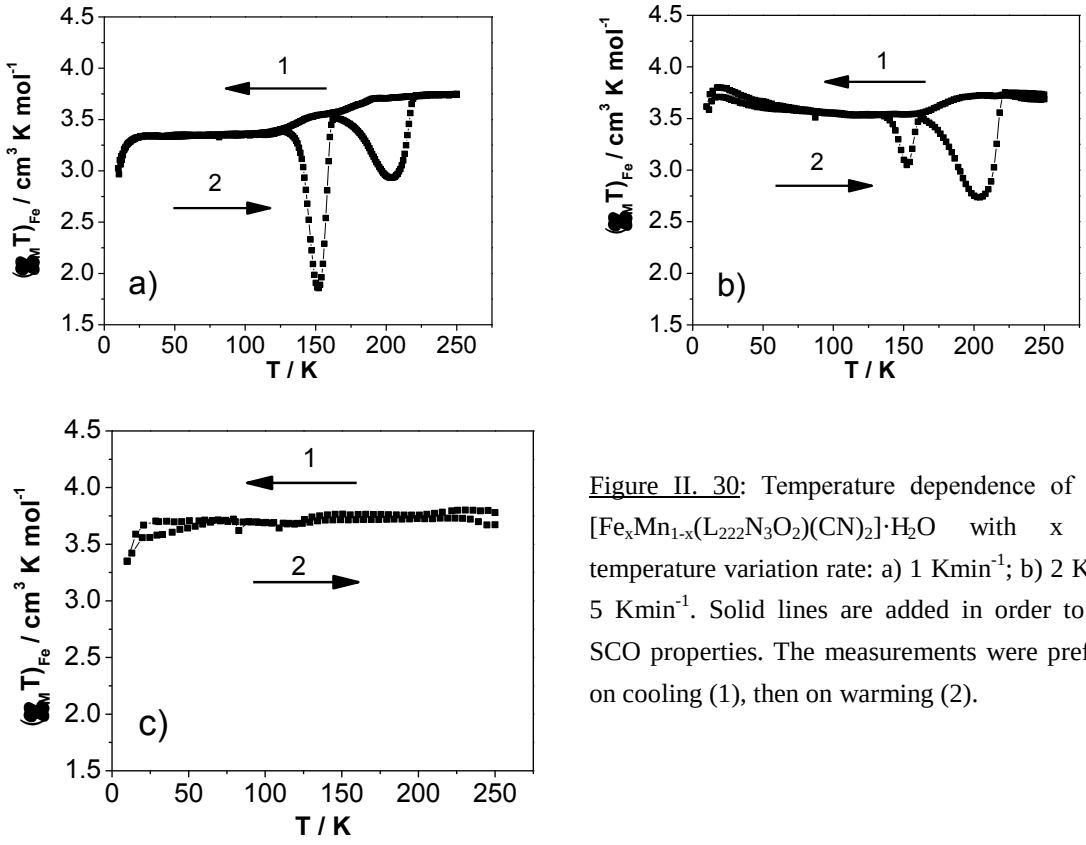

Figure II. 30: Temperature dependence of $(\chi_MT)_{Fe}$ for $[Fe_xMn_{1-x}(L_{222}N_3O_2)(CN)_2]\cdot H_2O$ with x = 0.949: temperature variation rate: a) 1 $Kmin^{-1}$; b) 2 $Kmin^{-1}$ and c) 5 $Kmin^{-1}$. Solid lines are added in order to follow the SCO properties. The measurements were preformed first on cooling (1), then on warming (2).

In regard to x = 0.966 (Figure II. 29) and the pure Fe(II) complex (Figure II. 15), the insertion of Mn(II) ions with x = 0.946 into the lattice strongly affects the SCO properties. If we consider for instance a constant cooling rate of 1 $Kmin^{-1}$, the metal diluted complex (x = 0.949) displayed a very high HS residual fraction (Figure II. 30a), while for x = 1 (Figure II. 15) and x = 0.966 (Figure II. 29a), a HS to HS/LS mixed state transition can be observed. This tendency is confirmed at a rate of 5 $Kmin^{-1}$, where no transition can be observed for x = 0.949. It seems that by increasing the percentage of the Mn(II) ions, the kinetics of the SCO phenomenon is slowed down. We have then decided to investigate the SCO properties at a rate of 0.5 $Kmin^{-1}$ on the complex x = 0.949.

Figure II. 31 presents the temperature dependence of $(\chi_M T)_{Fe}$ for x = 0.949 with a cooling rate of 0.5 $Kmin^{-1}$. The complex presents two-step SCO behavior with a first step from 200 K to 160 K, where the $(\chi_M T)_{Fe}$ value decreases from 3.74 to 2.45 $cm^3mol^{-1}K$ (γ_{HS} = 0.66). The second step appears after 150 K, reaching a $(\chi_M T)_{Fe}$ value of 2.02 $cm^3mol^{-1}K$ at 120 K (γ_{HS} = 0.54). On warming, two steps are observed at respectively 160 K and 210 K. It seems consequently that by using a cooling rate of 0.5 $Kmin^{-1}$, we have approached the transition between HS state and HS/LS mixed state. Of course, we can decide to futher use a lowest rate of cooling. Nevertheless, in regard to the time and helium, such experiment was not performed with our SQUID equipment.

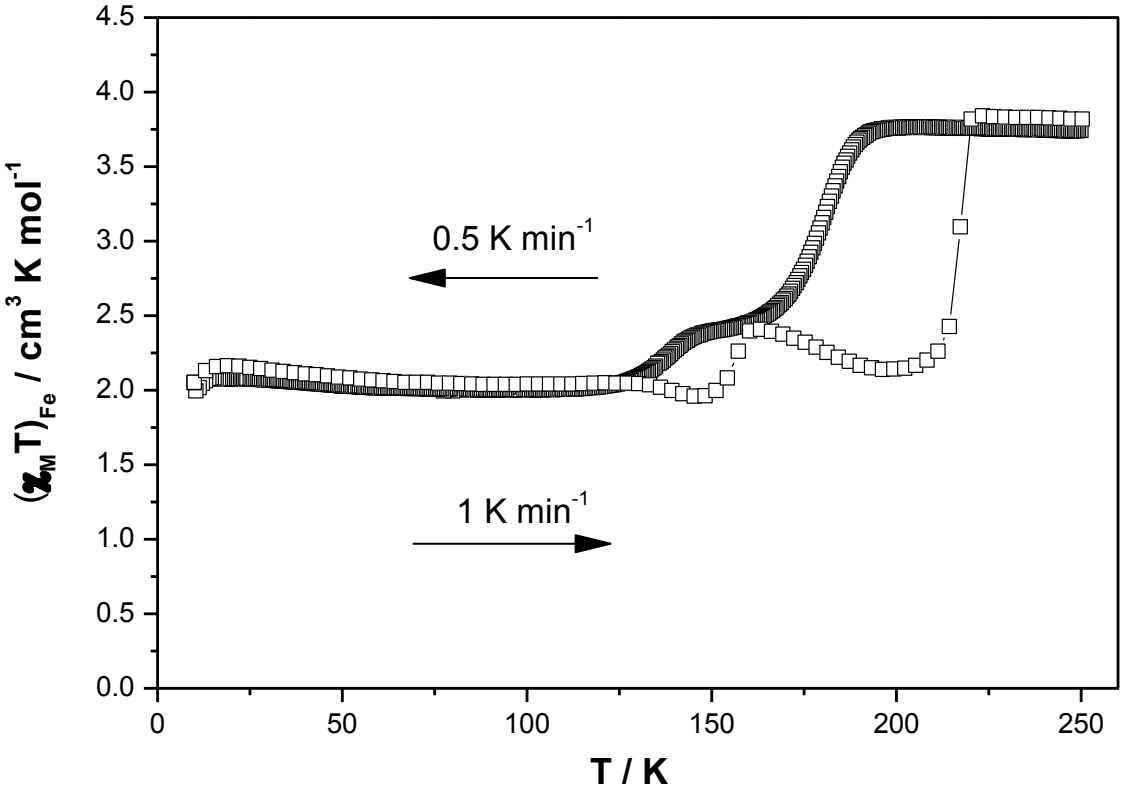

Figure II. 31: Temperature dependence of $(\chi_M T)_{Fe}$ for $[Fe_xMn_{1-x}(L_{222}N_3O_2)(CN)_2]\cdot H_2O$ with x = 0.949 on cooling to 10 K (0.5 $Kmin^{-1}$) and on warming to 250 K (1 $Kmin^{-1}$).

c) Concluding remarks

To sum up, the magnetic behavior of $[Fe_xMn_{1-x}(L_{222}N_3O_2)(CN)_2]\cdot H_2O$ series is totally different from the pure $[Fe(L_{222}N_3O_2)(CN)_2]\cdot H_2O$ complex. Several remarks can be done:

i) On the first cooling experiment for none of the metal diluted complexes, it was possible to record the HS to LS transition. It seems that the insertion of Mn(II) ions tends to block the phase transition between the seven-coordinated structure (HS state) to the pure six-coordinated structure (LS state), and favors the transition toward the HS/LS mixed state.

ii) For most of the measurements, on warming, $(\chi_M T)_{Fe}$ vs.T curve displays two minima

at almost the same temperatures. Only the proportion is changed as function of the metal dilution.

iii) The insertion of Mn(II) metal ions seems to strongly affect the kinetic of the SCO process. When the metal dilution increase, it is necessary to decrease the cooling rate for observing the SCO phenomenon. In other words, the lower rate applied, the higher possibility to reach the HS/LS mixed state was obtained, while the higher rate applied, the higher possibility to quench the complex was obtained.

II.4.5. Quenching effect in metal diluted $[Fe_xMn_{1-x}(L_{222}N_3O_2)(CN)_2]\cdot H_2O$ series

a) Case of x = 0.966

For x = 0.966 two quenching experiments are performed. On the first experiment the magnetic signal is recorded immediately after trapping with a warming rate of 1 $Kmin^{-1}$ (Figure II. 32a). The complex is in the metastable HS state up to 120 K and then in a few kelvins the $(\chi_MT)_{Fe}$ product drops drastically (position 2, Figure II. 32a) to reach a minimum $(\chi_MT)_{Fe}$ value at 148 K (0.59 $cm^3mol^{-1}K$). This $(\chi_MT)_{Fe}$ product remains stable when temperature was cooled back to 10 K (position 3). On the contrary, when the temperature overpass 150 K, the magnetic signal increases for reaching a maximum at 163 K (3.44 $cm^3mol^{-1}K$) then decrease down to 205 K (2.00 $cm^3mol^{-1}K$). A subsequent 1 hour kinetic experiment at 205 K did not further decreased the χ_MT value (position 5). The value remains even stable when temperature was further varied in the vicinity of 205 K – 10 K. From 205 K to 230 K the magnetic signal keeps increasing with a $T_{1/2}\uparrow$ = 220 K.

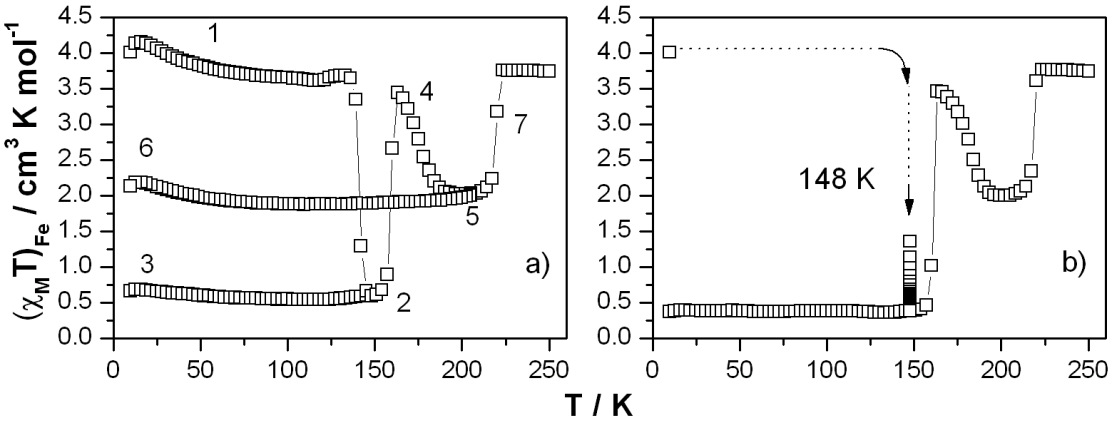

Figure II. 32: Temperature dependence of $(\chi_MT)_{Fe}$ for $[Fe_xMn_{1-x}(L_{222}N_3O_2)(CN)_2]\cdot H_2O$ with x = 0.966 in trapping measurement: a) measurement started from 10 K. The numbering has been added to follow sequence of the measurement; b) kinetic at 148 K. Solid lines and dashed lines are added in order to follow the SCO behavior.

The second set of experiment performed on x = 0.966 (Figure II. 32b) consists of trapping the sample at 10 K, in its 100% metastable HS state, and to record the kinetic at 148

K during 4 hours. During the first hour, the $(\chi_M T)_{Fe}$ product strongly decreases to reach a value of 0.38 $cm^3mol^{-1}K$ and then remains almost stable in the next 3 hours. Subsequent experiment by cooling temperature down to 10 K illustrated that this value is stable. From 148 K to 250 K the magnetic behavior seems to be similar with the first trapping experiment in Figure II. 32a i.e. the formation of a maximum (position 4) and a minimum (position 5) before coming back to room temperature (HS state).

b) Case of x = 0.946

Concerning the complex $[Fe_xMn_{1-x}(L_{222}N_3O_2)(CN)_2]\cdot H_2O$ with x = 0.949 (Figure II. 33) quenching experiments followed by heating with a warming rate of 1 $Kmin^{-1}$ were also performed. The first set of measurement corresponds to a quenching from 10 K (Figure II. 33a), and the second to study the relaxations at some selected temperature after trapping (Figure II. 33b).

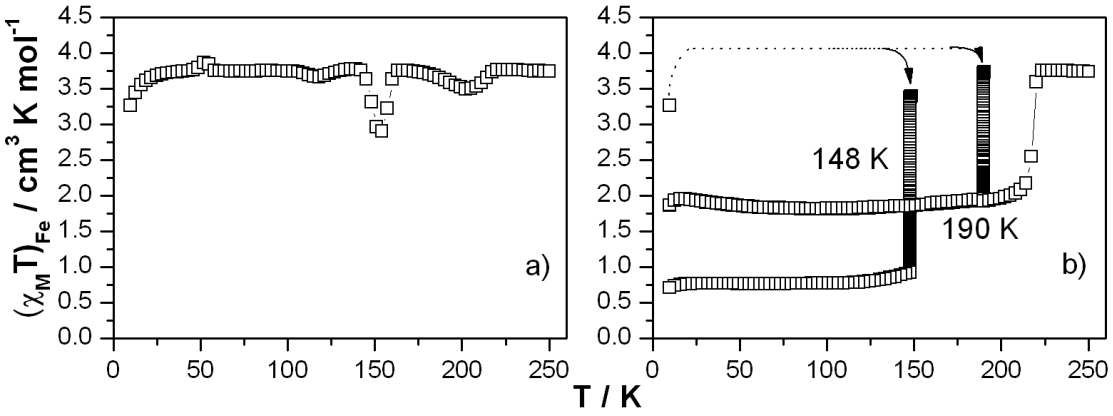

Figure II. 33: Temperature dependence of $(\chi_M T)_{Fe}$ for $[Fe_xMn_{1-x}(L_{222}N_3O_2)(CN)_2]\cdot H_2O$ with x = 0.949 in trapping measurement with a rate of 1 $Kmin^{-1}$: a) measurement started from 10 K; b) kinetics at 148 K and 190 K. Solid lines and dashed lines are added in order to follow the SCO properties.

From Figure II. 33a, it appears that under quenching at 10 K, the pure metastable HS state is populated. Then, the $(\chi_M T)_{Fe}$ value only slightly decreases from 3.77 $cm^3mol^{-1}K$ at 140 K to 2.90 $cm^3mol^{-1}K$ at 154 K, suggesting a partial SCO of about 23%. After that, the magnetic signal increases immediately to reach a $(\chi_M T)_{Fe}$ value of 3.75 $cm^3mol^{-1}K$ at 163 K. A very small decrease can be observed at around 160 K up to 202 K. Finally, the signal recovers its initial value.

The Figure II. 33b reports the results of the kinetics performed at 148 K and 190 K after trapping. It reveals that the LS state and the mixed HS/LS state are totally masked and can be in fact reached by performing some relaxation at selected temperature. Along that at 148 K, after a kinetic of about 6 hours, the relaxation saturates to a $(\chi_M T)_{Fe}$ value of 0.91 $cm^3mol^{-1}K$ (Figure II. 34). On cooling the $(\chi_M T)_{Fe}$ value reaches 0.76 $cm^3mol^{-1}K$ at around 100 K and then remains stable, which indicate the population of the LS state. At 190 K, the relaxation

after quenching was recorded during 9 hours. The $(\chi_M T)_{Fe}$ value saturates at a value of 1.93 $cm^3mol^{-1}K$ (Figure II. 34). Further cooling indicates an absence of any transition while on the on the warming mode, a $T_{1/2}\uparrow$ = 217 K is obtained in agreement with the population of the HS/LS mixed state.

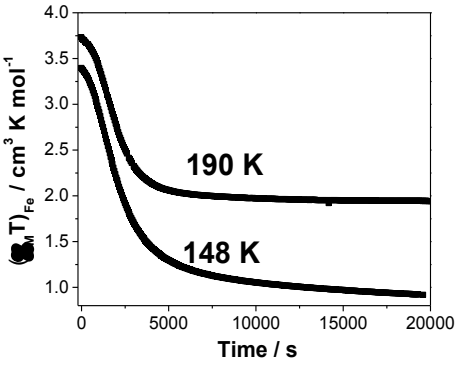

Figure II. 34: Relaxation recorded at 148 K and 190 K for complex $[Fe_xMn_{1-x}(L_{222}N_3O_2)(CN)_2]\cdot H_2O$ with x = 0.949.

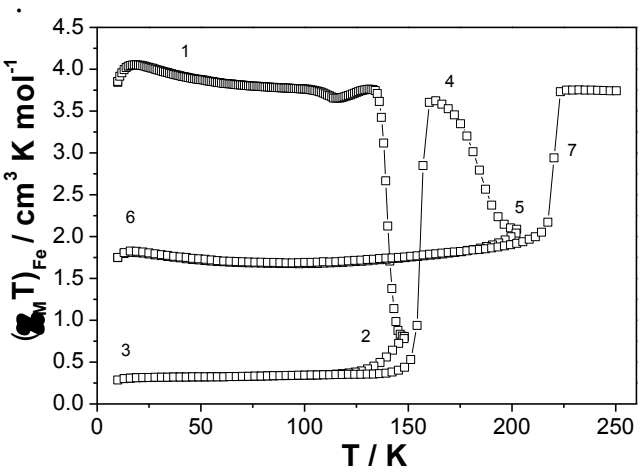

Figure II. 35: Temperature dependence of $(\chi_M T)_{Fe}$ for $[Fe_xMn_{1-x}(L_{222}N_3O_2)(CN)_2]\cdot H_2O$ with x = 0.949 for trapping measurement with a rate of 0.3 $Kmin^{-1}$. The numbering has been added to follow the route of the measurement.

From these series of results, it seems evident that kinetic effect controls the access of the LS and HS/LS state on the metal diluted x = 0.949. We have then decided to perform a new trapping at 10 K and to record the T(TIESST) curve with a rate of 0.3 $Kmin^{-1}$. The temperature dependence of $(\chi_M T)_{Fe}$ is presented in Figure II. 35. A T(TIESST) of 139 K is obtained. The shape of the curve is really reminiscent of the data observed with x = 0.966 (Figure II. 33a). All that confirms that the transition behavior of the diluted series $[Fe_xMn_{1-x}(L_{222}N_3O_2)(CN)_2]\cdot H_2O$ with x = 0.966 and x = 0.949 is highly depend on the temperature variation rate. The LS state can be reached only when rapid cooling is applied (100 % metastable HS state at 10 K). On the contrary, the mixed HS/LS state is reached by using a relatively low cooling rate.

II.4.6. Temperature regime of LS state and mixed HS/LS state in metal diluted series

To complete this analysis, we have performed TIESST measurements for a selection of metal diluted complex with x = 1, 0.949, 0.93, 0.912, 0.892 and 0.853. Temperature dependence of $(\chi_M T)_{Fe}$ is presented in Figure II. 36 and Table II. 10 collects the characteristic values.

a) TIESST measurement

Whatever the metal dilution, a first HS state (i.e HS_1) is obtained at 10 K, which corresponds to the metastable HS state obtained by quenching. On warming from 10 K, a decrease of magnetic signal is obtained in the vicinity of 130 K to 150 K. For convenience, we propose to name this state LS_1. The increase of Mn(II) percentage appears to rise the residual HS fraction as illustrated by the $(\chi_M T)_{Fe}$ value of LS_1. When the temperature is further increase up to 170 K, a new increase of the magnetic signal happens. We named the maximum HS_2. After that, the magnetic signal decreases to reach a minimum at around 205 K. In regard to the pure $[Fe(L_{222}N_3O_2)(CN)_2]\cdot H_2O$ we propose to name this state LS_2/HS_3. Similarly to what has been observed for the LS_1 state, the minimum $(\chi_M T)_{Fe}$ of LS_2/HS_3 also increases significantly with a increase of Mn(II) percentage (Table II. 10). Finally at around 220 K, the $(\chi_M T)_{Fe}$ value increases to recover its initial HS_4 value.

Sample	$(\chi_M T)_{Fe}$ at 148 K (LS_1)	$(\chi_M T)_{Fe}$ at 202 K (LS_2/HS_3)
x = 1	0.23	2.02
x = 0.949	0.71	2.16
x = 0.93	3.24	3.10
x = 0.912	3.59	3.42
x = 0.892	3.72	3.57
x = 0.853	3.72	3.72

Table II. 10: Minimum $(\chi_M T)_{Fe}$ value ($cm^3mol^{-1}K$) obtained in LS_1 and LS_2/HS_3 for different samples.

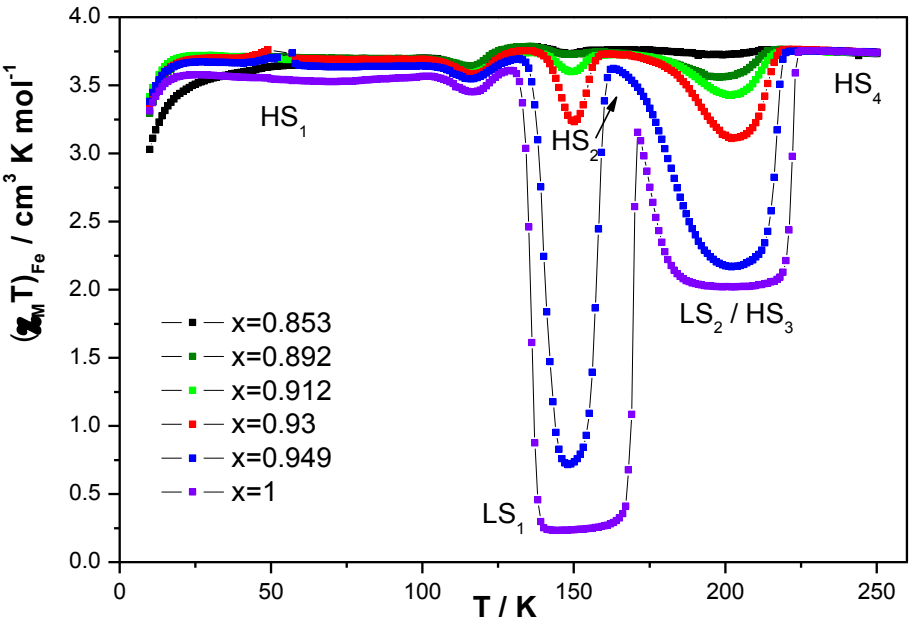

Figure II. 36: Temperature dependence of $(\chi_M T)_{Fe}$ for $[Fe_xMn_{1-x}(L_{222}N_3O_2)(CN)_2]\cdot H_2O$ of T(TIESST) experiment with x = 1 (in violet ■), 0.949 (in blue ■), 0.93 (in red ■), 0.912 (in green ■), 0.892 (in olive ■) and 0.853 (in black ■).

Several comments can be made:

i) Compared with the pure Fe(II), for all the metal diluted complexes, HS_1 and HS_4 are associated with the Phase B* and Phase A of the pure Fe(II) respectively. Attention has to be paid on the complex $[Fe_xMn_{1-x}(L_{222}N_3O_2)(CN)_2]\cdot H_2O$ with x = 0.853, which remains HS from 10 K to 250 K. In this case HS_1 and HS_4 can not be distinguished.

ii) The LS_1 of the metal diluted complexes is associated with Phase B of pure Fe(II). We noticed an important increase of the $\chi_M T$ product of the LS_1 with the metal dilution. This can be understood by the previous works performed on the well-know dilution series [27-32], where complexes with Mn(II) metal dilution favor the HS state.

iii) The LS_2/HS_3 in metal diluted system is associated with the Phase C of the pure iron complex (Figure II. 17). Similarly with LS_1, the LS_2/HS_3 is under the strong influence of dilution effect.

b) Phase diagram

Upon the TIESST experiments with a warming rate of 0.3 $Kmin^{-1}$, five characteristic temperatures for different Mn(II) percentage can be obtained. With an increase of temperature, those important temperatures appear in the following order (Figure II. 37): T(TIESST); T 1: where 50 % of LS_1 transits to HS_2; T 2: where obtain the maximum $(\chi_M T)_{Fe}$ value of HS_2 in between LS_1 and the mixed LS_2 / HS_3; T 3, where obtains 50 % transition of LS_2/HS_3; and $T_{1/2}\uparrow$. The values of those temperatures are listed in Table II. 11 .

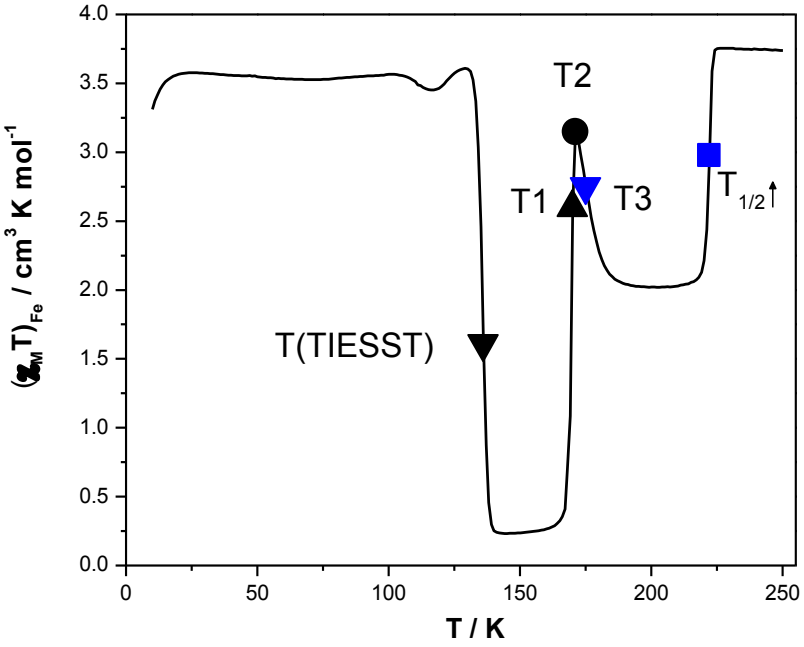

Figure II. 37: Illustration of the five characteristic temperatures on a T(TIESST) curve.

Sample	T(TIESST) / K	T 1 / K	T 2 / K	T 3 / K	$T_{1/2}\uparrow$ / K
x = 1	136	170	171	175	222
x = 0.949	140	158	163	182	217
x = 0.93	146	154	160	191	214
x = 0.912	145	153	157	191	212
x = 0.892	-	-	-	-	211
x = 0.853	-	-	-	-	-

Table II. 11: Seven important temperatures obtained during TLIESST experiment.

From x = 1 to x = 0.912, the five characteristic temperatures can be determined. For x = 0.892, since the sample stays almost in HS state during the TIESST measurement, only the $T_{1/2}\uparrow$ temperature can be barely determined. For x = 0.853, none of the five temperatures are obtained. With this series of characteristic temperatures, we built the phase diagram presented on Figure II. 38.

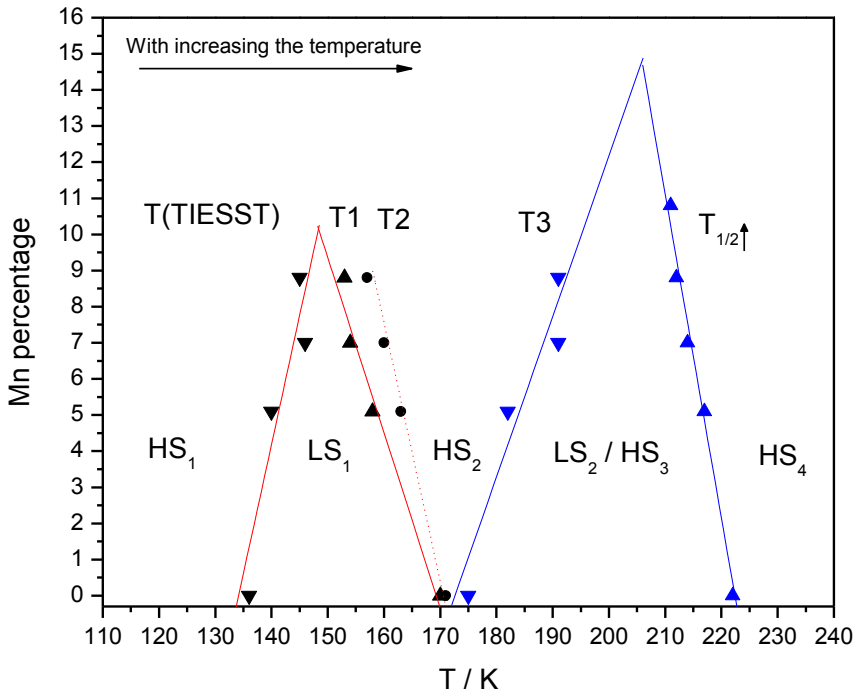

Figure II. 38: Phase diagram: characteristic temperatures for different Mn(II) percentage. ▼ T(TIESST); ▲ Temperature 1, ● Temperature 2; ▼ Temperature 3, and ▲ $T_{1/2}\uparrow$. Solid and dotted lines in red and blue are the linear fit of the corresponding temperatures.

Interestingly, the various characteristic temperatures indeed can be well fitted with a linear relation as a function of Mn(II) percentage. T(TIESST) and T1 define the regime where LS_1 can be obtained. T3 and $T_{1/2}\uparrow$ give the regime where the LS_2/HS_3 is formed. The linear fit of T(TIESST) and T1 meet at round 10.2 % Mn(II). In other words, above this percentage, the LS_1 could not be obtained. This is in perfect agreement with experimental result of the complex with x = 0.89, where the LS_1 can not be reached during the TIESST measurement (Figure II. 36). For LS_2/HS_3, the meeting point is predicted at 14.8 % of Mn(II). However at x = 0.892, the experiment results already show that the LS_2/HS_3 is barely observed.

Chapter II.5. Probing the hidden HS to LS_2/HS_3 state transition

II.5.1. The possibility of a hidden HS to LS_2/HS_3 state transition in the dilution system

In Chapter II.4, we have observed that the SCO properties of the metal diluted complex are strongly influenced by the kinetic effect. In consequence, the transition between HS and LS_2/HS_3 states can be hidden if we consider the sample with x = 0.892. For this reason, we have decided to investigate in more detail the hidden transition, i.e. to probe by thermal relaxation and/or light irradiation to study whether the predicted HS to LS_2/HS_3 transition may appear.

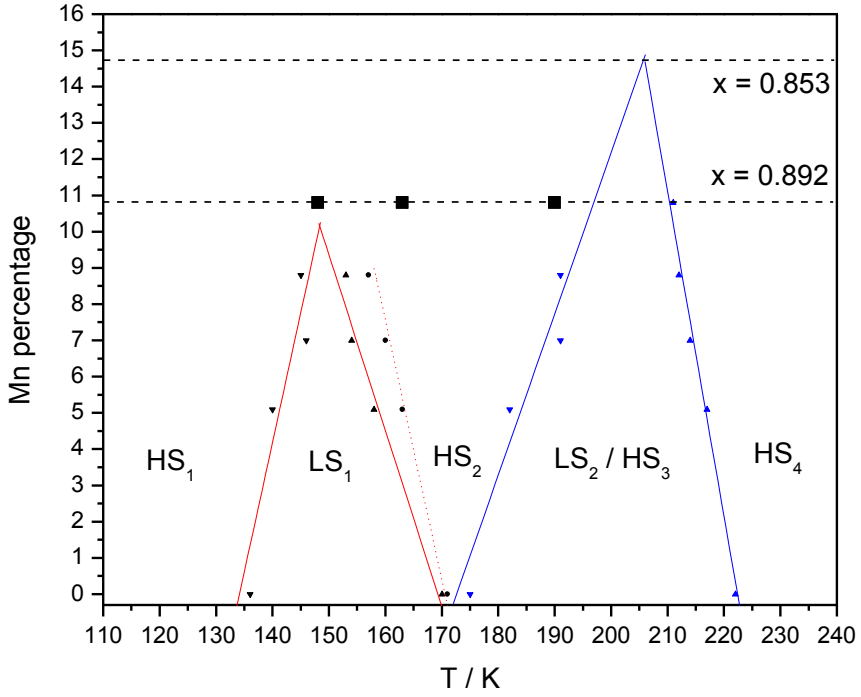

Figure II. 39: Phase diagram of the metal diluted complexes. Dashed line in black: illustration for x = 0.892 and 0.853 samples. In black ■: the selected temperatures (190 K, 163 K and 148 K) for investigation of the kinetic effect on the corresponding states.

We will first focus on the x = 0.892 sample to perform the thermal relaxation experiment at different temperature. The selected temperatures for relaxation are 190 K (i.e. at the vicinity of the LS_2/HS_3 state), 163 K (close to the HS_2 state), 148 K (i.e. LS_1 state) and 105 K (in the HS_1 regime)

II.5.2. Thermal relaxation to probe the hidden transition

The first selected temperature for thermal relaxation is 190 K. The sample with x = 0.892 was quenched as 190 K, and then kinetics was recorded. However, only after 2 hours, the magnetic product saturates at a $(\chi_M T)_{Fe}$ value of 3.6 cm^3 K mol^{-1} (Figure II. 40 in violet ■), which indicates that less than 4 % of the Fe(II) ions involve in a HS to LS_2/HS_3 state transition.

For other selected temperatures (163 K, 148K and 105 K) the thermal relaxation was also recorded for 2 hours. Similar with what has been observed at 190 K, the sample remains in HS state after relaxation (Figure II. 40).

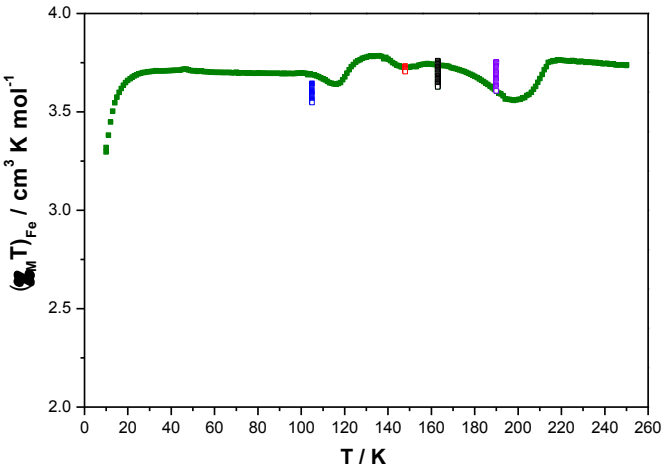

Figure II. 40: Kinetics experiment of $[Fe_xMn_{1-x}(L_{222}N_3O_2)(CN)_2]\cdot H_2O$ with x = 0.892 at different temperature for 2 hours (190 K in violet ■, 163 K in black ■, 148 K in red ■ and 105 K in blue ■). In green ■: TIESST experiment for comparison.

Figure II. 41 presents two cooling and warming experiment after kinetics at 163 K. For the first one, the sample with x = 0.892 was quenched directly at 163 K, and then a kinetics was recorded for 2 hours. After the kinetics, the sample was cooled to 10 K (Figure II. 41a). The $(\chi_M T)_{Fe}$ value remains stable at ca. 3.6 cm^3 K mol^{-1} in between 10 K and 200 K upon cooling. For the second experiment, the sample was quenched at 163 K and kinetics was recorded at 163 K for 2 hours. Then, the sample was warmed to 250 K. Between 163 K and 200 K, a decrease of $(\chi_M T)_{Fe}$ value can be observed. The minimum $(\chi_M T)_{Fe}$ value is ca. 3.4 cm^3 K mol^{-1} at around 190 K. It seems consequently that after the relaxation at 163 K, a partial HS to LS_2/HS_3 transition tends to take place upon warming, while upon cooling the sample remains almost in HS state.

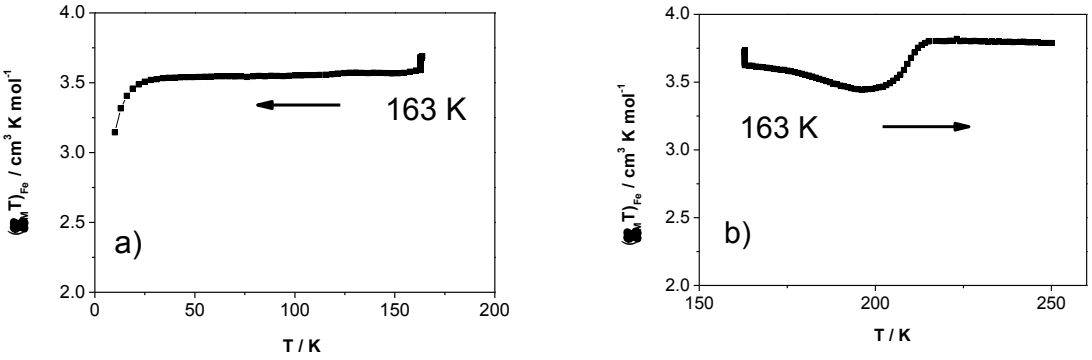

Figure II. 41: a) cooling and b) warming measurements of $[Fe_xMn_{1-x}(L_{222}N_3O_2)(CN)_2]\cdot H_2O$ with x = 0.892 after 2 hours kinetics at 163 K. Temperature variation rate:1 $Kmin^{-1}$.

II.5.3. The effect of thermal relaxation at 163 K

To investigate the effect of thermal relaxation at 163 K on the HS to LS_2/HS_3 transition, two sets of experiments are performed on a fresh sample with x = 0.892. For the first set, magnetic product is recorded during thermal cycles until selected temperatures (Figure II. 42): i.e. cycle from 250 K, down to 190 K (in black ■), to 163 K (in red ■) and to 148 K (in wine ■). During the thermal cycle between 250 K and 190 K, the complex remains in HS state, while on thermal cycle between 250 K and 163 K, a certain fraction of LS_2/HS_3 can be populated. This proportion increases by cooling down to 148 K.

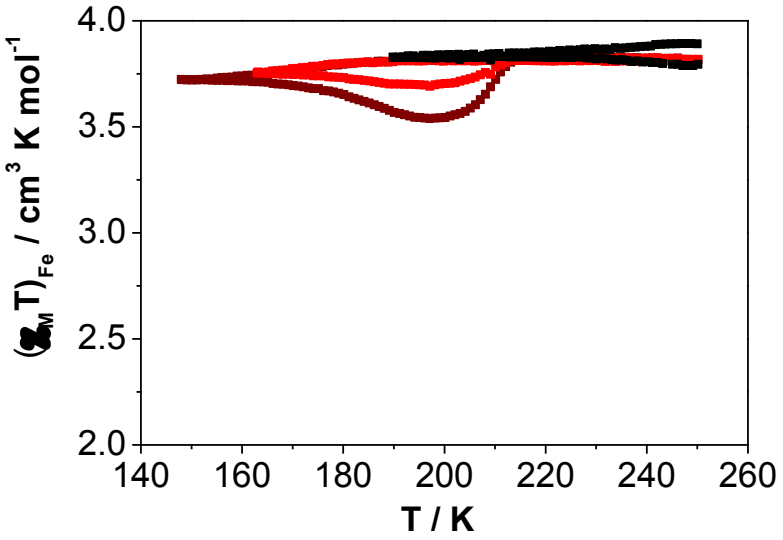

Figure II. 42: Temperature dependence of $(\chi_M T)_{Fe}$ for $[Fe_xMn_{1-x}(L_{222}N_3O_2)(CN)_2]\cdot H_2O$ with x = 0.892. Measurements were all performed with a rate of 1 $Kmin^{-1}$. Cooling from 250 K to 190 K (in black ■), 163 K (in red ■) and 148 K (in wine ■) then warming to 250 K.

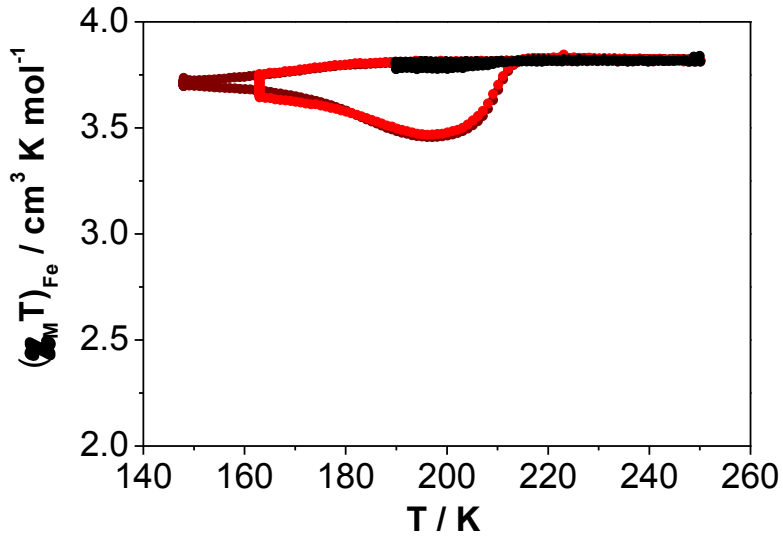

Figure II. 43: Temperature dependence of $(\chi_M T)_{Fe}$ for $[Fe_xMn_{1-x}(L_{222}N_3O_2)(CN)_2]\cdot H_2O$ with x = 0.892. Measurements were all performed with a rate of 1 $Kmin^{-1}$. Cooling from 250 K to 190 K (in black ●), 163 K (in red ●) and 148 K (in wine ●) followed by 2 hours kinetics at those temperatures, then warming to 250 K.

In the second set of experiment, the protocol is slightly different: relaxation of 2 hours was added after each cooling (Figure II. 43). For the thermal cycle down to 190 K, the addition of a kinetic of 2 hours induced no change. The HS fraction remains. For the thermal cycle down to 163 K, the addition of a kinetic increases the percentage of relaxation towards

the LS_2/HS_3 state. Interestingly, the addition of a kinetic on the thermal cycle down to 148 K induces no difference in regard to the curve recorded at 163 K.

II.5.4. An effective thermal treatment for the HS to LS_2/HS_3

Figure II. 44 presents the thermal treatment for the HS to LS_2/HS_3 transition in the metal diluted complex $[Fe_xMn_{1-x}(L_{222}N_3O_2)(CN)_2]\cdot H_2O$ with x = 0.892. The procedure is the following: a first thermal relaxation at 163 K is recorded for 2 hours, and then temperature is increased to 190 K with a rate of 0.3 $Kmin^{-1}$, following by a second thermal relaxation recorded at 190 K for 2 hours (position 1), after that, the system is cooled down to 10 K (position 2) then warmed to 250 K (position 3).

After the first relaxation at 163 K, the magnetic product slightly decreases to ca. 3.6 $cm^3mol^{-1}K$ ($\gamma_{HS} \approx 0.96$), which is in agreement with the above observation. Upon warming to 190 K, the magnetic product decreases to 3.27 $cm^3mol^{-1}K$, indicating that around 13 % of the Fe(II) ions involve the SCO. During the relaxation treatment at 190 K, the magnetic product decreases down to 2.48 $cm^3mol^{-1}K$ ($\gamma_{HS} \approx 0.66$). By lowering the temperature, the $(\chi_MT)_{Fe}$ product at 100 K is equal to 2.1$cm^3mol^{-1}K$, which indicates that around 44% of the Fe(II) ions center undergo the SCO. Upon warming at position 3, the $(\chi_MT)_{Fe}$ value recovers its initial value with $T_{1/2}\uparrow$ of 214 K.

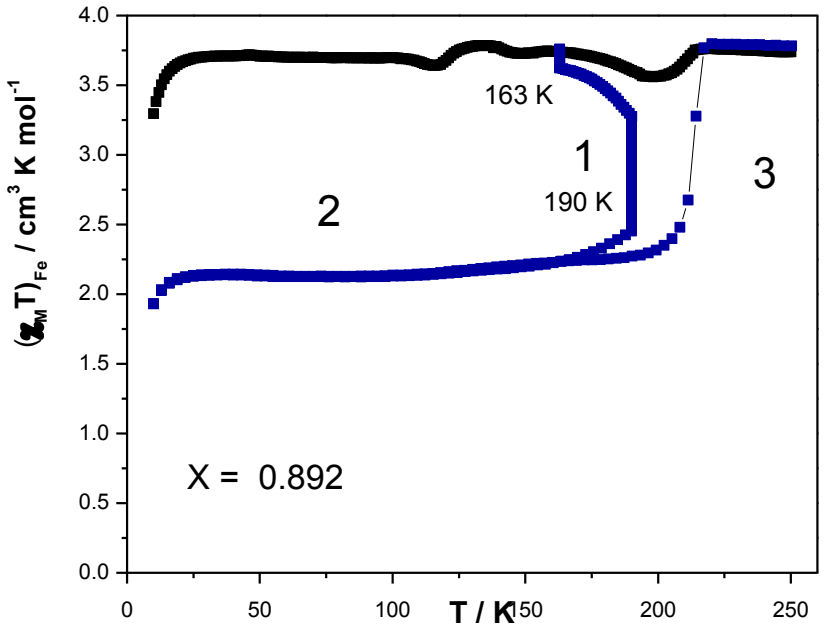

Figure II. 44: Temperature dependence of $(\chi_MT)_{Fe}$ for $[Fe_xMn_{1-x}(L_{222}N_3O_2)(CN)_2]\cdot H_2O$ with x = 0.892. TIESST measurements are presented in black ■. Thermal treatment procedure is presented in blue ■. The procedure follows the digital sequence from 1 to 3.

The above thermal treatment procedure is then used to probe the HS to LS_2/HS_3 state on

other metal diluted $[Fe_xMn_{1-x}(L_{222}N_3O_2)(CN)_2]\cdot H_2O$ samples. Figure II. 45 presents the temperature dependence of $(\chi_M T)_{Fe}$ for the selected metal diluted complexes with x = 0.930, x = 0.912 and x = 0.853. For these three complexes, the transition behavior is similar with the above x = 0.892, the only difference is the HS residue at low temperature after the thermal treatment, which in general rises with an increase of Mn(II) percentage.

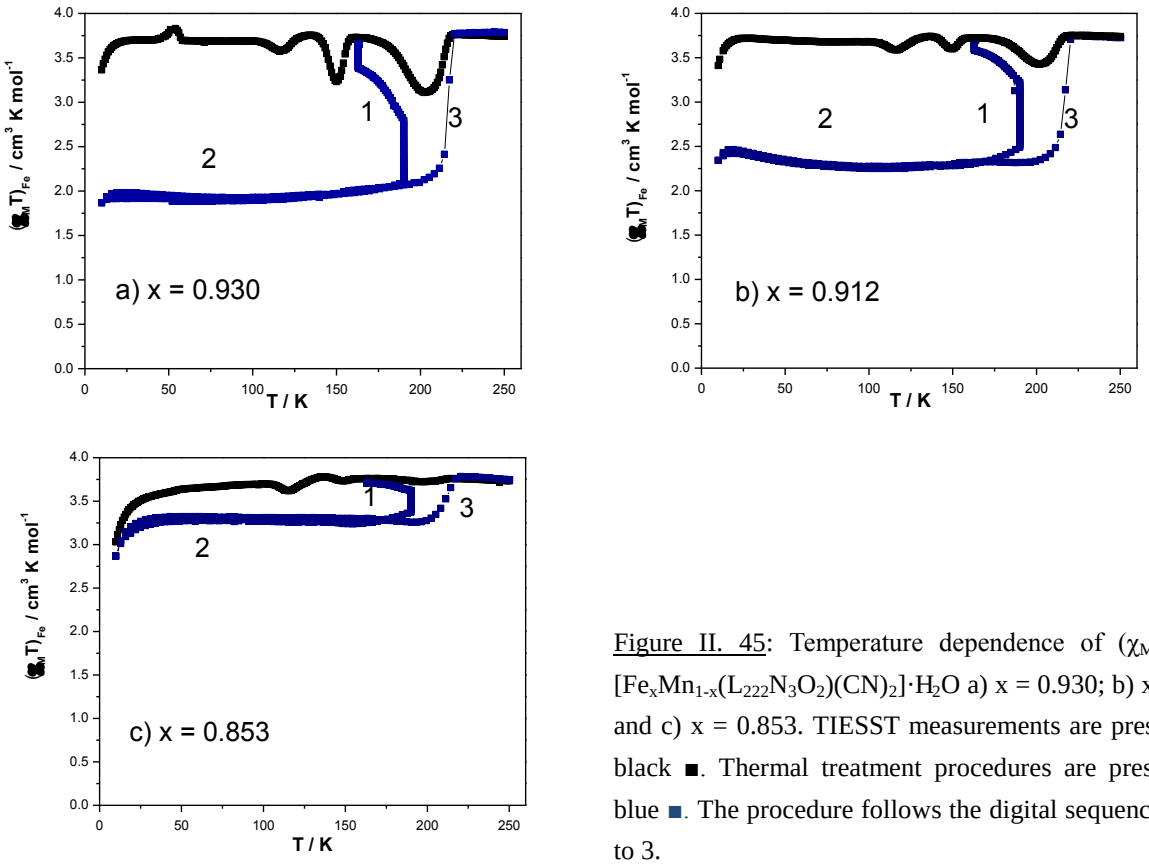

Figure II. 45: Temperature dependence of $(\chi_M T)_{Fe}$ for $[Fe_xMn_{1-x}(L_{222}N_3O_2)(CN)_2]\cdot H_2O$ a) x = 0.930; b) x = 0.912; and c) x = 0.853. TIESST measurements are presented in black ■. Thermal treatment procedures are presented in blue ■. The procedure follows the digital sequence from 1 to 3.

Several comments can be made:

i) The relaxation at 160 K in the thermal treatment protocol is essential to introduce the SCO to the LS_2/HS_3 state. In more detail, for instance the complex with x = 0.892, without a pretreatment at 160 K, the $(\chi_M T)_{Fe}$ value obtained at 190 K is 3.6 cm^3 K mol^{-1} (Figure II. 40); after the relaxation at 160 K, the γ_{HS} is 0.66, indicating around 40 % Fe(II) ions involve in the SCO (Figure II. 44).

ii) Before and after the relaxation at 160 K, the metal diluted complexes, for instance x = 0.892, remain in HS state. From the phase diagram (Figure II. 39), the temperature of 160 K is indeed in the HS_2 regime. Thus possibly during the relaxation, a transition from the thermally quenched HS state to the HS_2 state occurs. Consequently, the observed SCO to the mixed state is indeed a HS_2 to LS_2/HS_3 transition.

iii) The complex with x = 0.853 is at the border line of the LS_2/HS_3 regime in the phase

diagram, which predicts that the LS_2/HS_3 state can be barely obtained. After the thermal treatment, a partial SCO to the LS_2/HS_3 state is observed (Figure II. 45c), which is indeed in perfect agreement with the prediction from the phase diagram.

II.5.5. Light irradiation and thermal treatment on layer sample

a) Thermal treatment on layer sample

From the phase diagram, it is observed that the complex with x = 0.892 (Figure II. 39) is close to the LS_1 regime. However, the LS_1 can be reached neither from the metastable HS_1 state nor the thermal SCO transition. We have then decided to investigate if the application of light irradiation may allow to reach the LS_1 state. For the irradiation experiment, usually the sample is prepared as a thin layer of around 0.3 mg, which is attached on adhesive tape. Since it is a different preparation method, before the application of light we firstly investigate the thermal treatment on layer sample.

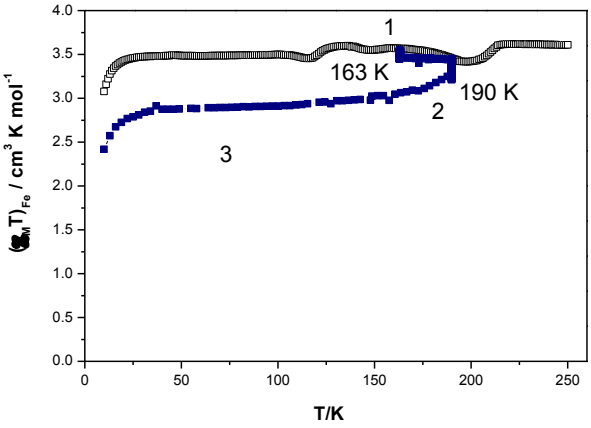

Figure II. 46: Temperature dependence of $(\chi_M T)_{Fe}$ for layer sample of $[Fe_xMn_{1-x}(L_{222}N_3O_2)(CN)_2]\cdot H_2O$ complex with x = 0.892. TIESST measurements are presented in black ■. Thermal treatment procedure is presented in blue ■. The procedure follows the sequence from 1 to 3.

Figure II. 46 presents the $(\chi_M T)_{Fe}$ product of a layer sample with x = 0.892 following the same thermal treatment which was performed to probe the LS_2/HS_3 state on the bulk sample (Figure II. 45). The transition behavior of layer sample is in general agreement with the bulk sample, the only difference is that the HS residue of the layer sample is much higher than the bulk. In more detail, the magnetic product decreases to 3.24 $cm^3mol^{-1}K$ ($\gamma_{HS} \approx 0.86$) during the relaxation at 190 K (position 2). By decreasing the temperature, the $(\chi_M T)_{Fe}$ product at 100 K (position 3) is equal to 2.9 $cm^3mol^{-1}K$ ($\gamma_{HS} \approx 0.78$).

Compared with the thermal treatment on the bulk sample with x = 0.892 ($\gamma_{HS} \approx 0.66$ after treatment, Figure II. 44), the obtained $(\chi_M T)_{Fe}$ value for layer sample is much higher. A set of thermal treatment is thus performed for introducing a more completed HS_2 to LS_2/HS_3 transition (Figure II. 47). The treatment is similar with the treatment on the bulk sample except that longer relaxation time is used at 190 K. Moreover, after every 2 hours a thermal cycle down to 150 K was recorded. It is observed that after around 6 hours of relaxation at 190 K and during the third thermal cycle down to 150 K, the $(\chi_M T)_{Fe}$ value reaches the same value as the bulk sample. It is therefore illustrated that on the layer sample the same LS_2/HS_3 state can be reached as the bulk sample but longer relaxation time at 190 K is required.

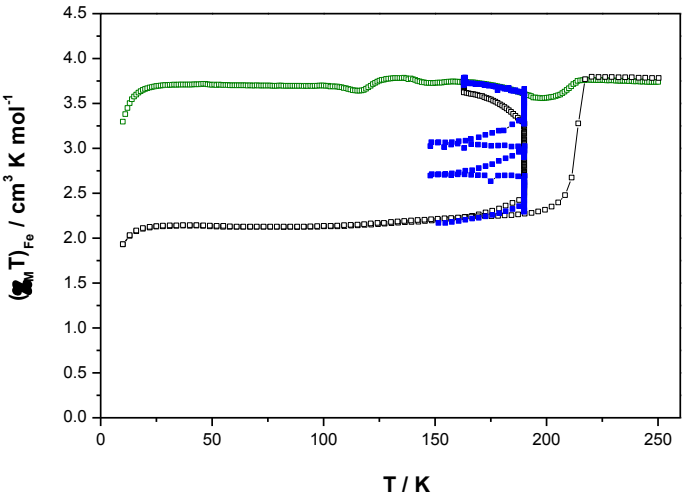

Figure II. 47: Thermal treatment procedure on layer sample with x = 0.892 (In blue ■). The treatment is preformed without irradiation. For comparison, the thermal treatment on bulk sample is presented in black □ and TIESST in green ■.

b) Photo-magnetic properties

Layer sample of x = 0.892 is prepared for two photomagnetic experiments. The first one is relaxation under light irradiation and the second is LITH experiment. For the relaxation under irradiation, the attempt was firstly performed at 148 K (Figure II. 48, position 1), after trapping at this temperature (HS state). For each selected wavelengths (λ = 488.0-514.5 nm, 530.9 nm, 647.1-679.4 nm, and 752.5-799.3 nm), the relaxation is performed for around 1 hour. However, after irradiation the sample is still in HS. Then the irradiation is performed at 148 K on the LS_2/HS_3 state with different wavelength (Figure II. 48, position 3). Similar with position 1, the sample remains in the LS_2/HS_3 state after irradiation.

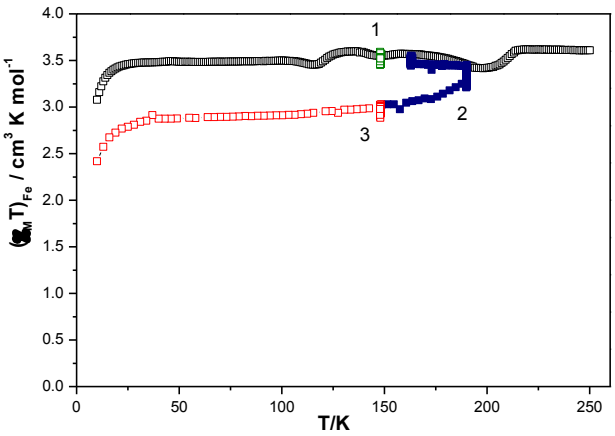

Figure II. 48: Photomagnetic experiments on $[Fe_xMn_{1-x}(L_{222}N_3O_2)(CN)_2]\cdot H_2O$ with x = 0.892. In black □: TIESST the bulk sample for reference. In green□: relaxation under irradiation at 148 K. In blue ■: thin layer sample under dark following the thermal treatment procedure for LS_2/HS_3 state. In red□: relaxation at 148 K after thermal treatment procedure.

Figure II. 49 presents the investigation of LITH properties on the LS_2/HS_3 state of complex with x = 0.892. The LS_2/HS_3 state is reached as previous describe for the layer sample (Figure II. 47). After reaching a $(\chi_M T)_{Fe}$ value of 2.5 cm^{3}mol^{-1}K at 190 K, LITH experiment is performed using Diode Laser (850 nm, 0.35mW/cm^2). A similar narrow LITH

loop as the pure Fe(II) is observed (Figure II. 49), which indicates the metal diluted complex with x = 0.892 remains similar LITH properties.

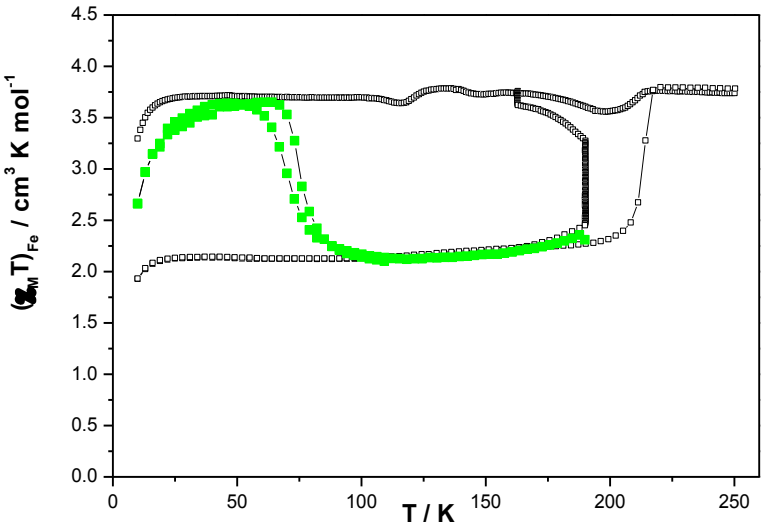

Figure II. 49: Temperature dependence of $(\chi_M T)_{Fe}$ for $[Fe_xMn_{1-x}(L_{222}N_3O_2)(CN)_2]\cdot H_2O$ with 0.892 in LITH experiment. In black □: TIESST and thermal treatment procedure of the bulk sample for reference. In green ■: LITH experiment.

Our last photomagnetic experiment concerns the T(LIESST) measurement on metal diluted complex (Figure II. 50). The selected sample is x = 0.966. The complex was first inserted in to SQUID chamber at 148 K, and then a relaxation of 1 hour was performed. A $(\chi_M T)_{Fe}$ value of around 0.34 cm^{3}mol^{-1}K at low temperature indicated that the complex reached a pure LS state. Then the complex was irradiated with green light (λ = 530.9 nm) for about 30 mins at 10 K. After the magnetic signal reached its maximum, a T(LIESST) experiment was performed following the standard procedure [44]. The obtained T(LIESST) curve is similar with the pure $[Fe(L_{222}N_3O_2)(CN)_2]\cdot H_2O$ complex (Figure II. 15a), and the T(LIESST) value is estimated at 136 K with a increase of 4 K in comparison with the pure $[Fe(L_{222}N_3O_2)(CN)_2]\cdot H_2O$ complex.

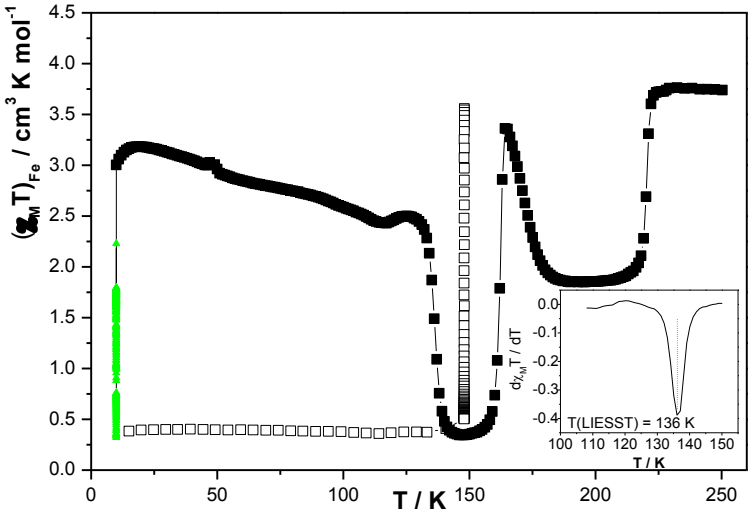

Figure II. 50: Temperature dependence of $(\chi_M T)_{Fe}$ for $[Fe_xMn_{1-x}(L_{222}N_3O_2)(CN)_2]\cdot H_2O$ with x = 0.966 in LIESST experiment. In black □: kinetics at 148 K and the following cooling. In green ▲: irradiation at 10 K. In black ■: T(LIESST) measurement. The T(LIESST) value is 136 K.

Several comments can be made:

i) Relaxation at 190 K requires only 2 hours for the bulk sample to reach the LS_2/HS_3 state, while it requires around 8 hours for the layer sample (including the time during cooling/warming to 150 K). This indicates a much stronger kinetic effect for the sample prepared in layer than in bulk.

ii) The layer sample for photomagnetic measurement consisted of a very thin layer of the compound, which is placed on a double-sided adhesive tape. During the preparation, pressure is usually applied to make sure that the powder sample sticks on the tape. As the pure complex $[Fe(L_{222}N_3O_2)(CN)_2]\cdot H_2O$ is sensitive to the pressure [40], further investigation on the layer sample need to be handle with caution.

iii) The attempt to introduce a HS_1 to LS_1 transition on the sample with x = 0.892 by light irradiation was unsuccessful. Possibly with stronger kinetic effect on the layer sample, it requires much longer time for relaxation under irradiation than the time actually applied.

iv) For the LITH and LIESST properties of the diluted series, it is evidenced that as soon as the LS_2/HS_3 and the pure LS state is reached, the photomagnetic properties of the diluted complexes are similar with the pure Fe(II) analogue, which is general agreement with previous studies on the Mn(II) metal diluted series [27-32].

II.5.6. Concluding remarks

In Part II, we have investigated the crystal structure of $[Mn(L_{222}N_3O_2)(CN)_2]\cdot H_2O$ and metal diluted $[Fe_xMn_{1-x}(L_{222}N_3O_2)(CN)_2]\cdot H_2O$ series. It was evidenced the metal centers were seven coordinated and the metal diluted series was isomorphous with the pure Mn(II) and Fe(II) analogues. From magnetic studies, strong kinetics effect was found in the powder samples of $[Fe_xMn_{1-x}(L_{222}N_3O_2)(CN)_2]\cdot H_2O$ series, which resulted in HS residual at low temperature depending on cooling rate. Upon warming, partial SCO from the HS state to the HS/LS mixed state occured on several metal diluted samples, which was under strong influence of the cooling/warming rate. We have then decided to systematically investigate the TIESST properties of the metal diluted series. It has been observed that when $x \leq 0.892$, the samples remain almost in HS state during the whole TIESST measurement. Moreover, five characteristic temperatures have been determined regarding to the T(TIESST) curves and a phase diagram was established based on these critical temperatures. In the phase diagram, the transition regimes (LS_1 and LS_2/HS_3 regimes) have been defined, which indicated that the LS_2/HS_3 state should be obtained in the metal diluted sample with x = 0.892. Several kintetic studies have been then perfomed. In some cases, the LS_2/HS_3 state could be partially reached. Finally, we have investigated the photomagnetic properties of the metal dilution series $[Fe_xMn_{1-x}(L_{222}N_3O_2)(CN)_2]\cdot H_2O$. It was evidenced that once the LS state and the LS_2/HS_3 state was reached, the photomagnetic properties such as LIESST and LITH remain similar with the pure Fe(II) analogue.

References

1 M. S. Haddad, W. D. Federer, M. W. Lynch, D. N, Hendrickson, *J. Am. Chem.* **1980**, *102*, 1468.
2 M. S. Haddad, W. D. Federer, M. W. Lynch, D. N, Hendrickson, *Inorg. Chem*. **1981**, *20*, 131.
3 D. N. Hendrickson, M. S. Haddad, W. D. Federer, M. W. Lynch, *Coord. Chem.* **1981**, *21*, 75.
4 P.S. Rao, A. Reuveni, B.R. Mc Garvey, P. Ganguli, P. Gütlich, *Inorg. Chem.* **1981**, *20*, 204.
5 P.S. Rao, B.R. Mc Garvey, P. Ganguli, *Inorg. Chem.* **1981**, *20*, 3682.
6 P. Ganguli, P. Gütlich, E.W. Müler, *Inorg. Chem.* **1982**, *21*, 3429.
7 V. Varma, J. R. Fernández, *Chem. Phys. Lett.* **1990**, *167*, 367.
8 M. Sorai, J. Ensling, P. Gütlich, *Chem. Phy. Lett.* **1976**, *18*, 199.
9 P. Gütlich, H. Köppen, R. Link, H. G. Steinhäuser, *Inorg. Chem.* **1978**, *17*, 2509.
10 P. Gütlich, R. Link, H. G. Steinhäuser, *J. Chem. Phys.* **1979**, *70*, 3977.
11 I. Sanner, E. Meissner, H. Köppen, H. Spiering, P. Gütlich, *Chem. Phys.* **1984**, *86*, 227.
12 P. Adler, L. Wiehl, E. Meissner, C. P. Köhler, H. Spiering, P. Gütlich., *J. Phys. Chem. Solids.* **1987**, *48*, 517.
13 H. Spiering, E. Meissner, H. Köppen, E.W. Müller, P. Gütlich, *J. Chem. Phys.* **1982**, *68*, 65.
14 H. Spiering, N. Willenbacher, *J. Phys. Condens. Matter* **1989**, *1*, 1089.
15 R. Jakobi, H. Spiering, L. Wiehl, E. Gmelin, P. Gütlich, *Inorg. Chem.* **1988**, *27*, 1823.
16 R. Jakobi, H. Spiering, P. Gütlich, *J. Phys. Chem. Solids.* **1992**, *53*, 267.
17 C. P. Köhler, R. Jakobi, E. Meisner, L. Wiehl, H. Spiering, P. Gütlich, *J. Phys. Chem. Solids.* **1990**, *51*, 239.
18 J. P. Martin, J. Zarembowifch, A. Dworkin, J.G. Haasnoot, E. Codjovil, *Inorg. Chem.* **1994**, *33*, 2617.
19 J. P. Martin, J. Zarembowitch, A. Bousseksou, A. Dworkin, J. G. Haasnoot, F. Varret, *Inorg. Chem.* **1994**, *33*, 6325.
20 H. Constant-Machado, J. Linares, F. Varret, J. G. Haasnoot, J. P. Martin, J. Zarembowitch, A. Dworkin, A. Bousseksou, *J. Phys.I.* **1996**, *6*, 1203.
21 W. Morscheidt, J. Jeftic, E. Codjovi, J. Linares, A. Bousseksou, H. Constant-Machado, F. Varret, *Meas. Sci. Technol.* **1998**, *9*, 1311.
22 N. Negre, M. Goiran, A. Bousseksou, J. Haasnoot, K. Boukheddaden, S. Askenazy, F. Varret, *Synthetic. Metals.* **2000**, *115*, 289.
23 E. Codjovi, N. Menendez, J. Jeftic, F. Varret, *C. R. Acad. Sci. Chim.* **2001**, *4*, 181.
24 A. Hauser, N. Amstutz, S. Delahaye, S. Schenker, A. Sadki, R. Sieber, M. Zerara, *in: Th. Schonherr (Ed.), Structure and Bonding, Springer, Berlin,* **2004**, *106*, 81.
25 A. Hauser, *Top. Curr. Chem*. **2004**, *234*, 155.
26 A. Hauser, C. Enachescu, M. L. Daku, A. Vargas, N. Amstutz, *Coord. Chem. Rev.* **2006**, *250*, 1642.
27 C. Baldé, C. Desplanches, A. Wattiaux, P. Guionneau, P. Gütlich, J.-F. Létard, *Dalton Trans,* **2008**, 2702.
28 C. Baldé, C. Desplanches, O. Nguyen, J.-F. Létard, E. Freysz, *J. Phys.: Conf. Ser.* **2009**, *148*, 012026
29 C. Baldé, C. Desplanches, P. Gütlich, E. Freysz, J.-F. Létard, *Inorg. Chim. Acta.*, **2008**, *361*, 3529.
30 C. Baldé, C. Desplanches, M.Grunert, Y. Wei, P. Gütlich, J.-F. Létard, *Eur. J. Inorg. Chem.* **2008**, 5382
31 C. Baldé, PhD Thesis, Université Bordeaux I, 2008.
32 N. Paradis, G. Chastanet, J.-F. Létard, *Eur. J. Inorg. Chem.* **2012**, 3618.
33 S. M. Nelson, P. D. A. Mcllroy, C. S. Stevenson, E. König, G. Ritter, J. Waigel, *J. Chem. Soc. Dalton Trans.*

1986, 991

34 M.G.B. Drew, A. H. bin Othman, S. M. Nelson, *J. Chem. Soc. Dalton Trans.* **1976**, 1394

35 E. König, G.Ritter, J. Dengler, S. M. Nelson *Inorg. Chem.* **1987**, *26*, 3582.

36 S. Hayami, Z. Gu, Y. Einaga, Y. Kobayasi, Y. Ishikawa, Y. Yamada, A. Fujishima, O. Sato, *Inorg. Chem.* **2001**, *40*, 3240.

37 H. Liu, A. Fujishima, O. Sato, *Appl. Phys. Lett.* **2004**, *85*, 2295.

38 P. Guionneau, J. S. Costa, J.-F. Létard, *Acta Cryst.* **2004**, *C60*, m587

39 P. Guionneau, F. Le Gac, A. Kaiba, J. S. Costa, D. Chasseau, J.-F. Létard, *Chem. Commun*. **2007**, *36*, 3723

40 J. S. Costa, P. Guionneau, J.-F. Létard, *J. Phys.: Conf. Ser.* **2005**, *21*, 67.

41 J. S. Costa, PhD Thesis, Université Bordeaux I, 2005.

42 S. M. Nelson, P. D. A. Mcllroy, C. S. Stevenson, E. König, G. Ritter, J. Waigel, *J. Chem. Soc. Dalton Trans.* **1986**, 991.

43 F. Bonadio, M.-C. Senna, J. Ensling, A. Sieber, A. Neels, H. Stoeckli-Evans, S. Decurtins, *Inorg. Chem.* **2005**, *44*, 969.

44 J.-F. Létard, P. Guionneau, O. Nguyen, J. S. Costa, S. Marcén, G. Chastanet, M. Marchivie, L. Goux-Capes, *Chem. Eur. J.* **2005**, *11*, 4582.

Part III. Modification of macrocyclic ligand

Chapter III.1. Chemical modifications on macrocyclic ligand

In this chapter, we will focus on the influence of chemical modifications on the SCO properties of macrocyclic complexes. First of all, some recent developments on the macrocyclic ligands will be introduced. These selected studies offer a brief overview of the modification of macrocyclic units which are comparable with the $L_{222}N_3O_2$ ligand. Then we will describe the various chemical modifications proposed on the macrocyclic unit and finally focus on changing the length of chains involved between the coordination atoms.

III.1.1. Recent modifications on macrocyclic ligands

Recently, many macrocylic ligands have been developed [1-9]. Scheme III. 1 presents some selected ligands possessing comparable structures with the macrocyclic ligands of $[Fe(L_{222}N_3O_2)(CN)_2]\cdot H_2O$ and $[Fe(L_{222}N_5)(CN)_2]\cdot H_2O$. Nevertheless most of these ligands (L1 to L9) have been used to synthesize Mn(II) coordinated complexes. Only Ligand L10 and L11 have been described to synthesized Fe(II) coordinated complexes. We will consider hereafter each of the different ligands

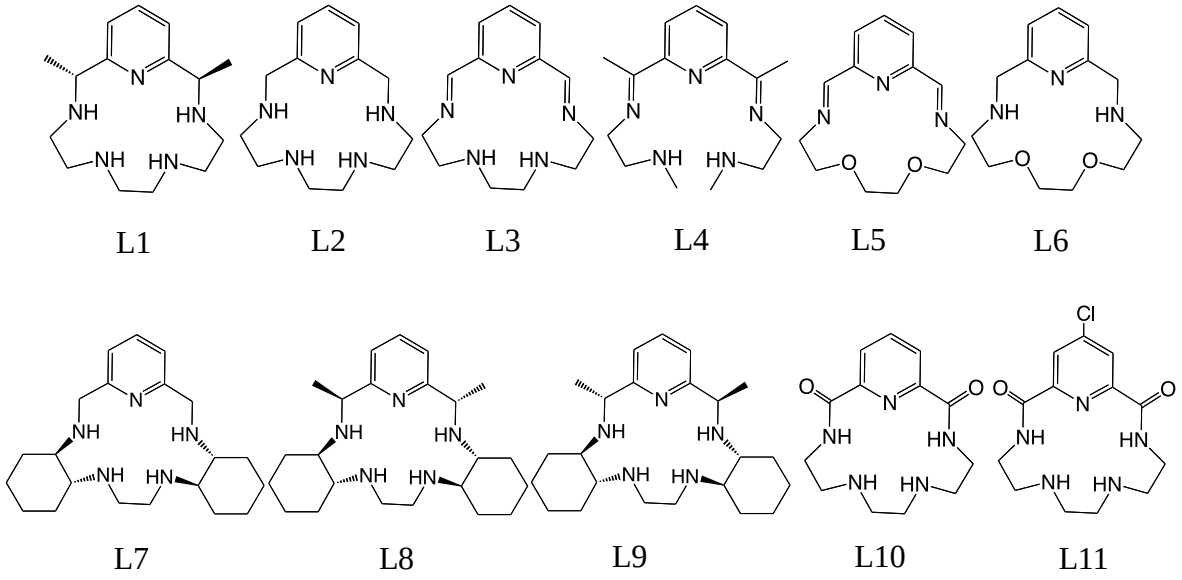

Scheme III. 1: Variety of modification on macrocyclic ligands

A. Dees et al. [1] have focused on the synthesis of Mn(II) coordinated complexes $[Mn(L1)Cl_2]$ and $[Mn(L2)Cl_2]$. The $[Mn(L1)Cl_2]$ complex was synthesized from the $[Mn(L)Cl_2]\cdot xH_2O$ (L = dichloro-2,-13-dimethyl-3,6,9,12,18-pentaazabicyclo[12.3.1]-octadeca-1(18),2,-12,14,16-pentaene) complex [2]. The complex $[Mn(L1)Cl_2]\cdot MeOH$ was obtained by reduction of $[Mn(L)Cl_2]$ with $NaBH_4$ [3] (Figure III. 1a). The complex $[Mn(L2)Cl_2]$ was obtained from the precursor bisimine complex $[Mn(L3)Cl_2]$ reduced with $NaBH_4$

A. Dees et al. [1] also described the open-shape ligand L4 and the complex $[Mn(L4)Cl_2]$. The synthesis involves the condensation of a diketone and two diamines [1]. The crystal structure of $[Mn(L4)Cl_2]$ has confirmed that the Mn(II) center is coordinated to one L4 ligand and two Cl atoms (Figure III. 1b).

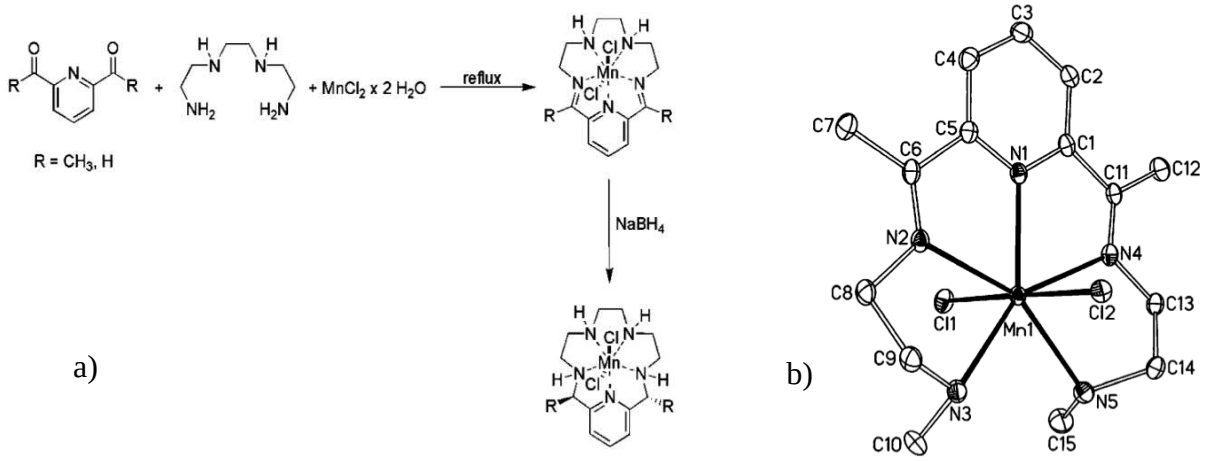

Figure III. 1: a) Synthesis of $[Mn(L1)Cl_2]$ and $[Mn(L2)Cl_2]$. b) Structure of $[Mn(L4)Cl_2]$. [1]

Ligands L5 and L6 were obtained by B. Drahoš et al. [4]. The synthesis of L5, as already described in chapter 2, involves the condensation of pyridine-2,6-dicarbaldehyde and 1,8-diamino-3,6-dioxaoctane, The pyridine-2,6-dicarbaldehyde is commercially available, but can be also prepared from the commercially available pyridine-2,6-dicarboxylic acid by its esterification to diethyl ester [5]. Ligand L6 was obtained by reduction of L5 with $NaBH_4$ (Scheme III. 2).

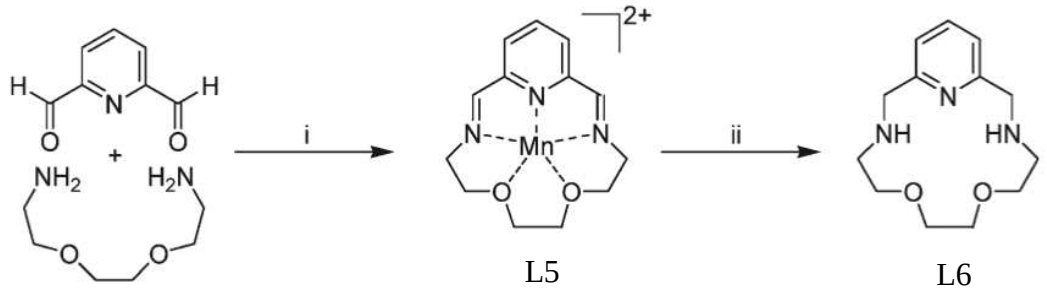

Scheme III. 2: Synthesis of ligand L5 and L6: (i) $MnCl_2$, MeOH, 60 °C, 2h; (ii) $NaBH_4$, H_2O on air [4].

Concerning the ligands L7-L9, the corresponding Mn(II) complexes have been synthesized [6-9]. Structural studies have shown that the Mn(II) is seven coordinated in those complex [9]. The synthesis procedure is a condensation reaction using Mn(II) as template (Scheme III. 3).

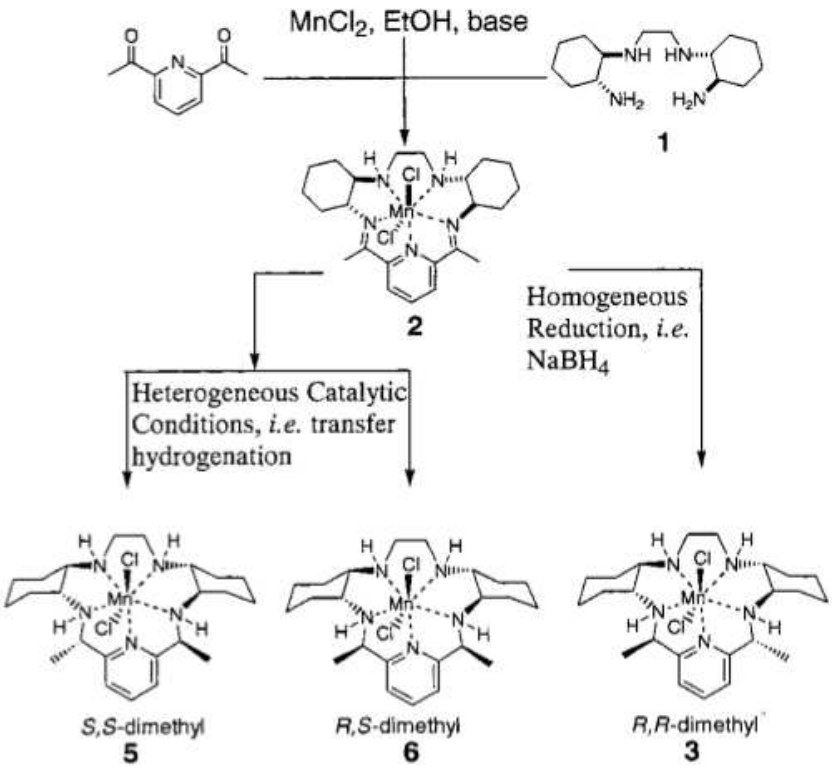

Scheme III. 3: Synthesis of a variety of Mn(II) macrocyclic complexes containing L8 type ligands [9]

In addition to Mn(II) complexes, Fe(II) complexes containing ligands L10 and L11 were synthesized [11]. These complexes (Figure III. 2) are in HS state whatever the temperature. Nevertheless, depending on the complex, the Fe(II) center adopts different coordination number. Complex $[FeL10](MeOH)_2$ and $[FeL11](MeOH)_2$ are seven coordinated, while complexes [FeL10](Cl)(MeOH) and [FeL11](MeOH) are six coordinated. In fact for the six coordinated complexes, the macrocyclic ligand is tetradentate, while for the seven coordinated system the ligand is pentadentate. In the peculiar case of $[FeL11](MeOH)_2$ the exchange of one MeOH ligand by a Cl^- ligand leads to the de-coordination of one nitrogen atom of the macrocyclic ligand.

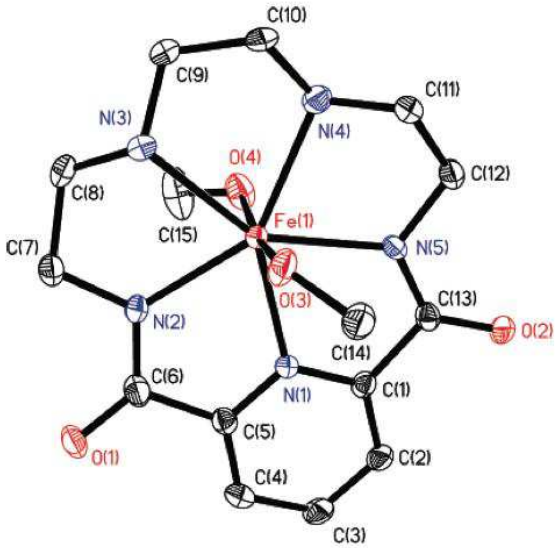

$[FeL10](MeOH)_2$

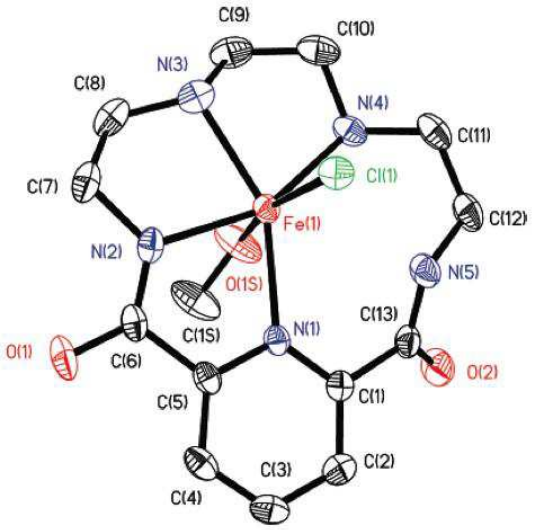

[FeL10](Cl)(MeOH)

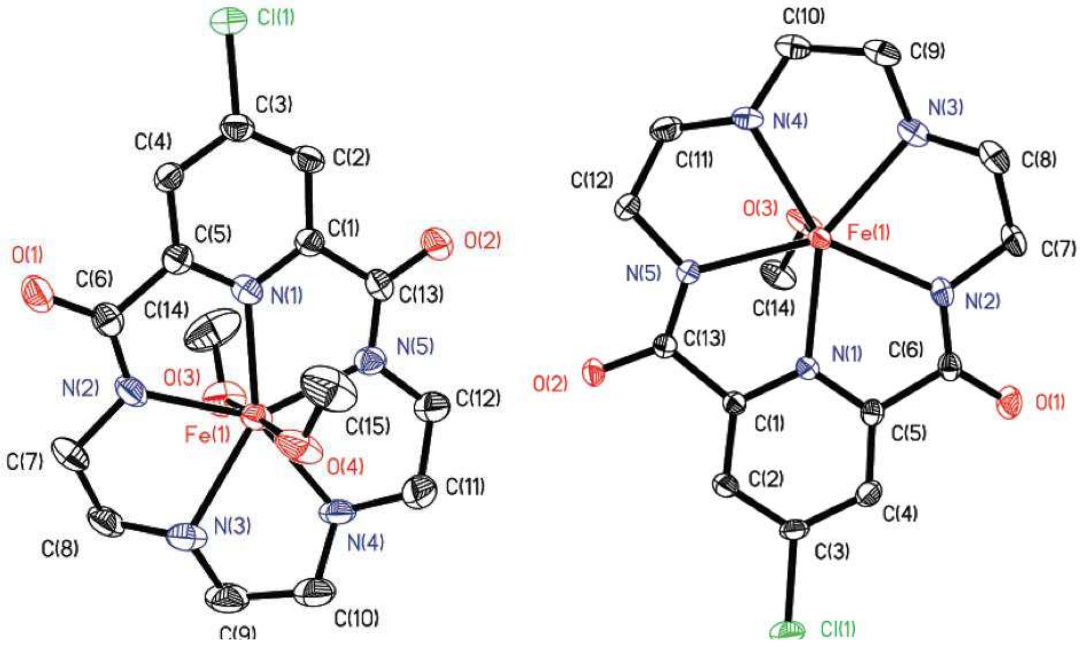

[FeL11](MeOH)$_2$ [FeL11](MeOH)

Figure III. 2: Fe(II) complexes containing L10 and L11. Fe(II) center adopts different coordination number.

III.1.2. Strategies for chemical modification on $[Fe(L_{222}N_3O_2)(CN)_2]\cdot H_2O$ complex.

The influence of some chemical modification on SCO properties of the $[Fe(L_{222}N_3O_2)(CN)_2]\cdot H_2O$ complex has been initially investigated in the PhD work of J. S. Costa [12]. The strategies developed are (Scheme III. 4):

a) To create an open-shape ligand.
b) To increase the rigidity of the system by adding aromatic units around the macrocyclic ligand.
c) To change the oxygen atoms by atoms of nitrogen or sulfur.
d) To change the length of chains in between coordination atoms.

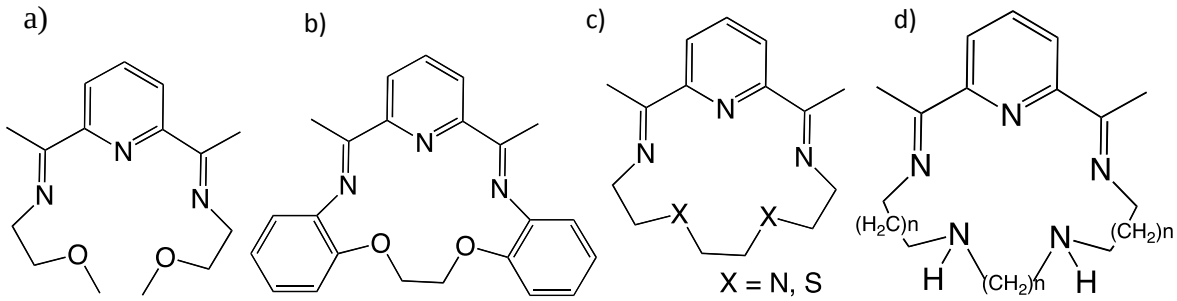

L12 L13 L14 L15

Scheme III. 4: Modification strategies. [12]

Many unsuccessful attempts to synthesize the complex with open-shape ligand $[Fe(L12)](CN)_2$ (L12 being presented in Scheme III. 4a) have been performed by J. S. Costa. The reason was attributed to the high affinity of the Fe(II) ion with the nitrogen atom, which favor the metal center to coordinate with two ligands L12, resulting in a octahedral symmetry with six coordinating nitrogen atoms. This hypothesis was confirmed by the structure of the complex $[Fe(L16)](X_2)$ obtained by J. S. Costa, where the ligand is an analogue of L12 with two ethyl groups instead of the two phenyl groups (Figure III. 3a). X-ray diffraction on single crystal of $[Fe(L16)](X_2)$ clearly demonstrate that the Fe(II) is coordinated to 6 nitrogen atoms with the two open-shape ligands. Therefore, it was concluded that the modification using open-shaped ligand with Fe(II) metal is quite limited.

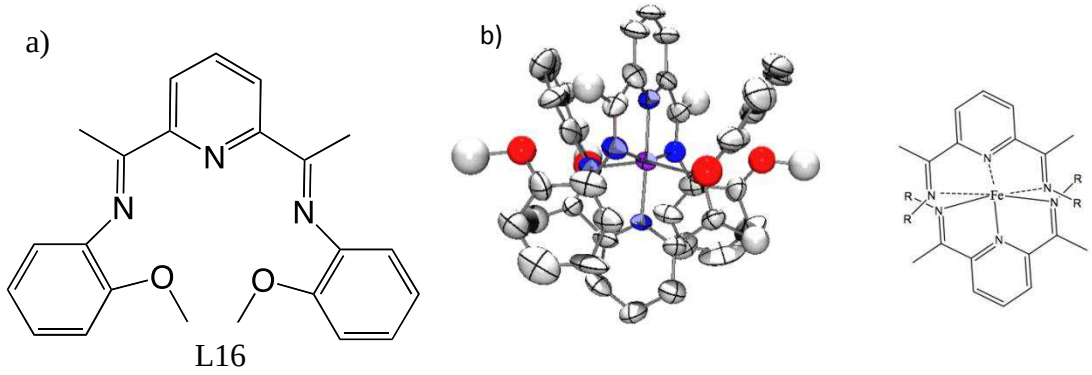

Figure III. 3: a) Ligand L16. b) Structure of obtained complex and schematic representation of the coordination: Fe(II) is coordinated by two ligands.

The introduction of macrocyclic ligands L13 and L14 were then investigated by J. S. Costa [12] to modulate the system in comparison with $L_{222}N_3O_2$ ligand. Unfortunately, the various attempts were also unsuccessful. The reason given by J. S. Costa is related to the study of Gryko et al. [13] which demonstrated that competition occurs between the formation of pyridinophanes and macrocycles of bis-amides, tetra-amides or polyamides (Figure III. 4).

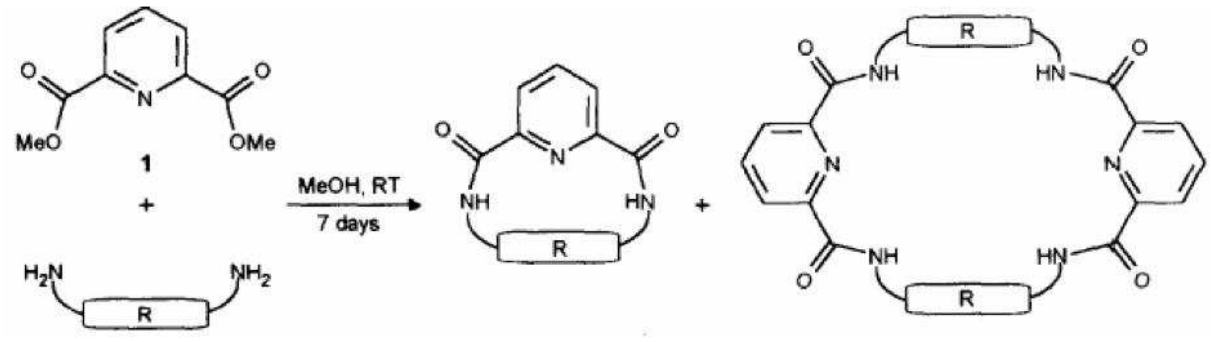

Figure III. 4: General process of synthesis of pyridinophanes.[13]

The synthesis of $[Fe(L_{222}N_5)(CN)_2]\cdot H_2O$ complex with ligand L14 (X = N, i.e ligand $L_{222}N_5$) was originally described by Nelson et al. [10]. The ligand $L_{222}N_5$ is similar to the ligand $L_{222}N_3O_2$ with the exception that the two oxygen atoms have been replaced by NH groups, (Figure III. 5 insert). Later on, J. S. Costa et al. [14] have reproduced the synthesis and investigated the photomagnetic properties. These authors demonstrate that this complex

which is LS state from room temperature to 10 K (Figure III. 5) [14], can be fully photoconverted into the metastable HS state. The T(LIESST) value was estimated at 105 K, which is a remarkably high value for a LS complex (Figure III. 5).

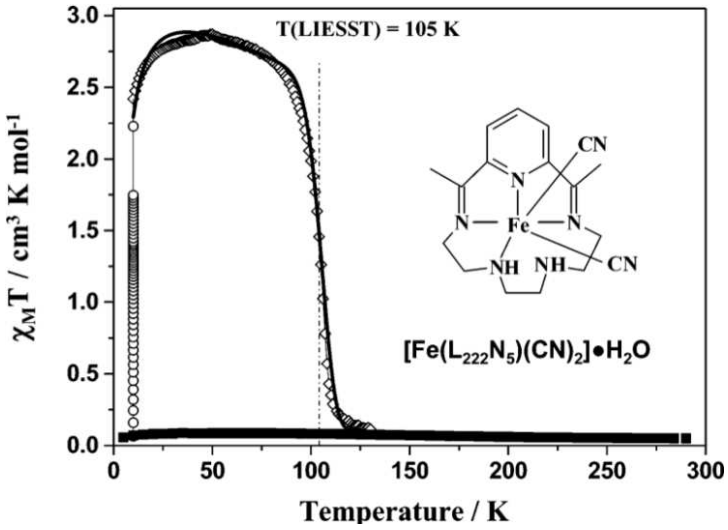

Figure III. 5: Magnetic and photomagnetic properties recorded for a polycrystalline sample of $[Fe(L_{222}N_5)(CN)_2]\cdot H_2O$ [14].

III.1.3. The objective of Part III

To sum up, J. S. Costa [12] has attempted several chemical modifications, with more or less success, to study the influence on the SCO properties. In the following chapter, our strategy is to pursue these synthetic efforts. We will investigate in particular the $[Fe(L_{xyz}N_5)(CN)_2]$ family and investigate the magnetic and photomagnetic properties. A comparison with the previously described complex $[Fe(L_{222}N_5)(CN)_2]\cdot H_2O$ will be done.

The family of compounds $[Fe(L_{xyz}N_5)(CN)_2]$ with $L_{xyz}N_5$ = $L_{232}N_5$, $L_{223}N_5$ and $L_{323}N_5$ (Scheme III. 5) has been selected for the following reasons:

i) The length of chains between the nitrogen coordination atoms will be changed and consequence on the SCO and photomagnetic properties will be studied. The Ligand $L_{222}N_5$ contains a HN–CH_2–CH_2–NH ethylene fragment at the center of the amine part, while ligand $L_{232}N_5$ contains a more flexible HN–CH_2–CH_2–CH_2–NH propylene fragment at the same position, and ligand $L_{323}N_5$ contains two propylene fragments at the two ends of the amine part.

ii) The symmetry of the ligand will be also changed. The ligand $L_{223}N_5$ contains the same propylene fragment in comparison with its symmetric analogue $L_{232}N_5$. However, instead of being located at the center of the amine part, the propylene fragment in ligand $L_{223}N_5$ is placed at one end of the amine part. The ligand $L_{223}N_5$ is thus an asymmetric macrocyclic ligand.

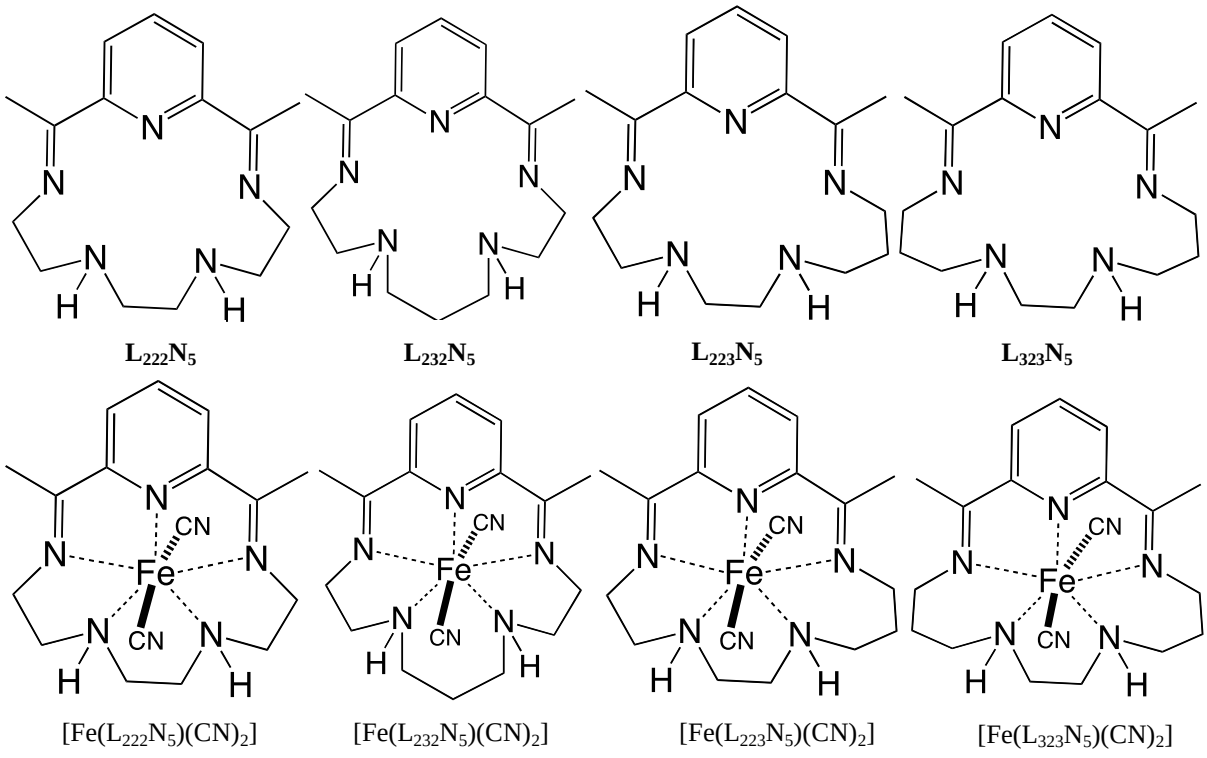

Scheme III. 5: Ligands and complexes $[Fe(L_{xyz}N_5)(CN)_2]\cdot H_2O$ with $L_{xyz} = L_{222}$, L_{232}, L_{223} and L_{323}

Chapter III.2. Synthesis of $[Fe(L_{xyz}N_5)(CN)_2]\cdot nH_2O$ family

III.2.1. Synthesis of $[Fe(L_{xyz}N_5)(CN)_2]\cdot nH_2O$ family

The synthesis of $[Fe(L_{222}N_5)(CN)_2]\cdot H_2O$ ($L_{222}N_5$ = 2,13-dimethyl-3,6,9,12,18-pentaazabicyclo[12.3.1]-octadeca-1(18),2,12,14,16-pentaene) is presented in Scheme III. 6, as described in previous work [14]. 1.20 g (6 mmol) of iron chloride tetrahydrate, 1 g (6 mmol) of 2,6-diacetylpyridine, and 0.1 g of sodium dithionite (used as reducing agent to remove traces of trivalent iron ion) were dissolved in 15 mL of methanol and 10 mL of water. The triethylenetetramine (0.876 g, 6 mmol) was added dropwise. The mixture was kept under nitrogen reflux at 75 °C for 16 h approximately (formation of $[Fe(L_{222}N_5)(Cl)_2]$). After filtration to remove traces of impurities, 15 mL of aqueous solution containing an excess of sodium cyanide NaCN (4g; 0.08 mol) and 0.1 g of sodium dithionite was added. This solution was then kept stirring for ca. 6 hours at room temperature. A polycrystalline powder is formed. The solid formed is then filtered and washed with 10 mL of degassed water and dried under vacuum. Finally 0.9 g (yield ~ 40%) of dark purple powder was collected.

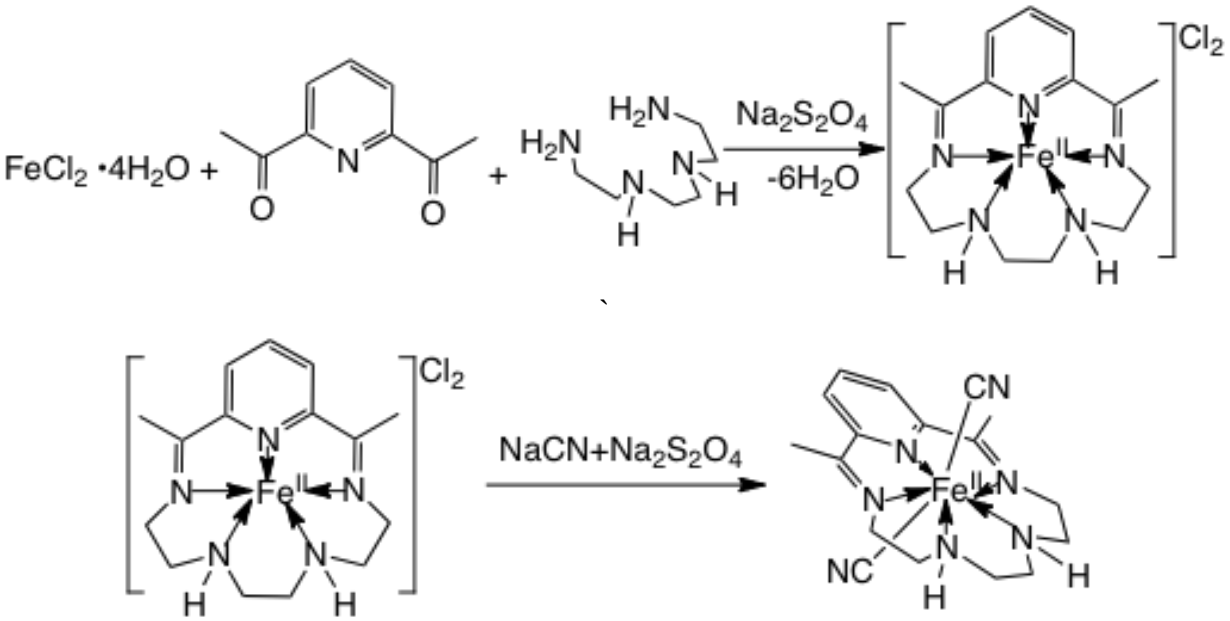

Scheme III. 6: Synthesis of $[FeL_{222}N_5(CN)_2]\cdot H_2O$ complex.

The synthesis of $[Fe(L_{232}N_5)(CN)_2]\cdot 2.5H_2O$ ($L_{232}N_5$=2,14-dimethyl-3,6,10,12,19-pentaazabicyclo[13.3.1]-nonadeca-1(19),2,13,15,17-pentaene), $[Fe(L_{223}N_5)CN)_2]\cdot 2.5H_2O$ ($L_{223}N_5$= 2,14-dimethyl-3,7,10,13,19-pentaazabicyclo[13.3.1]-nonadeca-1(19),2,13,15,17-pentaene) and $[Fe(L_{323}N_5)(CN)_2]\cdot 1.5H_2O$ ($L_{323}N_5$=2,15-dimethyl-3,7,10,14,20-pentaazabicyclo[14.3.1]-icosan-1(20),2,14,16,18-pentaene) has been originally described by Nelson et al. [10]. The protocol used is very similar to the one described for the elaboration of the complex $[Fe(L_{222}N_5)(CN)_2]\cdot H_2O$. The amine precursors are N,N'-Bis(2-aminoethyl)-1,3-propane-diamine, N-(2-aminoethyl)-N'-(3-aminopropyl)ethylene-diamine tetrahydrochloride and 1,2-Bis(3- aminopropylamino)-ethane, respectively. For $[Fe(L_{223}N_5)CN)_2]\cdot 2.5H_2O$, the amine N-(2-Aminoethyl)-N'-(3- aminopropyl)ethylene-diamine tetrahydrochloride (1.84 g, 6 mmol)

was dissolved in 5 mL of aqueous solution containing NaOH (0.96 g, 24 mmol) for deprotonation.

The chemical analyses for the four complexes are listed in Table III. 1, which demonstrate that the studied complexes are relatively pure. Nevertheless, even though the protocol is similar with the $[Fe(L_{222}N_5)(CN)_2]\cdot H_2O$, these three complexes are often found to contain impurities. Washing process with water is thus needed, which unfortunately reduces the final yield: ca. 30% for the three complexes.

Complex	C	H	N	Fe
$[Fe(L_{222}N_5)(CN)_2]\cdot H_2O$	50.89 (51.14)	6.23 (6.31)	24.49 (24.56)	14.13 (13.99)
$[Fe(L_{232}N_5)(CN)_2]\cdot 2.5H_2O$	49.31 (49.10)	6.19 (6.87)	23.16 (22.27)	12.75 (12.68)
$[Fe(L_{223}N_5)(CN)_2]\cdot 2.5H_2O$	48.59 (49.10)	6.87 (6.87)	22.08 (22.27)	13.64 (12.68)
$[Fe(L_{323}N_5)(CN)_2]\cdot 1.5H_2O$	53.01 (52.30)	7.14 (6.93)	22.28 (22.47)	13.38 (12.80)

Table III. 1: Elemental microanalyses of the $[Fe(L_{xyz}N_5)(CN)_2]\cdot nH_2O$ family [found, % (calcd, %)].

Powder X-ray diffraction patterns are presented in Figure III. 6, showing that the four synthesized complexes are in polycrystalline form. From X-ray diffraction patterns, it can be observed that the crystallinity of the $[Fe(L_{222}N_5)(CN)_2]\cdot H_2O$ is higher than the other complexes.

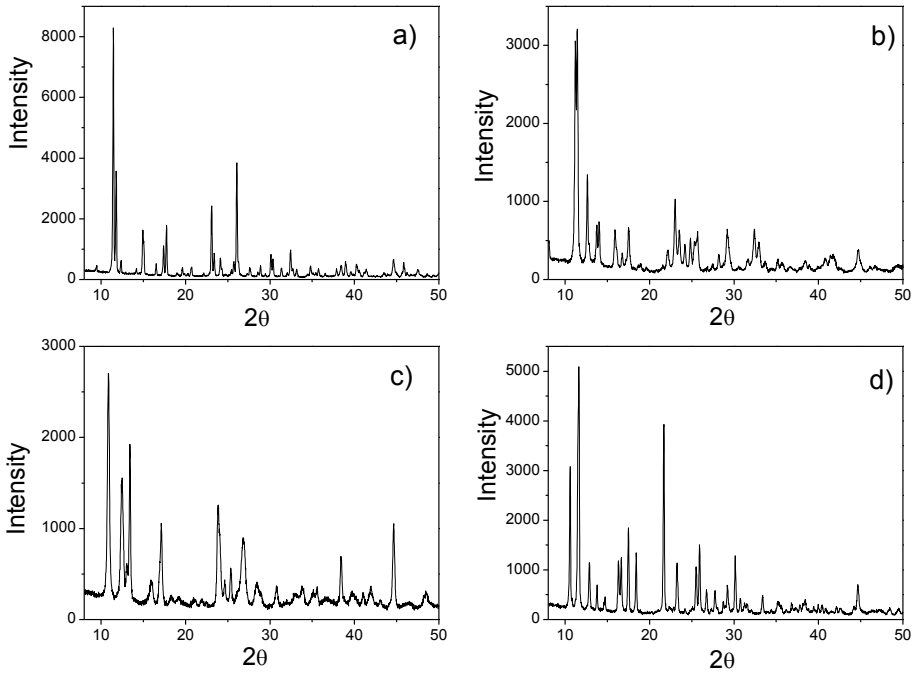

Figure III. 6: Powder X-ray diffraction patterns for a) $[Fe(L_{222}N_5)(CN)_2]\cdot H_2O$, b) $[Fe(L_{232}N_5)(CN)_2]\cdot 2.5H_2O$; c) $[Fe(L_{223}N_5)CN)_2]\cdot 2.5H_2O$ and d) $[Fe(L_{323}N_5)(CN)_2]\cdot 1.5H_2O$.

Many attempts to obtain single crystal of the four complexes have been carried out during this thesis. Methods such as slow diffusion, vapor diffusion using different glassware such as H shape tube, schlenk tube and U shape tube have been tried. Different solvents such as water, methanol and chloroform were also used for the attempts of crystallization. However those attempts were not successful.

III.2.2. Thermal analysis

The thermal analyses of the four complexes have been performed following the same procedure. The sample was first left in nitrogen flux for 3 hours at room temperature, then the temperature was increased up to 450 K with a rate of 1 K min^{-1}. Later on, the temperature was decreased back to room temperature slowly. The mass of the sample was continuously measured during the whole process. Figure III. 7 shows the TGA results for all the four complexes, presented in mass change percentage as function of temperature. All complexes show an important mass loss until ca. 400 K and then up to 450 K nothing changes.

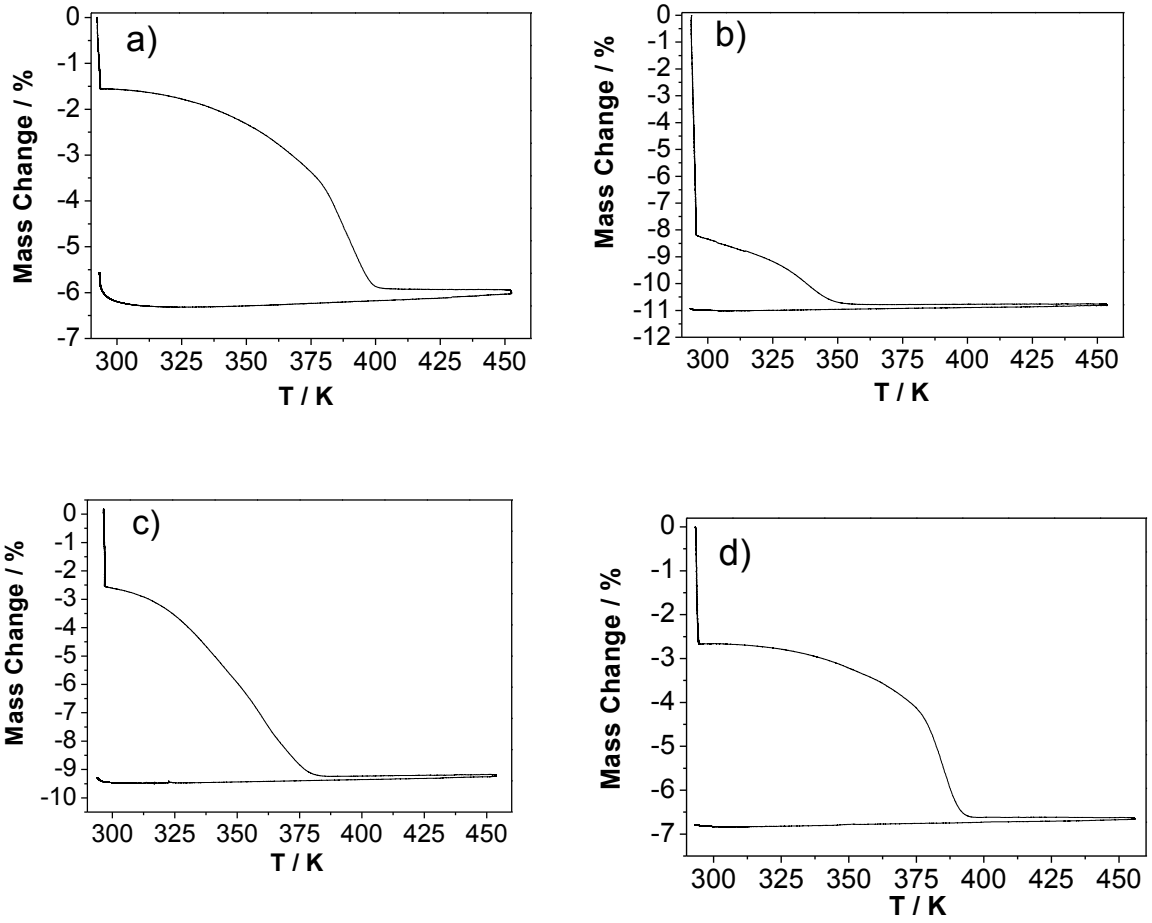

Figure III. 7: TGA analysis presented in mass change percentage as a function of temperature for a) $[Fe(L_{222}N_5)(CN)_2]\cdot H_2O$, b) $[Fe(L_{232}N_5)(CN)_2]\cdot 2.5H_2O$; c) $[Fe(L_{223}N_5)CN)_2]\cdot 2.5H_2O$ and d) $[Fe(L_{323}N_5)(CN)_2]\cdot 1.5H_2O$.

For $[Fe(L_{222}N_5)(CN)_2]\cdot H_2O$ (Figure III. 7a), starting from room temperature and under nitrogen flux for 3 hours, a weight loss of 1.5% can be observed even without any increase of temperature. When the temperature was increased, a further loss of mass of 4.4% was observed between room temperature and 425 K. Then up to 450 K and when the sample was cooled down, no further mass change was observed. The one water molecule proposed in the chemical formula $[Fe(L_{222}N_5)(CN)_2]\cdot H_2O$ corresponds to the obtained 4.5% of the total mass of the compound. Therefore the mass loss of 4.4%, observed by heating the compound, is in agreement with a loss of one water molecule. The supplementary 1.5% mass loss at room temperature is possibly due to some water adsorbed at the surface of the compound.

For $[Fe(L_{232}N_5)(CN)_2]\cdot 2.5H_2O$ (Figure III. 7b) a weight loss of 8.3% can be observed at room temperature and a further loss of mass of 2.4% was observed between room temperature and 360 K. Therefore the global mass loss of 10.7%, including the 8.3% mass loss at room temperature and 2.4% mass loss until 360 K, is in agreement with a loss of 2.5 water molecules (i.e. 10.2% of mass in respect to the chemical formula).

For $[Fe(L_{223}N_5)(CN)_2]\cdot 2.5H_2O$ (Figure III. 7c) a weight loss of 2.5% at 290 K and a further loss of 6.7% between room temperature and 380 K can be observed. The total mass loss of around 9.2% is in reasonable agreement with the 2.5 water molecule proposed in the chemical formula, which corresponds to 10.2% of mass.

For $[Fe(L_{323}N_5)(CN)_2]\cdot 1.5H_2O$ (Figure III. 7d), a weight loss of 2.6% can be observed at room temperature. When the temperature was increased, a further loss of mass of 4.1% was observed between room temperature and 400 K. The 1.5 water molecule proposed in the chemical formula corresponds to 6.6% of mass. Therefore the global mass loss of 6.7%, including the 2.6% mass loss at room temperature and 4.1% mass loss until 380 K, is in agreement with a loss of 1.5 water molecules.

To sum up, thermal analysis has demonstrated that the calculated solvent percentage is in quite good agreement with observed mass loss. This TGA analysis also suggests that two types of water molecules may exist in these series of complexes. The first type, which can be easily removed at room temperature under nitrogen flux for 3 hours, may be attributed to some adsorption at the surface. The second type, which imposes a warming process is certainly linked to water molecules in the crystal lattice, since more energy is required for the departure of this type of molecule.

Chapter III.3. Properties of $[Fe(L_{xyz}N_5)(CN)_2]\cdot nH_2O$ family

III.3.1. Magnetic properties

The magnetic properties of the four complexes have been investigated with the following procedure. For the measurement at low temperature, two apparatus can be used, namely SQUID (10 K – 380 K) and liquid nitrogen susceptometer (77 K – 360 K). For higher temperature region (up to 500 K) high-temperature susceptometer has been used. The measurement of a sample was firstly recorded by SQUID from 10 K to 350 K, then the sample was taken out and introduced rapidly into a high-temperature susceptometer and the magnetic properties were measured by warming to ca. 500 K and then cooling to 290 K. Finally the sample was taken out and introduced into SQUID or nitrogen susceptometer in order to measure the magnetic behavior down to ca. 80 K. The product of molar magnetic susceptibility χ_M by the temperature T (i.e. $\chi_M T$) as a function of temperature in the range of 10 K to 450 K is shown in Figure III. 8 and Figure III. 9: for the four different compounds

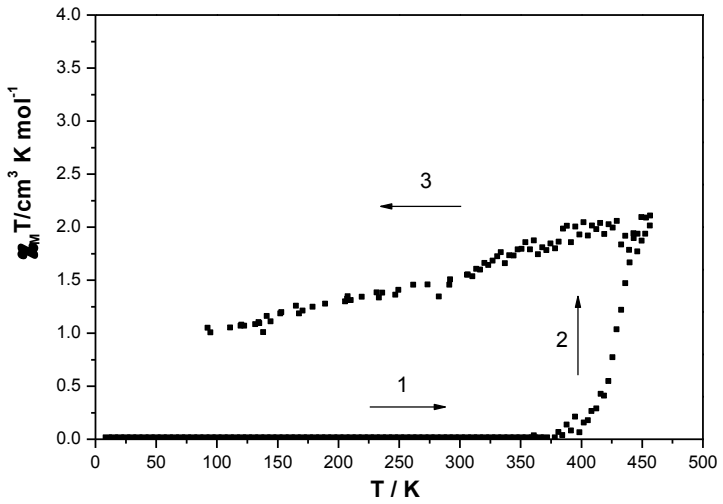

Figure III. 8: Product of molar magnetic susceptibility χ_M by the temperature T as a function of temperature for $[Fe(L_{222}N_5)(CN)_2]\cdot H_2O$. Step 1 and 2: heating. Step 3: cooling.

Figure III. 8 presents the magnetic properties of $[Fe(L_{222}N_5)(CN)_2]\cdot H_2O$, showing that this complex is diamagnetic from 10 K to 370 K in perfect agreement with previously reported measurements [14]. In higher temperature region, it shows an increase of $\chi_M T$ value starting at ca. 400 K. When the temperature increases above 425 K, $\chi_M T$ increases sharply to reach about 2.0 cm^3 K mol^{-1} at ca. 450 K. When the temperature is then decreased, the $\chi_M T$ value decreases very slowly to reach about 1.0 cm^3 K mol^{-1} at 80 K. In conclusion, after an initial thermal treatment up to 400 K, the magnetic properties of $[Fe(L_{222}N_5)(CN)_2]\cdot H_2O$ never come back to the initial diamagnetic state.

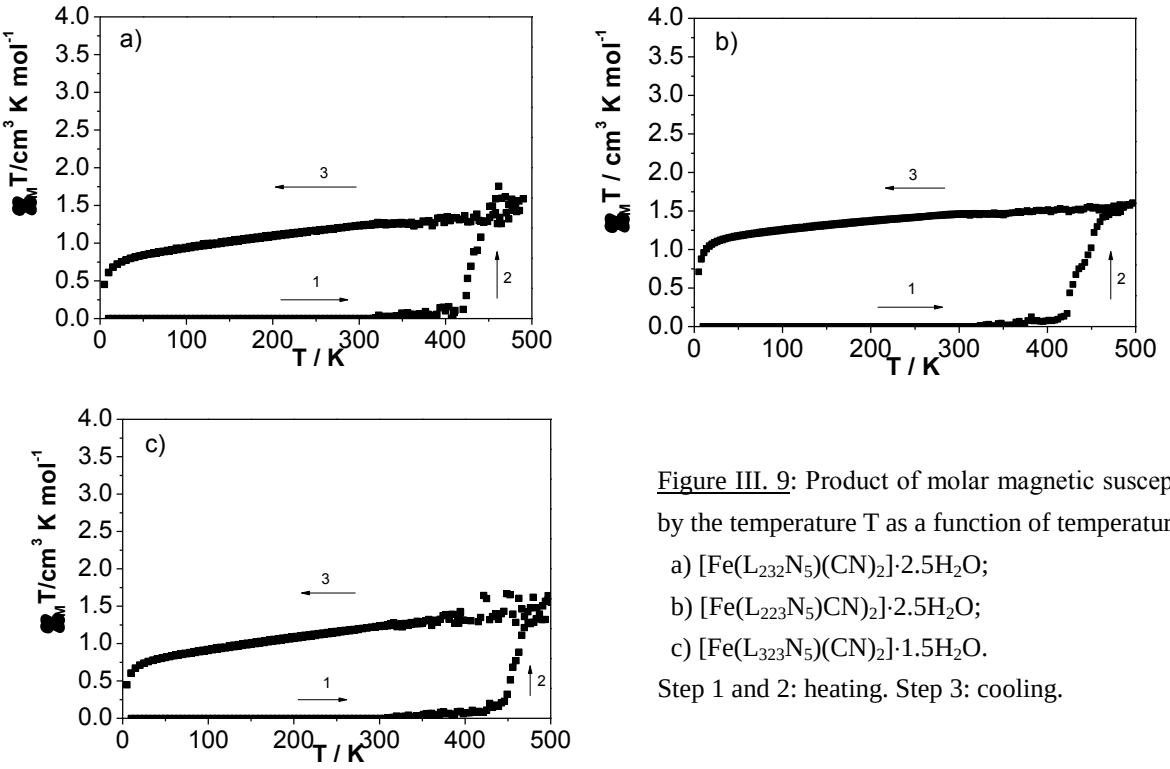

Figure III. 9: Product of molar magnetic susceptibility χ_M by the temperature T as a function of temperature for:
a) $[Fe(L_{232}N_5)(CN)_2]\cdot 2.5H_2O$;
b) $[Fe(L_{223}N_5)CN)_2]\cdot 2.5H_2O$;
c) $[Fe(L_{323}N_5)(CN)_2]\cdot 1.5H_2O$.
Step 1 and 2: heating. Step 3: cooling.

Figure III. 9 presents the magnetic properties of $[Fe(L_{232}N_5)(CN)_2]\cdot 2.5H_2O$ (Figure III. 9a), $[Fe(L_{223}N_5)CN)_2]\cdot 2.5H_2O$ (Figure III. 9b) and $[Fe(L_{323}N_5)(CN)_2]\cdot 1.5H_2O$(Figure III. 9c). Magnetic behaviors of the three complexes are similar to $[Fe(L_{222}N_5)(CN)_2]\cdot H_2O$. These complexes are diamagnetic from 10 K to 370 K. On warming to higher temperature region, an increase of χ_MT value can be found at 420 K, 420 K and 450 K respectively for the three complexes. The maximum χ_MT value is 1.5 cm^3 K mol^{-1} for all the three complexes at ca. 500 K. On cooling, the χ_MT value decreases very slowly. At 50 K, χ_MT value reaches 0.8 cm^3 K mol^{-1} for $[Fe(L_{232}N_5)(CN)_2]\cdot 2.5H_2O$, 1.2 cm^3 K mol^{-1} for $[Fe(L_{223}N_5)CN)_2]\cdot 2.5H_2O$ and 0.8 cm^3 K mol^{-1} for $[Fe(L_{323}N_5)(CN)_2]\cdot 1.5H_2O$. Thus the increases of χ_MT are irreversible for these three complexes. Moreover, when those complexes are left at ambient atmosphere for several months after the above experiment, the χ_MT values for all the four complexes are still around 1 cm^3 K mol^{-1} at room temperature, which further confirms that the increases of χ_MT are irreversible.

There are at least two possibilities to explain this irreversible increase of χ_MT value. The first one is that the complex exhibits a spin transition with an extremely large hysteresis of more than 400 K. Nevertheless, this idea appears unrealistic, in regard to the hysteresis loop up to now encountered for SCO materials which never exceed 60 K [4]. The second one is that a decomposition and/or dehydration process takes place at high temperature, which means that the chemical nature of the complexes has been irreversibly modified.

To find out whether the increase is due to a dehydration and/or a decomposition process, magnetic properties have been compared with TGA properties. Magnetic measurements

clearly demonstrate that, for the four complexes, the changes between the LS and the HS states occur at about 420 K. That is in the same region where the TGA measurements indicate the departure of water. It seems consequently reasonable to assume that the increases of $\chi_M T$ value at high temperature are linked to solvent departure, rather that decomposition of the complexes.

If we consider now the influence of the ligand on the thermal SCO properties, the four complexes involve ligand with different chain length, but all of them are in LS state at room temperature. It seems that the magnetic properties of those macrocyclic complexes are independent with chain length on macrocyclic ring. The coming question is whether the chain length will influence LIESST properties. To investigate this, reflectivity measurements and photomagnetic measurements were performed.

III.3.2. Reflectivity properties

It is now well known through the work of Kahn and Varret that the SCO phenomenon can be followed by the color change of the material [11-13]. A reflectivity experiment consists in continuously irradiating the sample with white light and collecting the light reflected as function of the temperatures and wavelengths. Thus, any change in the reflectivity signal can be directly used to monitor the thermal spin transition and the photo-induced spin transition on the surface of the sample. In our case, the reflectivity signal was recorded between 500 and 900 nm from 280 K down to 10 K for the three complexes: $[Fe(L_{232}N_5)(CN)_2]\cdot 2.5H_2O$, $[Fe(L_{223}N_5)(CN)_2]\cdot 2.5H_2O$ and $[Fe(L_{323}N_5)(CN)_2]\cdot 1.5H_2O$

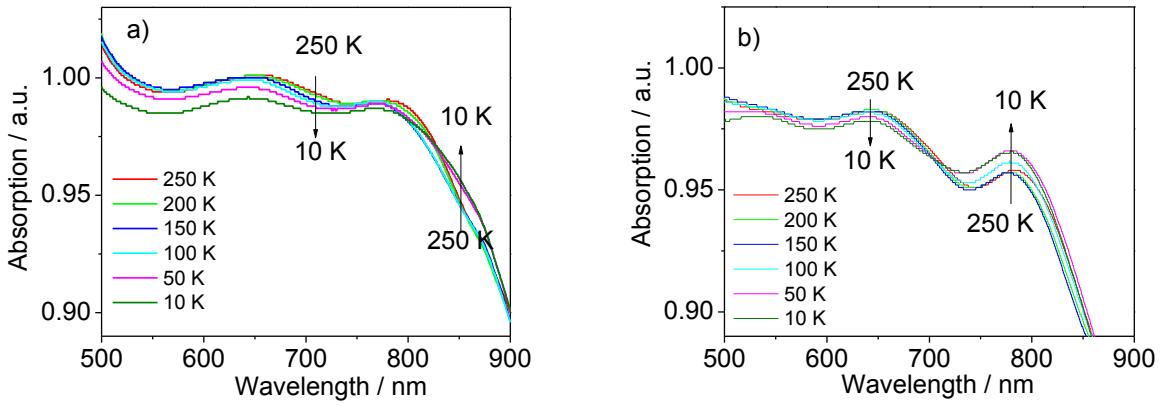

Figure III. 10: Changes in the diffuse absorption spectra of a) $[Fe(L_{232}N_5)(CN)_2]\cdot 2.5H_2O$ and b) $[Fe(L_{223}N_5)(CN)_2]\cdot 2.5H_2O$ upon cooling under light irradiation

Figure III. 10: presents the absorption spectra of the $[Fe(L_{232}N_5)(CN)_2]\cdot 2.5H_2O$ and $[Fe(L_{223}N_5)(CN)_2]\cdot 2.5H_2O$. For both compounds, a decrease of the temperature between 250 and 10 K leads to a slight increase of absorption between 800 and 850 nm and a decrease of absorption between 500 and 650 nm. The increase of the 800–850 nm band characterizes the appearance of the d–d transition associated to the HS state. The decrease of the 500–650 nm

transition is assigned to the decrease of both d–d and MLCT (metal-to-ligand charge transfer) bands of the LS iron metal center [23]. Such an increase of d–d HS transition at 800–850 nm band from room temperature to 10 K under irradiation suggests that at the surface of the samples a photoconversion process may occur according to the well-known LIESST effect [16-19]. Nevertheless, the increase of d–d HS transition for both $[Fe(L_{232}N_5)(CN)_2]\cdot 2.5H_2O$ and $[Fe(L_{223}N_5)(CN)_2]\cdot 2.5H_2O$ complexes is extremely small, namely 3% of absorption intensity.

Figure III. 11 presents the absorption spectra of $[Fe(L_{323}N_5)(CN)_2]\cdot 1.5H_2O$ between 500 nm and 900 nm. From 250 K to 10 K, a continuous decrease can be observed in a broad range from 500 to 900 nm. In contrast to the two above complexes, the complex $[Fe(L_{323}N_5)(CN)_2]\cdot 1.5H_2O$ does not exhibit an increase of d–d HS transition band (800-850 nm) at low temperature under irradiation. This complex may not present some LIESST properties at low temperatures.

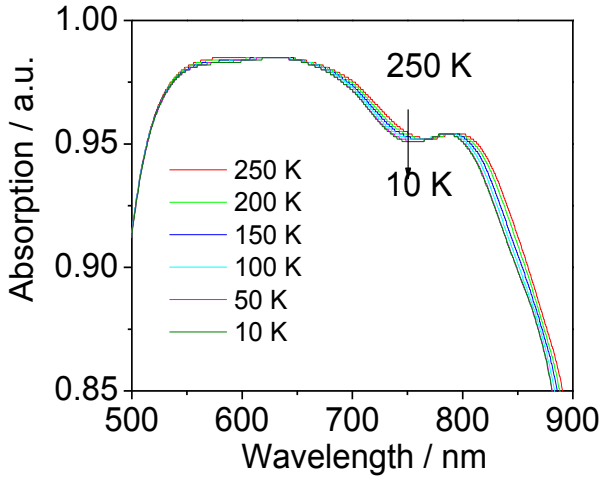

Figure III. 11: Changes in the diffuse absorption spectra of $[Fe(L_{323}N_5)(CN)_2]\cdot 1.5H_2O$ upon cooling under light irradiation

To complete this analysis, Figure III. 12 reports the total reflectivity as a function of the temperature of the four compounds. For $[Fe(L_{222}N_5)(CN)_2]\cdot H_2O$ (Figure III. 12a), upon cooling, the total reflectivity shows a sharp increase at around 100 K. The maximum is found to be at ca. 60 K for the cooling branch. On further cooling, the total reflectivity signal keeps stable until 10 K. Upon warming a sharp decrease of intensity can be found at ca. 100 K. At ca. 175 K the intensity of the warming branch reaches similar level as compared to the cooling branch. This type of behavior corresponds to Light Induced Thermal Hysteresis (LITH) introduced in 1998 for the $[Fe(PM\text{-}BiA)_2(NCS)_2]$ complex [24]. In our cases the width of the LITH loop is ca. 30 K.

For $[Fe(L_{232}N_5)(CN)_2]\cdot 2.5H_2O$ (Figure III. 12b), the intensity of total reflectivity increases gradually starting at ca. 100 K upon cooling. On warming, the intensity decreases gradually from 10 K, merging with the cooling branch at ca. 120 K. In comparison with the $[Fe(L_{222}N_5)(CN)_2]\cdot H_2O$ complex, the size of the thermal hysteresis is smaller and the magnitude of the change in reflectivity at low temperature is about 4.5 times smaller. Moreover, the shape of the LITH loop is really gradual. For $[Fe(L_{223}N_5)(CN)_2]\cdot 2.5H_2O$

(Figure III. 12c), under irradiation the change of reflectivity signal is very small (Figure III. 12 insert), giving a tiny LITH loop at round 100 K. The intensity of the LITH loop is about 10 times smaller than the one for $[Fe(L_{232}N_5)(CN)_2]\cdot 2.5H_2O$. Finally for $[Fe(L_{323}N_5)(CN)_2]\cdot 1.5H_2O$ (Figure III. 12d) in agreement with the previous expectation, no change of reflectivity is observed.

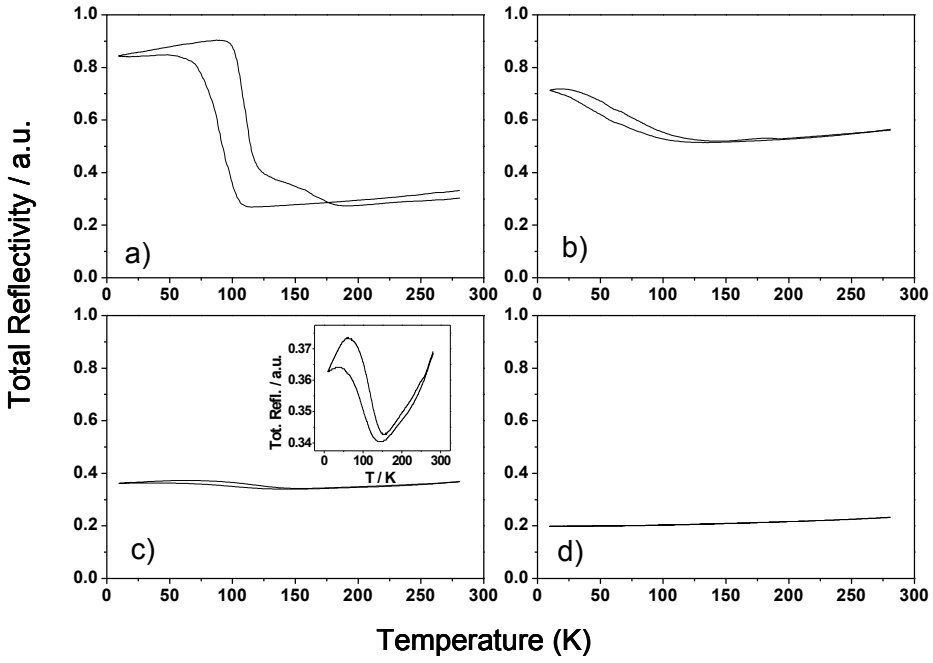

Figure III. 12: Total reflectivity of compounds a) $[Fe(L_{222}N_5)(CN)_2]\cdot H_2O$, b) $[Fe(L_{232}N_5)(CN)_2]\cdot 2.5H_2O$, c) $[Fe(L_{223}N_5)(CN)_2]\cdot 2.5H_2O$ and d) $[Fe(L_{323}N_5)(CN)_2]\cdot 1.5H_2O$. Insert: Enlarged graph for total reflectivity of $[Fe(L_{223}N_5)(CN)_2]\cdot 2.5H_2O$

As a remark, we observed changes of total reflectivity for the three complexes ($[Fe(L_{222}N_5)(CN)_2]\cdot H_2O$, $[Fe(L_{232}N_5)(CN)_2]\cdot 2.5H_2O$, and $[Fe(L_{223}N_5)(CN)_2]\cdot 2.5H_2O$), and attributed this to the presence of LIESST effect. From the warming branch of the LITH loop, it may be anticipate a relatively long lifetime of the photo-induced HS state as the change of reflectivity occurs at around 100 K. Nevertheless, we have also noticed that the change of intensity in reflectivity is strongly dependent on the nature of the ligands. Complex $[Fe(L_{222}N_5)(CN)_2]\cdot H_2O$ having the ligand $L_{222}N_5$ shows the highest level of change. When the chain length of the ligands increases, i.e. when ligand $L_{222}N_5$ is replaced by $L_{232}N_5$ or $L_{223}N_5$ ligands, a decrease in the intensity is observed and a decrease of the size of LITH loop is also observed. Finally the $[Fe(L_{323}N_5)(CN)_2]\cdot 1.5H_2O$ shows no increase in the total reflectivity.

III.3.3. Photomagnetic properties

Figure III. 13 presents the photomagnetic experiments performed on $[Fe(L_{222}N_5)(CN)_2]\cdot H_2O$, $[Fe(L_{232}N_5)(CN)_2]\cdot 2.5H_2O$, and $[Fe(L_{223}N_5)(CN)_2]\cdot 2.5H_2O$. These measurements have been carried out following the standard procedure [16-19]. The sample was firstly cooled down to 10 K inside the SQUID cavity and then irradiated with green light (λ = 514 nm). Under irradiation, the $\chi_M T$ product increases slowly to reach a maximum value of $\chi_M T$. The value reached after irradiation depends on the compound: 3.5 cm^3 K mol^{-1} for $[Fe(L_{222}N_5)(CN)_2]\cdot H_2O$, 2.5 cm^3 K mol^{-1} for **[**$Fe(L_{232}N_5)(CN)_2]\cdot 2.5H_2O$ and 1.5 cm^3 K mol^{-1} for **[**$Fe(L_{223}N_5)(CN)_2]\cdot 2.5H_2O$. It should be noticed that the photoconversion of the compound has required long time of photo-irradiation and quite large power of irradiation: 2 hours (10 K, 50 mW) for $[Fe(L_{222}N_5)(CN)_2]\cdot H_2O$, 3 hours (3 K, 200 mW) for **[**$Fe(L_{232}N_5)(CN)_2]\cdot 2.5H_2O$ and 10 hours (3 K, 200 mW) for **[**$Fe(L_{223}N_5)(CN)_2]\cdot 2.5H_2O$. As far as **[**$Fe(L_{323}N_5)(CN)_2]\cdot 1.5H_2O$ is concerned, irradiation at 3 K with P = 200 mW for several hours did not lead to any increase of magnetic susceptibility, and thus LIESST effect has not been observed. Moreover, several attempts have been done to change the wavelength (λ = 488.0-514.5 nm, 530.9 nm, 647.1-679.4 nm, and 752.5-799.3 nm) but excitation at 514 nm has been found the most efficient.

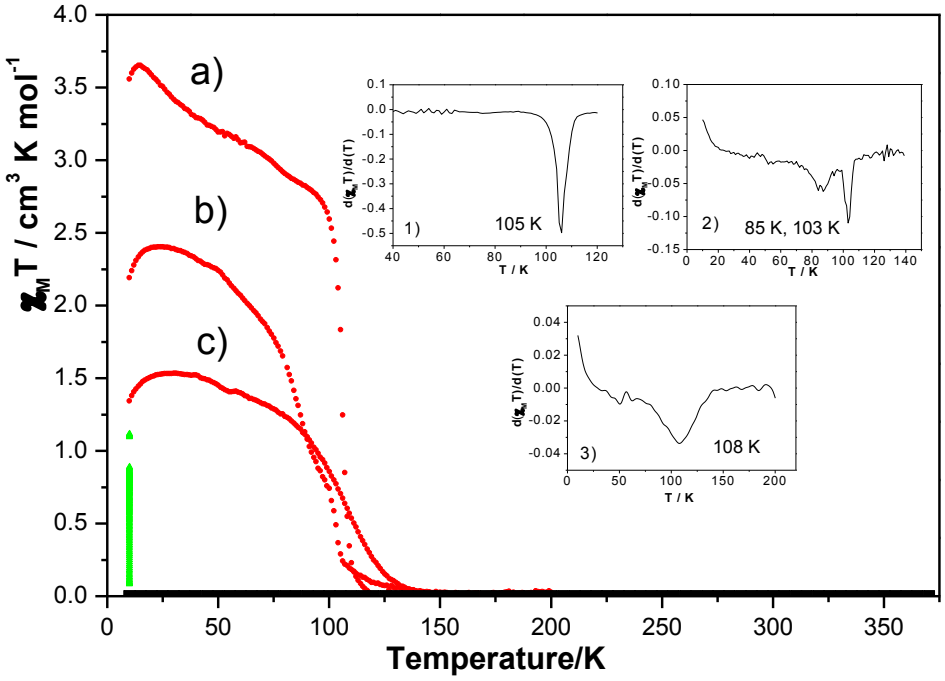

Figure III. 13: Figure 1 Magnetic and photomagnetic behaviours of a) $[Fe(L_{222}N_5)(CN)_2]\cdot H_2O$, b) $[Fe(L_{232}N_5)(CN)_2]\cdot 2.5H_2O$, and c) $[Fe(L_{223}N_5)(CN)_2]\cdot 2.5H_2O$. Magnetic measurements in the dark are represented in black, under irradiation at 10 K in green and measurements registered by increasing the temperature in the dark after irradiation are represented in red. T(LIESST) values are presented in inserted graphs: 1) 105 K for $[Fe(L_{222}N_5)(CN)_2]\cdot H_2O$, 2) 85 K and 103 K for $[Fe(L_{232}N_5)(CN)_2]\cdot 2.5H_2O$, and 3) 108 K for $[Fe(L_{223}N_5)(CN)_2]\cdot 2.5H_2O$.

T(LIESST) measurements were performed for the different complexes. After reaching the photosaturation at 10 K under irradiation, the laser was switched off and the temperature increased at a defined rate of 0.3 K min^{-1}. For complex **[**$Fe(L_{222}N_5)(CN)_2]\cdot H_2O$, the shape and the T(LIESST) value (105 K) are in agreement with the work of J. S. Costa [12]. For complex **[**$Fe(L_{232}N_5)(CN)_2]\cdot 2.5H_2O$, the shape of the T(LIESST) curve displays two steps at 85 K and 103 K respectively (Figure III. 13 inserted 2). For $[Fe(L_{223}N_5)(CN)_2]\cdot 2.5H_2O$, the T(LIESST) value is estimated at 108 K (Figure III. 13c).

Concerning the presence of two T(LIESST) values for $[Fe(L_{232}N_5)(CN)_2]\cdot 2.5H_2O$, let us describe the following experiment. Instead of using an irradiation power of 200 mW, we reproduce the experiment with an intensity of 150 mW. The recorded $\chi_M T$ vs. T curve is presented in Figure III. 14. The photostationary limit found at 10 K under this condition provides a $\chi_M T$ value of 1.7 cm^3 K mol^{-1}, which is lower than the one obtained by irradiation with 200 mW light. But what is more interesting is that in such condition, the T(LIESST) curve presents only one minimum at 80 K (Figure III. 14), that is at lower value of the two minima recorded by applying 200 mW of irradiation. It seems that with a lower power, only one T(LIESST) value is recorded at 80 K, while when higher power is applied, the T(LIESST) value shifts to higher temperature, reaching ca. 100 K. Consequently, the two T(LIESST) values observed on Figure III. 13b can be attributed respectively on domains of the sample with different level of saturation of photoconversion. Of course it would be interesting to apply higher power for irradiation. Unfortunately in SQUID cavity, the use of higher power destabilize of the temperature.

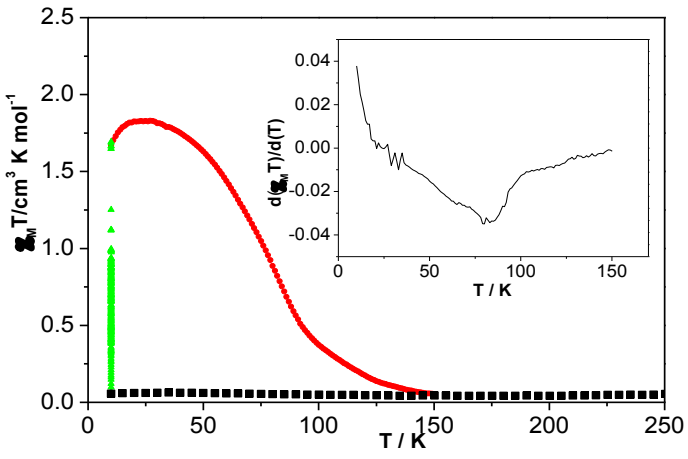

Figure III. 14: Figure 2 Magnetic and photomagnetic behaviors of $[Fe(L_{232}N_5)(CN)_2]\cdot 2.5H_2O$ with irradiation at 10 K for ca. 10 hours (10 K, 150 mW). The minimum of the derivative of $\chi_M T$ vs. T curve is found to be at 80 K.

III.3.4. Discussion and conclusion

In this part, we have reported the synthesis and the characterization of a new Fe(II) macrocyclic family with nitrogen coordination atoms on macrocyclic unit. In this family, the length of chains between the nitrogen atoms was increased and the consequence on the properties of the individual complex was investigated. From thermal analysis, it was illustrated that all the four studied complexes contained two different types of water molecule,

i.e. the water of surface adsorption and the water in the crystal lattice. From magnetic studies, it was demonstrated that all the four complexes were in LS state bellow 420 K and presented an irreversible increase of $\chi_M T$ product at around 420 K, which indicated that the magnetic properties of the family is independent with the chain length. Then we reported the reflectivity properties of the complexes, which demonstrated that three of them could be photoexcited to the metastable HS state. The photomagnetic studies further confirmed that the three complexes exhibited T(LIESST) value around 100 K. However, depending on the nature of the ligands, the level of photoexcitation is different. The highest level was found for $[Fe(L_{222}N_5)(CN)_2]\cdot H_2O$, while the lowest level was for $[Fe(L_{223}N_5)(CN)_2]\cdot 2.5H_2O$ complex.

Concerning the stability of the photoinduced state, let us first note that the three complexes $[Fe(L_{222}N_5)(CN)_2]\cdot H_2O$, $[Fe(L_{232}N_5)(CN)_2]\cdot 2.5H_2O$ and $[Fe(L_{223}N_5)(CN)_2]\cdot 2.5H_2O$ display similar T(LIESST) value of about 100 K. It seems consequently that the nature of the ligand in this macrocyclic family affects the easiness of photoexcitation (illustrated by different levels of photosaturation) but not the stability of the lifetime. In fact, if we consider the energy gap law approach [28], it is not expected that an Fe(II) material with a LS state presents a photoinduced HS state with a long lifetime. In our case, the three complexes display exceptional long lived lifetime for Fe(II) materials in LS state at room temperature.

One of the reason for such atypical stability of the photoinduced HS state may be linked to the 6 to 7 coordination change observed with $[Fe(L_{222}N_3O_2)(CN)_2]\cdot H_2O$ complex. In this context, the structures of the complexes in both LS and photoinduced HS state need to be investigated. Unfortunately, up to now no structure is available and our effort to get single crystals failed. It is consequently difficult to conclude on the presence of such 6/7 coordination change. An alternative reason of the high T(LIESST) may be linked to the role of the distortion involved along the relaxation process. Nevertheless by changing the nature of the ligand and by incorporating the Fe(II) metal ion into a macrocyclic sphere, these physical parameters have been certainly affected. The similar T(LIESST) found for all the $[Fe(L_{xyz}N_5)(CN)_2]\cdot nH_2O$ complexes seems to suggest that it is not the critical parameter.

Based on the photomagnetic properties recorded for the three complexes, we may complete the T(LIESST)/$T_{1/2}$ database by using the thermal temperature $T_{1/2}$ (recorded along the LS to HS transition measured by magnetic measurements), and the T(LIESST) values (deduced from the photomagnetic properties). Of course such analysis may be questionable in reason of the interplay between the SCO transition and the dehydration process. Nevertheless, it is interesting to note that the three new data points (Figure III. 15, sample **50-52**) are far above the T_0 = 180 K line for the macrocyclic sample, and towards a higher T_0 = 220 K line.

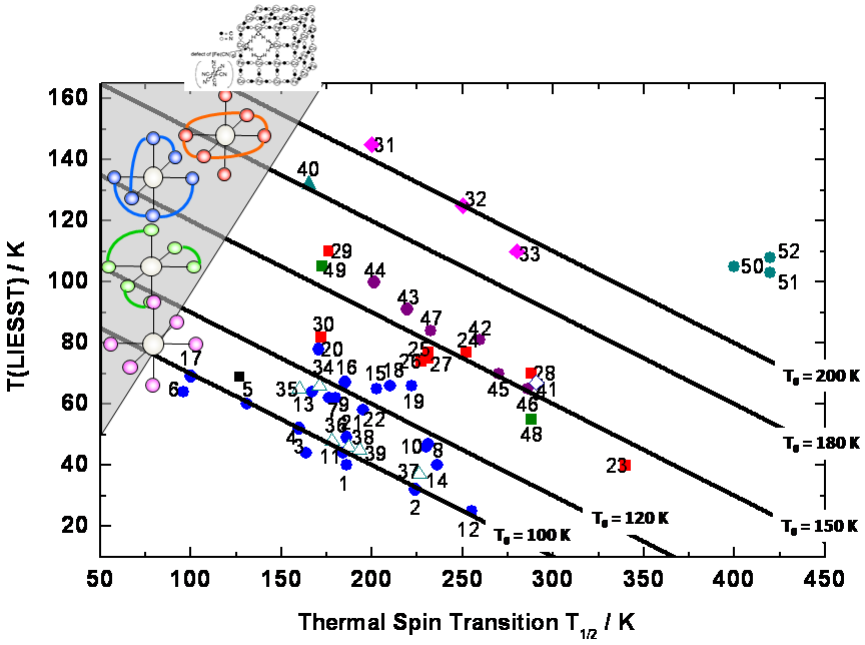

Figure III. 15: Figure 3 Variation of T(LIESST) versus $T_{1/2}$ for spin crossover compounds. Samples **50**-**52** are relative to the complexes $[Fe(L_{222}N_5)(CN)_2]\cdot H_2O$, $[Fe(L_{232}N_5)(CN)_2]\cdot 2.5H_2O$ and $[Fe(L_{223}N_5)(CN)_2]\cdot 2.5H_2O$ respectively.

References

1 A. Dees, A. Zahl, R. Puchta, N. J. R. van Eikema Hommes, F. W. Heinemann, I. Ivanović-Burmazović, *Inorg. Chem*. **2007**, *46*, 2459

2 O. Jiménez-Sandoval, D. Ramírez-Rosales, M. Rosales-Hoz, M. E. Sosa-Torres, R. Zamorano-Ulloa, *J. Chem. Soc., Dalton Trans.* **1998**, 1551.

3 K. Aston, N. Rath, A. Naik, U. Slomczynska, O. F. Schall, D. P. Riley, *Inorg. Chem.* **2001**, *40*, 1779.

4 B. Drahoš, J. Kotek, P. Hermann, I. Lukeš, É. Tóth, *Inorg. Chem.* **2010**, *49*, 3224.

5 B. Su, J. Zhao, *Synth. Commun.* **2005**, *35*, 2317.

6 A. Maroz, G. F. Kelso, R. A. J. Smith, D. C. Ware, R. F. Anderson, *J. Phys. Chem. A* **2008**, *112*, 4929.

7 D. Salvemini, Z. Q. Wang, J. L. Zweier, A. Samouilov, H. Macarthur, T. P. Misko, M. G. Currie, S. Cuzzocrea, J. A. Sikorski, D. P. Riley, *Science* **1999**, *286*, 304.

8 D. P. Riley, W. L. Neumann, S. L. Henke, P. Lennon, K. W. Aston, D. Salvemini, J. A. Sikorski, Y. M. Fobian, M. L. Grapperhaus, C. L. Kusturin, US Patent 6214187, 2001.

9 K. Aston, N. Rath, A. Naik, U. Slomczynska, O. F. Schall, D. P. Riley, *Inorg. Chem.* **2001**, *40*, 1779.

10 S. M. Nelson, P. D. A. Mcllroy, C. S. Stevenson, E. König, G. Ritter, J. Waigel, *J. Chem. Soc. Dalton Trans.* **1986**, 991.

11 I. V. Korendovych, O. P. Kryatova, W. M. Reiff, E. V. Rybak-Akimova, *Inorg. Chem.* **2007**, *46*, 4197.

12 J. S. Costa, PhD Thesis, Université Bordeaux I, **2005.**

13 D. T. Gryko, P. Piatek, A. Pecak, M. Palys, J. Jurczak, *Tetrahedron* **1998**, *54*, 7505.

14 J. S. Costa, C. Baldé, C. Carbonera, D. Denux, A. Wattiaux, C. Desplanches, J.-P. Ader, P. Gütlich, J.-F. Létard, *Inorg. Chem.* **2007**, *46*, 4114

15 Spin Crossover in Transition Metal Compounds, in Topics in Current Chemistry, ed. P. Gütlich and H. A. Goodwin, Springer-Verlag, Berlin– Heidelberg–New York, **2004**, vol. I, II and III.

16 J.-F. Létard, L. Capes, G. Chastanet, N. Moliner, S. Létard, J. A. Real, O. Kahn, *Chem. Phys. Lett.* **1999**, *313*, 115.

17 S. Marcén, L. Lecren, L. Capes, H. A. Goodwin, J.-F. Létard, *Chem. Phys. Lett.* **2002**, *358*, 87.

18 J.-F. Létard, P. Guionneau, O. Nguyen, J. S. Costa, S. Marcén, G. Chastanet, M. Marchivie, L. Goux-Capes, *Chem. Eur. J.* **2005**, *11*, 4582.

19 J.-F. Létard, *J. Mater. Chem.* **2006**, *16*, 2550.

20 O. Kahn, E. Codjovi, *Phil. Trans. R. Soc. London A.* **1996**, *354*, 359.

21 E. Codjovi, L. Sommier, O. Kahn, C. Jay, *New. J. Chem.* **1996**, *20*, 503.

22 W. Morscheidt, J. Jeftic, E. Codjovi, J. Linares, A. Bousseksou, H. Constant-Machado, F. Varret, *Meas. Sci. Technol.* **1998**, *9*, 1311.

23 J.-F. Létard, C. Carbonera, E. Courcot, J. S. Costa, *Bull. Mater. Sci.*, **2006**, *29*, 567.

24 J.-F. Létard, P. Guionneau L.Rabardel, J. A. K. Howard, A. E. Goeta, D. Chasseau, O. Kahn, *Inorg. Chem.* **1998**, *37*, 4432

25 S. Bonhommeau, N. Bréfuel, V. K. Pálfi, G. Molnár, A. Zwick, L. Salmon, J.-P. Tuchagues, J. S. Costa, J.-F. Létard, H. Paulsen, A. Bousseksou, *Phys. Chem. Chem. Phys.*, **2005**, *7*, 2909.

26 C. Enachescu, J. Linares, F. Varret, K. Boukheddaden, E. Codjovi, S. G. Salunke, R. Mukherjee, *Inorg. Chem.* **2004**, *43*, 4880.

27 P. Guionneau, F. Le Gac, A. Kaiba, J. S. Costa, D. Chasseau, J.-F. Létard, *Chem. Comm.* **2007**, *36*, 3723.

28 A. Hauser, A Vef, P. Adler, *J. Chem. Phys.* **1991**, 95, 8710

Part IV. Modification on the anionic ligand

Chapter IV.1. Introduction

IV.1.1. Influence of anionic ligand on the SCO properties of macrocyclic complexes

Each kind of ligand presents different ligand field strength. It is thus possible to play on the diversity of ligand field strength by connecting several different anionic ligands to a same metal center. This method has been applied to change the SCO properties in many complexes [1-6]. In Part III, we have investigated the macrocyclic family $[Fe(L_{xyz}N_5)(CN)_2]$, and observed that those cyano coordinated complexes are in LS state from 10 K to 400 K. If we consider the NCX^- (X = S, Se) anionic ligand, it is well known that the ligand field is lower than CN^- ligand. Therefore, the replacement of the cyano group by the thiocyanate or the selenocyanate ligand may be a possible method to modify the SCO properties in the $[Fe(L_{222}N_3O_2)(NCX)_2]$ (X = S, Se) family and recover the SCO properties in the $[Fe(L_{xyz}N_5)(NCX)_2]$ (X = S, Se) family. Indeed, starting from a LS complex and replacing ligand by another one with lower ligand field strength may hopefully allow obtaining a SCO complex.

Moreover, structural study of the $[Fe(L_{222}N_3O_2)(CN)_2]\cdot H_2O$ complex confirmed that it adopts a hepta-coordinate geometry in the HS state (HS-7 $FeN_3C_2O_2$) and a hexa-coordinate geometry in the LS state (LS-6 FeN_3C_2O) [9-11]. One of the two oxygen atoms in the macrocyclic ligand, which locates in planar position, exhibits a reversible metal–ligand bond break associated to the SCO. This phenomenon is unique in the SCO complexes so far. Remarkably, the modification of the coordination of the metal centre occurs in the solid state and corresponds to a drastic phase transition but without degradation of the crystalline character of the sample. It is thus a unique example of a single-crystal to single-crystal transition corresponding to a spin crossover with a change of coordination. This phenomenon is still under study and the exact nature of the parameters that give rise to the change of coordination is still debated. However, it is already interesting to question the character exceptional or even unique of such phenomenon. For this reason, it will be interesting to perform the structural investigation on the thiocyanate / selenocyanate coordinated macrocyclic complexes to check whether those complexes exhibit, or not, a similar metal–ligand bond break.

In the literature, some structures of the $[Fe(L_{222}N_3O_2)(NCX)_2]$ and $[Fe(L_{xyz}N_5)(NCX)_2]$ (X = S, Se) families have already been investigated. Nelson et al. [7] in 1976 studied at room temperature the structure of the two macrocyclic Fe(II) complexes $[Fe(L_{222}N_5)(NCS)_2]$ and $[Fe(L_{232}N_5)(NCS)_2]$. These authors indicated that the two metal ions behave in HS state and are seven coordinated (Figure IV. 1)

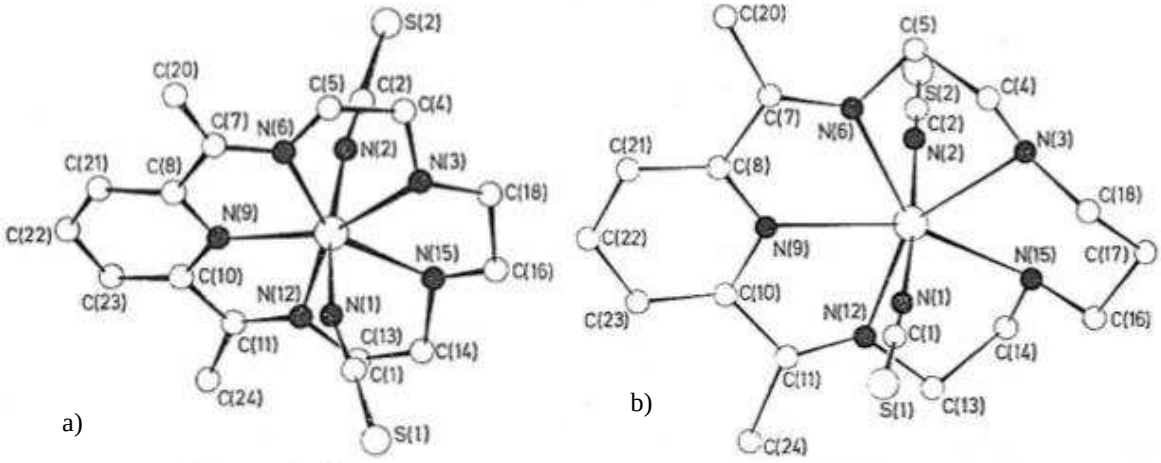

Figure IV. 1: Molecular structures of seven coordinated Fe(II) complexes: a) $[Fe(L_{222}N_5)(NCS)_2]$ b) $[Fe(L_{232}N_5)(NCS)_2]$ [7].

In 2005, J. S. Costa [8] described some structures and magnetic properties of $[Fe(L_{222}N_3O_2)(NCX)_2]$ (X = S, Se) analogue. Magnetic measurements on the $[Fe(L_{222}N_3O_2)(NCX)_2]$ (X = S, Se) samples revealed that the two complexes remain HS whatever the temperature. Structures of the $[Fe(L_{222}N_3O_2)(NCS)_2]$ complex determined on single crystal at room temperature revealed that the Fe(II) center is seven coordinated (Figure IV. 2).

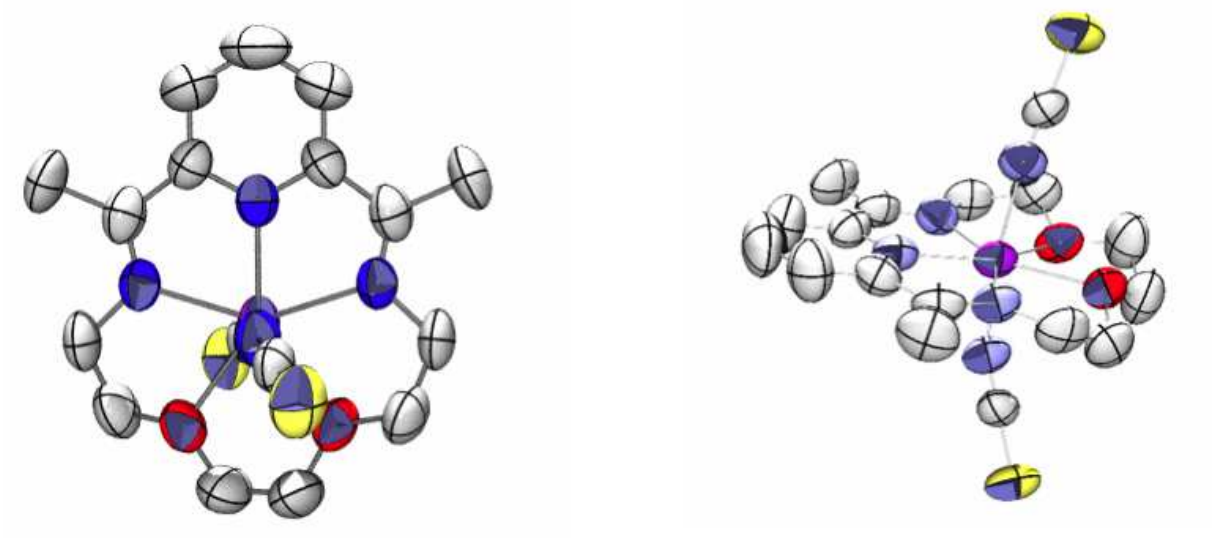

Figure IV. 2: Molecular structure of $[Fe(L_{222}N_3O_2)(NCS)_2]$ complex [8].

IV.1.2. Objective of Part IV

In the Part IV, we will report the synthesis and the efforts made to obtain single crystals of eight compounds having the formula $[Fe(L)(X)_2]$ (ligand L = $L_{222}N_3O_2$, $L_{222}N_5$, $L_{232}N_5$, or $L_{223}N_5$, X = NCS or NCSe) (Scheme IV. 1). The main purpose is to perform a systematic structural investigation on those complexes, notably the relation between the SCO, the metal-coordination modifications and the low temperature structural phase transition.

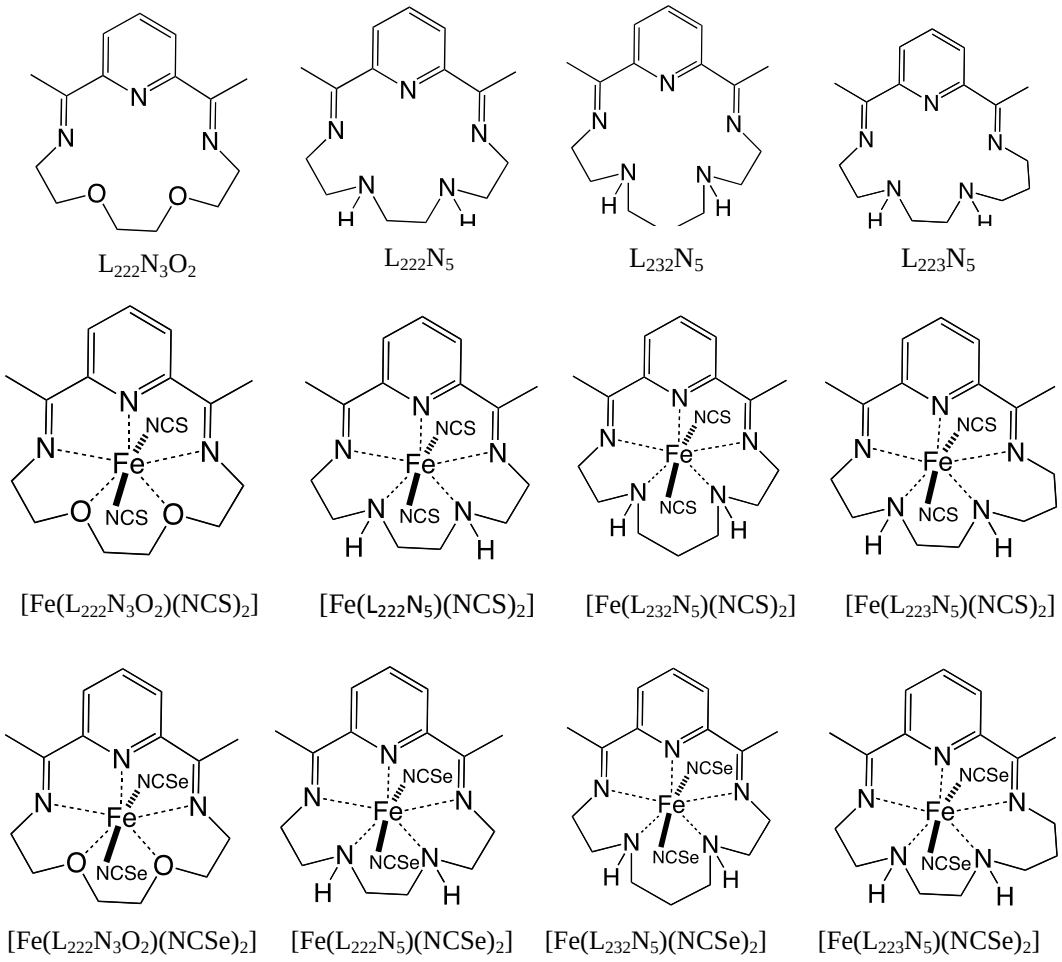

Scheme IV. 1: Ligands (top) and complexes (low) and the corresponding nomenclature used in this chapter

Chapter IV.2. Synthesis and crystallization

IV.2.1. Synthesis of $[Fe(L)(X)_2]\cdot nH_2O$

The synthesis of the eight samples $[Fe(L)(NCX)_2]$ (X = S or Se) were performed as described by Nelson et al. for the synthesis of $[Fe(L_{222}N_3O_2)(CN)_2]$ complex [12]. All the reactions were carried out under anaerobic condition and all solvents were degassed.

The synthesis route of $[Fe(L_{222}N_3O_2)(NCS)_2]$ is presented in Figure IV. 3. It is a two step procedure which involves a template reaction in the first step. The synthesis was carried out in 15 mL of methanol and 10 mL of water in which were dissolved 1.20 g (6 mmol) of iron chloride tetrahydrate, 1.0 g (6 mmol) of 2,6-diacetylpyridine, and 0.1 g of sodium dithionite (used as reducing agent to remove traces of trivalent iron ion). Then 3,6-diamine dioxaoctane-1,8-diamine (0.92mL, 6 mmol) was added dropwise. The mixture was kept under nitrogen reflux at 75 °C for 16 h approximately (formation of $[Fe(L_{222}N_3O_2)(Cl)_2]$). After filtration, 15 mL of aqueous solution containing an excess of potassium thiocyanate KNCS (2g, 0.02 mol) and 0.1 g of sodium dithionite was added. This solution was then kept stirring for ca. 6 hours at room temperatu're. The polycrystalline powder formed was then filtered and washed with 10 mL of degassed water and dried under vacuum. Finally 0.9 g (yield ~ 40%) of powder was collected. The synthesis of $[Fe(L_{222}N_3O_2)(NCSe)_2]$ complex was similar. The only difference was the replacement of KCN by KNCSe in the step 2.

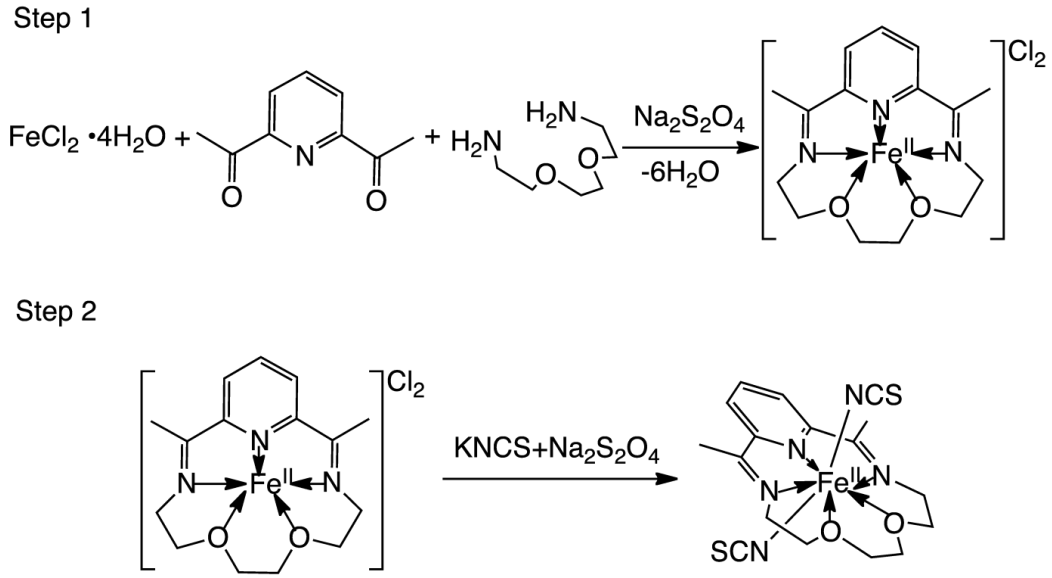

Figure IV. 3: Synthesis of $[Fe(L_{222}N_3O_2)(NCS)_2]$ complex.

The synthesis of $[Fe(L_{222}N_5)(NCX)_2]$, $[Fe(L_{232}N_5)(NCX)_2]$ and $[Fe(L_{223}N_5)(NCX)_2]$ (X=S or Se), are similar with the one of $[Fe(L_{222}N_3O_2)(NCX)_2]$ described above. The amine parts, are triethylenetetramine (for $L_{222}N_5$), N,N'-Bis(2-aminoethyl)-1,3-propanediamine (for $L_{232}N_5$), and N-(2-aminoethyl)- N'-(3-aminopropyl)ethylene-diamine tetrahydrochloride (for $L_{223}N_5$), respectively. In the peculiar case of the $[Fe(L_{223}N_5)(NCX)_2]$, N-(2-aminoethyl)-N'-(3-aminopropyl) ethylene-diamine tetrahydrochloride (1.84 g, 6 mmol) was dissolved in 5 mL

of aqueous solution containing NaOH (0.96 g, 24 mmol) to deprotonate the amine.

Polycrystalline powders of the eight complexes were obtained. The chemical analyses listed in Table IV. 1 indicate a good agreement between experimental and calculated data. In the cases of $[Fe(L_{232}N_5)(NCX)_2]$ and $[Fe(L_{223}N_5)(NCX)_2]$ (X=S or Se), the elemental analysis suggests the presence of water molecules.

Complex	C	H	N	S/Se	Fe
$[Fe(L_{222}N_3O_2)(NCS)_2]$	44.99(45.64)	4.59(4.73)	15.36(15.65)	13.73(14.34)	12.26(12.48)
$[Fe(L_{222}N_3O_2)(NCSe)_2]$	37.57(37.73)	3.85(3.91)	12.69(12.94)	28.72(29.18)	10.83(10.32)
$[Fe(L_{222}N_5)(NCS)_2]$	45.26(45.84)	5.13(5.21)	21.73(22.01)	13.33(14.40)	13.23(12.54)
$[Fe(L_{222}N_5)(NCSe)_2]$	37.28(37.87)	4.16(4.30)	17.69(18.18)	28.52(29.29)	11.05(10.36)
$[Fe(L_{232}N_5)(NCS)_2]\cdot H_2O$	45.43(45.28)	5.06(5.70)	20.41(20.54)	12.32(13.43)	12.44(11.70)
$[Fe(L_{232}N_5)(NCSe)_2]\cdot H_2O$	37.98(37.85)	4.43(4.76)	16.80(17.16)	28.31(27.65)	10.14(9.78)
$[Fe(L_{223}N_5)(NCS)_2]\cdot H_2O$	45.64(45.28)	5.18(5.70)	20.57(20.54)	13.22(13.22)	11.89(11.70)
$[Fe(L_{223}N_5)(NCSe)_2]\cdot 2H_2O$	36.92(36.69)	4.19(4.96)	16.55(16.64)	27.25(26.80)	10.26(9.48)

Table IV. 1: Elemental microanalyses of the $[Fe(L_{222}N_3O_2)(NCX)_2]$ and $[Fe(L_{xyz}N_5)(NCX)_2]\cdot nH_2O$ (X=S or Se) family [found, % (calcd, %)].

IV.2.2. Crystallization of $[Fe(L_{222}N_3O_2)(NCX)_2]$ and $[Fe(L_{xyz}N_5)(CN)_2]\cdot nH_2O$ family

Slow diffusion method in H shape tubes was used to crystallize the complexes. Precisely, after the step 1 of the synthesis, solution containing $[Fe(L)(Cl)_2]$ and aqueous solution containing KNCS or KNCSe were added to the two bottoms of the H tube separately. Water was then slowly added in the H tube for slow diffusion. After a few weeks, crystals were found at the bottom of the H tube.

To complete this study, other solvents, like methanol, ethanol, $CHCl_3$, CH_2Cl_2 and the different mixture of those solvents, were used to analyze the influence of solvent on the diffusion process.

Chapter IV.3. Magnetic and X-ray diffraction structural investigations

Thanks to the help of A. Kaiba (Post-doc) and C. Sinito (Master thesis) single crystals of eight complexes were obtained. We will hereafter report for each of them the magnetic and X-ray structures.

IV.3.1. Magnetic properties

The temperature dependence of $\chi_M T$ for the eight complexes is presented in Figure IV. 4 and 5. These properties were determined on polycrystalline powders by using the SQUID magnetometer from room temperature down to 10 K. For all the complexes, the $\chi_M T$ product is close to 3.5 $cm^3mol^{-1}K$ between room temperature and 25 K. Below 25 K, a slight decrease of $\chi_M T$ is observed, which can be attributed to the zero field splitting and/or interaction between Fe(II) centers. This magnetic behavior is coherent with the fact that all the complexes are in HS state in the studied temperature range. No SCO is therefore observed in the investigated temperature range and experimental conditions.

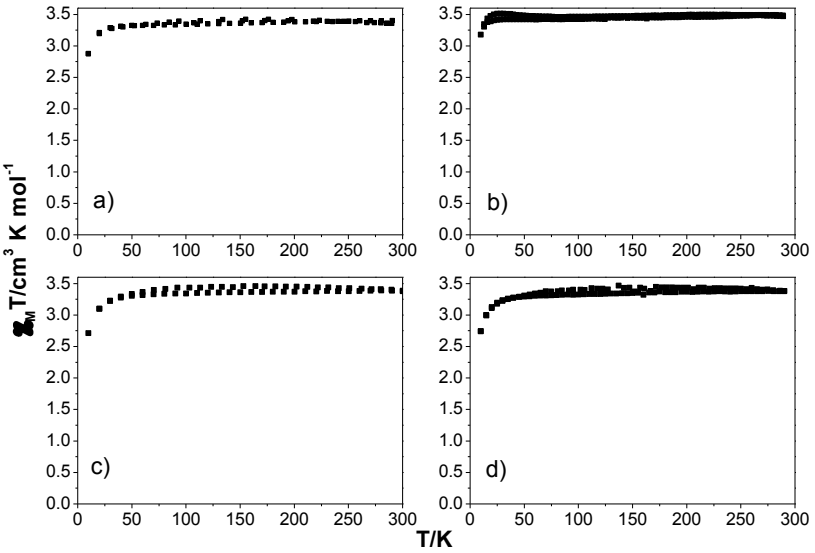

Figure IV. 4: Temperature dependence of $\chi_M T$ for thiocyanate coordinated complexes. a) $[Fe(L_{222}N_3O_2)(NCS)_2]$, b) $[Fe(L_{222}N_5)(NCS)_2]$, c) $[Fe(L_{232}N_5)(NCS)_2]\cdot H_2O$ and d) $[Fe(L_{223}N_5)(NCS)_2]\cdot H_2O$

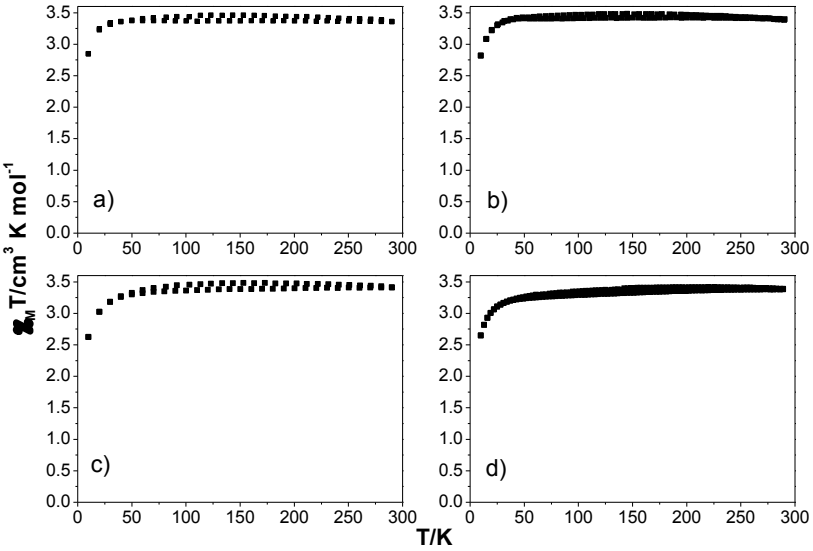

Figure IV. 5: Temperature dependence of $\chi_M T$ for selenocyanate coordinated complexes. a) $[Fe(L_{222}N_3O_2)(NCSe)_2]$, b) $[Fe(L_{222}N_5)(NCSe)_2]$, c) $[Fe(L_{232}N_5)(NCSe)_2]\cdot H_2O$ and d) $[Fe(L_{223}N_5)(NCSe)_2]\cdot 2H_2O$

IV.3.2. Crystal structures of $[Fe(L_{222}N_3O_2)(NCS)_2]$ and $[Fe(L_{222}N_3O_2)(NCSe)_2]$

a) Case of the $[Fe(L_{222}N_3O_2)(NCS)_2]$ complex

The complex $[Fe(L_{222}N_3O_2)(NCS)_2]$ crystallizes in a monoclinic P 2/n space group at room temperature, with a unit cell volume of 1007.31(8) Å^3 (Table IV. 2). The Fe(II) is hepta-coordinated, with a pentagonal bipyramidal environment (Figure IV. 6a). The Fe(II) atom is located in a twofold axis and the Fe–O bonds are therefore geometrically identical by symmetry (Table IV. 3). These bond distances characterize unambiguously a high spin state. The Fe–O bond distance is 2.302(2) Å. The volume of the coordination sphere, calculated from the atomic positions using IVTON, is 16.4 Å^3. The crystal packing is presented in Figure IV. 6b. The S atom makes a short contact with the neighboring S atom characterized by a short distance of 3.4983(8) Å.

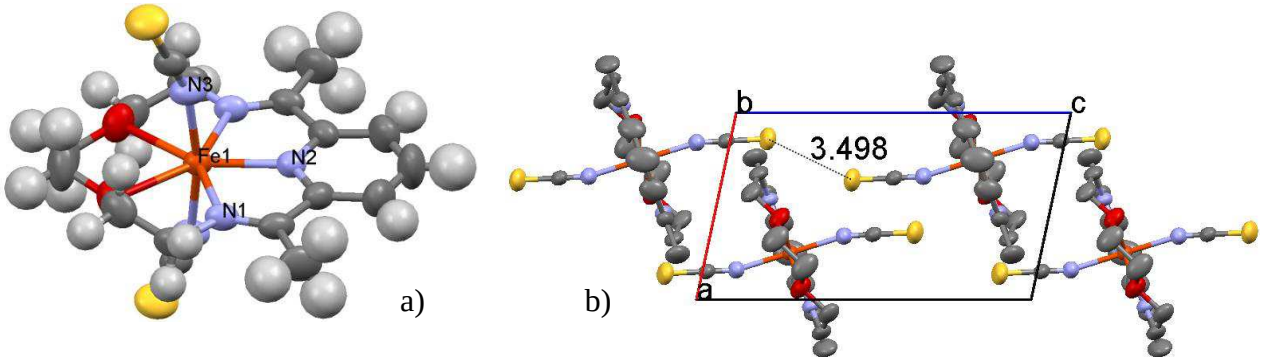

Figure IV. 6: a) Molecular structure and b) Crystal packing of $[Fe(L_{222}N_3O_2)(NCS)_2]$ at 293 K. Hydrogen atoms have been omitted for clarity.

Compound	$[Fe(L_{222}N_3O_2)(NCS)_2]$	
Formula	$C_{17}H_{21}FeN_5O_2S_2$	$C_{17}H_{21}FeN_5O_2S_2$
M_r (g.mol^{-1})	447.38	447.38
Colour	black	black
Crystal size (mm^3)	0.75 × 0.75 × 0.38	0.75 × 0.75 × 0.38
Crystal morphology	plate	plate
Temperature (K)	293(2)	120(2)
Crystal system	monoclinic	triclinic
Space group	P 2/n	P -1
a (Å)	7.0540(2)	7.0081(14)
b (Å)	11.7587(6)	11.651(4)
c (Å)	12.4200(6)	12.321(3)
α (°)	90	88.883(14)
β (°)	102.097(3)	78.274(15)
γ (°)	90	87.09(2)
V (Å^3)	1007.31(8)	983.7(5)
Z	2	2
Density (g.cm^{-3})	1.475	1.510
μ (mm^{-1})	0.978	1.001
No. of total reflections	1957	798
R_{obs}	0.0387	0.0699
$wR2_{obs}$	0.1078	0.1633
S	1.021	1.072

Table IV. 2: Crystal data of $[Fe(L_{222}N_3O_2)(NCS)_2]$

293 K		120 K	
Fe1 — O1	2.302(2)	Fe1 — O1a	2.27(1)
		Fe1 — O1b	2.30(1)
Fe1 — N1	2.200(1)	Fe1 — N1a	2.176(9)
		Fe1 — N1b	2.203(9)
Fe1 — N2	2.119(2)	Fe1 — N2	2.15(1)
Fe1 — N3	2.103(2)	Fe1 — N3a	2.070(9)
		Fe1 — N3b	2.086(9)

Table IV. 3: Selected geometric parameters (Å) for $[Fe(L_{222}N_3O_2)(NCS)_2]$ at 293 K and 120 K.

The same crystal was then cooled to 120 K and the crystal structure was determined. Interestingly, a phase transition is observed since, at this temperature, it adopts a triclinic P -1 space group, with a unit cell volume of 983.7(5) Å^3. The Fe–N bond distances are still in the range of 2.1 Å - 2.2 Å and the coordination sphere volume is 16.08 Å^3, characterizing a HS-7 metal centre. Therefore the sample does not undergo a SCO nor a metal coordination modification but it undergoes a pure structural transition corresponding to a loss of symmetry. If the Fe(II) ion is still hepta-coordinated, however it is now located in a general position, with a loss of the twofold axis (Figure IV. 7a). The Fe–O bonds are not anymore identical: 2.27(1) Å for Fe1–O1a and 2.30(1) Å for Fe1–O1b. The crystal packing is presented in Figure IV. 7b. The S atom is still in short contact with neighboring S atom, but to a distance shortened to 3.456(3) Å.

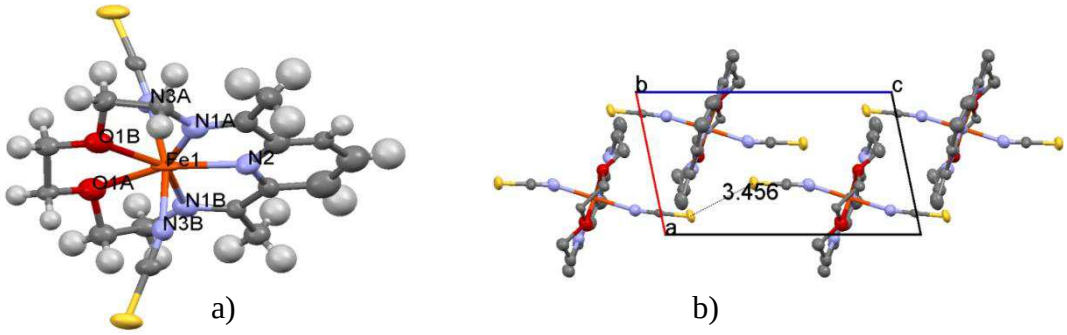

Figure IV. 7: a) Molecular structure and b) Crystal packing of $[Fe(L_{222}N_3O_2)(NCS)_2]$ at 120 K. Hydrogen atoms have been omitted for clarity.

b) Case of the $[Fe(L_{222}N_3O_2)(NCSe)_2]$ complex

The structure of the $[Fe(L_{222}N_3O_2)(NCSe)_2]$ complex obtained by slow diffusion in water was determined at 300 K. It adopts the P -1 space group, with one molecular complex in the asymmetric unit and no water molecule (Table IV. 4). The Fe(II) ion is hepta-coordinated, and it lies in a pentagonal bipyramidal environment. The Fe(II) atom is located in a general position. Oxygen atoms are located in non symmetrical positions. However, it should be emphasized that the final goodness of fit is 1.652 and can not be further improved. It indicates that crystallinity of the selected crystal is not good enough to comment further in details.

The crystal structure of the $[Fe(L_{222}N_3O_2)(NCSe)_2]$ complex obtained by diffusion in ethanol was also determined at 100 K. It adopts the same triclinic P -1 space group as the one obtained in water. In this crystal there is still one molecule in the asymmetric unit as the one obtained in water (Table IV. 4). The Fe(II) ion is hepta-coordinated, being in a pentagonal bipyramidal environment (Figure IV. 8a). The Fe(II) atom is located in a general position. Oxygen atoms are located in non symmetrical positions. The Fe–O distances are 2.309(3) Å for Fe1–O1 and 2.286(2) Å for Fe1–O2. Fe–N bond distances are still in the range of 2.1 Å - 2.2 Å. Selected metal—ligand bond lengths are listed in Table IV. 5. Those distances characterize a high spin state. The crystal packing is presented in Figure IV. 8b. The selenium atom is in short contact with neighboring Se atom. The distance between the two Se atoms is 3.5106(5) Å.

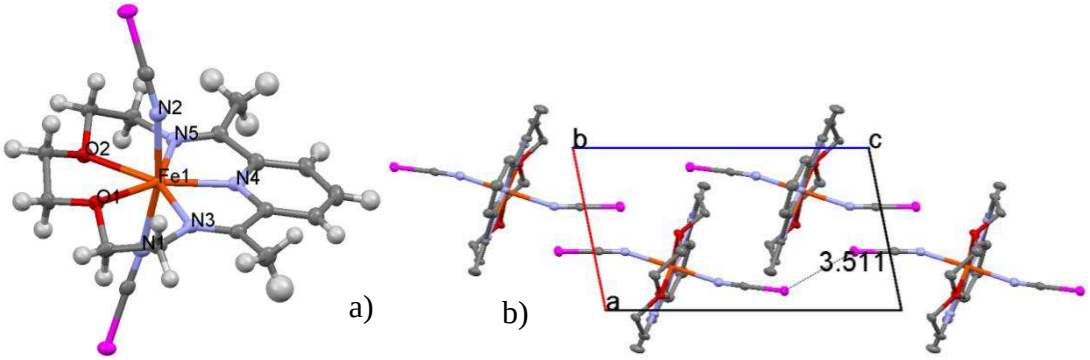

Figure IV. 8: a) Molecular structure and b) Crystal packing of $[Fe(L_{222}N_3O_2)(NCSe)_2]$ at 100 K. Hydrogen atoms have been omitted for clarity.

Compound	$[Fe(L_{222}N_3O_2)(NCSe)_2]$	
Formula	$C_{17}H_{21}FeN_5O_2Se_2$	$C_{17}H_{21}FeN_5O_2Se_2$
M_r (g.mol^{-1})	541.16	541.16
Colour	black	black
Crystal size (mm^3)	0.25 × 0.05 × 0.03	0.25 × 0.2 × 0.2
Crystal morphology	rectangular	rectangular
Temperature (K)	293(2)	100(2)
Crystal system	triclinic	triclinic
Space group	P-1	P-1
a (Å)	7.1138(5)	7.0655(3)
b (Å)	11.8204(8)	11.6012(5)
c (Å)	12.7513(8)	12.5957(5)
α (°)	88.872(5)	87.073(3)
β (°)	77.488(5)	78.284(3)
γ (°)	87.918(5)	83.751(3)
V (Å^3)	1046.00(12)	1004.49(7)
Z	2	2
Density (g.cm^{-3})	1.718	1.789
μ (mm^{-1})	4.222	4.397
No. of total reflections	4698	4503
R_{obs}	0.1501	0.0386
$wR2_{obs}$	0.4288	0.1073
S	1.652	1.158

Table IV. 4: Crystal data of $[Fe(L_{222}N_3O_2)(NCSe)_2]$

Fe1 — O1	2.309(3)	Fe1 — N1	2.107(4)
Fe1 — O2	2.286(2)	Fe1 — N2	2.112(4)
Fe1 — N4	2.119(4)	Fe1 — N3	2.214(3)
		Fe1 — N5	2.219(3)

Table IV. 5: Selected geometric parameters (Å) for $[Fe(L_{222}N_3O_2)(NCSe)_2]$ at 100 K

c) Conluding remarks

The crystal structures of two $[Fe(L_{222}N_3O_2)(NCX)_2]$ complexes (X= S and Se) have thus been determined, both remain in HS-7 whatever the temperature. Crystal data show that the complexes are isomorphous at low temperature but not at room temperature. Indeed, while $[Fe(L_{222}N_3O_2)(NCS)_2]$ presents a structural transition from monoclinic P 2/n to triclinic P -1 on cooling, $[Fe(L_{222}N_3O_2)(NCSe)_2]$ adopts the triclinic P-1 space group on the entire temperature range.

Compared with the cyano coordinated $[Fe(L_{222}N_3O_2)(CN)_2]\cdot H_2O$* (Part II, Chapter II), several similarities can be found in the structure of $[Fe(L_{222}N_3O_2)(NCS)_2]$. In both complexes,

* At room temperature: C 2/c space group with a = 17.326(5) Å, b = 12.054(5) Å, c = 10.125(5) Å, , β = 116.270(10) °; At 120 K: P 2_1/c space group with a = 10.6243(4) Å, b = 11.9157(4) Å, c = 14.6759(5) Å, β = 105.082(5) °.

a structural transition is observed on changing the temperature, which results in the loss of the twofold axis on Fe(II) leading to the differentiation of the two Fe-O lengths. However, in the cyano complex, this differentiation is much more pronounced since it corresponds to the change of the metal coordination. Note that, at room temperature, the Fe(II) coordination environments are close for the two complexes $[Fe(L_{222}N_3O_2)(NCS)_2]$ and $[Fe(L_{222}N_3O_2)(CN)_2]\cdot H_2O$. The coordination volume of $[Fe(L_{222}N_3O_2)(NCS)_2]$ is 16.4 $Å^3$, similar to the one of $[Fe(L_{222}N_3O_2)(CN)_2]\cdot H_2O$, i.e.17.0 $Å^3$. The Fe–O distances are also close: 2.302(2) Å for $[Fe(L_{222}N_3O_2)(NCS)_2]$ and 2.3342 (18) Å for $[Fe(L_{222}N_3O_2)(CN)_2]\cdot H_2O$. Only the coordination atom in axial position is different. Elsewhere, from 293 K to 120 K, the change of the unit cell volume is 2.3% for $[Fe(L_{222}N_3O_2)(NCS)_2]$, which is due to the thermal contraction effects and correspond to the usual value for this kind of mononuclear molecular SCO complexes [13]. For $[Fe(L_{222}N_3O_2)(CN)_2]\cdot H_2O$, the unit cell volume decreases by 5.4% from 293 K to 120 K but in this case it corresponds to the sum of the SCO and the thermal effects. Moreover, a significant difference in crystal packing is observed comparing the two complexes. In the $[Fe(L_{222}N_3O_2)(CN)_2]\cdot H_2O$ complex at high temperature, the water molecule is linked to the cyano group, and a one dimensional chain is thus formed by hydrogen bond with N…O distances of ca. 2.8 Å [9], while in the $[Fe(L_{222}N_3O_2)(NCS)_2]$ complex, no such one dimensional chain is formed by hydrogen bond. A comparable interaction along the axial position in the $Fe(L_{222}N_3O_2)(NCS)_2]$ complex is the S…S short contact with distances of ca. 3.4 Å, which is longer than the N…O distances in the $[Fe(L_{222}N_3O_2)(CN)_2]\cdot H_2O$ complex. Therefore our current study reveals that by replacing the cyano group axial position with thiocyanate group, which possess weaker ligand field strengths, the thermal spin transition and the associated change of coordination are suppressed. In parallel, interestingly, it shows that, in the thiocyanate complex, a pure structural transition corresponding to a loss of symmetry still occurs at low temperature. The structural study as a function of temperature to locate the exact temperature of transition is still undergoing.

IV.3.3. Crystal structures of $[Fe(L_{222}N_5)(NCS)_2]$ and $[Fe(L_{222}N_5)(NCSe)_2]$

The structural determination of the $[Fe(L_{222}N_5)(NCS)_2]$ complex was performed at both 250 K and 110 K. It adopts a triclinic P -1 space group at both temperatures (Table IV. 6). The asymmetric unit of this complex contains two crystallographically independent molecules (Figure IV. 9a). Both of the two independent Fe(II) centers are hepta-coordinated at 250 K and 110 K. The bond lengths (Table IV. 7) characterize the HS state at both temperatures. The coordination sphere volumes are c.a. 17.2 $Å^3$ for the two Fe(II) centers at 250 K and 110 K. Consequently, there is nor SCO nor structural phase transition in this complex. At 110 K, the Fe–N distances are in the range of 2.1 Å to 2.3 Å.

Compound	$[Fe(L_{222}N_5)(NCS)_2]$	
Formula	$C_{17}H_{23}FeN_7S_2$	$C_{17}H_{23}FeN_7S_2$
λ (Å)	0.71073	0.71073
M_r (g.mol^{-1})	445.41	445.41
Colour	black	black
Crystal size (mm^3)	0.1 × 0.05 × 0.03	0.38 × 0.25 × 0.25
Crystal morphology	prism	prism
Temperature (K)	250(2)	110(2)
Crystal system	triclinic	triclinic
Space group	P-1	P-1
a (Å)	10.0780(2)	10.02920(10)
b (Å)	12.7955(4)	12.64680(10)
c (Å)	16.6985(5)	16.6405(2)
α (°)	76.0790(10)	76.6240(10)
β (°)	80.178(2)	79.8490(10)
γ (°)	89.127(2)	88.9120(10)
V (Å^3)	2058.69(10)	2020.72(4)
Z	4	4
Density (g.cm^{-3})	1.437	1.464
μ (mm^{-1})	0.952	0.970
No. of total reflections	9357	17674
R_{obs}	0.0431	0.0314
$wR2_{obs}$	0.0838	0.0768
S	1.002	1.019

Table IV. 6: Crystal data of $[Fe(L_{222}N_5)(NCS)_2]$ complex

250 K		110 K	
Fe1 — N1	2.168(2)	Fe1 — N1	2.1429(9)
Fe1 — N2	2.136(2)	Fe1 — N2	2.1238(9)
Fe1 — N3	2.183(2)	Fe1 — N3	2.1797(9)
Fe1 — N4	2.249(2)	Fe1 — N4	2.2847(9)
Fe1 — N5	2.119(2)	Fe1 — N5	2.313(1)
Fe1 — N6	2.103(2)	Fe1 — N6	2.2739(8)
Fe1 — N7	2.256(2)	Fe1 — N7	2.251(1)
Fe2 — N8	2.299(3)	Fe2 — N8	2.320(1)
Fe2 — N9	2.284(2)	Fe2 — N9	2.2572(8)
Fe2 — N10	2.179(2)	Fe2 — N10	2.179(1)
Fe2 — N11	2.250(3)	Fe2 — N11	2.2580(9)
Fe2 — N12	2.270(2)	Fe2 — N12	2.2863(9)
Fe2 — N13	2.154(2)	Fe2 — N13	2.1366(9)
Fe2 — N14	2.130(2)	Fe2 — N14	2.1624(8)

Table IV. 7: Selected geometric parameters (Å) for $[Fe(L_{222}N_5)(NCS)_2]$ at 250 K and 110 K

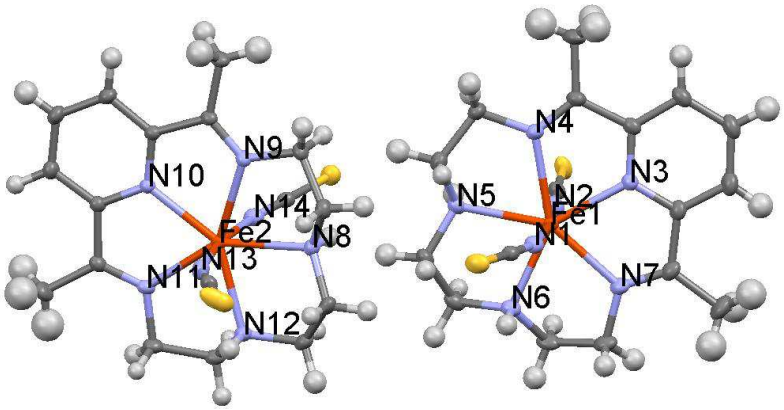

Figure IV. 9: Molecular structure of $[Fe(L_{222}N_5)(NCS)_2]$ at 110 K. Hydrogen atoms have been omitted for clarity.

The crystal packing of $[Fe(L_{222}N_5)(NCS)_2]$ at both 250 K and 110 K is presented in Figure IV. 10. At 250 K, the sulfur atom S3, having Fe2 as metal center, is in short contact with the neighboring S3 atom of molecule Fe2 (Figure IV. 10a). The distance between the two S3 atoms is 3.240(1) Å. However, the distance between two sulfur atoms having Fe1 as metal center are much longer: 3.662(2) Å. At 110 K, sulfur atom S2 is disordered. It can be resolved into S2A and S2B, having occupation factor of 40 % and 60 %. The S2 atom and the S3 atom are in short contact with neighboring sulfur atom (Figure IV. 10b). The distances between sulfur atoms are 3.1832(3) Å for S3–S3, 3.576(7) Å for S2B–S2B and 3.59(1) Å for S2A–S2A.

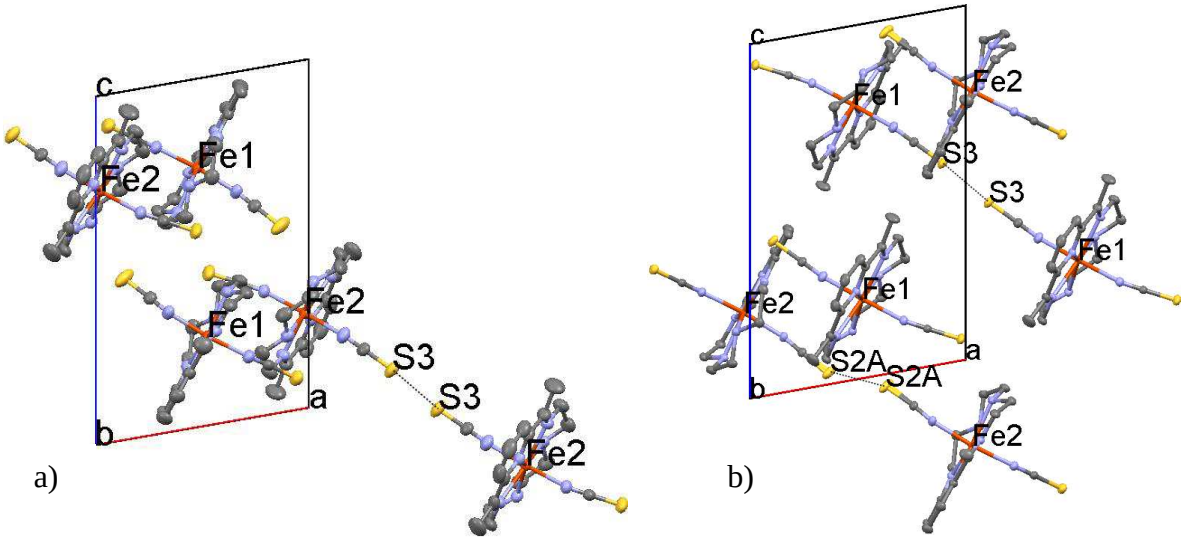

Figure IV. 10: Crystal packing of $[Fe(L_{222}N_5)(NCS)_2]$ at a) 250 K, and b)110 K. Hydrogen atoms have been omitted for clarity.

In parallel, the structure of the $[Fe(L_{222}N_5)(NCSe)_2]$ complex was determined at both room temperature and 100 K. It adopts a triclinic P -1 space group at the two temperatures (Table IV. 8). The asymmetric unit of this complex contains one molecule. The Fe(II) center locates in a general position (Figure IV. 11a). According to the bond lengths (Table IV. 9), the complex is in the HS state with a seven coordination environment at both temperatures. This is confirmed by the coordination sphere volumes of c.a. 17.3 $Å^3$ at 293 K and at 100 K.

Compound	$[Fe(L_{222}N_5)(NCSe)_2]$	
Formula	$C_{17}H_{23}FeN_7Se_2$	$C_{17}H_{23}FeN_7Se_2$
M_r (g.mol^{-1})	539.19	539.19
Colour	black	black
Crystal size (mm^3)	0.50 × 0.50 × 0.20	0.50 × 0.50 × 0.20
Crystal morphology	plate	plate
Temperature (K)	293(2)	100(2)
Crystal system	triclinic	triclinic
Space group	P-1	P-1
a (Å)	7.275(2)	7.2421(2)
b (Å)	11.692(4)	11.5317(4)
c (Å)	12.760(4)	12.6415(3)
α (°)	85.868(2)	84.884(2)
β (°)	76.764(2)	77.206(2)
γ (°)	85.302(2)	83.702(2)
V (Å^3)	1051.4(6)	1021.02(5)
Z	2	2
Density (g.cm^{-3})	1.703	1.754
μ (mm^{-1})	4.196	4.321
No. of total reflections	4224	4595
R_{obs}	0.0344	0.0378
$wR2_{obs}$	0.0859	0.1035
S	1.03	1.036

Table IV. 8: Crystal data of $[Fe(L_{222}N_5)(NCSe)_2]$ complex

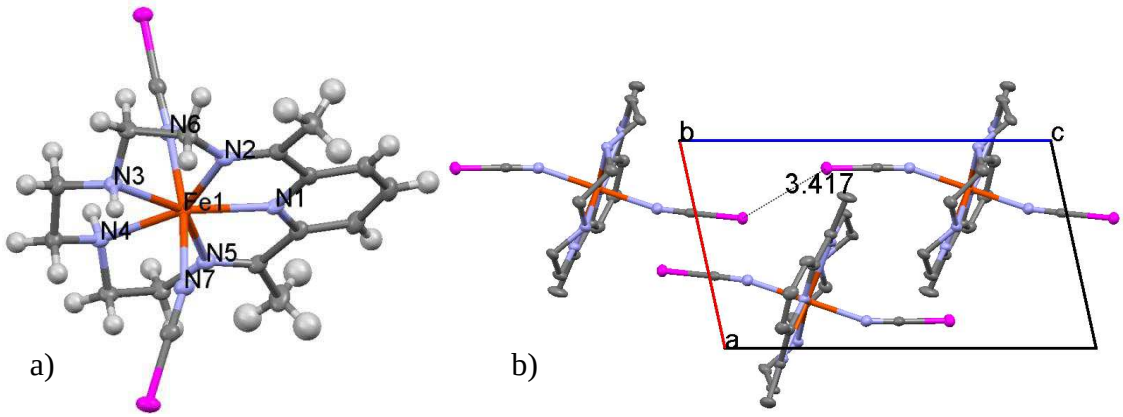

Figure IV. 11: a) Molecular structure and b) Crystal packing of $[Fe(L_{222}N_5)(NCSe)_2]$ at 100 K. Hydrogen atoms have been omitted for clarity.

The crystal packing (Figure IV. 11b) is based on the Se…Se short contact between neighboring atoms as shown by the Se-Se distance of 3.439(1) Å at 293 and 3.4175(3) Å at 100 K.

293 K		100 K	
Fe1 — N1	2.182(2)	Fe1 — N1	2.180(2)
Fe1 — N2	2.255(2)	Fe1 — N2	2.265(2)
Fe1 — N3	2.300(2)	Fe1 — N3	2.306(2)
Fe1 — N4	2.303(2)	Fe1 — N4	2.297(2)
Fe1 — N5	2.260(2)	Fe1 — N5	2.259(2)
Fe1 — N6	2.146(3)	Fe1 — N6	2.141(2)
Fe1 — N7	2.146(3)	Fe1 — N7	2.135(2)

Table IV. 9: Selected geometric parameters (Å) for $[Fe(L_{222}N_5)(NCSe)_2]$ at 293 K and 100 K

To sum up, the two $L_{222}N_5$ based complexes present neither spin transition nor structural transition. Their structural properties are very close and all adopt a triclinic P -1 packing.

IV.3.4. Crystal structures of $[Fe(L_{232}N_5)(NCS)_2]\cdot 0.5H_2O$ and $[Fe(L_{232}N_5)(NCSe)_2]\cdot 0.25H_2O$

The structural determination of the $[Fe(L_{232}N_5)(NCS)_2]\cdot 0.5H_2O$ complex was performed at 300 K and 110 K. At both temperatures, there is one macrocyclic molecule in the asymmetric unit and 0.5 water molecule per Fe(II) center. At 300 K, it adopts a P $2_1/n$ monoclinic space group (Table IV. 10). The Fe(II) ion is located in a general position (Figure IV. 12a). The Fe–N bond distances for nitrogen atom at the NH–CH_2–CH_2–CH_2–NH propylene fragment are 2.366(2) Å for Fe1–N3 and 2.300(2) Å for Fe1–N4. The Fe–N bond distances for axial thiocyanate group are 2.147(3) Å for Fe1–N1 and 2.165(3) Å for Fe1–N2. Other Fe–N bond distances are listed in Table IV. 11. All those bond lengths characterize the HS state.

The crystal packing at 300 K is presented in Figure IV. 12b. Water molecule is linked to the sulfur atom S2 on one side, with a distance of 3.066(8) Å for O1–S2. On the other side, it is linked to N4 and N2 atom of the macrocyclic molecule by two hydrogen bonds. N4 is a nitrogen atom which locates at the NH–CH_2–CH_2–CH_2–NH propylene fragment, while N2 locates at the thiocyanate group. The distance of these contacts are 3.038(9) Å for O1– N4 and 2.999(9) Å for O1– N2.

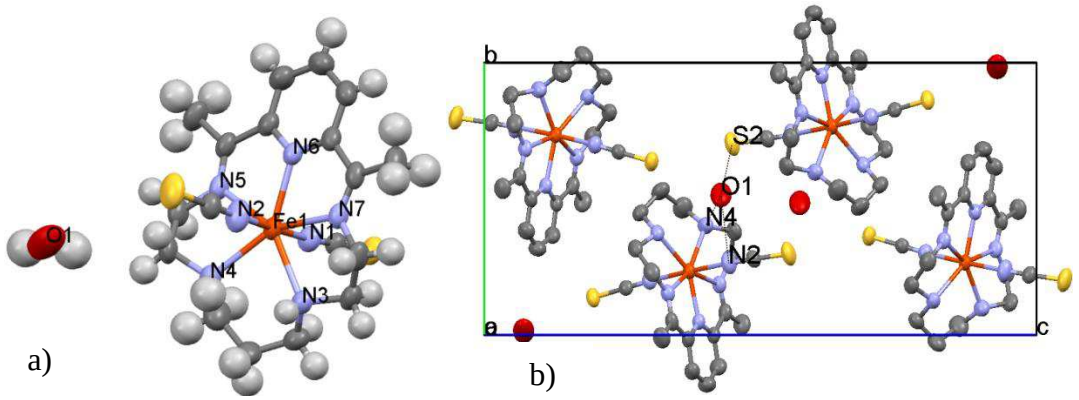

Figure IV. 12: a) Molecular structure and b) Crystal packing of $[Fe(L_{232}N_5)(NCS)_2]\cdot 0.5H_2O$ at 300 K. Hydrogen atoms have been omitted for clarity.

Compound	$[Fe(L_{232}N_5)(NCS)_2]\cdot 0.5H_2O$	
Formula	$C_{36}H_{52}Fe_2N_{14}OS_4$	$C_{36}H_{52}Fe_2N_{14}OS_4$
M_r (g.mol^{-1})	936.90	936.90
Colour	dark blue	dark blue
Crystal size (mm^3)	0.85 × 0.38 × 0.25	0.38 × 0.15 × 0.15
Crystal morphology	rectangular	prism
Temperature (K)	300(2)	110(2)
Crystal system	monoclinic	monoclinic
Space group	$P2_1/n$	$P2_1/n$
a (Å)	7.7530(3)	7.66640(10)
b (Å)	11.7757(5)	11.6061(2)
c (Å)	24.0225(10)	23.8228(4)
β (°)	96.556(2)	96.2370(10)
V (Å^3)	2178.84(15)	2107.13(6)
Z	2	2
Density (g.cm^{-3})	1.428	1.477
μ (mm^{-1})	0.905	0.936
No. of total reflections	4923	8312
R_{obs}	0.0482	0.0376
$wR2_{obs}$	0.1333	0.1012
S	1.067	1.043

Table IV. 10: Crystal data of $[Fe(L_{232}N_5)(NCS)_2]\cdot 0.5H_2O$ complex

300 K		100 K	
Fe1 — N1	2.147(3)	Fe1 — N1	2.226(1)
Fe1 — N2	2.165(3)	Fe1 — N2	2.257(1)
Fe1 — N3	2.366(2)	Fe1 — N3	2.370(1)
Fe1 — N4	2.300(2)	Fe1 — N4A	2.491(6)
Fe1 — N5	2.270(2)	Fe1 — N4B	2.302(2)
Fe1 — N6	2.227(2)	Fe1 — N5	2.273(1)
Fe1 — N7	2.254(2)	Fe1 — N6	2.141(1)
		Fe1 — N7A	2.19(1)
		Fe1 — N7B	2.12(1)

Table IV. 11: Selected geometric parameters (Å) for $[Fe(L_{232}N_5)(NCS)_2]\cdot 0.5H_2O$ at 300 K and 100 K

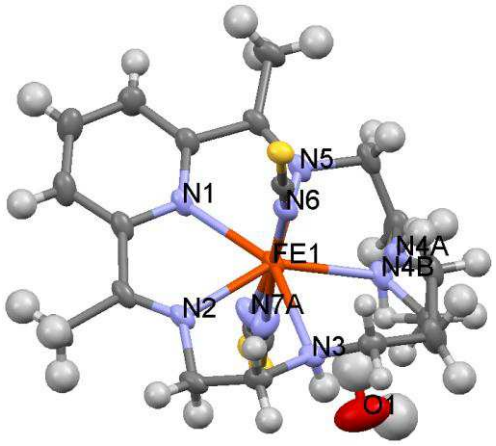

Figure IV. 13: Molecular structure of $[Fe(L_{232}N_5)(NCS)_2]\cdot 0.5H_2O$ at 110 K.

At 110 K, the structure adopts the same monoclinic P 2_1/n space group as at 300 K. The Fe(II) ion is still located in a general position (Figure IV. 13). One of nitrogen atoms on the propylene fragment satisfies with 100% occupation, while the other nitrogen atom is disordered. The Fe–N bond distance for the 100% occupation on propylene ring is 2.370(1) Å (Fe1–N3), while the disordered nitrogen as well as its neighboring carbon atoms can be determined in two possible positions. The Fe–N bond distances and occupations for the two possibilities are 75% of 2.302(2) Å for Fe1–N4B and 25% of 2.491(6) Å for Fe1–N4A. The difference between the two Fe–N bond distances is 0.19 Å. The positions of disordered carbon atom can be resolved with the same occupations as the nitrogen, i.e. 75% for one position and 25 % for the other. Another disorder can be observed at one of the thiocyanate group at axial positions. While the other thiocyanate group is satisfied with 100% occupation, the position of this disordered one can be determined into two possibilities with 50% occupation for each. The Fe–N bond distances for the two possibilities are 2.19(1) Å for Fe1–N7A and 2.12(1) Å for Fe1–N7B with an average of 2.155 Å. The other Fe–N bond distance for thiocyanate group in the opposite axial position is 2.141(1) Å (Fe1–N6), which is close to the average of the above two possibilities. Despite of the disordered N atoms, all the metal—ligand bond lengths describe a HS state.

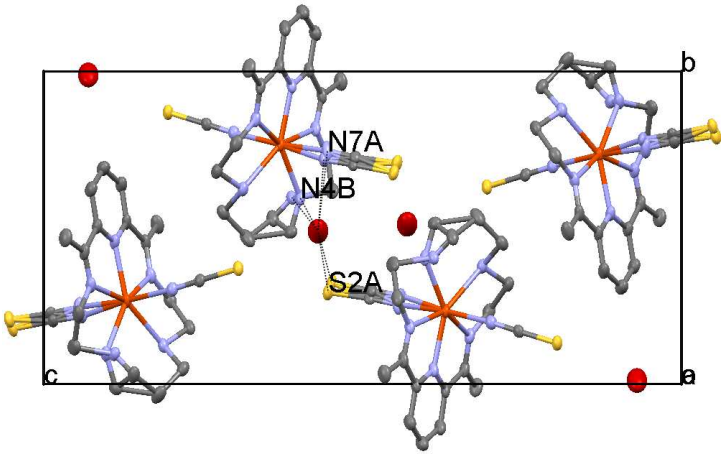

Figure IV. 14: Crystal packing of $[Fe(L_{232}N_5)(NCS)_2]\cdot 0.5H_2O$ at 110 K. Hydrogen atoms have been omitted for clarity.

The crystal packing at 100 K is presented in Figure IV. 14. The basic description of the packing is unchanged as compared to the packing at 300 K. The water molecule is still linked to one sulfur atom and two nitrogen atoms by hydrogen bonds. However, all the three linked atoms are disordered. The distance of these contacts are 3.115(5) Å for O1–S2A, 2.730(5) Å for O1–S2B; 3.028(9) Å for O1–N7A, 2.692(8) Å for O1–N7B; and 3.503(8) Å for O1–N4A, 2.954(6) Å for O1–N4B.

To understand the origin of the disorders, we would like to analyze the structure from two different aspects: the disorder of the thiocynate group and the disorder of the propylene fragment. The angle of S2B–Fe1–S2A is 5.05 degree, while the C2B–Fe1–C2A is 5.3 degree. They are quite close. The difference between the two Fe–N bond distances is 0.07 Å, which is relatively small. This disorder of thiocyanate group at axial position probably describes a vibration circlewise around Fe(II) center. However the disorder at the propylene fragment may describe an entirely different phenomenon. When the metal–ligand bond break occurs in

$[Fe(L_{222}N_3O_2)(CN)_2]\cdot H_2O$, inversion of the $O–CH_2–CH_2–O$ ethylene fragment conformation can be observed [11]. For the $[Fe(L_{232}N_5)(NCS)_2]\cdot 0.5H_2O$, the disorder of both nitrogen and carbon atoms in the propylene fragment may be due to a 25 % of inversion at nitrogen position. This can be proven by the change of Fe–N bond lengths at two temperatures, since the lengths of Fe1–N4B (2.302(2) Å) and Fe1–N3 (2.370(1) Å) at 110 K are close to the lengths of Fe1–N4 (2.300(2) Å) and Fe1–N3 (2.366(2) Å) at 300 K. The existence of 25 % Fe1–N4A (2.491(6) Å), with an increase of 0.19 Å from Fe1–N4B, can be thus interpreted as an initial departure of the nitrogen from the Fe(II) center. It has been verified that with the above change in the structure, no phase transition can be observed and no superstructure appears. Therefore, the above departure probably presents a randomly occurrence in the crystal. However, it is worth noting that this departure is observed only in structures where the water molecule is present within the crystal packing. This is to keep in mind since the presence of water participating efficiently to the crystal cohesion is suspected to play a role in the exceptional behavior of $[Fe(L_{222}N_3O_2)(CN)_2]\cdot H_2O$ [8,11 ,14].

The structural determination of the $[Fe(L_{232}N_5)(NCSe)_2]\cdot 0.25H_2O$ complex was performed at both room temperature (293 K) and 110 K. It adopts a monoclinic $P2_1/n$ space group at both room temperature and 110 K (Table IV. 12). There is 0.25 water molecule per Fe(II) center. The bond lengths at both temperatures are listed in Table IV. 13.

Compound	$[Fe(L_{232}N_5)(NCSe)_2]\cdot 0.25H_2O$	
Formula	$C_{72}H_{102}Fe_4N_{28}OSe_8$	$C_{72}H_{102}Fe_4N_{28}OSe_8$
M_r (g.mol^{-1})	2230.90	2230.90
Colour	dark blue	dark blue
Crystal size (mm^3)	0.6 × 0.35 × 0.15	0.6 × 0.35 × 0.15
Crystal morphology	prism	prism
Temperature (K)	293(2)	110(2)
Crystal system	monoclinic	monoclinic
Space group	$P2_1/n$	$P2_1/n$
a (Å)	15.5939(3)	15.4575(2)
b (Å)	11.7657(2)	11.6172(2)
c (Å)	24.7536(5)	24.5781(2)
β (°)	102.3730(10)	102.4380(10)
V (Å^3)	4436.13(14)	4309.97(10)
Z	2	2
Density (g.cm^{-3})	1.670	1.719
μ (mm^{-1})	3.982	4.098
No. of total reflections	10146	14994
R_{obs}	0.042	0.0392
$wR2_{obs}$	0.1063	0.092
S	1.029	1.020

Table IV. 12: Crystal data of $[Fe(L_{232}N_5)(NCSe)_2]\cdot 0.25H_2O$ complex

293 K		110 K	
Fe1 — N1	2.231(2)	Fe1 — N1	2.233(2)
Fe1 — N2	2.271(3)	Fe1 — N2	2.274(2)
Fe1 — N3	2.311(4)	Fe1 — N3A	2.297(3)
		Fe1 — N3B	2.500(9)
Fe1 — N4	2.364(3)	Fe1 — N4	2.364(2)
Fe1 — N5	2.247(3)	Fe1 — N5	2.255(2)
Fe1 — N6	2.155(3)	Fe1 — N6	2.146(2)
Fe1 — N7	2.163(3)	Fe1 — N7	2.146(2)
Fe2 — N8	2.232(2)	Fe2 — N8	2.227(2)
Fe2 — N9	2.279(3)	Fe2 — N9	2.280(2)
Fe2 — N10A	2.26(1)	Fe2 — N10A	2.277(5)
Fe2 — N10B	2.47(1)	Fe2 — N10B	2.466(5)
Fe2 — N11	2.370(3)	Fe2 — N11	2.370(2)
Fe2 — N12	2.262(3)	Fe2 — N12	2.261(2)
Fe2 — N13	2.150(3)	Fe2 — N13	2.135(2)
Fe2 — N14	2.142(3)	Fe2 — N14	2.145(2)

Table IV. 13: Selected geometric parameters (Å) for $[Fe(L_{232}N_5)(NCSe)_2]\cdot 0.25H_2O$ at 293 K and 110 K

At room temperature, nitrogen atom N10 is found to be disordered (Figure IV. 15). It locates at the NH–CH_2–CH_2–CH_2–NH propylene fragment, of Fe2 iron (II) center. The bond Fe–N distances for the two possible occupations are 50% of 2.26(1) Å and 50% of 2.47(1) Å. There are 0.21 Å of difference between the two bonds. On the contrary, the corresponding nitrogen atoms N3 and N4 of the Fe1 metal center satisfy 100% occupation.

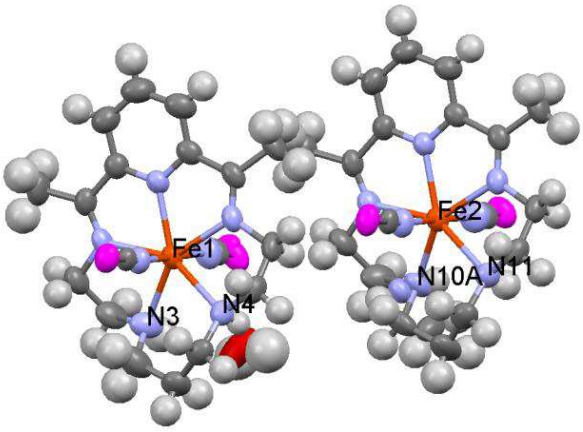

Figure IV. 15: Molecular structure of $[Fe(L_{232}N_5)(NCSe)_2]\cdot 0.25H_2O$ at 293 K. Hydrogen atoms have been omitted for clarity.

At 110 K, disorders are found in two nitrogen atoms N3 and N10 (Figure IV. 16). The two nitrogen atoms locate at two different propylene fragments. Bond Fe–N distances and occupations are 50% of 2.277(5) Å for Fe1–N10A and 50% of 2.466(5) Å for Fe1–N10B; 75% of 2.297(3) Å for Fe2–N3A and 25% of 2.500(9) Å for Fe2–N3B. It seems that the disorder of N10 at 110 K corresponds to the disorder of N10 at 293 K. Thus this atom keeps the same disorder ratio at both 293 K and 110 K. However, no corresponding disorder of the N3 atom

can be found at 293 K. Therefore, interestingly, at low temperature, the N3 atom tends to break the metal–ligand bond by increasing it by ca. 0.2 Å. This bond breaking can be estimated to affect about 25 % of the complexes.

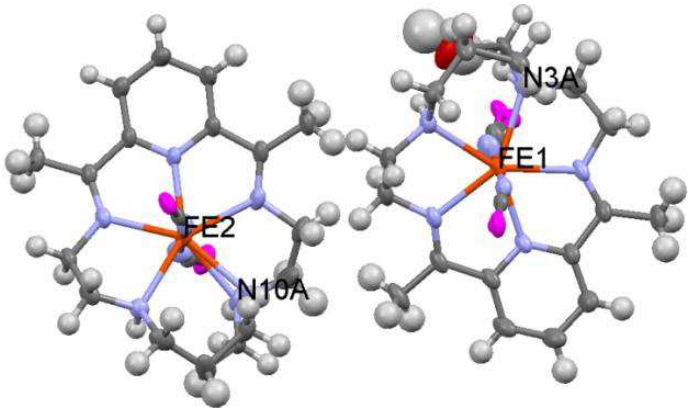

Figure IV. 16: Molecular structure of [Fe(L232N5)(NCSe)2]·0.25H2O at 110 K. Hydrogen atoms have been omitted for clarity.

Consequently, in both complexes, a partial departure of one nitrogen atom from the FeN_6 coordination sphere is observed at low temperature. To understand why both of these $L_{232}N_5$ complexes present this initial departure, we would like to underline two aspects: the nature of the ligand and the influence of the water molecule. Since none of the $L_{222}N_5$ complexes shows a similar change, the above properties are likely associated with chain length of $L_{232}N_5$ ligand, which consist of one more carbon atom comparing to $L_{222}N_3O_2$, and $L_{222}N_5$ ligand. Moreover, no water molecule was found in any $L_{222}N_3O_2$, and $L_{222}N_5$ complexes with thiocyanate / selenocyanate in axial position. However, in the two $L_{232}N_5$ contained complexes, the water molecule is directly linked with the nitrogen atom which presents this departure. Therefore, hydrogen bond from water molecule may play important roles in this initial departure of nitrogen atom.

Crystal packing of the complex $[Fe(L_{232}N_5)(NCSe)_2]\cdot 0.25H_2O$ at 293 K is presented in Figure IV. 17. Water molecules are linked to three nitrogen atoms: N4 of the selenocyanate group, N5 and N9 of the propylene fragment. All these three nitrogen atoms locate on the molecule having Fe1 as metal center. The distance of these contacts are 3.027(9) Å for O1–N7, 3.414(8) Å for O1–N4 and 3.081(9) Å for O1–N3.

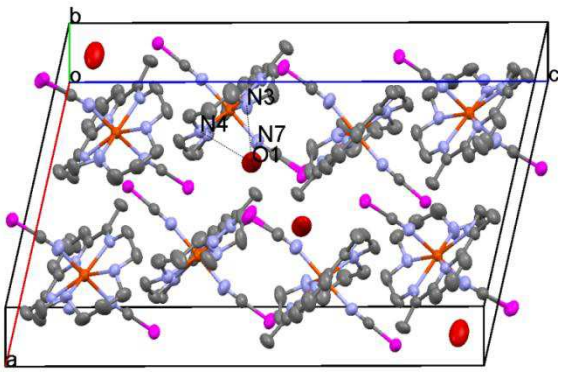

Figure IV. 17: Crystal packing of $[Fe(L_{232}N_5)(NCSe)_2]\cdot 0.25H_2O$ at 293 K. Hydrogen atoms have been omitted for clarity.

Crystal packing of the complex $[Fe(L_{232}N_5)(NCSe)_2]\cdot 0.25H_2O$ at 110 K is presented in Figure IV. 18. Water molecule is linked to three nitrogen atoms: N7 of the selenocyanate group, N3A and N4 of the propylene fragment. N3 atom shows the 75% - 25% disorder. All these three nitrogen atoms locate on the molecule having Fe1 as metal center. The distance of these contacts are 2.938(9) Å for O1–N7, 3.429(7) Å for O1–N4, 2.954(8) Å for O1–N3A and 3.60(1) Å for O1–N3B. Since the water molecule is linked to the nitrogen atom N3, which is found to be disordered at 110 K, it can be confirmed that the water molecules in the lattice play an important role on the change of coordination property of the macrocyclic complex, even when it is only an partial change.

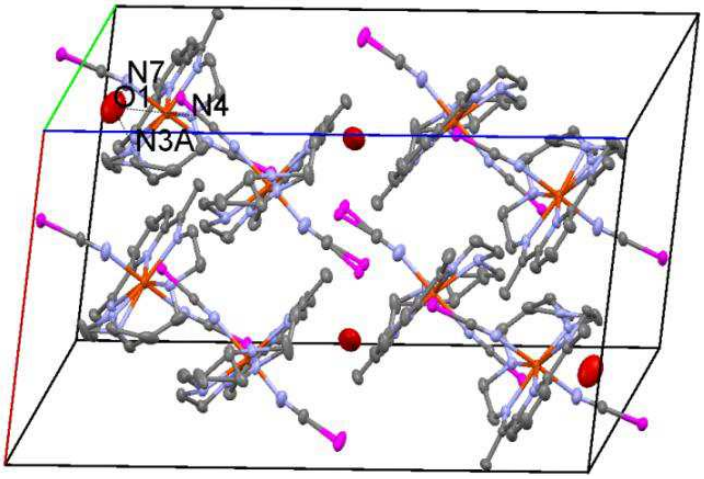

Figure IV. 18: Crystal packing of $[Fe(L_{232}N_5)(NCSe)_2]\cdot 0.25H_2O$ at 110 K. Hydrogen atoms have been omitted for clarity.

To sum up, both $[Fe(L_{232}N_5)(NCS)_2]\cdot 0.5H_2O$ complex and $Fe(L_{232}N_5)(NCSe)_2]\cdot 0.25H_2O$ complex adopts monoclinic P $2_1/n$ space group. In the both complexes, the departure of a nitrogen atom from the coordination sphere can be observed at low temperature. This departure is just partial in these case and concern about 25 % of the metal centers with a random distribution all along the crystal structure. This departure is observed on one nitrogen atom of the propylene fragments. To this regard, it may be considered as very similar, even though partial to the metal-ligand bond break observed on complex $[Fe(L_{222}N_3O_2)(CN)_2]\cdot H_2O$.

IV.3.5. Structures of $[Fe(L_{223}N_5)(NCS)_2]$ and $[Fe(L_{223}N_5)(NCSe)_2]$

Ligand $L_{223}N_5$ is an isomer of ligand $L_{232}N_5$. While the $NH–CH_2–CH_2–CH_2–NH$ propylene fragment locates in the center of amine part in $L_{232}N_5$, it is connected with pyridine part in $L_{223}N_5$. It thus forms an asymmetric macrocyclic ligand.

The structural determination of the $[Fe(L_{223}N_5)(NCS)_2]$ complex is performed at 293 K and 110 K. It adopts monoclinic P $2_1/n$ space group at both 293 K and 110 K (Table IV. 14). There is one molecule in the asymmetric unit and the Fe(II) ion locates in a general position. No water molecule is found within the packing. However the structure of the molecule is highly disordered at the amine part. At room temperature, the disorder can not be resolved. At

110 K, the disorder can be determined (Figure IV. 19). The bond coordination bond lengths characterize HS state at 110 K (Table IV. 15), The sulfur is in short contact with neighboring sulfur atom. The distance between sulfur atoms is 3.5208(7) Å. The disorder of the amine part may be due to the asymmetric conformation of ligand $L_{223}N_5$, and it is thus difficult to comment further such disorder.

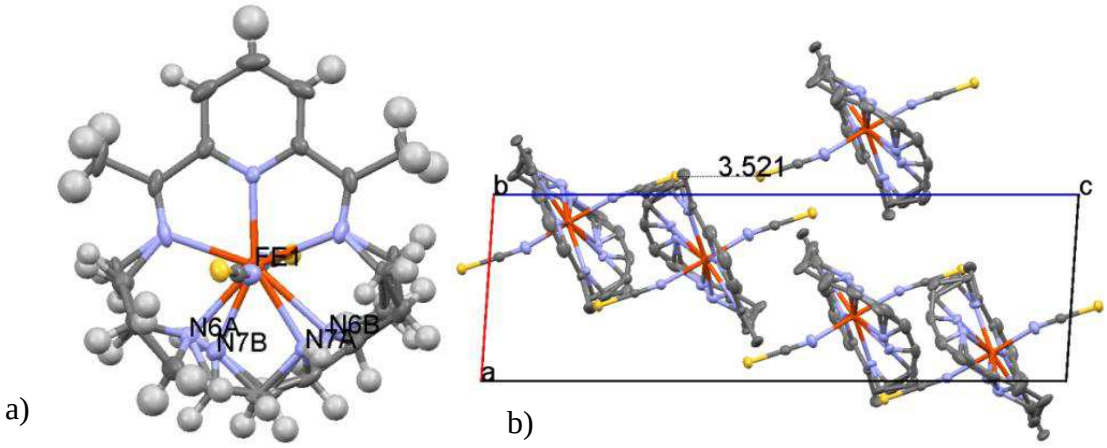

Figure IV. 19: a) Molecular structure and b) Crystal packing of $[Fe(L_{223}N_5)(NCS)_2]$ at 110 K. Hydrogen atoms have been omitted for clarity.

Compound	$[Fe(L_{223}N_5)(NCS)_2]$	
Formula	$C_{18}H_{25}FeN_7S_2$	$C_{18}H_{25}FeN_7S_2$
M_r (g.mol^{-1})	459.44	459.44
Colour	dark blue	dark blue
Crystal size (mm^3)	0.6 × 0.35 × 0.15	0.38 × 0.13 × 0.08
Crystal morphology	prism	prism
Temperature (K)	293(2)	110(2)
Crystal system	monoclinic	monoclinic
Space group	$P2_1/n$	$P2_1/n$
a (Å)	7.6865(2)	7.61060(10)
b (Å)	11.5038(4)	11.3658(2)
c (Å)	24.0051(7)	23.8383(5)
β (°)	85.856(2)	93.8260(10)
V (Å^3)	2117.08(11)	2057.43(6)
Z	4	4
Density (g.cm^{-3})	1.441	1.483
μ (mm^{-1})	0.928	0.955
No. of total reflections	6165	6008
R_{obs}	0.0585	0.0421
$wR2_{obs}$	0.1557	0.0836
S	1.076	1.161

Table IV. 14: Crystal data of $[Fe(L_{223}N_5)(NCS)_2]$ complex

$[FeL_{223}N_5(NCS)_2]$		$[FeL_{223}N_5(NCSe)_2]$	
Fe1 — N1	2.214(2)	Fe1 — N1	2.279(2)
Fe1 — N2	2.279(2)	Fe1 — N2	2.215(2)
Fe1 — N3	2.316(2)	Fe1 — N3	2.315(2)
Fe1 — N4	2.151(2)	Fe1 — N4	2.125(2)
Fe1 — N5	2.120(2)	Fe1 — N5A	2.329(5)
Fe1 — N6A	2.357(3)	Fe1 — N6A	2.380(5)
Fe1 — N7A	2.350(3)	Fe1 — N7	2.159(2)
Fe1 — N6B	2.452(7)	Fe1 — N5B	2.295(8)
Fe1 — N7B	2.298(8)	Fe1 — N6B	2.410(8)

Table IV. 15: Selected geometric parameters (Å) for $[Fe(L_{223}N_5)(NCS)_2]$ and $[FeL_{223}N_5(NCSe)_2]$ at 110 K.

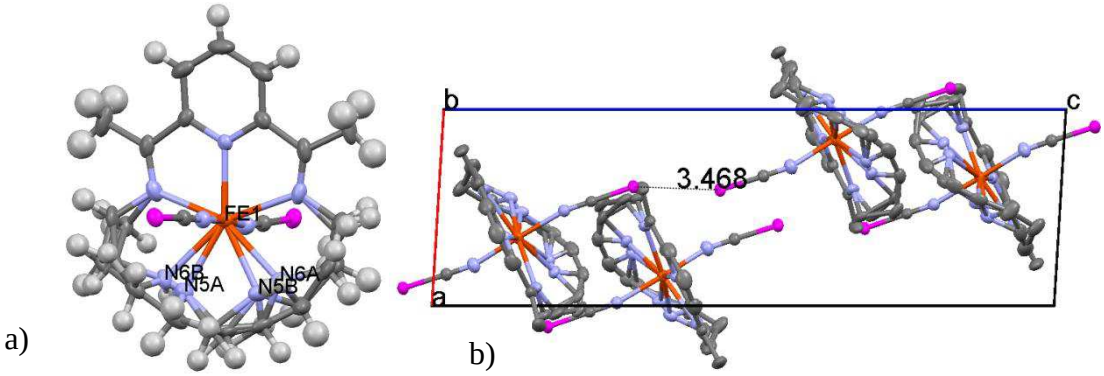

Figure IV. 20: a) Molecular structure and b) Crystal packing of $[Fe(L_{223}N_5)(NCSe)_2]$ at 110 K. Hydrogen atoms have been omitted for clarity.

Complex $[Fe(L_{223}N_5)(NCSe)_2]$ adopts monoclinic P $2_1/n$ space group at 293 K and 110 K (Table IV. 16). There is one molecule in the asymmetric unit (Figure IV. 20a). No water molecule is involved in the crystal packing (Figure IV. 20b).The amine part of the molecule is highly disordered. At 110 K, the disorder can be determined. The bond coordination bond lengths characterize HS state at 110 K (Table IV. 15). The selenium is in short contact with neighboring selenium atom. The distance between selenium atoms is 3.4680(4) Å. Similar with $[Fe(L_{223}N_5)(NCS)_2]$ complex, it is difficult to comment further due to the disorder.

Compound	[Fe($L_{223}N_5$)(NCSe)$_2$]	
Formula	$C_{18}H_{25}FeN_7Se_2$	$C_{18}H_{25}FeN_7Se_2$
M_r (g.mol^{-1})	553.22	553.22
Colour	dark blue	dark blue
Crystal size (mm^3)	0.13 × 0.13 × 0.05	0.25 × 0.13 × 0.13
Crystal morphology	prism	prism
Temperature (K)	293(2)	110(2)
Crystal system	monoclinic	monoclinic
Space group	$P2_1/n$	$P2_1/n$
a (Å)	7.7266(3)	7.6680(2)
b (Å)	11.5898(5)	11.4447(2)
c (Å)	24.3459(9)	24.1613(5)
β (°)	93.458(2)	93.4600(10)
V (Å^3)	2176.20(15)	2116.48(8)
Z	4	4
Density (g.cm^{-3})	1.689	1.736
μ (mm^{-1})	4.057	4.171
No. of total reflections	4001	6153
R_{obs}	0.0461	0.0358
$wR2_{obs}$	0.0956	0.0772
S	0.958	1.037

Table IV. 16: Crystal data of [Fe($L_{223}N_5$)(NCSe)$_2$] complex

IV.3.6. Discussion and conclusion

In this part, we have firstly described the synthesis and crystallization of eight Fe(II) macrocyclic complexes with thiocyanate or selenocyanate anionic ligand. The magnetic studies of polycrystalline powder sample demonstrated that all eight studied complexes are HS. A systematic investigation on the crystal structures of the eight complexes at both high and low temperatures was then reported. It was observed that the complex [Fe($L_{222}N_3O_2$)(NCS)$_2$] presented a structural transition from monoclinic P 2/n to triclinic P -1 space group upon cooling, while the other seven complexes adopt the same space group at both room temperature and at low temperature: complexes [Fe($L_{222}N_3O_2$)(NCSe)$_2$], [Fe($L_{222}N_5$)(NCS)$_2$] and [Fe($L_{222}N_5$)(NCSe)$_2$] adopt the triclinic P -1 space group, while complexes [Fe($L_{232}N_5$)(NCS)$_2$]·0.5H_2O, [Fe($L_{232}N_5$)(NCSe)$_2$]·0.25H_2O, [Fe($L_{223}N_5$)(NCS)$_2$], and [Fe($L_{223}N_5$)(NCSe)$_2$] adopt the monoclinic P 2_1/n space group.

More importantly, at low temperature in the [Fe($L_{232}N_5$)(NCS)$_2$]·0.5H_2O and [Fe($L_{232}N_5$)(NCSe)$_2$]·0.25H_2O complexes, an elongation of Fe-N bond distance from the coordination sphere was clearly demonstrated. As it was carefully verified that no superstructure appeared, the molecules presenting an elongated bond were therefore randomly distributed inside the crystal structure. Then from structural determination, it was illustrated that this elongation concerned about 25 % of the metal centers for both complexes. This elongation could certainly be attributed to an initial departure of the nitrogen atom from the coordination center upon cooling. Finally, since this departure was observed on one nitrogen

atom of the propylene fragments, it may be considered as very similar, even though partial, to the metal-ligand bond break observed on complex $[Fe(L_{222}N_3O_2)(CN)_2]\cdot H_2O$. Thus we believe by modifying the anionic ligand in the Fe(II) macrocyclic complexes, new samples with the change of coordination properties can be obtained.

References

1 L. Capes, J.-F. Létard, O. Kahn *Chem. Eur. J.* **2000**, *6*, 2246

2 N. Moliner, M. C. Muñoz, S. Létard, J.-F. Létard, X. Solans, R. Burriel, M. Castro, O. Kahn, J. A. Real, *Inorg. Chim. Acta* **1999**,*291*, 279.

3 G. Chastanet, A. B. Gaspar, J. A. Real, J.-F. Létard, *Chem. Commun.* **2001**, 819.

4 G. Chastanet, C. Carbonera, C. Mingotaud, J.-F. Létard, *J. Mater. Chem*. **2004,** *14*, 3516.

5 E. Trzop, M. Buron-Le Cointe, H. Cailleau, L. Toupet, G. Molnar, A. Bousseksou, A. B. Gaspar, J. A. Real, E. Collet, *J. Appl. Cryst.* **2007**. *40*, 158.

6 N. O. Moussa, S. Mouri, G. Molnár, K. Tanaka, J. A. Real, A. Bousseksou, *J. Inorg. Organomet. Polym.* **2008,** *18*,195.

7 M. G. B. Drew, A.H. bin Othman, S.M. Nelson, *J. Chem. Soc., Dalton Trans.***1976**, 1394.

8 J. S. Costa, PhD Thesis, Université Bordeaux I, 2005.

9 S. Hayami, Z. Gu, Y. Einaga, Y. Kobayasi, Y. Ishikawa, Y. Yamada, A. Fujishima, O. Sato *Inorg. Chem.* **2001**, *40*, 3240

10 P. Guionneau, J. S. Costa, J-F Létard, *Acta Cryst*. **2004,** *C60*, m587

11 P. Guionneau, F. Le Gac, A. Kaiba, J. S. Costa, D. Chasseau, J.-F. Létard *Chem. Commun.* **2007**, *36*, 3723

12 S. M. Nelson, P. D. A. Mcllroy, C. S. Stevenson, E. König, G. Ritter, J. Waigel, *J. Chem. Soc. Dalton Trans.* **1986**, 991.

13 Spin Crossover in Transition Metal Compounds, in Topics in Current Chemistry, ed. P. Gütlich and H. A. Goodwin, Springer-Verlag, Berlin– Heidelberg–New York, 2004, vol. II.

14 S. Lakhloufi, PhD Thesis, Université Bordeaux I, 2013.

Part V.Modification of solvent molecule

Chapter V.1. The complexes $[FeL_{222}N_3O_2(CN)_2]$·solv (solv = H_2O and $2CHCl_3$)

V.1.1. Introduction

Recently, some SCO complexes have been found to present strong solvent dependence on the magnetic properties [1-5]. Regarding to the macrocyclic system, however, the investigation is quite limited. J. S. Costa in his PhD thesis [6] described an unusual phenomenon on the rehydration of $[FeL_{222}N_3O_2(CN)_2]\cdot H_2O$ complex. After the rehydration process, the T(TIESST) value increase to more than 150 K (Figure V. 1). To further study this unusual phenomenon, a systematic investigation on the solvent dependence of $[FeL_{222}N_3O_2(CN)_2]\cdot H_2O$ complex will be presented in Part V.

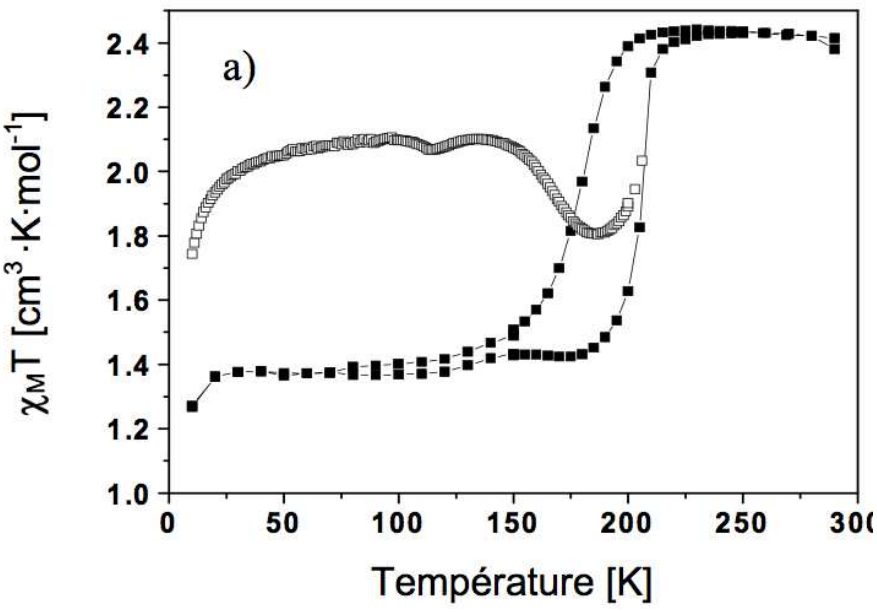

Figure V. 1: T(LIESST) measurement of rehydrated $[FeL_{222}N_3O_2(CN)_2]\cdot H_2O$

To investigate the role of solvent molecule on the macrocyclic $[FeL_{222}N_3O_2(CN)_2]\cdot H_2O$ complex, we have adopted two strategies. The first one deals with the replacement of the water molecule by other solvent molecules. The second one concerns the dehydration and rehydration of $[FeL_{222}N_3O_2(CN)_2]\cdot H_2O$ complex.

V.1.2. Synthesis

Complex $[FeL_{222}N_3O_2(CN)_2]\cdot H_2O$ was obtained as described by Nelson et al. [7]. All the reactions were carried out under anaerobic condition and all solvents used were degassed. The reaction was carried out in two steps (Scheme V. 1).

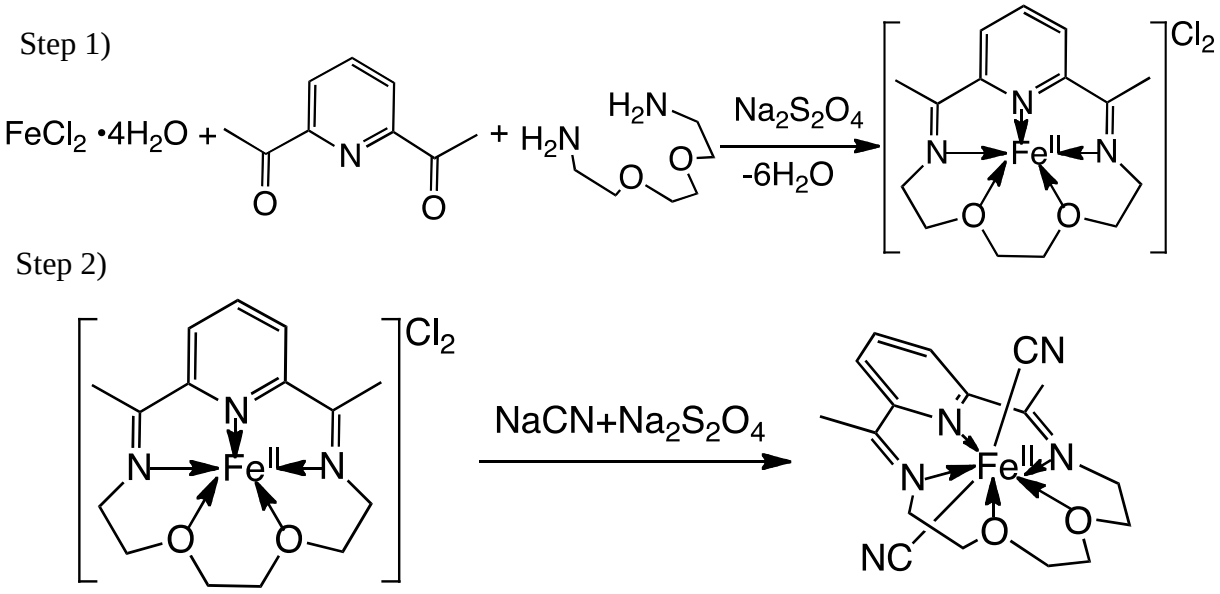

Scheme V. 1: The synthesis of $[FeL_{222}N_5(CN)_2]\cdot H_2O$.

Step 1) Aqueous solution with 15 mL of methanol and 10 mL of water was prepared, in which were dissolved 1.20 g (6 mmol) of iron(II) chloride tetrahydrate, 1 g (6 mmol) of 2,6-diacetylpyridine, and 0.1 g of sodium dithionite (used as reducing agent to remove traces of trivalent iron ion). 3,6-dioxacoctane-1,8-diamine. (0.92 mL, 6 mmol) was added dropwise. The mixture was kept under nitrogen reflux at 75 °C for 16 h approximately (formation of $[FeL_{222}N_3O_2(Cl)_2]$).

Step 2) After filtration of the above mixture, 15 mL of aqueous solution containing an excess of sodium cyanide NaCN (4g, 0.08 mol) and 0.1 g of sodium dithionite was added. This solution was then kept in fridge for ca. 6 hours at around 10 °C. A polycrystalline powder is formed. The solid formed is then filtered and washed with 10 mL of degassed water and dried under vacuum. Finally 1.06 g (yield ~ 45%) of in dark purple powder was collected. Chemical analysis: Anal. Calc.: C, 50.89; H, 5.78; N, 17.45; Fe, 13.92% Found: C, 50.78; H, 5.88; N, 17.61; Fe, 14.22%

V.1.3. Crystallization of $[FeL_{222}N_3O_2(CN)_2]\cdot$solv (solv = H_2O and $2CHCl_3$)

Re-crystallization of the $[FeL_{222}N_5(CN)_2]\cdot H_2O$ polycrystalline powder was performed several times. The vapor diffusion technique was found to be the most effective method. This method was also applied in Part II.1 for the diluted series. An excess of approximately 3 mg of $[FeL_{222}N_3O_2(CN)_2]\cdot H_2O$ was dissolved in 3 mL of dichloromethane (SIGMA-ALDRICH ACS reagent, ≥ 99.9% (GC) without degassing). After 30 minutes stirring, a suspension is formed and filtered. This residual solution (1 mL) was put into a small tube (ca. 1 cm in diameter and 3 cm deep). The tube was then carefully introduced into a bigger bottle (ca. 2.5 cm in diameter and 5 cm deep). For the process of vapor diffusion, 10 mL of ether was added in this bottle. This bottle was closed tightly and left in the fridge for a week, and dark blue

rectangular crystals were obtained.

The structure of the crystals $[FeL_{222}N_5(CN)_2]\cdot H_2O$ was determined at room temperature. The existence of one water molecule was confirmed [8,9]. This provide an alternative method for obtaining the single crystal of the $[FeL_{222}N_3O_2(CN)_2]\cdot H_2O$ complex.

Single crystals of $[FeL_{222}N_3O_2(CN)_2]\cdot 2CHCl_3$ were obtained by A. Kaiba and the structure determination was performed. The crystallization of $[FeL_{222}N_3O_2(CN)_2]\cdot 2CHCl_3$ was performed using slow diffusion method in a U shape tube (Scheme V. 2). Indeed, the product of Step 1 (the synthesis of powder), i.e. $[FeL_{222}N_3O_2(Cl)_2]$ solution was added into the U shape tube which was previously filled with chloroform. Then aqueous solution containing NaCN was prepared and added into U shape tube from the other side. Crystals were found at the bottom of U tube after several weeks.

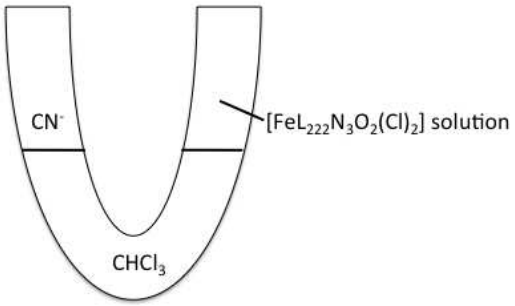

Scheme V. 2: Crystallization of $[FeL_{222}N_3O_2(CN)_2]\cdot 2CHCl_3$ by slow diffusion in U shape tube

V.1.4. Crystal structures of $[FeL_{222}N_3O_2(CN)_2]\cdot 2CHCl_3$

The crystal structure of the complex $[FeL_{222}N_3O_2(CN)_2]\cdot 2CHCl_3$ is solved at room temperature. It adopts a monoclinic C 2/c space group. The Fe(II) ion is hepta-coordinated. It is located in a pentagonal bipyramidal environment and lies on a twofold axis. The Fe–O bonds are geometrically identical by symmetry. The bond lengths are 2.114(2) Å for Fe-N7, 2.209(2) Å for Fe–N6, 2.155(3) Å for Fe-C16 and 2.335(2) Å for Fe-O1. There are two $CHCl_3$ molecules per Fe(II) center. They link to the nitrogen atom of cyano group by hydrogen bonds with a C-N distance of 3.124(4) Å.

At 100 K the crystal slightly cracked. Structure determination shows that the complex adopts the same C 2/c space group. The Fe(II) ion is still hepta-coordinated in the same pentagonal bipyramidal environment (Figure V. 2). Bond lengths are only slightly reduced. The packing is also similar. The $CHCl_3$ molecules link to the nitrogen atom of cyano group by hydrogen bonds with a C-N distance of 3.104(4) Å. Comparing to the structure of $[FeL_{222}N_3O_2(CN)_2]\cdot H_2O$ in the HS state**,** the main difference concerns the hydrogen bond interaction. In the $[FeL_{222}N_3O_2(CN)_2]\cdot 2CHCl_3$. The coordination bond lengths around Fe(II) in both temperatures is characteristic of a metal ion in HS state and no structural modification has been detected. Moreover, there is no evidence for the presence of solvent interactions forming one dimensional chain. It seems consequently that by replacing water molecules by $CHCl_3$, the number of interaction is reduced and the HS state is favored.

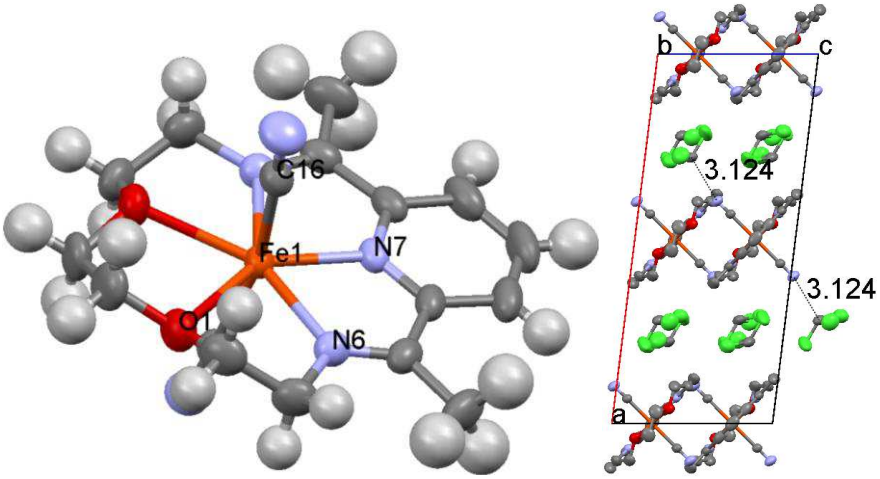

Figure V. 2: Crystal structure and packing of $[Fe(L_{222}N_3O_2)(CN)_2]\cdot 2CHCl_3$ at room temperature. The hydrogen atoms have been omitted for clarity.

Desolvation has been attempted on the $[Fe(L_{222}N_3O_2)(CN)_2]\cdot 2CHCl_3$ by A. Kaiba (Post-doc), using a vacuum pump. Unfortunately, the structure was found similar to the original $[FeL_{222}N_3O_2(CN)_2]\cdot H_2O$ single crystal [8,9]. Structural determination at room temperature revealed that single crystals after treatment under vacuum contained water molecules. In other words, after desolvation, the single crystals rehydrated and the final complex corresponds to the $[FeL_{222}N_3O_2(CN)_2]\cdot H_2O$ complex.

V.1.5. Dehydration and rehydration of $[FeL_{222}N_3O_2(CN)_2]\cdot H_2O$

Figure V. 3a displays TGA experiment. The mass loss process starts at around 320 K and finishes at around 385 K. Total mass loss at 385 K is about 4.46 %, and corresponds to one water molecule (4.49 %, calculated).

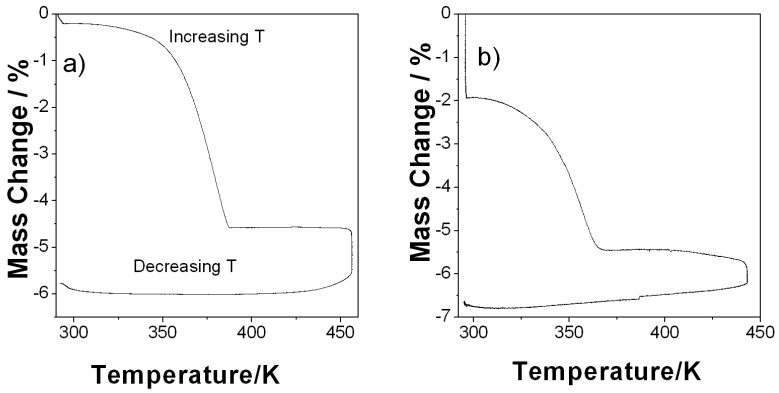

Figure V. 3: TGA measurements of complex $[FeL_{222}N_3O_2(CN)_2]\cdot H_2O$.

The sample after the first TGA measurement (recorded up to 430 K) was left at ambient atmosphere for around one month, and then the experiment was repeated (Figure V. 3b). The

shape of the second TGA curve was different from the previous one, with the occurrence of two steps. The first step corresponds to a mass loss of around 1.9 % which occurs at 295 K under just N_2 flux of 3 hours. The second step, which represents a mass loss of 3.53 % is associated with the increase of temperature up to 370 K. The mass loss for the second step corresponds to a main lost of 0.8 water molecule per complex. Based on previous studies, it is reasonable to attribute the mass loss observed at room temperature to the water molecule adsorbed at the surface while the behavior recorded during the heating process corresponds to 0.8 water molecule into the crystal lattice.

From the crystallographic work done on the $[FeL_{222}N_3O_2(CN)_2]\cdot H_2O$ single crystal [8,9], we have learned that the water molecules form hydrogen bonds through the two cyanide nitrogen atoms in the axial positions with an infinitive one dimensional chain [8,9]. The TGA experiments reveal that at high temperature the water molecules in the lattice can be removed. The hydrogen bonds between water molecule and nitrogen are consequently broken, and the one dimensional character of the structure lost. Of course rehydration effect may reconstruct this chain. However this reconstructed chain is certainly incomplete, since the mass loss observed by TGA is lower (loss 0.8 molecule of water) than for the original sample (loss of 1 molecule of water).

Figure V. 4 presents the diffraction patterns on $[FeL_{222}N_3O_2(CN)_2]\cdot H_2O$ single crystal at different temperatures. At 25 °C, the diffraction pattern is consistent with the single crystal nature, while after 3 hours at 60 °C, a loss of crystallinity can be observed (Figure V. 4b). After 15 hours at 60 °C, the diffraction patterns correspond to a complex in polycrystalline form. This experiment confirms that the dehydration process induces the rupture of the cohesion of the crystal certainly by removing the hydrogen interaction associated to the water molecules.

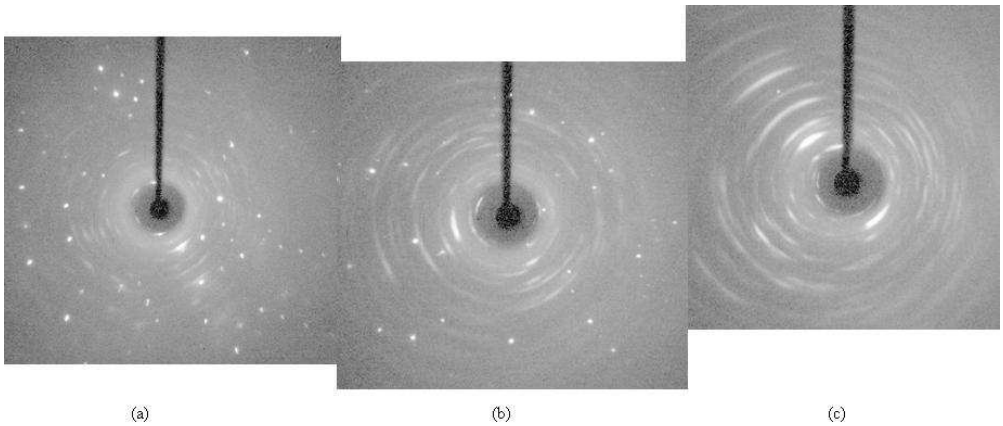

Figure V. 4: Diffraction figure of a single crystal of the compound at 25°C (a), at 60°C after staying at that temperature 3 hours (b) and at 60°C after 12 more hours.

Figure V. 5 describes the powder X-ray patterns between 303 K and 403 K. Between 303 K and 373 K, the diffraction patterns are very similar. At 383 K, new diffraction peaks start to appear and at 393 K and 403 K, the patterns are totally different. The change in the patterns between 373 K and 393 K can be attributed to the dehydration of the complex in agreement with TGA experiment.

The diffraction patterns at 403 K were refined using X-CELL (Figure V. 6). The complex adopts a triclinic P -1 space group, instead of the C 2/c space group for the original sample. The unit cell volume decrease to 829 $Å^3$ (Table V. 1). However, without molecular structure, further comparison is difficult.

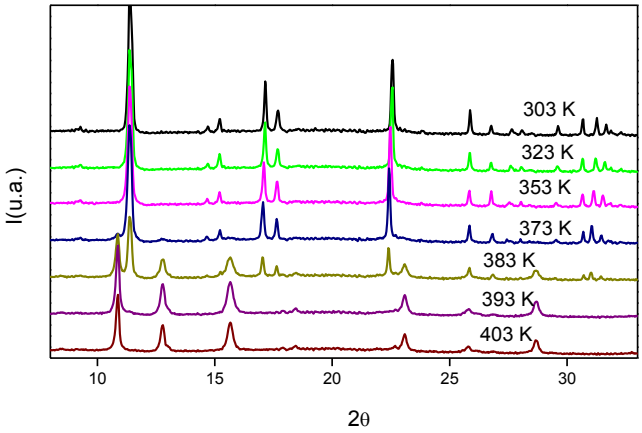

Figure V. 5: *In-situ* Powder X-ray diffraction patterns during dehydration process.

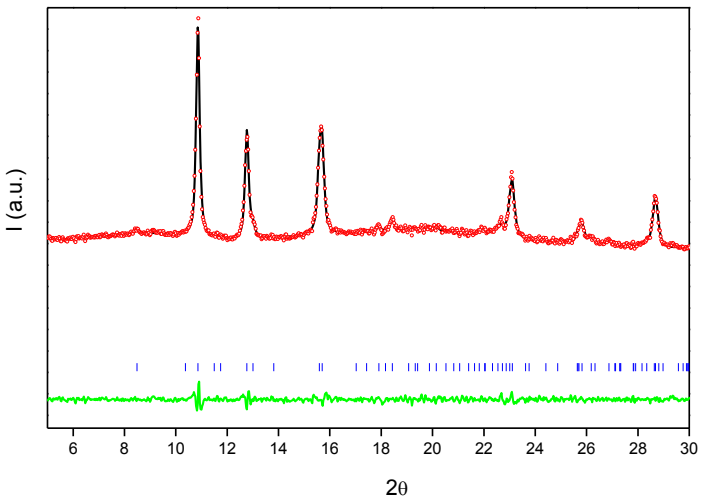

Figure V. 6: Refined powder X-ray pattern at 403 K. The observed and calculated values are drawn with red points and dark lines respectively, reflection positions are marked with vertical ticks and difference curve is shown at the bottom.

	Hydrated Phase	Dehydrated Phase
T (K)	290	403
Crystal system	Monoclinic	triclinic
Space group	C2/c	P – 1
a (Å)	17.326(5)	10.871(2)
b (Å)	12.054(5)	9.387(2)
c (Å)	10.125(5)	9.327(2)
α (°)		114.53(2)
β (°)	116.27(1)	106.464(7)
γ (°)		86.32(2)
V ($Å^3$)	1896.2(1)	829(11)
$R_{wp}^{w/o\ bck}$(%)		14

Table V. 1: Crystal data of hydrated phase (290 K) and refined dehydration phase (403 K)

Figure V. 7 presents the structural comparison between the rehydrated and original

samples on the powder diffraction patterns. The rehydrated sample is the one obtained by leaving the sample after a first TGA experiment at ambient atmosphere for around one month. For the two samples, the diffraction peaks appear at the same 2Θ angle. The main difference is that the rehydrated sample presents significantly broadening diffraction peaks.

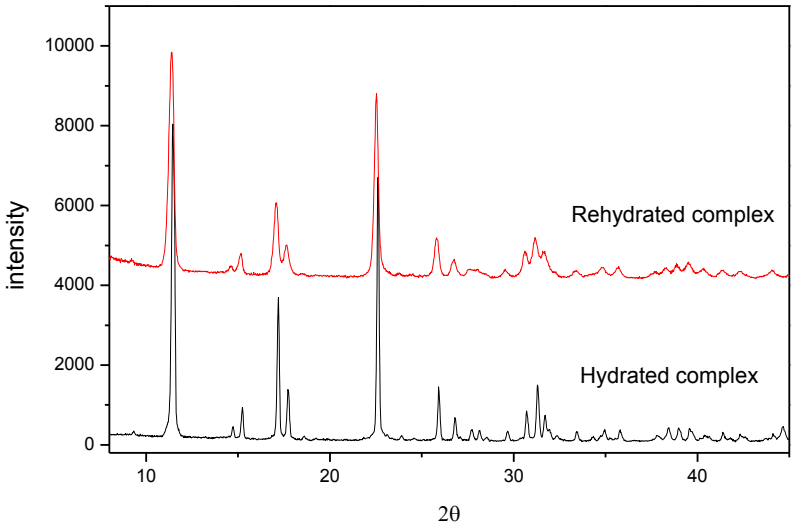

Figure V. 7: X-ray powder diffraction patterns of hydrated and rehydrated samples.

V.1.6. Concluding remarks

To sum up, in this chapter we have proven that it was possible to modify the solvent molecule in the $[FeL_{222}N_3O_2(CN)_2]\cdot H_2O$ complex. First of all, we have observed that the replacement of the water molecule by $CHCl_3$ favors the HS state. Then, by TGA experiments, dehydration and rehydration process have been evidenced on the $[FeL_{222}N_3O_2(CN)_2]\cdot H_2O$. Finally, X-ray diffraction measurement as a function of the temperature revealed that the dehydrated complex adopted different structures from the original $[FeL_{222}N_3O_2(CN)_2]\cdot H_2O$ complex. In the following chapter, we will investigate the magnetic properties of dehydrated and rehydrated complex in order to further study the influence of solvent on the SCO properties.

Chapter V.2. Solvent dependence of magnetic properties

V.2.1. Magnetic properties of dehydrated and rehydrated $[FeL_{222}N_3O_2(CN)_2]\cdot H_2O$

Figure V. 8 shows the $\chi_M T$ product of the dehydrated $[FeL_{222}N_3O_2(CN)_2]\cdot H_2O$ complex. The dehydration was induced *in-situ* inside the SQUID chamber. Sample (ca. 10 mg) was firstly placed at ambient temperature then at 380 K inside SQUID for 90 mins. Purging was performed during this time to eliminate the released water molecule. Cooling down to 10 K and warming up to 300 K were performed with a rate of 1.2 $Kmin^{-1}$. On cooling from 300 K to 80 K, $\chi_M T$ value drops at around 130 K from 3.08 $cm^3mol^{-1}K$ to 0.85 $cm^3mol^{-1}K$. Thermal SCO transition is observed at around $T_{1/2}\downarrow$ = 125 K. On warming a $T_{1/2}\uparrow$ = 130 K is obtained, forming a 5 K hysteresis. TIESST experiment was performed following the standard procedure [10-13], i.e. the sample was rapidly trapped at 10 K. A $\chi_M T$ value of 1.43 $cm^3mol^{-1}K$ is obtained and the T(TIESST) temperature is determined at 69 K. The T(TIESST) curve reaches the warming branch at around 75 K.

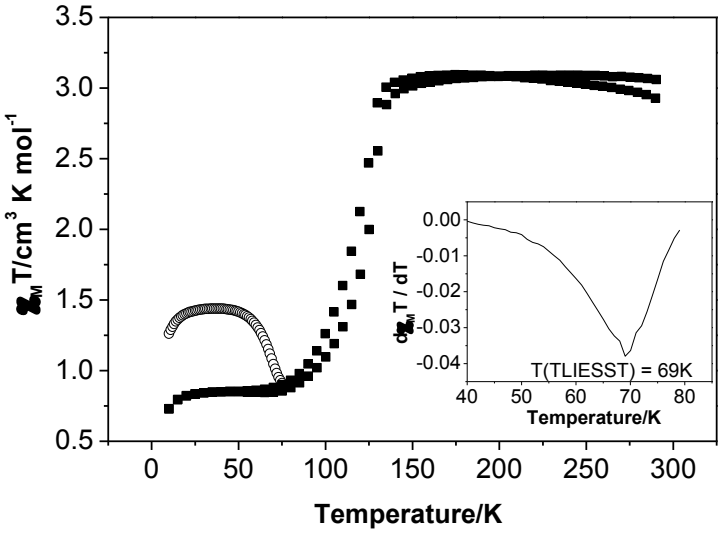

Figure V. 8: Temperature dependence of $\chi_M T$ for $[Fe(L_{222}N_3O_2)(CN)_2]\cdot H_2O$ after dehydration at 380 K for 90 mins inside SQUID chamber: ■ cooling and warming after dehydration, ○ TIESST experiment.

The thermal transition was measured for several thermal cycles, and the shape remains unchanged. Interestingly, the magnetic behavior is different from the original $[FeL_{222}N_3O_2(CN)_2]\cdot H_2O$ sample [13-17]. From the previous TGA and X-ray diffraction experiments, we may attribute this behavior to the fully dehydrated $[FeL_{222}N_3O_2(CN)_2]\cdot H_2O$ complex. In fact, if the dehydration phenomenon is not complete, a mixture of dehydrated and hydrated complexes may happen, and a transition in steps may be observed around 160 K and 200 K, where the transitions of original $[FeL_{222}N_3O_2(CN)_2]\cdot H_2O$ take place.

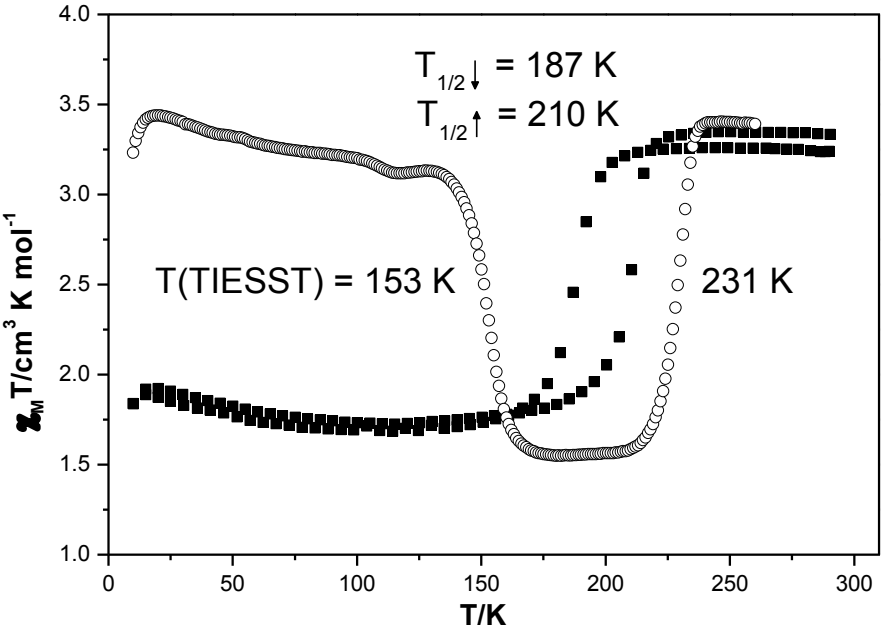

Figure V. 9: Temperature dependence of $\chi_M T$ for $[Fe(L_{222}N_3O_2)(CN)_2]\cdot H_2O$ after rehydration in ambient atmosphere for one week: ■ cooling and warming after dehydration, ○ TIESST experiment.

In order to study the rehydration phenomenon (evidenced by TGA), the *in-situ* dehydrated sample was left at ambient atmosphere during one week and the magnetic properties were reinvestigated in SQUID. The temperature dependence of $\chi_M T$ product is presented in Figure V. 9. On cooling, spin transition occurs at around $T_{1/2}\downarrow$ = 187 K. $\chi_M T$ value drops from 3.23 $cm^3mol^{-1}K$ (at 213 K) to 1.72 $cm^3mol^{-1}K$ (at 130 K). On warming a $T_{1/2}\uparrow$ = 210 K is obtained, forming a 23 K hysteresis. TIESST experiment was then performed. At 30 K, after the quench cooling, the $\chi_M T$ value is 3.40 $cm^3mol^{-1}K$, indicating that ca. 100% metastable HS state can be reached. On warming the T(TIESST) limit is estimated at 153 K. On further warming, unusual behavior is observed. The T(IESST) curve does not follow the warming branch of the SCO curve. For instance, at 180 K the $\chi_M T$ value is 1.83 $cm^3mol^{-1}K$, instead of 1.97 $cm^3mol^{-1}K$ for thermal SCO curve. Finally a $T_{1/2}\uparrow$ of 231 K is obtained and the curve merges into SCO curve at 235 K. We have repeated the thermal SCO measurement after the TIEEST experiment, and found that the SCO curve remains identical.

After one month of rehydration in ambient atmosphere, the transition behavior was reinvestigated for the second time. The temperature dependence of $\chi_M T$ is shown in Figure V. 10. On cooling, spin transition occurs at around $T_{1/2}\downarrow$ = 180 K. The $\chi_M T$ value drops from 3.34 $cm^3mol^{-1}K$ (at 213 K) to 1.94 $cm^3mol^{-1}K$ (at 130 K)and on warming a $T_{1/2}\uparrow$ = 210 K is obtained, forming a 30 K hysteresis. TIESST experiment was also performed. At 30 K, the $\chi_M T$ value is 3.53 $cm^3mol^{-1}K$ and the T(TIESST) limit is estimated at156 K. Here also, the T(TIESST) curve does not follow the warming branch of SCO curve. A $T_{1/2}\uparrow$ of 223 K is obtained and the curve merges into SCO curve at 235 K.

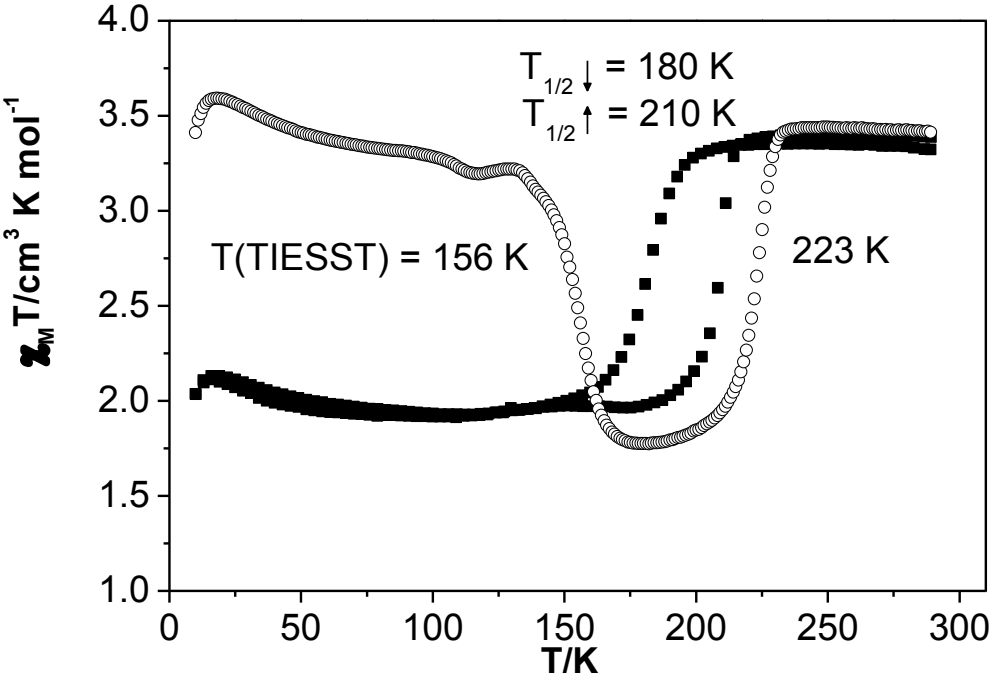

Figure V. 10: Temperature dependence of $\chi_M T$ for $[Fe(L_{222}N_3O_2)(CN)_2]\cdot H_2O$ after rehydration in ambient atmosphere for one month: ■ cooling and warming after dehydration, ○ TIESST experiment.

V.2.2. Other attempts for dehydration outside the SQUID chamber

In parallel to the dehydration process performed *in-situ* in to the SQUID chamber, we have attempted to perform *ex-situ* treatment. The first method is to dehydrate the sample firstly in a vacuum line and then rehydrate the material under ambient atmosphere during 24 hours. Along that, two samples were placed under the vacuum at 100°C for respectively 2 mins and 5 mins, and then rehydrated under a flux of ambient air for 24 hours. TIESST measurements on the two were presented on Figure V. 11.

The sample heated during 2 mins (Figure V. 11 in blue) is characterized by $\chi_M T$ product of 3.3 $cm^3mol^{-1}K$ after the frozen effect, and the T(TIESST) is estimated at 135 K. On further warming, an increase of $\chi_M T$ value is observed at 171 K (2.7 $cm^3mol^{-1}K$), and then decrease at 190 K (1.6 $cm^3mol^{-1}K$). Finally at 221 K, the magnetic response recovers the initial HS fraction. $T_{1/2}\uparrow$ (TIESST) of 221 K is obtained.

The second sample heated during 5 mins (Figure V. 11 in red) presents a magnetic response for the trapped form at 30 K of 3.3 $cm^3mol^{-1}K$. The whole T(TIESST) behavior is similar to the previous sample. The only difference deals with the HS residual obtained at 150 K, which is much higher than for the previous sample.

The TIESST measurement was also performed on a sample after TGA experiment. The

TGA experiment was performed as described in above chapter V.3.2**.** Briefly, the sample was placed under nitrogen flux at room temperature for 3 hours, and then heated up to 400 K. the heating was limited to this temperature in order to avoid decomposition of the complex. The T(TIESST) curve is presented in Figure V. 11. In such experiment the HS residual fraction at 150 K is even higher than the two previous experiments.

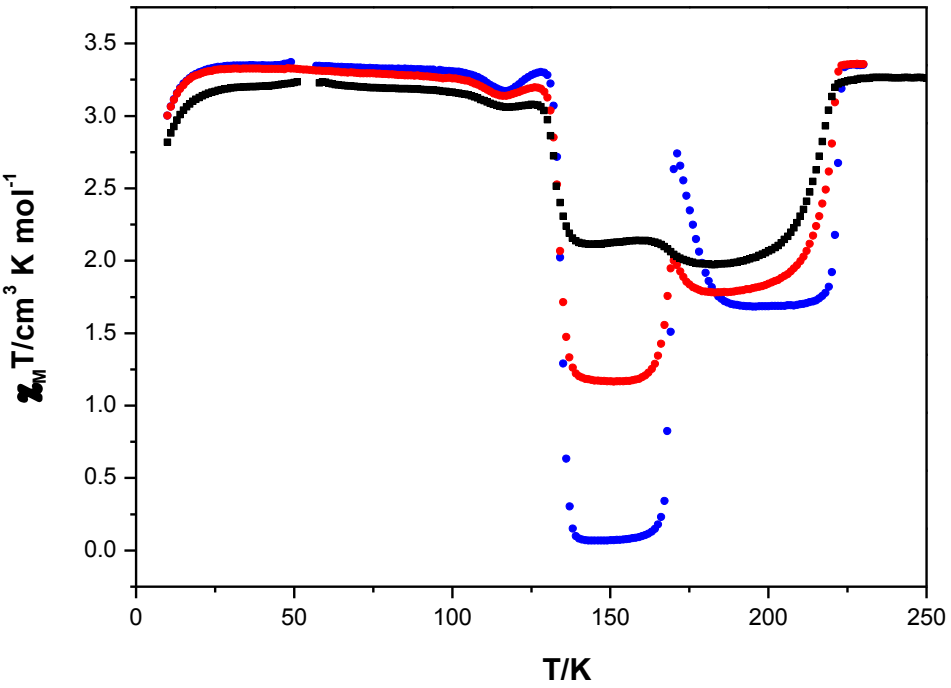

Figure V. 11: Temperature dependence of $\chi_M T$ for the TIESST behavior of complex $[Fe(L_{222}N_3O_2)(CN)_2]\cdot H_2O$ after short time dehydration with vacuum pump: 2 mins (in blue) and 5 mins (in red) dehydration at 100°C; In black line : dehydration by TGA experiment.

In conclusion, it seems that when sample is placed at 100°C for 5 mins, the dehydration process is almost complete while for 2 mins the phenomenon is incomplete. However, when sample is place at 100°C for 2 mins, it seems that no dehydration would take place in such short time. The influence of long-time dehydration in vacuum line is still under investigation

V.2.3. Photomagnetic properties

LIESST experiments were performed on the layer samples (ca. 0.3 mg) of both *in-situ* dehydrated (i.e. dehydration in SQUID) and rehydrated samples. The LIESST experiments were performed according to the standard procedure [10-13]. The complexes of both dehydrated and rehydrated samples were slowly cooled to 10 K, and then irradiated with green light (λ = 530.9 nm) for 30 mins. When the photostationary limit was reached, the T(LIESST) measurement was performed at rate of 0.3 $Kmin^{-1}$.

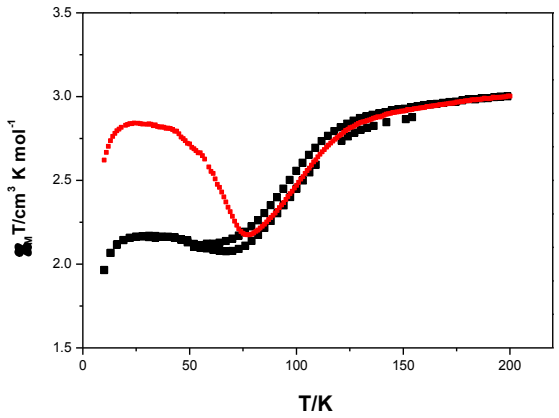

Figure V. 12: Temperature dependence of $\chi_M T$ for $[Fe(L_{222}N_3O_2)(CN)_2]\cdot H_2O$ after dehydration at 380 K for 90 mins inside SQUID chamber: ■ cooling and warming after dehydration, ■ LIESST experiment.

Figure V. 12 presents the $\chi_M T$ product vs. temperature of the sample dehydrated. T(LIESST) obtained after photoexcitation at 10 K was equal to 66 K; i.e. a value close to the T(TIESST) of 69 K determined for the trapping experiment (Figure V. 8). The main difference concerns the HS residual fraction at low temperature. Before irradiation, on the sample prepared in thin layer, a relatively high HS residue is obtained at low temperature (2.25 $cm^3mol^{-1}K$), while for the bulk material the residue is low (0.85 $cm^3mol^{-1}K$) (see Figure V. 8). Such difference is to now unclear. Possibly, the complex is sensitive to pressure, applied during the preparation of the layer.

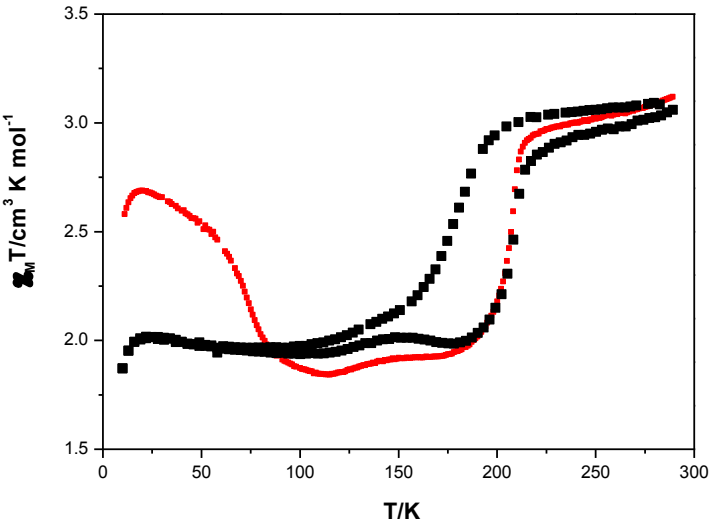

Figure V. 13: Temperature dependence of $\chi_M T$ for $[Fe(L_{222}N_3O_2)(CN)_2]\cdot H_2O$ after rehydration in ambient atmosphere for one month: ■ cooling and warming after dehydration, ■ LIESST experiment.

After one month of rehydration at ambient atmosphere, the LIESST property was reinvestigated (Figure V. 13). A thermal hysteresis of 28 K is observed with $T_{1/2}\downarrow$ = 180 K $T_{1/2}\uparrow$ = 208 K. This behavior agrees with the 30 K loop already reported for the bulk sample (Figure V. 10) and it is characteristic for the thermal hysteresis of hydrated $[FeL_{222}N_3O_2(CN)_2]\cdot H_2O$ in its second thermal cycle [17].

A T(LIESST) of 74 K was obtained, which is much lower than the T(TIESST) of 156 K for the trapping experiment (Figure V. 10). However this T(LIESST) for rehydrated complex

is very similar with what has been observed on hydrated $[FeL_{222}N_3O_2(CN)_2]\cdot H_2O$ in the second thermal cycle, which is 73 K [161]. TGA experiments have illustrated that after the dehydration, a rehydration process occurred at ambient atmosphere.

V.2.4. Concluding remarks

In this part, we mainly focused on the solvent dependence of magnetic and photomagnetic properties of macrocyclic complexes $[FeL_{222}N_3O_2(CN)_2]\cdot$solv (solv = H_2O and $2CHCl_3$). First, we have recalled the structural investigation on the $[FeL_{222}N_3O_2(CN)_2]\cdot 2CHCl_3$ complex, which demonstrated that after replacing water molecule by $CHCl_3$, the complex was HS at both high and low temperatures. Then our attention was focused on the dehydration and rehydration of $[FeL_{222}N_3O_2(CN)_2]\cdot H_2O$ complex. Powder X-ray diffraction patterns demonstrated that the rehydrated complex is isomorphous with the original hydrated complex, while the dehydrated complex adopted a different space group from the former ones. From magnetic studies, it was demonstrated that the thermal SCO behavior of both the dehydrated and rehydrated samples was different from the original hydrated complex. More importantly, we reported on the rehydrated $[FeL_{222}N_3O_2(CN)_2]\cdot H_2O$ complex, a new T(TIESST) record of 156 K for mononuclear Fe(II) complexes.

The reason why T(TIESST) curve of rehydrated complex does not follow SCO curve is still under investigation. Since the T(TIESST) value of this complex is close to its $T_{1/2}$ value, it is possible that thermal SCO process is under the influence of kinetic effect. Further attention will be focused on the relaxation kinetics in the thermal SCO region.

Based on the T(TIESST) and $T_{1/2}\downarrow$ values of *in-situ* dehydration and rehydration data can be completed in the T(LIESST) database. It is marked in Figure V. 14 as samples **53** (rehydration) and **54** (dehydration). Previous studies on the solvent dependence of $[Fe(bpp)_2]X_2\cdot nH_2O$ family [11] have shown that hydrated and anhydrous analogues follow the same 150 K T_0 line. For instance **23** and **24** represent respectively the hydrated $[Fe(bpp)_2](BF_4)_2\cdot 5H_2O$ and its anhydrous analogue. Similar behavior can be also found for $[Fe(bpp)_2]Br_2\cdot 3H_2O$ (sample **28**) and its anhydrous analogue (sample **29**). Based on these previous results, the T(TIESST)/$T_{1/2}$ couples of dehydrated and rehydrated $[FeL_{222}N_3O_2(CN)_2]\cdot H_2O$ should be predicted to follow the T_0 = 180 K line as well. However, the plotted T(TIESST)/$T_{1/2}$ couples in Figure V. 14 (sample **53, 54**, together with the original hydrated complex $[FeL_{222}N_3O_2(CN)_2]\cdot H_2O$, namely sample **40)** surprisingly define a line perpendicular to T_0 = 180 K. This situation contrasts with the T(LIESST)/ T(decomposition) relation of the $[Fe(L_{xyz}N_5)(CN)_2]\cdot nH_2O$ family (sample **50-52**) and the T(TIESST) / $T_{1/2}$ for the rehydrated $[FeL_{222}N_3O_2(CN)_2]\cdot H_2O$ (sample **53**), which defines a new T_0 line can be drawn with a value of 220 K. This new T_0 line indicates the possibility to further increase the T(LIESST) value by modifying the macrocyclic complexes.

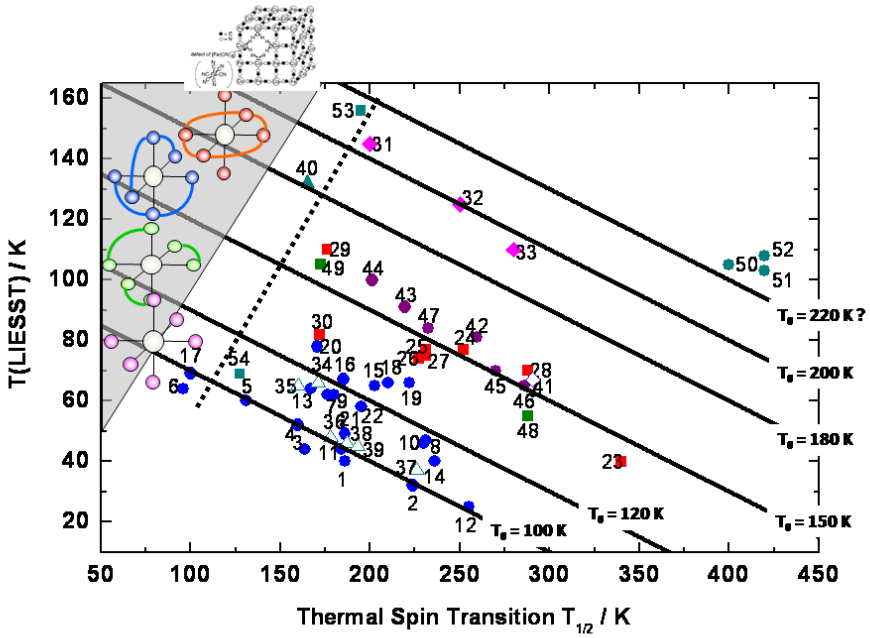

Figure V. 14: Variation of T(LIESST) versus $T_{1/2}$ for spin crossover compounds

References

1 M. Seredyuk, A. B. Gaspar, V. Ksenofontov, M. Verdaguer, F. Villain, P. Gütlich, *Inorg. Chem*. **2009**, *48*, 6130

2 I. Šalitroš, J. Pavlik, R. Boča, O. Fuhr, C. Rajaduraia, M. Ruben, *Cryst. Eng. Comm.* **2010**, *12*, 2361.

3 M. C. Giménez-López, M. Clemente-León, E. Coronado, F. M. Romero, S. Shova, J.-P. Tuchagues, *Eur. J. Inorg. Chem*. **2005**, 2783.

4 E. Coronado, M. C. Giménez-López, C. Giménez-Saizab, F. M. Romero, *Cryst. Eng. Comm.,* **2009**, *11*, 2198.

5 B. A. Leita, S. M. Neville, G. J. Halder, B. Moubaraki, C. J. Kepert, J.-F. Létard, K. S. Murray, *Inorg. Chem.* **2007**, *46*, 8784.

6 J. S. Costa, PhD Thesis, Université Bordeaux I, 2005.

7 S. M. Nelson, P. D. A. Mcllroy, C. S. Stevenson, E. König, G. Ritter, J. Waigel, *J. Chem. Soc. Dalton Trans.* **1986**, 991.

8 S. Hayami, Z. Gu, Y. Einaga, Y. Kobayasi, Y. Ishikawa, Y. Yamada, A. Fujishima, O. Sato, *Inorg. Chem.* **2001**, *40*, 3240;

9 P. Guionneau, J. S. Costa, J.-F. Létard, *Acta Cryst.* **2004,** *C60*, m587

10 J.-F. Létard, L. Capes, G. Chastanet, N. Moliner, S. Létard, J. A. Real, O. Kahn, *Chem. Phys. Lett*. **1999**, *313*, 115;

11 S. Marcén, L. Lecren, L. Capes, H. A. Goodwin, J.-F. Létard, *Chem. Phys. Lett.* **2002**, *358*, 87 ;

12 J.-F. Létard, P. Guionneau, O. Nguyen, J. S. Costa, S. Marcén, G. Chastanet, M. Marchivie, L. Goux-Capes, *Chem. Eur. J*. **2005**, *11*, 4582.

13 J.-F. Létard, J. *Mater. Chem.* **2006**, *16*, 2550.

14 S. M. Nelson, P. D. A. Mcllroy, C. S. Stevenson, E. König, G. Ritter, J. Waigel *J. Chem. Soc. Dalton Trans.* **1986**, 991-995.

15 E. Konig, G. Ritter, J. Dengler, S. M. Nelson, *Inorg. Chem.* **1987**, *26*, 3582.

16 H. Liu, A. Fujishima, O. Sato, *Appl. Phys. Lett*. **2004,** *85*, 2295.

17 J. S. Costa, P. Guionneau, J.-F. Létard, *J. Phys.: Conf. Ser.* **2005**, *21*, 67.

Conclusion

In this manuscript we have focused our attention on the influence of chemical modification on the SCO properties of macrocyclic complexes. The modification was carried out on the different parts of the complex, i.e. the metal center, the macrocyclic ligand, the anionic ligand and the solvent.

The modification of the Fe(II) metal center by dilution with the Mn(II) ions (Part II) led us to observe strong kinetics effect in the powder samples of $[Fe_xMn_{1-x}(L_{222}N_3O_2)(CN)_2]\cdot H_2O$ series, which resulted in high HS residual at low temperature upon cooling. Upon warming, partial SCO from the HS state to the HS/LS mixed state occurred on several metal diluted samples. By a systematical investigation of the TIESST properties, it has been demonstrated that when x was less than 0.892, the samples remained almost in HS state. A phase diagram was then established based on five critical temperatures, which were determined from the T(TIESST) curve. In the phase diagram, the transition regimes (LS_1 and LS_2/HS_3 regimes) have been defined, which indicated that the LS_2/HS_3 state should be obtained in the metal diluted sample with x = 0.892. Based on an effective thermal treatment protocol we were able to reach the LS_2/HS_3 state. Finally, the photomagnetic properties of the $[Fe_xMn_{1-x}(L_{222}N_3O_2)(CN)_2]\cdot H_2O$ metal dilution series were demonstrated to be similar to the pure Fe(II) analogue.

The modification of the macrocyclic ligand (Part III) was done by changing the carbon numbers between the nitrogen coordination atoms on the $[Fe(L_{222}N_5)(CN)_2]\cdot H_2O$ complex. By doing this, we observed that all the four studied complexes, namely $[Fe(L_{222}N_5)(CN)_2]\cdot H_2O$, **[**$Fe(L_{232}N_5)(CN)_2]\cdot 2.5H_2O$, $[Fe(L_{223}N_5)(CN)_2]\cdot 2.5H_2O$ and $[Fe(L_{323}N_5)(CN)_2]\cdot 1.5H_2O$ were LS from 10 K to 420 K. We also noticed for the four complexes above 420 K an irreversible departure of water molecules associated with a LS to HS conversion. The study of the photomagnetic properties demonstrated that depending on the nature of the ligands, the level of photoexcitation was different. In contrast, the stability of the photoinduced state of the three $[Fe(L_{222}N_5)(CN)_2]\cdot H_2O$, **[**$Fe(L_{232}N_5)(CN)_2]\cdot 2.5H_2O$ and $[Fe(L_{223}N_5)(CN)_2]\cdot 2.5H_2O$ complexes was similar: the three T(LIESST) values were about 100 K. In conclusion, it seemed that the nature of the ligand in this macrocyclic family did not affect the stability of the lifetime, but just the easiness of photoexcitation. Moreover, it was interesting to note that these three complexes display exceptional long lived lifetime for Fe(II) materials in LS state.

Concerning the modification of anionic ligand (Part IV), our strategy was to change the cyano group of the $[Fe(L_{222}N_3O_2)(CN)_2]\cdot H_2O$ and $[Fe(L_{xyz}N_5)(CN)_2]\cdot nH_2O$ complexes by thiocyanate / selenocyanate group. Eight complexes were investigated at both high and low temperatures. All these complexes were in HS state from magnetic measurement. The complex $[Fe(L_{222}N_3O_2)(NCS)_2]$ presented a structural transition from monoclinic P 2/n to triclinic P -1 space group upon cooling, while the other complexes adopted the same space group at both room and low temperatures. More interestingly, in the $[Fe(L_{232}N_5)(NCS)_2]\cdot 0.5H_2O$ and $[Fe(L_{232}N_5)(NCSe)_2]\cdot 0.25H_2O$ complexes, an elongation of the Fe-N bond distance was observed on one nitrogen atom of the propylene fragments. This elongation was attributed to an initial departure of the nitrogen atom from the coordination center upon cooling.

In the Part V, we have investigated the solvent dependence on the SCO properties of the $[Fe(L_{222}N_3O_2)(CN)_2]\cdot H_2O$ complex. Powder X-ray diffraction patterns demonstrated that the rehydrated complex is isomorphous with the original hydrated complex, but from magnetic studies the thermal SCO behavior of both the dehydrated and rehydrated samples was different from the original hydrated complex. More importantly, we reported on the rehydrated $[FeL_{222}N_3O_2(CN)_2]\cdot H_2O$ complex, a new T(TIESST) record of 156 K for a mononuclear Fe(II) material.

Finally, we introduced the new complexes into the T(LIESST)/$T_{1/2}$ database (Figure a). For the LS complex of Part III, we used the thermal temperature $T_{1/2}$ recorded along the LS to HS transition and their T(LIESST) values deduced from the photomagnetic properties. The three complexes in the T(LIESST)/$T_{1/2}$ database were the sample **50**-**52**. Of course such analysis might be questionable in reason of the interplay between the SCO transition and the dehydration process. Nevertheless, it was interesting to note that those three new data were above the T_0 = 180 K line. For the complexes of Part V, we used the T(TIESST) value deduced form the trapping measurements to introduce the two dehydrated (sample **54**) and rehydrated complexes (sample **53**) in the database. Interestingly, none of these macrocyclic complexes follows the T_0 = 180 K line of the macrocyclic complex $[Fe(L_{222}N_3O_2)(CN)_2]\cdot H_2O$ (sample **40**). Indeed, the LS macrocyclic complexes (**50**-**52)** as well as the rehydrated complex (**53)** allowed to define a new line with a T_0 of 220 K, which represented the upper record now reported for SCO materials.

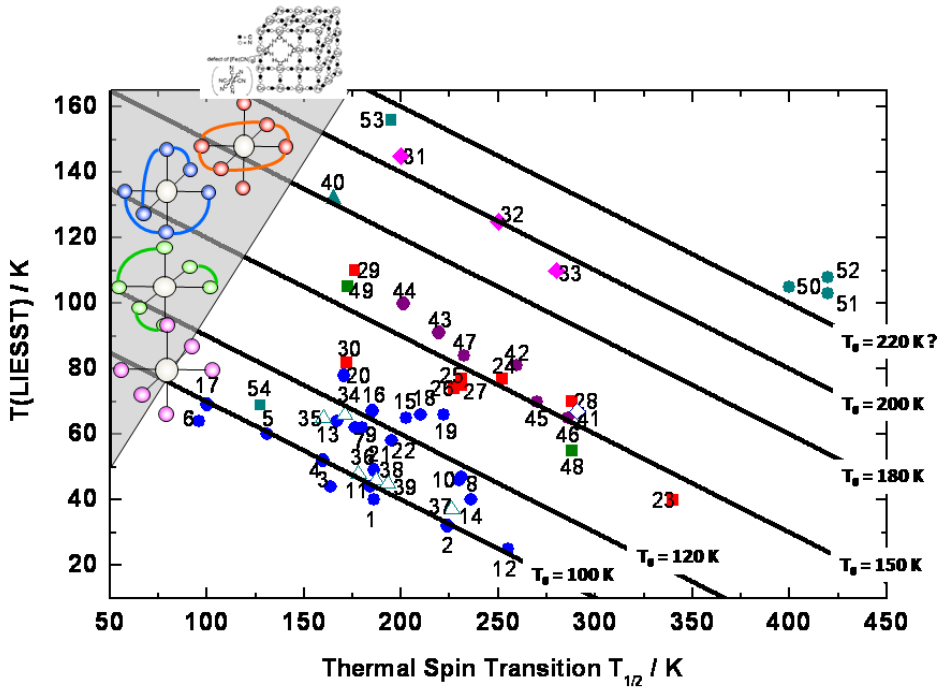

Figure a. Variation of T(LIESST) versus $T_{1/2}$ for spin crossover compounds

As a perspectives, the effort on X-ray diffraction study has to be pursued, the expected HS_4 to HS_2 transition $[Fe_xMn_{1-x}(L_{222}N_3O_2)(CN)_2]\cdot H_2O$ at around 160 K in the metal diluted system should be verified by crystallography, which is the key to understand why the HS to

LS_2/HS_3 state transition is hidden in some diluted complexes. In parallel, we have to extend the synthesis for new Fe(II) macrocylic complexes. We may expect to define new samples with optimized properties of coordination change, light induced metastability with long lived lifetime as well as high T(LIESST) value towards room temperature to be used in some applications. Particularly, if we consider that in the last 10 years, the T(LIESST) record has been progressively shifted from 60 K in the late 1990s to 130 K for a pure Fe(II) SCO material and even 150 K in Prussian Blue analogs. Today, the record is held by a molecular cluster with a value of about 180 K. Clearly, the T(LIESST) limit has not been reached.

Annexes

Elemental analysis

CHNS

Elemental analyzes C, H, N and S were performed on an automatic elemental analyzer FlashEA^{TM} 1112. The sample is weighed thoroughly (1 to 2 mg) in tin capsules, and then placed in a furnace oxidation / reduction at 900 ° C. The reaction of the oxygen with the tin capsules at high temperature generates an exothermic reaction which raises the temperature to 1800 ° C for a few seconds. At this temperature, the organic and inorganic compounds are converted to elemental gas. These gases after several reductions are separated by column chromatography, and finally detected by a thermal conductivity detector highly sensitive.

Microprobe analysis of metal

The measurements were performed on an electron microprobe X-ray emission (CAMECA SX 100) with 3 WDS and EDS spectroscopy-sddd (Bruker AXS) the "Center for Advanced Materials Characterization" - The CeCaMA of ICMCB.

X-ray diffraction on powder and single crystals

Records of powder diffractograms were made by E. Lebraud (ICMCB) using diffractometer (Philips PW1820, PANalytical X'Pert) with Bragg-Bentano geometry (λ = 1.5406 Å). The angular range extends from 5 to 60 ° with a speed of 0.02 ° / s. The indexing of the diffraction peaks was performed using the software and DICVOLGV TREOR.

Diffraction data on single crystal X were recorded using Bruker-Nonius diffractometer K-CCD (λ = 0.7170 Å). The crystal structures were determined by direct methods and atomic parameters were refined using SHELX-97 programs SIR97 and WinGX.

Optical reflectivity measurements

The apparatus of reflectivity, developed at ICMCB, consists of a halogen lamp (Fiber Optic Iluminator Model 77501) equipped with a filter centered at 530 cm^{-1}. The sample, placed in a quartz sample holder, is continuously measured on the surface by the white light emitted by the halogen lamp. The device is equipped with a SM240 spectrometer (Opton Laser International) and coupled to cryogenic helium. This equipment allows simultaneous recording, diffuse absorption spectra between 450 and 950 nm at a given temperature but also changes depending on the temperature (10-290 K) of the reflected signal. The scanning speed is 3 $Kmin^{-1}$. The spectrum of the reflected light was calibrated with carbon black as standard black and barium sulfate ($BaSO_4$) as standard white.

Magnetic susceptibility measurements

Two susceptometers were used: i) The susceptometer nitrogen, operating in the range from 77 to 350 K, is equipped with a continuous flow cryostat of liquid nitrogen, a Brüker electromagnet (2 T), and a temperature controller type TBT. The rate of change of temperature of 3 $Kmin^{-1}$. ii) The high temperature susceptometer, operating in the range 300-800 K, is equipped with a 2 T electromagnet and a Eurotherm temperature controller.

Magnetic and photomagnetic measurements

The magnetic properties were recorded using a SQUID magnetometer (Superconducting Quantum Interference Device) Quantum Design MPMS-5S. The measurements can be performed between 10 K and room temperature for applied magnetic fields of 2 T. The thermal contact between the sample and the helium tank is by means of exchange gas (helium) flowing through the sample compartment..

Photomagnetic Experiments are performed using the apparatus SQUID coupled to a light source which can be either a LASER (Krypton, Kr +) at wavelengths 514.5 nm (472.2 - 501.7 nm), 647 nm (676.4 - 752.5 nm) or a laser diode which emits at 830 nm. The cane of SQUID measurement allows the passage of an optical fiber which guides the beam to the sample deposited on a straw attached to the end of the rod. The compound is deposited as a thin layer (the amount of product is estimated to be around 0.3 mg) on a horizontal support inside the straw. This technique of sample preparation minimizes the absorption effects. However, this requires the use of a strong magnetic field (2 T in our case) and does not allow an accurate estimate of the mass of product. For this, the magnetic measurement is performed compared to the spin transition recorded previously from a mass accurately weighed. The intensity of irradiation is set to be around 5 mW/cm^2 to minimize the effects of heating of the sample. The choice of the wavelength of irradiation requires knowledge of the absorption spectrum of the compound.

Infrared spectra of $[Fe(L_{xyz}N_5)(CN)_2]\bullet nH_2O$ family

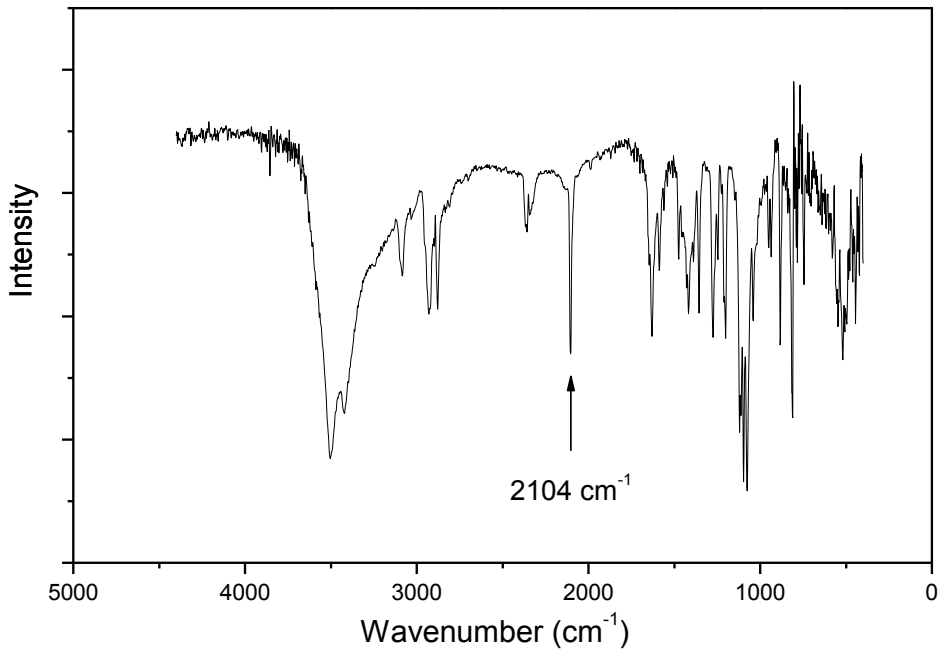

Figura a. Infrared spectra of $[Fe(L_{222}N_5)(CN)_2]\cdot H_2O$ complex

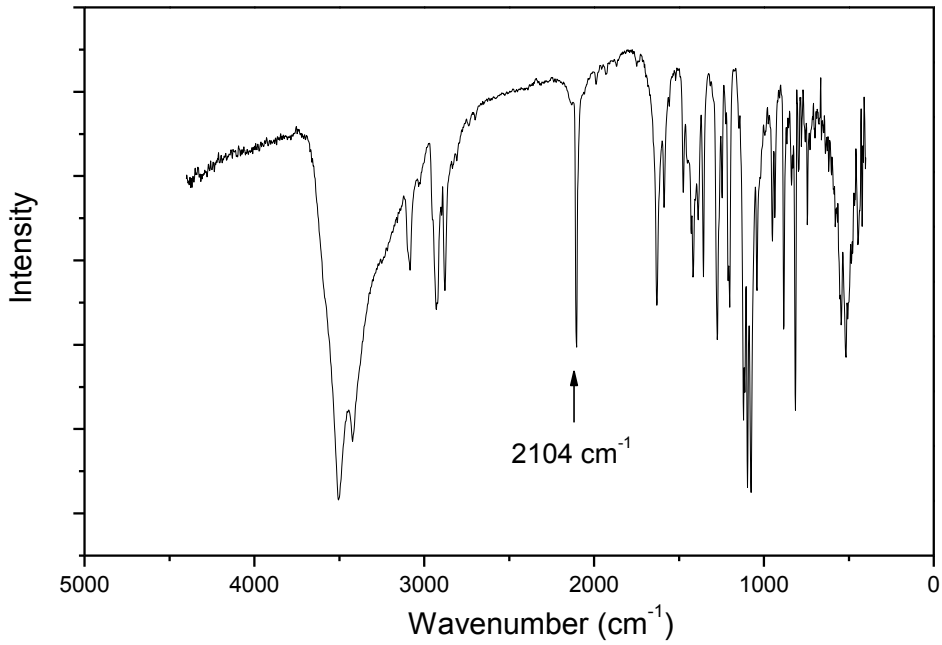

Figura b. Infrared spectra of $[Fe(L_{232}N_5)(CN)_2]\cdot 2.5H_2O$ complex

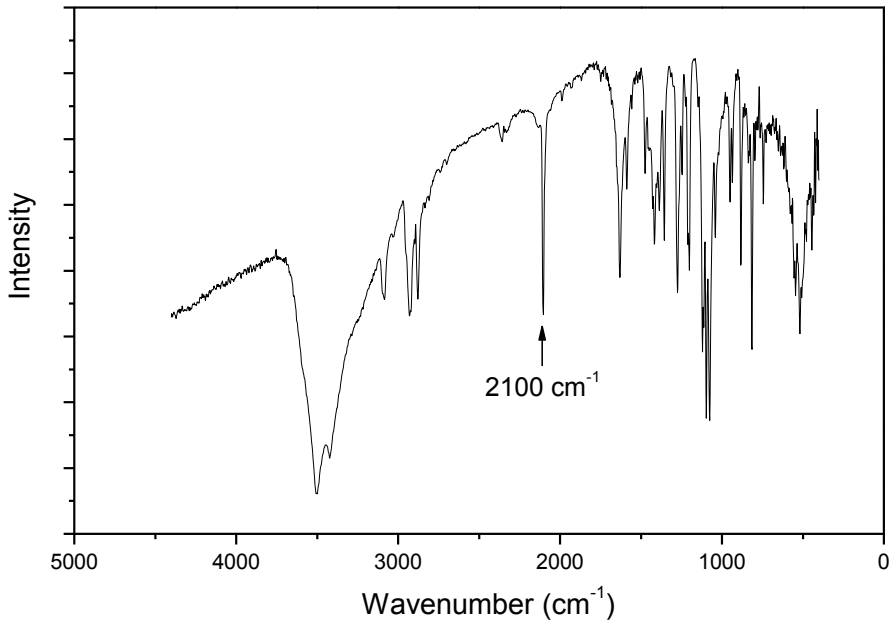

Figura c. Infrared spectra of $[Fe(L_{223}N_5)CN)_2]\cdot 2.5H_2O$ complex

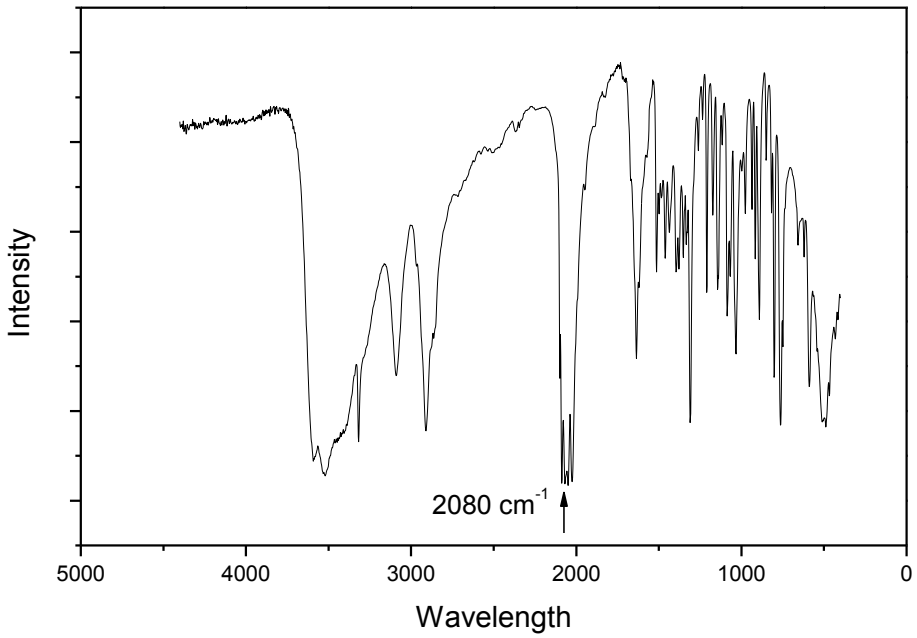

Figura d. Infrared spectra of $[Fe(L_{323}N_5)(CN)_2]\cdot 1.5H_2O$ complex

Résumé :

Les complexes à transition de spin sont des molécules qui peuvent être commutées entre deux états, l'un diamagnétique et l'autre paramagnétique. Cette commutation peut s'effectuer, entre autre, à l'aide d'une excitation lumineuse, ouvrant la voie vers un possible stockage de l'information au niveau d'une molécule unique. Toutefois, l'information photo-inscrite n'est stable qu'au-dessous d'une certaine température appelée T(LIESST).

L'objectif principal de cette thèse a constitué en des modifications chimiques (modification du ligand organique, désolvatation, modifications d'anion,…) d'un complexe macrocyclique de Fe(II) qui présente à l'heure actuelle l'un des T(LIESST) les plus élevés (134 K), et ce afin d'augmenter encore cette valeur. Parmi les divers résultats expérimentaux, un T(LIESST) de 160 K a été obtenu.

Mots clés :

• Transition de spin • Complexes de Fe(II) •Effet LIESST
• Effets de solvant • Déshydratation

Title : Optimization of bistable molecular materials.

Abstract :

Spin transition complexes are molecules that can be commuted between two different states, one being diamagnetic and the other one paramagnetic. This commutation can be triggered by different ways, including light irradiation, opening a way to the storage of information at molecular level. However, the photo-inscribed information is stable only below a given temperature called T(LIESST).

The main goal of this thesis has been to modify chemically (modification of organic ligand, desolvation, modification of anions, …) a Fe(II) macrocyclic ligand presenting one of the highest T(LIESST) known today (134 K) with the aim to further increase this temperature. Among the different results obtained, a T(LIESST) of 160 K has been reached.

Keywords :

• Spin transition • Fe(II) complexes • LIESST effect
• Solvent effects • Desolvatation